Imperial/TP/12/AH/01

Brane Tilings and Reflexive Polygons

Amihay Hanany and Rak-Kyeong Seong

Theoretical Physics Group, The Blackett Laboratory, Imperial College London, Prince Consort Road, London SW7 2AZ, UK

E-mail: a.hanany@imperial.ac.uk, rak-kyeong.seong@imperial.ac.uk

Abstract: Reflexive polygons have attracted great interest both in mathematics and in physics. This paper discusses a new aspect of the existing study in the context of quiver gauge theories. These theories are 4d supersymmetric worldvolume theories of D3 branes with toric Calabi-Yau moduli spaces that are conveniently described with brane tilings. We find all 30 theories corresponding to the 16 reflexive polygons, some of the theories being toric (Seiberg) dual to each other. The mesonic generators of the moduli spaces are identified through the Hilbert series. It is shown that the lattice of generators is the dual reflexive polygon of the toric diagram. Thus, the duality forms pairs of quiver gauge theories with the lattice of generators being the toric diagram of the dual and vice versa.

arXiv:1201.2614v2 [hep-th] 6 Feb 2012

Contents

1 Introduction **2**

2 Background and Motivation **4**
- 2.1 Reflexive Polytopes 4
- 2.2 The Brane Tiling and the Forward Algorithm 9
- 2.3 Hilbert Series and Lattice of Generators 13

3 Model 1: $\mathbb{C}^3/\mathbb{Z}_3 \times \mathbb{Z}_3$ $(1,0,2)(0,1,2)$ **17**

4 Model 2: $\mathbb{C}^3/\mathbb{Z}_4 \times \mathbb{Z}_2$ $(1,0,3)(0,1,1)$ **21**

5 Model 3: $L_{1,3,1}/\mathbb{Z}_2$ $(0,1,1,1)$ **25**
- 5.1 Model 3 Phase a 25
- 5.2 Model 3 Phase b 30

6 Model 4: $\mathcal{C}/\mathbb{Z}_2 \times \mathbb{Z}_2$ $(1,0,0,1)(0,1,1,0)$, $\mathbf{PdP}_5$ **32**
- 6.1 Model 4 Phase a 32
- 6.2 Model 4 Phase b 36
- 6.3 Model 4 Phase c 39
- 6.4 Model 4 Phase d 41

7 Model 5: $\mathbf{PdP}_{4b}$ **44**

8 Model 6: $\mathbf{PdP}_{4a}$ **50**
- 8.1 Model 6 Phase a 50
- 8.2 Model 6 Phase b 56
- 8.3 Model 6 Phase c 58

9 Model 7: $\mathbb{C}^3/\mathbb{Z}_6$ $(1,2,3)$, $\mathbf{PdP}_{3a}$ **61**

10 Model 8: $\mathbf{SPP}/\mathbb{Z}_2$ $(0,1,1,1)$, $\mathbf{PdP}_{3c}$ **65**
- 10.1 Model 8 Phase a 65
- 10.2 Model 8 Phase b 69

11 Model 9: $\mathbf{PdP}_{3b}$ **72**
11.1 Model 9 Phase a 72
11.2 Model 9 Phase b 76
11.3 Model 9 Phase c 78

12 Model 10: $\mathbf{dP}_3$ **81**
12.1 Model 10 Phase a 81
12.2 Model 10 Phase b 85
12.3 Model 10 Phase c 87
12.4 Model 10 Phase d 89

13 Model 11: $\mathbf{PdP}_2$ **92**

14 Model 12: $\mathbf{dP}_2$ **96**
14.1 Model 12 Phase a 96
14.2 Model 12 Phase b 100

15 Model 13: $\mathbb{C}^3/\mathbb{Z}_{4,(1,1,2)}$, $Y^{2,2}$ **102**

16 Model 14: $\mathbf{dP}_1$ **106**

17 Model 15: $\mathcal{C}/\mathbb{Z}_2$ $(1,1,1,1)$, $\mathbb{F}_0$ **110**
17.1 Model 15 Phase a 110
17.2 Model 15 Phase b 114

18 Model 16: $\mathbb{C}^3/\mathbb{Z}_3$ $(1,1,1)$, $\mathbf{dP}_0$ **116**

19 Seiberg Duality Trees **121**

20 Specular Duality and Conclusions **127**

A The theory for $\mathbb{C}^3/\mathbb{Z}_4 \times \mathbb{Z}_4$ $(1,0,3)(0,1,3)$ **129**

B Review: Seiberg Duality, Integrating out Mass Terms, and the Higgs Mechanism **130**
B.1 Seiberg Duality 130
B.2 Integrating out mass terms 132
B.3 Higgs Mechanism 133

1 Introduction

The study of $\mathcal{N} = 1$ supersymmetric gauge theories living on D-branes probing singular non-compact Calabi-Yau 3-folds has been an immensely active and fruitful endeavour in string theory. The matter content of the 4 dimensional worldvolume theories is encoded in a graph known as the **quiver** [1].[1] An interesting subset of these theories possess mesonic moduli spaces which are toric and are associated to convex lattice polygons. These polygons are known as **toric diagrams** [4] of the Calabi-Yau singularity.

In the last two decades, a particular type of polytope caught the attention in string theory in the context of **mirror symmetry** [5–11]. This polytope is known as a **reflexive polytope**.

A reflexive polytope is a convex lattice polytope which possesses a single internal lattice point.[2] For a long time, del Pezzo surfaces [12–16] and more generally Fano varieties [17–27] have been associated to a range of reflexive polytopes.

When Type II superstring theory is compactified on a Calabi-Yau 3-fold, its worldsheet theory is a $\mathcal{N} = (2, 2)$ superconformal field theory. By swapping the Hodge numbers h_{11} and h_{12} associated to the Calabi-Yau 3-fold, one obtains another Calabi-Yau 3-fold. If one flips the signs of the U(1) R-charges of the left and right moving components of the theory's superalgebra, one obtains another superconformal field theory which is the one compactified on the "mirror" of the original Calabi-Yau 3-fold.

Reflexive polytopes have played an important role in studying the relationship between mirror paired Calabi-Yau manifolds and the corresponding superconformal field theories. The reflexive polytopes are used for constructing Calabi-Yau manifolds as hypersurfaces in toric varieties. The underlying property of reflexive polytopes is that they have a polar dual partner which in turn is reflexive and relates to the mirror Calabi-Yau manifold. This property led to a systematic study of mirror paired Calabi-Yau manifolds. The resulting classification [28–33] found connections to for instance heterotic string compactifications [34–36] or to F-theory backgrounds [37–40].

In the following work, reflexive polygons are used to study mesonic moduli spaces of 4d supersymmetric quiver gauge theories dual to Type IIB string theory on $\mathrm{AdS}_5 \times X_5$ where X_5 is a Sasaki-Einstein 5-manifold. There are 16 distinct reflexive polygons and the corresponding theories are worldvolume theories of D3-branes probing Calabi-Yau 3-fold singularities. The mesonic moduli spaces are toric Calabi-Yau 3-folds and the reflexive polygons are the corresponding toric diagrams.

The aim of the following work is to identify all $4d$ supersymmetric quiver gauge theories whose moduli space is represented by a reflexive polygon. In order to do so,

[1] For more mathematical reviews on quivers see for example [2, 3].

[2] From Latin *reflexus*, Medieval Latin *reflexivus*, meaning to be turned back or reflected.

extensive use is made of **brane tilings** [41, 42][3] which combine the matter content and the superpotential of the quiver theory on a periodic graph on $\mathbb{T}^2$.

Every consistent brane tiling relates to a consistent quiver gauge theory. Starting from the brane tiling for the orbifold of the form $\mathbb{C}^3/\mathbb{Z}_4 \times \mathbb{Z}_4$ with orbifold action $(1,0,3)(0,1,3)$ [48–52], one applies the **Higgs mechanism** [14] and uses **Seiberg duality** [12, 13, 15, 53–56] on brane tilings in order to find that there exist exactly 30 quiver gauge theories corresponding to the 16 reflexive polygons. Seiberg duality, also known as toric duality in this context, relates theories with different matter content and superpotential to the same mesonic moduli space.

In order to have a complete classification of the mesonic moduli spaces, the moduli space generators for all 30 quiver gauge theories are found by computing a generating function known as the **Hilbert series** [57–61]. The Hilbert series encodes information about the moduli space generators. They are identified using a method known as **plethystics** [62]. The lattice of generators formed by the mesonic charges is the dual reflexive polygon for the 16 toric diagrams. It is shown that this is the case for all 30 quiver gauge theories.

The complete classification of $4d$ $\mathcal{N} = 1$ supersymmetric gauge theories corresponding to the 16 reflexive polygons leads to new observations. The most important observation is that of a new duality which we name **specular duality**. It relates quiver theories with different mesonic moduli spaces under a swap of external and internal points of the toric diagram. Specular duality partitions the set of 30 quiver gauge theories in dual pairs and illustrates interesting physics at work. An illustration of this new duality is given at the concluding section, and it is of great interest to explore it further in future work.

The work is structured as follows. In section §2, the concepts and motivations behind studying reflexive polygons are reviewed. In addition, the ideas behind brane tilings and the mesonic Hilbert series are reviewed. A key ingredient of the discussion is the lattice of mesonic generators which is reviewed in section §2. Sections §3 to §18 summarize the 30 quiver gauge theories associated to reflexive polygons, and illustrate the duality between the toric diagram and generator lattices. In section §19, the trees illustrating the relationships between toric (Seiberg) dual brane tiling models corresponding to the same reflexive polygon are presented. For the purpose of having a self-contained discussion, appendix §B reviews the concepts of toric (Seiberg) duality and the Higgs mechanism in the context of brane tiling models. As part of the concluding section, the concept behind specular duality of the 30 brane tiling models corresponding to reflexive polygons is introduced.

[3] For applications of brane tilings see for example [43–47].

2 Background and Motivation

2.1 Reflexive Polytopes

Mirror Symmetry. Reflexive polytopes have been introduced in string theory in the context of mirror symmetry [5–11]. A way to study mirror symmetry is to consider Type II superstring theory compactified on a Calabi-Yau 3-fold. Its string worldsheet theory is a $\mathcal{N} = (2, 2)$ superconformal field theory. It contains a superalgebra with left and right moving components. When one flips the signs of the $U(1)$ R-symmetry charges of the left and right moving components, the Calabi-Yau transitions to a different Calabi-Yau manifold with its Hodge numbers h_{11} and h_{12} being interchanged.

The understanding of mirror symmetry in the context of compactified superstring theory led to a search of mirror paired Calabi-Yau manifolds. Batyrev-Borisov [7, 9] laid the foundations for industrialising the search for mirror paired Calabi-Yau manifolds by formulating the construction of Calabi-Yau manifolds as hypersurfaces in toric varieties represented by reflexive polytopes. These reflexive polytopes are on a lattice with the dual polytope and hence corresponding mirror Calabi-Yau manifold being identified by a straightforward geometrical transformation.

Let the following summary review the notion of a reflexive polytope and the concept of its dual:

- A **reflexive polytope** is a convex polytope with points in a lattice $\mathbb{Z}^d$ and the origin $(0, \ldots, 0)$ being the unique interior point of the polytope.

- A **dual (polar) polytope** exists for every reflexive polytope. The dual of polytope Δ, Δ°, is another lattice polytope with points

$$\Delta^\circ = \{v^\circ \in \mathbb{Z}^d \mid \langle v^\circ, v\rangle \geq -1 \ \forall v \in \Delta\} \tag{2.1}$$

  The dual of every reflexive polygon is another reflexive polygon. A reflexive polygon can be self-dual, $\Delta = \Delta^\circ$.

- A **classification of reflexive polytopes** [29–31] is available for the dimensions $d \leq 4$ with the number of reflexive polytopes given in Table 1. It is unknown how many exist for higher dimensions.

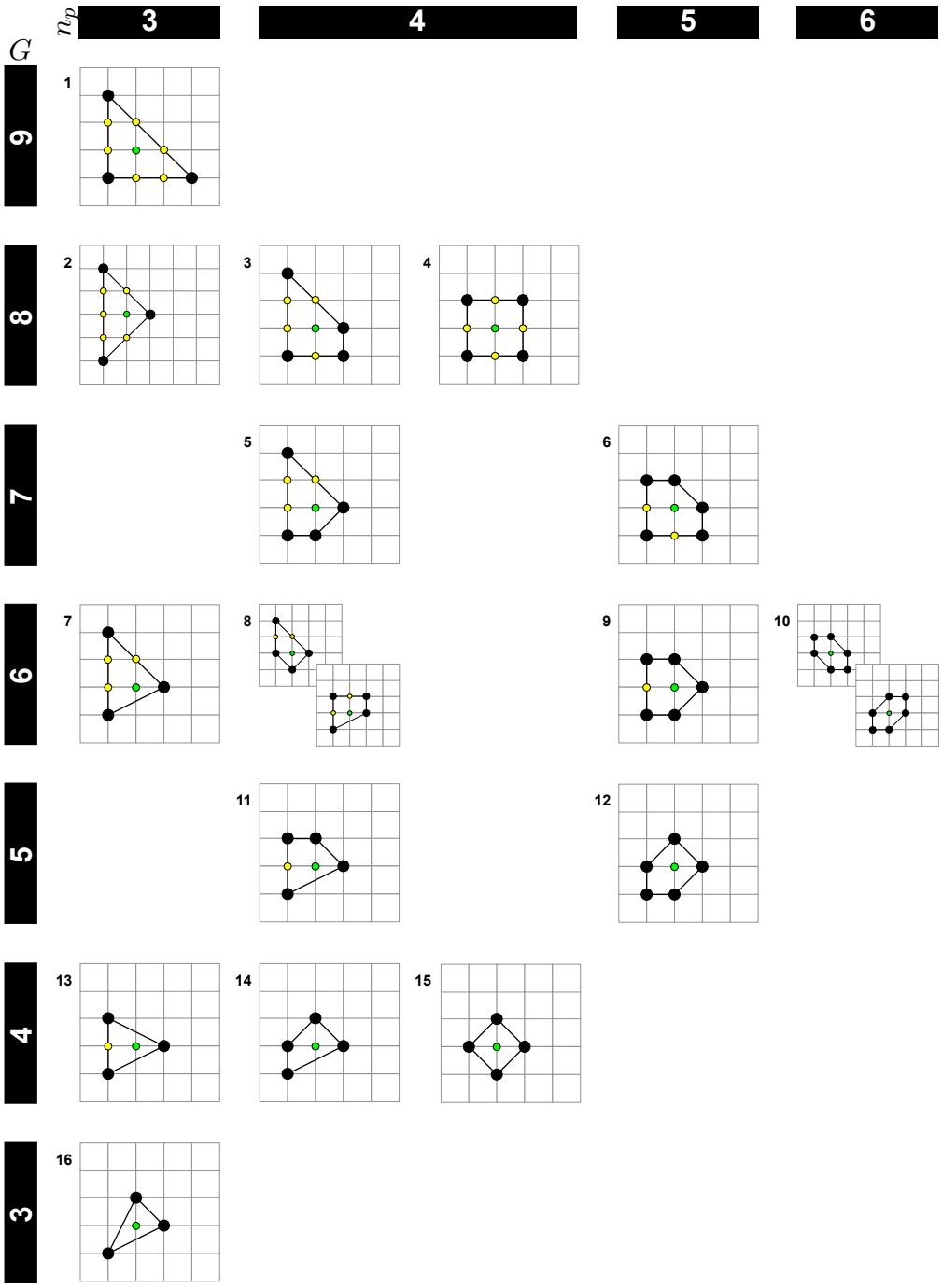


Figure 1. The 16 convex polygons which are reflexive. The polygons have been $GL(2,\mathbb{Z})$ adjusted to reflect the duality under (2.1). The green internal points are the origins. G is the area of the polygon with the smallest lattice triangle having normalized area 1, and n_G is the number of extremal points which are in black. The 4 polygons with $G = 6$ are self-dual. The paired polygons in 8 and 10 are $GL(2,\mathbb{Z})$ equivalent and are each others dual polygon.

d	Number of Polytopes
1	1
2	16
3	4319
4	473800776

Table 1. Number of reflexive lattice polytopes in dimension $d \leq 4$. The number of polytopes forms a sequence which has the identifier A090045 on OEIS.

D-branes on Calabi-Yau. Next to the study of mirror symmetry, reflexive polytopes are playing an interesting role in a different context in string theory. Witten described in 1993 an $\mathcal{N} = (2, 2)$ supersymmetric field theory with $U(1)$ gauge groups [63] in the language of what is today known as gauge linear sigma models (GLSM). He illustrated how the Fayet-Iliopoulos parameter of the $\mathcal{N} = (2, 2)$ supersymmetric field theory interpolates between the Landau-Ginzburg and Calabi-Yau phases of the theory. The large parameter limit leads to the space of classical vacua as toric Calabi-Yau spaces determined by the D- and F-terms of the supersymmetric field theory. The formulation of GLSM is going to be used in the context of D-brane gauge theories in this work even though the FI terms will not play a crucial role during the discussion.

Let the focus be on worldvolume theories living on a stack of D3-branes probing Calabi-Yau 3-fold singularities. The gravity dual of these theories is Type IIB string theory on the background $AdS_5 \times X_5$ where X_5 is a Sasaki-Einstein 5-manifold. The worldvolume theories are $4d$ $\mathcal{N} = 1$ supersymmetric quiver gauge theories whose space of vacua being toric Calabi-Yau 3-fold are described by lattice polygons on $\mathbb{Z}^2$ known as the toric diagrams.

A restriction that the toric diagrams are reflexive polygons is introduced for the purpose of the study. A motivation for introducing the restriction is the fact that there are only a finite number 16 of these reflexive polygons. The natural question to ask, and the question which is fully answered in the following discussion, is which supersymmetric quiver gauge theories exist whose space of vacua correspond to the 16 reflexive polygons.

There are useful properties of the quiver gauge theories which are considered in this work. These properties provide the essential tools for finding all quiver gauge theories corresponding to reflexive polygons:

- **Brane Tilings (Dimers)** [41–47] can be used to represent D3-brane worldvolume theories whose vacuum moduli space is toric Calabi-Yau. A brane tiling encodes the bifundamental matter content (quiver) and superpotential of the

gauge theory. Every consistent brane tiling represents a consistent combination of a quiver and superpotential, and hence a consistent quiver gauge theory.

- The **Higgs Mechanism** [14] in the context of quiver gauge theories has a natural interpretation in terms of the geometrical blow down, i.e. 'higgsing', or blow up, i.e. 'un-higgsing', of the toric variety corresponding to the gauge theory vacuum moduli space. All 16 reflexive polygons and the corresponding toric varieties can be related by the geometrical blow downs starting from the abelian orbifold of the form $\mathbb{C}^3/\mathbb{Z}_4 \times \mathbb{Z}_4$ with orbifold action $(1,0,3)(0,1,3)$ [48–52]. For the purpose of a self-contained discussion, the Higgs mechanism in the context of brane tiling theories is reviewed in Appendix §B.3.

- **Toric (Seiberg) Duality** [12, 13, 15, 53–56] in the context of quiver gauge theories relates theories with the same vacuum moduli space. In other words, two toric dual theories relate to the same reflexive polygon. Consequently, a single toric variety can be the vacuum moduli space of multiple quiver gauge theories. Such dual quiver gauge theories are known as *toric phases* of the moduli space. More generally, Seiberg duality relates an infinite number of quiver gauge theories by allowing the ranks of gauge groups in the theory to be greater than one. In the following discussion based on brane tilings, only $U(1)$ gauge groups are taken. The search for brane tilings corresponding to the 16 reflexive polygons uses toric duality in order to identify all toric phases. It turns out that there are 30 brane tiling theories corresponding to the 16 reflexive polygons. For the purpose of a self-contained discussion, toric (Seiberg) duality in the context of quiver gauge theories and their brane tilings is reviewed in Appendix §B.1.

Many of the quiver gauge theories related to reflexive polygons have been studied in the past. A selection of the available literature is given in Table 2. With the following work, a complete classification of all 30 quiver gauge theories related to reflexive polygons in Witten's language of **GLSM fields** is provided for the first time. GLSM fields relate the points of the toric diagram with the matter fields of the quiver gauge theory. The F-term and D-term constraint charges on the GLSM fields are used to obtain the **mesonic Hilbert series**. The mesonic Hilbert series encodes the moduli space **generators**.

An intriguing property of theories corresponding to reflexive polygons, which is exemplified in the work below, is as follows:

The global charges on moduli space generators form a lattice polygon on $\mathbb{Z}^2$ which is reflexive and which is precisely the dual polygon of the toric diagram.

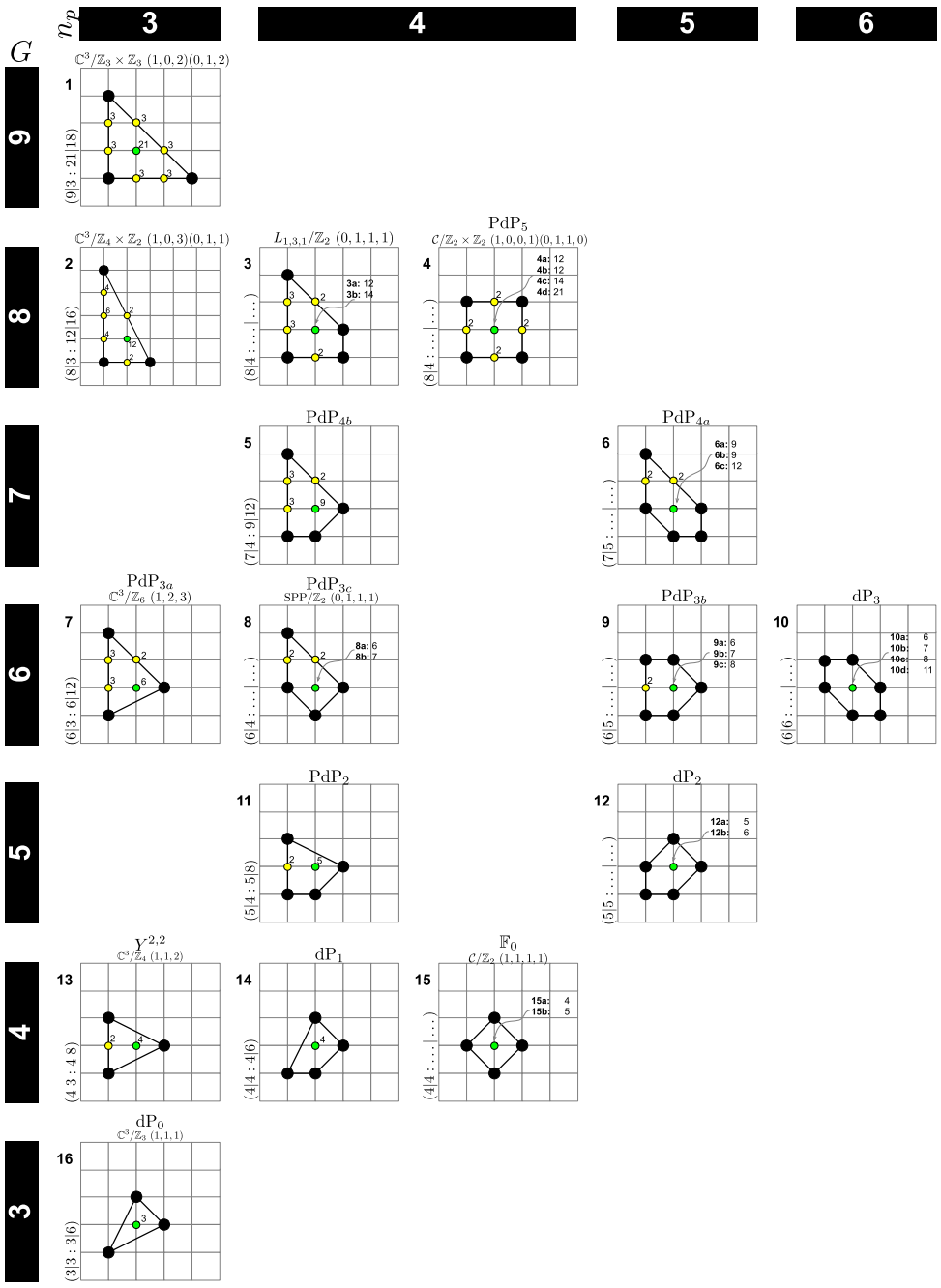


Figure 2. The 16 reflexive polygons as toric diagrams for 30 brane tilings. The 16 polygons have been $GL(2,\mathbb{Z})$ transformed to illustrate the blow down from $\mathbb{C}^3/\mathbb{Z}_4\times\mathbb{Z}_4$ $(1,0,3)(0,1,3)$ whose toric diagram contains all 16 reflexive polygons. Each polygon is labelled by $(G|n_p : n_i|n_W)$, where G corresponds to the number of $U(n)$ gauge groups, n_p to the number of GLSM fields with non-zero R-charge (number of extremal points in the toric diagram or just the order of the polygon), n_i to the multiplicity of the single interior point of the toric diagram, and n_W to the number of superpotential terms. A reflexive polygon can correspond to multiple quiver gauge theories which are related by toric (Seiberg) duality and distinguished via n_i and n_W.

Model #	Model Name	Quiver & W (Brane Tiling)	Toric Data	Mesonic HS	Generators & Generator Lattice
1	$\mathbb{C}^3/\mathbb{Z}_3 \times \mathbb{Z}_3$ $(1,0,2)(0,1,2)$	[41, 55]			
2	$\mathbb{C}^3/\mathbb{Z}_4 \times \mathbb{Z}_2$ $(1,0,3)(0,1,1)$	[41]			
3	$L_{1,3,1}/\mathbb{Z}_2$ $(0,1,1,1)$	[43, 64]	[64]		
4	PdP_5 , $\mathcal{C}/\mathbb{Z}_2 \times \mathbb{Z}_2$ $(1,0,0,1)(0,1,1,0)$	[14, 41, 42, 65]	[14, 42, 65]		
5	PdP_{4b}				
6	PdP_{4a}	[14, 65, 66]	[14, 65, 66]	[57]	
7	PdP_{3a} , $\mathbb{C}^3/\mathbb{Z}_6$ $(1,2,3)$	[41, 55]	[41]		
8	PdP_{3c} , $\mathrm{SPP}/\mathbb{Z}_2$ $(0,1,1,1)$	[14, 55, 67]	[14, 67]		
9	PdP_{3b}	[14, 55, 67]	[14, 67]		
10	dP_3	[14, 15, 42, 55, 65, 67, 68]	[13, 14, 42, 65, 67, 68]	[57]	
11	PdP_2	[14, 67]	[14, 67]		
12	dP_2	[15, 42, 65, 67–71]	[13, 42, 65, 67, 68, 70]	[57]	[70]
13	$Y^{2,2}$, $\mathbb{C}^3/\mathbb{Z}_4$ $(1,1,2)$	[41, 42]	[72]	[57]	[73, 74]
14	$Y^{2,1}$, dP_1	[15, 42, 65, 67, 69, 71]	[13, 65, 67, 72]	[57, 60]	[73, 74]
15	$\mathbb{F}_0$, $Y^{2,0}$, $\mathcal{C}/\mathbb{Z}_2$ $(1,1,1,1)$	[13, 41, 42, 65, 67, 68, 71, 75]	[13, 65, 67, 68, 72, 75]	[57]	[73, 74]
16	dP_0 , $\mathbb{C}^3/\mathbb{Z}_3$ $(1,1,1)$	[15, 41, 44, 71, 76]	[13, 14, 76]	[57, 60, 76]	

Table 2. A selection of the literature on quiver gauge theories corresponding to reflexive polygons.

The two sections below provide a review of the physical concepts involved in order to proceed with the complete classification of quiver gauge theories corresponding to reflexive polygons.

2.2 The Brane Tiling and the Forward Algorithm

The worldvolume theory of a stack of n D3-branes probing singular non-compact Calabi-Yau 3-folds is a $3+1$ dimensional $\mathcal{N}=1$ supersymmetric gauge theory. The corresponding Lagrangian is specified by the theory's gauge groups, matter content and superpotential.

The probed Calabi-Yau 3-fold is toric, and is the mesonic moduli space of the worldvolume theory. It is of great interest to associate to each worldvolume theory the corresponding mesonic moduli space. For the purpose of a self-contained discussion, a brief review on the **forward algorithm** [12, 77] which translates the gauge theory information into toric data is provided below.

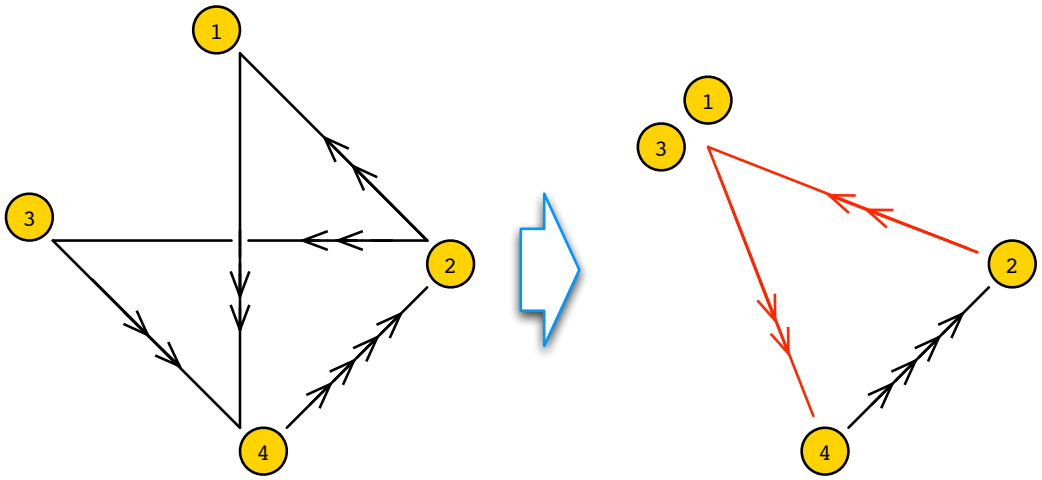


Figure 3. The quiver for phase b of the Hirzebruch $\mathbb{F}_0$ model. Vertices 1 and 3 share the same incidence information with no matter fields between them. They are combined into a block. All matter fields intersecting the block are colored red and are combined such that a red arrow represents all possible connections from and to all vertices within the block.

Quiver $\mathcal{Q}$. The matter content of the gauge theory is specified by a graph known as the **quiver** [1–3]. It consists of the following components:

- **Vertices** in $\mathcal{Q}$ correspond to $U(n_i)$ gauge groups with $i = 1, \ldots, G$.
- **Edges** in $\mathcal{Q}$ correspond to the matter fields X_{ij}. The matter fields are bifundamental and transform under the fundamental of $U(n_i)$ and antifundamental of $U(n_j)$, imposing a direction on the quiver edges, $i \to j$. The anomaly cancellation condition for the quiver gauge theory sets the number of incoming and outgoing edges on a quiver vertex to be equal. Every matter field appears precisely once in a positive and negative term in W, with the number of positive and negative terms in W being the same. This is known as the **toric condition** [15].
- The **incidence matrix** $d_{G\times E}$ for E bifundamental matter fields encodes the quiver. Its entry for a gauge group $U(n_i)$ is -1 for X_{ij}, $+1$ for X_{ji}, and 0 otherwise. The matrix $d_{G\times E}$ has $G-1$ independent rows which can be collected in a new matrix called $\Delta_{(G-1)\times e}$.

If two or more quiver vertices share the same intersection number with other quiver vertices and have no matter fields between any two of them, then the quiver vertices can be grouped into a **block** [78, 79]. This property is illustrated in the example for

phase b of the Hirzebruch $\mathbb{F}_0$ model as shown in Figure 3.

Brane Tilings/Dimers: The superpotential and the quiver can be combined into a single representation of the supersymmetric gauge theory. The representation is known as a brane tiling or dimer [2, 41–43]. It is a periodic bipartite graph on $\mathbb{T}^2$ and has the following components:

- **White (resp. black) nodes** correspond to positive (negative) terms in the superpotential. They have a clockwise (anti-clockwise) orientation.
- **Edges** connect to nodes and correspond to the bifundamental fields in the superpotential. Going along the induced orientations around nodes, one can identify the matter fields associated to a specific superpotential term in the correct cyclic order.
- **Faces** correspond to $U(n_i)$ gauge groups. Every edge X_{ij} in the tiling has two neighbouring faces corresponding to $U(n_i)$ and $U(n_j)$. The quiver orientation of the bifundamental field X_{ij} is given by the orientation around the black and white nodes at the two ends of the corresponding tiling edge.

The fundamental domain of the 2-torus on which the brane tiling is drawn is interpreted as a section of the periodic tiling which contains the quiver and superpotential information without repetition. Copying the domain along the fundamental cycles of the torus reproduces the complete brane tiling.

Perfect Matchings/GLSM fields and F-and D-term charges. A new basis of fields can be defined from the set of bifundamental matter fields. The purpose of the new basis of fields is to describe both F-term and D-term constraints of the supersymmetric gauge theory with a common setting. The new fields are known as gauge linear sigma model fields (GLSM) and are represented as perfect matchings in the brane tiling. They have the following properties:

- A **perfect matching** p_α is a set of bifundamental fields which connect all nodes in the brane tiling uniquely once. The perfect matchings corresponding to **extremal** (corner) points of the toric diagram have non-zero $U(1)_R$ R-charge. The internal as well as all **non-extremal** toric points on the perimeter of the toric diagram have zero R-charge. All points on the perimeter are called **external**, including extremal ones. They can be summarized in a matrix $P_{E\times c}$ where E is the number of matter fields and c the number of perfect matchings.

- **F-terms** are encoded in the perfect matching matrix $P_{E\times c}$. The charges under the F-term constraints are given by the kernel,

$$Q_{F\ (c-G-2)\times c} = \ker\left(P_{E\times c}\right) \quad . \tag{2.2}$$

- **D-terms** are of the form [63],

$$D_i = -e^2(\sum_a d_{ia}|X_a|^2 - \zeta_i) \quad , \tag{2.3}$$

where X_a is the matter field corresponding to the a-th column of the incidence matrix $d_{G\times E}$, i runs over the $U(n)$ gauge groups in the quiver, e is the gauge coupling, and ζ_i is the Fayet-Iliopoulos (FI) parameter. The D-terms are encoded via the reduced quiver matrix $\Delta_{(G-1)\times E}$[4] and are related to the perfect matching matrix as follows,

$$\Delta_{(G-1)\times E} = Q_{D\ (G-1)\times c}.P^t_{c\times E} \quad , \tag{2.4}$$

where the $Q_{D\ (G-1)\times c}$ matrix is the charge matrix under D-term constraints. Equivalently, in terms of an interim matrix $\tilde{Q}_{G\times c}$, which maps perfect matchings into their quiver charges, one has the relation

$$d_{G\times E} = \tilde{Q}_{G\times c}.P^t_{c\times E} \quad . \tag{2.5}$$

Overall, the charge matrices Q_F and Q_D can be concatenated to form a $(c-3)\times c$ matrix,

$$Q_t = \begin{pmatrix} Q_F \\ Q_D \end{pmatrix} \quad . \tag{2.6}$$

The kernel of the charge matrix,

$$G_t = \ker\left(Q_t\right) \quad , \tag{2.7}$$

precisely encodes the coordinates of the **toric diagram** points with columns and hence perfect matchings and GLSM fields corresponding to points of the toric diagram.

[4]Since the sum of rows in $d_{G\times E}$ vanishes, there are $G-1$ independent rows giving the reduced matrix $\Delta_{(G-1)\times E}$.

2.3 Hilbert Series and Lattice of Generators

The generating function of mesonic gauge invariant operators (GIOs) is known as the **mesonic Hilbert series** [57–61]. The Hilbert series encodes the generators of the associated moduli space. These are essential for a complete classification of the mesonic moduli spaces of brane tilings corresponding to reflexive polygons. The moduli space generators can be extracted from the Hilbert series using a method known as **plethystics**. These carry charges under the **mesonic symmetry**. The charges on a $\mathbb{Z}_2$ lattice form a convex polygon which is the dual polygon of the toric diagram.

Let the section below provide a review of the concepts involved.

Mesonic Symmetry. The mesonic moduli space of a given brane tiling is a non-compact toric Calabi-Yau 3-fold. The mesonic symmetry of the associated quiver gauge theory takes one of the following forms,

- $U(1)_{f_1} \times U(1)_{f_2} \times U(1)_R$
- $SU(2)_x \times U(1)_f \times U(1)_R$
- $SU(2)_{x_1} \times SU(2)_{x_2} \times U(1)_R$
- $SU(3)_{x_1,x_2} \times U(1)_R$,

where the lower case indices denote fugacities of the gauge group with the exemption of the R-symmetry group $U(1)_R$. The fugacity associated to the $U(1)_R$ charge is t.

The above global symmetries derive from the isometry group of the Calabi-Yau 3-fold. The enhancement of a $U(1)$ flavour to $SU(2)$ or $SU(3)$ is indicated by repeated columns in the total charge matrix Q_t.

Mesonic Hilbert Series. The mesonic moduli space is the space of invariants under F-term charges Q_F and D-term charges Q_D. The c GLSM fields corresponding to perfect matchings of the brane tiling form the space $\mathbb{C}^c$ known as the space of perfect matchings.

- The **Symplectic Quotient**

$$\mathcal{M}^{mes} = (\mathbb{C}^c//Q_F)//Q_D \quad . \tag{2.8}$$

  is the *mesonic moduli space* of the quiver gauge theory.[5] The invariants under the symplectic quotient are mesonic GIOs.

[5]The symplectic quotient $\mathcal{F}^\flat = \mathbb{C}^c//Q_F$ is known as the *Master space* [65, 68, 75, 76, 80, 81] and is the space of invariants including both mesonic and baryonic degrees of freedom.

- The **mesonic Hilbert series** is a generating function which counts mesonic GIOs on the moduli space. The mesonic Hilbert series is obtained via the Molien integral formula,

$$g_1(y_\alpha;\mathcal{M}^{mes}) = \prod_{i=1}^{c-3}\oint_{|z_i|=1}\frac{\mathrm{d}z_i}{2\pi i z_i}\prod_{\alpha=1}^{c}\frac{1}{(1-y_\alpha\prod_{j=1}^{c-3}z_j^{(Q_t)_{j\alpha}})} \quad , \tag{2.9}$$

where c is the number of perfect matchings labelled by $\alpha = 1,\ldots,c$ and Q_t is the total charge matrix in (2.6). GLSM fields corresponding to extremal perfect matchings p_α carry non-zero R-charges and have fugacities denoted by $y_\alpha = t_\alpha$. For all other GLSM fields s_m with zero R-charges one assigns the fugacity $y_\alpha = y_{s_m}$. The perfect matchings associated to these fields are non-extremal. Certain products of non-extremal perfect matchings such as $s = \prod_m s_m$ are assigned a single fugacity denoted by y_s.

- The **plethystic logarithm** of the Hilbert series encodes information about the generators of the moduli space and the relations formed by them. It is defined as

$$PL[g_1(y_\alpha;\mathcal{M})] = \sum_{k=1}^{\infty}\frac{\mu(k)}{k}\log\left[g_1(y_\alpha^k;\mathcal{M})\right] \quad , \tag{2.10}$$

where $\mu(k)$ is the Möbius function. If the expansion of the plethystic logarithm is finite, the moduli space is a *complete intersection* generated by a finite number of generators subject to a finite number of relations. If the expansion is infinite, the moduli space is a non-complete intersection. The first positive terms of the expansion refer to generators of the moduli space.[6] All higher order terms refer to relations among generators and relations among relations called *syzygies*.

R-charges.[7] The mesonic moduli space is a toric Calabi-Yau cone over a Sasaki-Einstein 5-manifold whose volume is related under minimization to the $U(1)$ R-charges of the *divisors* of the toric geometry [84–86]. The toric divisors relate to the extremal points of the toric diagram and the corresponding GLSM fields.

The volume of the Sasaki Einstein 5-manifold X_5 is

$$\mathrm{Vol}(r_\alpha;X_5) = \frac{8\pi^3}{27}\lim_{\mu\to 0}\mu^3 g_1(t_\alpha = e^{-\mu r_\alpha};\mathcal{M}=\mathcal{C}(X_5)) \quad . \tag{2.11}$$

[6] The Groebner basis of the set of gauge invariant operators forms the generators of the moduli space.

[7] We review here volume minimisation as a means to calculate R-charges. For alternative methods see for example [64, 82, 83].

where $g_1(t_\alpha;\mathcal{M})$ is the mesonic Hilbert series in (2.9), t_α is the fugacity for GLSM field p_α, and r_α is the corresponding minimization parameter. The Hilbert series related to the divisor D_α and the corresponding GLSM field p_α is obtained through the following modified Molien integral,

$$\begin{aligned} g^{D_\alpha}(t_\alpha;\mathcal{M}^{mes}) &= \prod_{i=1}^{c-3}\oint_{|z_i|=1}\frac{\mathrm{d}z_i}{2\pi i z_i}\ \left(t_\alpha\ \prod_{k=1}^{c-3} z_k^{(Q_t)_{k\alpha}}\right)^{-1}\ g_1(t_\alpha,z_i;\mathbb{C}^c) \\ &= \prod_{i=1}^{c-3}\oint_{|z_i|=1}\frac{\mathrm{d}z_i}{2\pi i z_i}\ \prod_{\beta=1}^{c}\frac{\left(t_\alpha\ \prod_{k=1}^{c-3} z_k^{(Q_t)_{k\alpha}}\right)^{-1}}{1-t_\beta\ \prod_{j=1}^{c-3} z_j^{(Q_t)_{j\beta}}}\quad . \end{aligned} \tag{2.12}$$

The associated R-charge is then

$$R_\alpha = \lim_{\mu\to 0}\frac{1}{\mu}\left[\frac{g^{D_\alpha}(e^{-\mu r_\alpha};\mathcal{M}^{mes})}{g^{mes}(e^{-\mu r_\alpha};\mathcal{M}^{mes})}-1\right]\quad . \tag{2.13}$$

For superconformality, the superpotential has R-charge 2 which sets the following restriction on the R-charges

$$\sum_\alpha R_\alpha = 2. \tag{2.14}$$

Lattice of Generators. The lattice of generators is determined by the mesonic charges carried by the generators of the mesonic moduli space. Ignoring the $U(1)_R$ factor, the remaining flavour symmetries have ranks which sum up to 2. Hence, there are always 2 fugacities which count flavour charges. The pair of flavour charges carried by each generator is taken as coordinates of a point on the plane. The convex hull of the collection of points corresponding to the collection of moduli space generators forms a convex polygon. This is known as the lattice of generators.

For a non-vanishing convex polygon on $\mathbb{Z}^2$, the flavour charges are subject to the following constraints:

- The pairs of flavour charges carried by all n_p extremal perfect matchings form a pair of n_p-dimensional charge vectors. For a non-trivial choice of flavour charges, the charge vectors are linearly independent.
- The elements of the n_p-dimensional charge vectors sum up to zero.
- The charges on GLSM fields are scaled such that the charges on mesonic moduli space generators take integer values and the lattice of generators is on $\mathbb{Z}^2$.

The lattice of generators subject to the constraints above still exhibits a remaining $GL(2,\mathbb{Z})$ degree of freedom. Moreover, each generator also carries a R-charge which plays the role of a third coordinate for each point in the lattice of generators. In order to remove these remaining degrees of freedom, one makes use of a particular property of generator lattices introduced below.

Duality between Generator Lattices and Toric Diagrams.

The lattice of generators of a brane tiling is the dual of the toric diagram.

The duality between *reflexive* polygons follows (2.1). Hence, for reflexive polygons as toric diagrams, the lattice of generators is another reflexive polygon in $\mathbb{Z}^2$. Accordingly, the remaining $GL(2,\mathbb{Z})$ degree of freedom on the lattice of generators can be removed by making the duality for reflexive polygons exact as defined in (2.1). In addition, for reflexive polygons the lattice of generators always lies on $\mathbb{Z}^2$.

When the lattice of generators is considered as a toric diagram of a new brane tiling, the duality between reflexive polygons manifestly relates between two quiver gauge theories with toric moduli spaces. In terms of the number of $U(n)$ gauge groups G and the number of GLSM fields with non-zero R-charge n_p, the duality map takes the form

$$\begin{array}{rcl} \text{Model A} & \leftrightarrow & \text{Model B} \\ G & \leftrightarrow & 12-G \\ n_p & \leftrightarrow & n_p \end{array} \tag{2.15}$$

as illustrated in Figure 2.

In the following sections, all 30 quiver gauge theories with their brane tilings corresponding to the 16 reflexive polygons are classified. All 30 quiver gauge theories are obtained by higgsing and toric (Seiberg) dualizing the theory related to the abelian orbifold of the form $\mathbb{C}^3/\mathbb{Z}_4\times\mathbb{Z}_4$ with orbifold action $(1,0,3)(0,1,3)$. The details for the *parent* theory for all reflexive polygon theories are given in appendix §A.

3 Model 1: $\mathbb{C}^3/\mathbb{Z}_3 \times \mathbb{Z}_3\ (1,0,2)(0,1,2)$

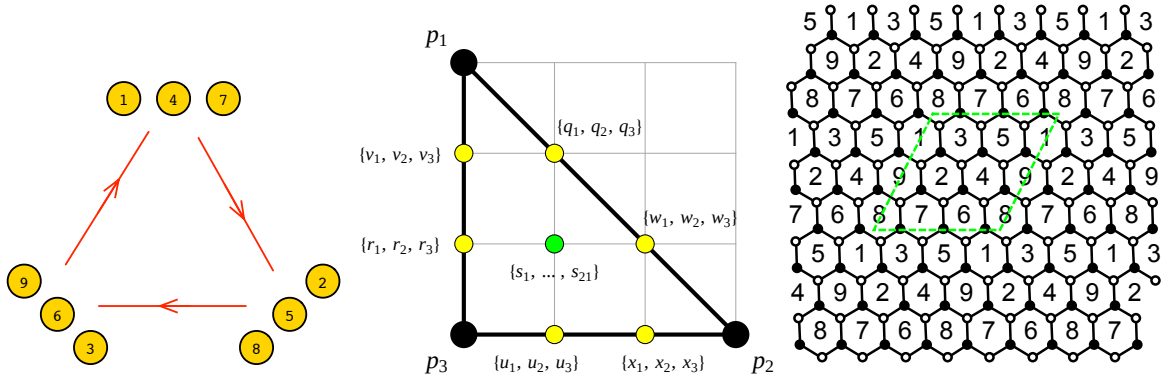


Figure 4. The quiver, toric diagram, and brane tiling of Model 1. The red arrows in the quiver indicate all possible connections between blocks of nodes.

The superpotential is

$$\begin{aligned} W = &+X_{15}X_{56}X_{61} + X_{29}X_{91}X_{12} + X_{31}X_{18}X_{83} + X_{42}X_{23}X_{34} + X_{53}X_{37}X_{75} + X_{67}X_{72}X_{26} \\ &+X_{78}X_{89}X_{97} + X_{86}X_{64}X_{48} + X_{94}X_{45}X_{59} - X_{15}X_{59}X_{91} - X_{29}X_{97}X_{72} - X_{31}X_{12}X_{23} \\ &-X_{42}X_{26}X_{64} - X_{53}X_{34}X_{45} - X_{67}X_{75}X_{56} - X_{78}X_{83}X_{37} - X_{86}X_{61}X_{18} - X_{94}X_{48}X_{89}\ . \end{aligned} \tag{3.1}$$

The perfect matching matrix is

$P =$

	p_1	p_2	p_3	q_1	q_2	q_3	r_1	r_2	r_3	u_1	u_2	u_3	v_1	v_2	v_3	w_1	w_2	w_3	x_1	x_2	x_3	s_1	s_2	s_3	s_4	s_5	s_6	s_7	s_8	s_9	s_{10}	s_{11}	s_{12}	s_{13}	s_{14}	s_{15}	s_{16}	s_{17}	s_{18}	s_{19}	s_{20}	s_{21}
X_{89}	1	0	0	1	1	0	1	0	0	0	0	0	1	0	1	1	0	0	0	0	0	0	0	1	1	0	0	0	0	0	0	1	0	0	0	0	0	0	1	1	1	1
X_{37}	1	0	0	1	1	0	0	1	0	0	0	0	0	1	1	1	0	0	0	0	0	0	0	0	0	0	0	0	0	1	1	1	1	1	1	1	0	0	1	0	0	0
X_{45}	1	0	0	1	1	0	0	0	1	0	0	0	1	1	0	1	0	0	0	0	0	0	0	1	1	1	1	1	0	0	1	0	1	0	0	0	0	0	0	0	0	0
X_{64}	1	0	0	1	0	1	1	0	0	0	0	0	1	0	1	0	1	0	0	0	0	0	0	0	0	0	1	1	0	1	0	1	1	0	1	0	0	1	0	0	0	0
X_{18}	1	0	0	1	0	1	0	1	0	0	0	0	0	1	1	0	1	0	0	0	0	1	1	0	0	1	1	0	1	0	0	1	0	0	1	0	0	0	0	0	0	0
X_{23}	1	0	0	1	0	1	0	0	1	0	0	0	1	1	0	0	1	0	0	0	0	1	0	1	0	1	0	0	0	0	0	0	0	0	0	0	1	1	0	1	1	0
X_{72}	1	0	0	0	1	1	1	0	0	0	0	0	1	0	1	0	0	1	0	0	0	0	1	0	1	0	1	1	1	1	0	0	0	0	0	0	0	0	0	0	0	1
X_{56}	1	0	0	0	1	1	0	1	0	0	0	0	0	1	1	0	0	1	0	0	0	1	1	0	0	0	0	0	0	0	0	0	0	1	0	1	1	0	1	1	0	1
X_{91}	1	0	0	0	1	1	0	0	1	0	0	0	1	1	0	0	0	1	0	0	0	0	0	0	0	1	0	1	0	0	1	0	1	1	1	1	0	0	0	0	0	0
X_{29}	0	1	0	1	0	0	0	0	0	1	0	0	0	0	0	1	1	0	1	0	1	1	0	1	0	1	0	0	0	0	0	1	0	0	0	0	0	0	1	1	1	0
X_{67}	0	1	0	1	0	0	0	0	0	0	1	0	0	0	0	1	1	0	0	1	1	0	0	0	0	0	0	0	0	0	1	1	1	1	1	0	1	0	0	1	0	0
X_{15}	0	1	0	1	0	0	0	0	0	0	0	1	0	0	0	1	1	0	1	1	0	0	0	1	1	1	1	0	1	0	1	0	0	1	0	0	0	0	0	0	0	0
X_{31}	0	1	0	0	1	0	0	0	0	1	0	0	0	0	0	1	0	1	1	0	1	0	0	0	0	0	1	0	1	0	1	1	0	1	1	0	0	1	0	0	0	0
X_{42}	0	1	0	0	1	0	0	0	0	0	1	0	0	0	0	1	0	1	0	1	1	0	1	0	1	0	1	1	0	0	1	0	1	0	0	0	0	0	0	0	0	1
X_{86}	0	1	0	0	1	0	0	0	0	0	0	1	0	0	0	1	0	1	1	1	0	0	0	1	1	0	0	0	0	0	0	0	0	0	1	0	1	1	0	1	1	
X_{78}	0	1	0	0	0	1	0	0	0	1	0	0	0	0	0	0	1	1	1	0	1	1	1	0	0	1	1	1	1	1	0	0	0	0	0	0	0	0	0	0	0	0
X_{53}	0	1	0	0	0	1	0	0	0	0	1	0	0	0	0	0	1	1	0	1	1	1	1	0	0	0	0	0	0	0	0	0	0	0	1	1	0	1	1	1		
X_{94}	0	1	0	0	0	1	0	0	0	0	0	1	0	0	0	0	1	1	1	1	0	0	0	0	0	0	0	0	1	1	0	0	0	1	1	1	1	1	0	0	0	0
X_{59}	0	0	1	0	0	0	1	1	0	1	1	0	0	0	1	0	0	0	0	0	1	1	1	0	0	0	0	0	0	0	0	1	0	0	0	0	0	0	1	1	1	1
X_{34}	0	0	1	0	0	0	1	1	0	1	0	1	0	0	1	0	0	0	1	0	0	0	0	0	0	0	0	1	1	0	1	0	1	1	1	0	0	1	0	0	0	0
X_{12}	0	0	1	0	0	0	1	1	0	0	1	1	0	0	1	0	0	0	0	1	0	0	1	0	1	0	1	0	1	0	1	0	0	1	0	0	0	0	0	0	0	1
X_{61}	0	0	1	0	0	0	1	0	1	1	1	0	1	0	0	0	0	0	0	0	1	0	0	0	0	0	0	1	0	1	0	1	1	0	1	0	1	0	0	1	0	0
X_{75}	0	0	1	0	0	0	1	0	1	1	0	1	1	0	0	0	0	0	1	0	0	0	0	1	1	1	1	1	1	0	0	0	0	0	0	0	0	0	0	0	0	0
X_{83}	0	0	1	0	0	0	1	0	1	0	1	1	1	0	0	0	0	0	0	1	0	0	0	1	1	0	0	0	0	0	0	0	0	1	1	0	1	1	1			
X_{48}	0	0	1	0	0	0	0	1	1	1	1	0	0	1	0	0	0	0	0	0	1	1	1	0	0	1	1	1	0	0	1	0	1	0	0	0	0	0	0	0	0	0
X_{26}	0	0	1	0	0	0	0	1	1	1	0	1	0	1	0	0	0	0	1	0	0	1	0	1	0	0	0	0	0	0	0	0	0	1	0	1	1	0	1	0		
X_{97}	0	0	1	0	0	0	0	1	1	0	1	1	0	1	0	0	0	0	0	1	0	0	0	0	0	0	0	0	0	1	0	1	1	1	1	1	1	0	0	0	0	0

The F-term charge matrix $Q_F = \ker(P)$ is

$Q_F =$

p_1	p_2	p_3	q_1	q_2	q_3	r_1	r_2	r_3	u_1	u_2	u_3	v_1	v_2	v_3	w_1	w_2	w_3	x_1	x_2	x_3	s_1	s_2	s_3	s_4	s_5	s_6	s_7	s_8	s_9	s_{10}	s_{11}	s_{12}	s_{13}	s_{14}	s_{15}	s_{16}	s_{17}	s_{18}	s_{19}	s_{20}	s_{21}
1	1	0	0	−1	0	0	0	0	0	0	0	0	0	0	0	−1	0	0	0	0	0	0	0	0	0	0	0	0	0	0	0	0	0	0	0	0	0	0	0	0	0
1	1	0	−1	0	0	0	0	0	0	0	0	0	0	0	0	0	−1	0	0	0	0	0	0	0	0	0	0	0	0	0	0	0	0	0	0	0	0	0	0	0	0
1	0	1	0	0	0	0	−1	0	0	0	0	−1	0	0	0	0	0	0	0	0	0	0	0	0	0	0	0	0	0	0	0	0	0	0	0	0	0	0	0	0	0
1	0	1	0	0	0	−1	0	0	0	0	0	0	−1	0	0	0	0	0	0	0	0	0	0	0	0	0	0	0	0	0	0	0	0	0	0	0	0	0	0	0	0
1	0	0	−1	−1	0	0	0	0	0	0	0	0	0	0	1	0	0	0	0	0	0	0	0	0	0	0	0	0	0	0	0	0	0	0	0	0	0	0	0	0	0
1	0	0	−1	0	−1	0	0	0	0	0	0	0	0	0	0	1	0	0	0	0	0	0	0	0	0	0	0	0	0	0	0	0	0	0	0	0	0	0	0	0	0
1	0	0	−1	0	0	0	−1	0	1	0	0	0	0	0	0	0	0	0	0	0	0	0	0	0	0	0	0	0	0	0	0	1	0	0	0	0	0	0	−1	0	0
1	0	0	0	−1	0	−1	0	0	1	0	0	0	0	0	0	0	0	0	0	0	0	0	0	1	0	0	0	0	0	0	0	0	0	0	0	0	0	−1	0	0	0
1	0	0	0	0	0	−1	0	0	1	1	0	0	0	0	0	0	0	0	0	0	−1	0	0	0	0	0	0	0	0	0	0	0	−1	0	0	0	0	0	0	0	0
0	1	1	0	0	0	0	0	0	0	−1	0	0	0	0	0	0	0	−1	0	0	0	0	0	0	0	0	0	0	0	0	0	0	0	0	0	0	0	0	0	0	0
0	1	1	0	0	0	0	0	0	−1	0	0	0	0	0	0	0	0	0	−1	0	0	0	0	0	0	0	0	0	0	0	0	0	0	0	0	0	0	0	0	0	0
0	0	1	1	0	0	−1	0	0	0	0	0	0	0	0	0	0	0	0	0	0	−1	1	0	0	0	0	0	0	0	0	0	−1	0	0	0	0	0	0	0	0	0
0	0	1	0	0	0	−1	−1	0	0	0	0	0	0	1	0	0	0	0	0	0	0	0	0	0	0	0	0	0	0	0	0	0	0	0	0	0	0	0	0	0	0
0	0	1	0	0	0	−1	0	−1	0	0	0	1	0	0	0	0	0	0	0	0	0	0	0	0	0	0	0	0	0	0	0	0	0	0	0	0	0	0	0	0	0
0	0	1	0	0	0	−1	0	0	0	−1	−1	0	0	0	0	0	0	0	0	1	0	0	0	0	0	0	0	0	0	0	0	0	0	0	0	0	0	0	0	0	0
0	0	1	0	0	0	0	0	0	−1	0	−1	0	0	0	0	0	0	1	0	0	0	0	0	0	0	0	0	0	0	0	0	0	0	0	0	0	0	0	0	0	0
0	0	1	0	0	0	−1	0	0	0	−1	0	0	0	0	0	0	0	−1	0	0	1	0	0	1	0	0	0	0	0	0	0	0	0	0	0	0	0	0	0	0	0
0	0	1	0	0	0	0	−1	0	0	0	0	0	0	0	1	0	0	0	0	−1	1	0	−1	0	0	0	0	0	0	0	0	0	0	0	0	0	0	0	0	0	0
0	0	1	0	0	0	0	−1	0	−1	0	0	0	0	0	0	0	0	0	0	0	1	0	0	0	0	0	0	1	0	0	0	0	0	0	0	0	0	0	0	0	−1
0	0	1	0	0	0	0	−1	0	0	−1	0	0	0	0	0	0	0	0	0	0	0	1	0	0	0	0	0	0	1	0	0	0	0	−1	0	0	0	0	0	0	0
0	0	0	0	0	1	0	0	0	0	1	0	0	0	0	0	0	0	0	0	0	0	−1	0	0	0	0	0	0	0	0	0	0	0	0	−1	0	0	0	0	0	0
0	0	0	0	0	1	0	0	0	1	0	0	0	0	0	0	0	0	0	0	0	−1	0	0	0	0	0	0	0	0	0	0	0	0	0	0	−1	0	0	0	0	0
0	0	0	0	0	1	0	0	0	0	0	0	0	0	0	0	0	0	0	0	0	1	0	0	0	0	0	0	0	0	0	0	0	0	0	0	0	−1	0	0	0	0
0	0	0	0	0	1	0	0	0	0	0	0	0	0	0	0	0	0	0	0	0	−1	0	0	0	0	0	0	0	0	0	0	0	0	0	0	0	0	−1	0	0	0
0	0	0	0	0	1	0	0	0	0	0	0	0	0	0	0	0	0	0	0	0	1	0	0	0	0	0	0	0	0	0	0	0	0	0	0	0	0	0	−1	1	0
0	0	0	0	0	1	0	0	0	0	0	0	0	0	0	0	0	0	0	0	0	1	−1	0	0	0	0	0	0	0	0	0	0	0	0	0	0	0	0	0	−1	0
0	0	0	0	0	1	0	0	0	0	0	0	0	0	0	0	0	0	0	0	0	1	−1	0	0	0	0	0	0	0	0	0	0	0	0	0	0	0	0	0	0	0

The D-term charge matrix is

$Q_D =$

p_1	p_2	p_3	q_1	q_2	q_3	r_1	r_2	r_3	u_1	u_2	u_3	v_1	v_2	v_3	w_1	w_2	w_3	x_1	x_2	x_3	s_1	s_2	s_3	s_4	s_5	s_6	s_7	s_8	s_9	s_{10}	s_{11}	s_{12}	s_{13}	s_{14}	s_{15}	s_{16}	s_{17}	s_{18}	s_{19}	s_{20}	s_{21}
0	0	0	0	0	0	0	0	0	0	0	0	0	0	0	0	0	0	0	0	0	1	−1	0	0	0	0	0	0	0	0	0	0	0	0	0	0	0	0	0	0	0
0	0	0	0	0	0	0	0	0	0	0	0	0	0	0	0	0	0	0	0	0	0	1	−1	0	0	0	0	0	0	0	0	0	0	0	0	0	0	0	0	0	0
0	0	0	0	0	0	0	0	0	0	0	0	0	0	0	0	0	0	0	0	0	0	0	0	1	−1	0	0	0	0	0	0	0	0	0	0	0	0	0	0	0	0
0	0	0	0	0	0	0	0	0	0	0	0	0	0	0	0	0	0	0	0	0	0	0	0	0	1	−1	0	0	0	0	0	0	0	0	0	0	0	0	0	0	0
0	0	0	0	0	0	0	0	0	0	0	0	0	0	0	0	0	0	0	0	0	0	0	0	0	0	0	1	−1	0	0	0	0	0	0	0	0	0	0	0	0	0
0	0	0	0	0	0	0	0	0	0	0	0	0	0	0	0	0	0	0	0	0	0	0	0	0	0	0	0	1	−1	0	0	0	0	0	0	0	0	0	0	0	0
0	0	0	0	0	0	0	0	0	0	0	0	0	0	0	0	0	0	0	0	0	0	0	0	0	0	0	0	0	1	−1	0	0	0	0	0	0	0	0	0	0	0
0	0	0	0	0	0	0	0	0	0	0	0	0	0	0	0	0	0	0	0	0	0	0	0	0	0	0	0	0	0	1	−1	0	0	0	0	0	0	0	0	0	0
0	0	0	0	0	0	0	0	0	0	0	0	0	0	0	0	0	0	0	0	0	0	0	0	0	0	0	0	0	0	0	1	−1	0	0	0	0	0	0	0	0	0
0	0	0	0	0	0	0	0	0	0	0	0	0	0	0	0	0	0	0	0	0	0	0	0	0	0	0	0	0	0	0	0	1	−1	0	0	0	0	0	0	0	0
0	0	0	0	0	0	0	0	0	0	0	0	0	0	0	0	0	0	0	0	0	0	0	0	0	0	0	0	0	0	0	0	0	1	−1	0	0	0	0	0	0	0
0	0	0	0	0	0	0	0	0	0	0	0	0	0	0	0	0	0	0	0	0	0	0	0	0	0	0	0	0	0	0	0	0	0	1	−1	0	0	0	0	0	0
0	0	0	0	0	0	0	0	0	0	0	0	0	0	0	0	0	0	0	0	0	0	0	0	0	0	0	0	0	0	0	0	0	0	0	1	−1	0	0	0	0	0

The total charge matrix Q_t exhibits no repeated columns. Accordingly, the global symmetry group is $U(1)_{f_1} \times U(1)_{f_2} \times U(1)_R$. Following the discussion on flavour symmetry and R-charges in section §2.3, the charges on GLSM fields with non-zero R-charges are chosen as shown in Table 3.

	$U(1)_{f_1}$	$U(1)_{f_2}$	$U(1)_R$	fugacity
p_1	1/3	0	2/3	t_1
p_2	-1/3	-1/3	2/3	t_2
p_3	0	1/3	2/3	t_3

Table 3. The GLSM fields corresponding to extremal points of the toric diagram with their mesonic charges (Model 1).

Products of non-extremal perfect matchings are labelled by a single variable as

follows,

$$q = q_1q_2q_3 \ , \ r = r_1r_2r_3 \ , \ u = u_1u_2u_3 \ , \ v = v_1v_2v_3 \ ,$$
$$w = w_1w_2w_3 \ , \ x = x_1x_2x_3 \ , \ s = \prod_{m=1}^{21} s_m \ . \tag{3.2}$$

The fugacities t_α count extremal perfect matchings corresponding to GLSM fields with non-zero R-charge. The fugacity of the form y_q counts the product of non-extremal perfect matchings q above.

The mesonic Hilbert series of Model 1 is calculated using the Molien integral formula in (2.9). It is

$$g_1(t_\alpha, y_q, y_r, y_u, y_v, y_w, y_x, y_s; \mathcal{M}_1^{mes}) = \frac{1 - y_q^3y_r^3y_u^3y_v^3y_w^3y_x^3y_s^3 \ t_1^3t_2^3t_3^3}{(1 - y_q^2y_r^2y_v^2y_wy_s \ t_1^3)(1 - y_qy_uy_w^2y_x^2y_s \ t_2^3)(1 - y_r^2y_u^2y_vy_xy_s \ t_3^3)(1 - y_qy_ry_uy_vy_wy_xy_s \ t_1t_2t_3)} \ . \tag{3.3}$$

The plethystic logarithm of the mesonic Hilbert series is

$$PL[g_1(t_\alpha, y_q, y_r, y_u, y_v, y_w, y_x, y_s; \mathcal{M}_1^{mes})] = y_qy_ry_uy_vy_wy_xy_s \ t_1t_2t_3 + y_q^2y_ry_v^2y_wy_s \ t_1^3$$
$$+y_r^2y_u^2y_vy_xy_s \ t_3^3 + y_qy_uy_w^2y_x^2y_s \ t_2^3 - y_q^3y_r^3y_u^3y_v^3y_w^3y_x^3y_s^3 \ t_1^3t_2^3t_3^3 \ . \tag{3.4}$$

The finite plethystic logarithm indicates that the mesonic moduli space is a complete intersection.

In terms of the fugacity map

$$f_1 = \frac{y_qy_v \ t_1^2}{y_uy_x \ t_2t_3} \ , \ f_2 = \frac{y_ry_u \ t_3^2}{y_qy_w \ t_1t_2} \ , \ t = y_q^{1/3}y_r^{1/3}y_u^{1/3}y_v^{1/3}y_w^{1/3}y_x^{1/3}y_s^{1/3} \ t_1^{1/3}t_2^{1/3}t_3^{1/3} \ , \tag{3.5}$$

where f_1, f_2 and t are the fugacities counting the mesonic charges, the above plethystic logarithm becomes

$$PL[g_1(t, f_1, f_2; \mathcal{M}_1^{mes})] = \left(1 + f_1 + f_2 + \frac{1}{f_1f_2}\right) t^3 - t^9 \tag{3.6}$$

The above plethystics logarithm identifies both the moduli space generators and the mesonic charges carried by them. The generators and the corresponding mesonic charges are summarized in Table 4. The generators can be presented on a charge lattice. It is a convex polygon as shown in Table 4 and is the dual reflexive polygon of the toric diagram of Model 16.

The relation formed among the generators is as follows,

$$A_1 A_2 A_3 = B^3 \quad . \tag{3.7}$$

Generator	$U(1)_{f_1}$	$U(1)_{f_2}$
$A_1 = p_1^3\ q^2\ r\ v^2\ w\ s$	1	0
$A_2 = p_2^3\ q\ u\ w^2\ x^2\ s$	-1	-1
$A_3 = p_3^3\ r^2\ u^2\ v\ x\ s$	0	1
$B = p_1 p_2 p_3\ q\ r\ u\ v\ w\ x\ s$	0	0

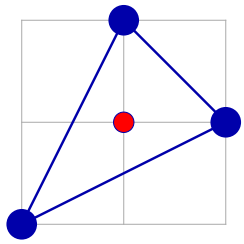


Table 4. The generators and lattice of generators of the mesonic moduli space of Model 1 in terms of GLSM fields with the corresponding flavor charges.

Generator	$U(1)_{f_1}$	$U(1)_{f_2}$
$X_{18}X_{89}X_{91} = X_{23}X_{37}X_{72} = X_{45}X_{56}X_{64}$	1	0
$X_{15}X_{53}X_{31} = X_{29}X_{94}X_{42} = X_{67}X_{78}X_{86}$	-1	-1
$X_{12}X_{26}X_{61} = X_{34}X_{48}X_{83} = X_{59}X_{97}X_{75}$	0	1
$X_{12}X_{23}X_{31} = X_{12}X_{29}X_{91} = X_{15}X_{56}X_{61} = X_{15}X_{59}X_{91} = X_{18}X_{83}X_{31} = X_{18}X_{86}X_{61} = X_{23}X_{34}X_{42} = X_{26}X_{64}X_{42} = X_{26}X_{67}X_{72}$ $= X_{29}X_{97}X_{72} = X_{34}X_{45}X_{53} = X_{37}X_{75}X_{53} = X_{37}X_{78}X_{83} = X_{45}X_{59}X_{94} = X_{48}X_{86}X_{64} = X_{48}X_{89}X_{94} = X_{56}X_{67}X_{75} = X_{78}X_{89}X_{97}$	0	0

Table 5. The generators in terms of bifundamental fields (Model 1).

With the following fugacity map

$$\begin{aligned} T_1 &= f_1^{1/3}\ t = y_q^{2/3} y_r^{1/3} y_v^{2/3} y_w^{1/3} y_s^{1/3} t_1 \ , \\ T_2 &= f_1^{-1/3} f_2^{-1/3}\ t = y_q^{1/3} y_u^{1/3} y_w^{2/3} y_x^{2/3} y_s^{1/3} t_2 \ , \\ T_3 &= f_2^{1/3}\ t = y_r^{2/3} y_u^{2/3} y_v^{1/3} y_x^{1/3} y_s^{1/3} t_3 \ , \end{aligned} \tag{3.8}$$

the mesonic Hilbert series becomes

$$g_1(T_1, T_2, T_3; \mathcal{M}_1^{mes}) = \frac{1 - T_1^3 T_2^3 T_3^3}{(1 - T_1^3)(1 - T_2^3)(1 - T_3^3)(1 - T_1 T_2 T_3)} \tag{3.9}$$

with the plethystic logarithm being

$$PL[g_1(T_1, T_2, T_3; \mathcal{M}_1^{mes})] = T_1 T_2 T_3 + T_1^3 + T_3^3 + T_2^3 - T_1^3 T_2^3 T_3^3 \quad . \tag{3.10}$$

The above refinement of the Hilbert series exemplifies the conical structure of the toric Calabi-Yau space.

4 Model 2: $\mathbb{C}^3/\mathbb{Z}_4 \times \mathbb{Z}_2\ (1,0,3)(0,1,1)$

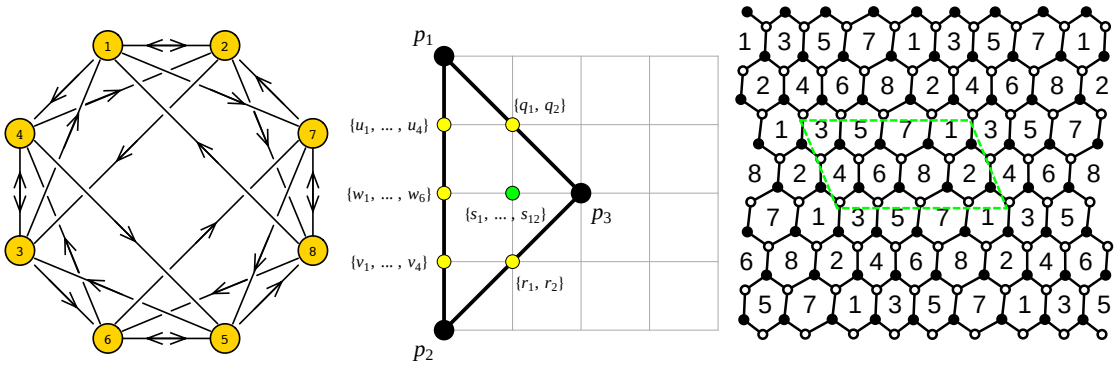


Figure 5. The quiver, toric diagram, and brane tiling of Model 2.

The superpotential is

$$\begin{aligned} W = &+X_{17}X_{72}X_{21} + X_{28}X_{81}X_{12} + X_{31}X_{14}X_{43} + X_{42}X_{23}X_{34} \\ &+X_{53}X_{36}X_{65} + X_{64}X_{45}X_{56} + X_{75}X_{58}X_{87} + X_{86}X_{67}X_{78} \\ &-X_{17}X_{78}X_{81} - X_{28}X_{87}X_{72} - X_{31}X_{12}X_{23} - X_{42}X_{21}X_{14} \\ &-X_{53}X_{34}X_{45} - X_{64}X_{43}X_{36} - X_{75}X_{56}X_{67} - X_{86}X_{65}X_{58}\ . \end{aligned} \tag{4.1}$$

The perfect matching matrix is

$P =$

	p_1	p_2	p_3	q_1	q_2	r_1	r_2	u_1	u_2	u_3	u_4	v_1	v_2	v_3	v_4	w_1	w_2	w_3	w_4	w_5	w_6	s_1	s_2	s_3	s_4	s_5	s_6	s_7	s_8	s_9	s_{10}	s_{11}	s_{12}
X_{67}	1	0	0	1	0	0	0	1	1	1	0	1	0	0	0	1	0	1	1	0	0	1	0	0	0	1	1	0	0	0	0	0	0
X_{45}	1	0	0	1	0	0	0	1	1	0	1	0	1	0	0	1	0	0	0	1	1	1	0	0	0	0	0	1	1	0	0	0	0
X_{58}	1	0	0	0	1	0	0	1	1	1	0	1	0	0	0	1	0	1	1	0	0	0	1	0	0	0	0	0	0	1	1	0	0
X_{36}	1	0	0	0	1	0	0	1	1	0	1	0	1	0	0	1	0	0	0	1	1	0	1	0	0	0	0	0	0	0	0	1	1
X_{23}	1	0	0	1	0	0	0	1	0	1	1	0	0	1	0	0	1	1	0	1	0	0	0	1	0	0	0	1	0	1	0	0	0
X_{81}	1	0	0	1	0	0	0	0	1	1	1	0	0	0	1	0	1	0	1	0	1	0	0	1	0	1	0	0	0	0	0	0	1
X_{14}	1	0	0	0	1	0	0	1	0	1	1	0	0	1	0	0	1	1	0	1	0	0	0	0	1	0	1	0	0	0	0	1	0
X_{72}	1	0	0	0	1	0	0	0	1	1	1	0	0	0	1	0	1	0	1	0	1	0	0	0	1	0	0	0	1	0	1	0	0
X_{28}	0	1	0	0	0	1	0	1	0	0	0	1	1	1	0	1	0	1	0	1	0	0	1	0	0	0	0	1	0	1	0	0	0
X_{31}	0	1	0	0	0	1	0	0	1	0	0	1	1	0	1	1	0	0	1	0	1	0	1	0	0	1	0	0	0	0	0	0	1
X_{17}	0	1	0	0	0	0	1	1	0	0	0	1	1	1	0	1	0	1	0	1	0	1	0	0	0	0	1	0	0	0	0	1	0
X_{42}	0	1	0	0	0	0	1	0	1	0	0	1	1	0	1	1	0	0	1	0	1	1	0	0	0	0	0	0	1	0	1	0	0
X_{64}	0	1	0	0	0	1	0	0	0	1	0	1	0	1	1	0	1	1	1	0	0	0	0	0	1	1	1	0	0	0	0	0	0
X_{75}	0	1	0	0	0	1	0	0	0	0	1	0	1	1	1	0	1	0	0	1	1	0	0	0	1	0	0	1	1	0	0	0	0
X_{53}	0	1	0	0	0	0	1	0	0	1	0	1	0	1	1	0	1	1	1	0	0	0	0	1	0	0	0	0	0	1	1	0	0
X_{86}	0	1	0	0	0	0	1	0	0	0	1	0	1	1	1	0	1	0	0	1	1	0	0	1	0	0	0	0	0	0	0	1	1
X_{65}	0	0	1	1	0	1	0	0	0	0	0	0	0	0	0	0	0	0	0	0	0	1	0	0	1	1	1	1	1	0	0	0	0
X_{21}	0	0	1	1	0	1	0	0	0	0	0	0	0	0	0	0	0	0	0	0	0	0	1	1	0	1	0	1	0	1	0	0	1
X_{43}	0	0	1	1	0	0	1	0	0	0	0	0	0	0	0	0	0	0	0	0	0	1	0	1	0	0	0	1	1	1	1	0	0
X_{87}	0	0	1	1	0	0	1	0	0	0	0	0	0	0	0	0	0	0	0	0	0	1	0	1	0	1	1	0	0	0	0	1	1
X_{78}	0	0	1	0	1	1	0	0	0	0	0	0	0	0	0	0	0	0	0	0	0	0	1	0	1	0	0	1	1	1	1	0	0
X_{34}	0	0	1	0	1	1	0	0	0	0	0	0	0	0	0	0	0	0	0	0	0	0	1	0	1	1	1	0	0	0	0	1	1
X_{12}	0	0	1	0	1	0	1	0	0	0	0	0	0	0	0	0	0	0	0	0	0	1	0	0	1	0	1	0	1	0	1	1	0
X_{56}	0	0	1	0	1	0	1	0	0	0	0	0	0	0	0	0	0	0	0	0	0	0	1	1	0	0	0	0	0	1	1	1	1

The F-term charge matrix $Q_F = \ker(P)$ is

$Q_F =$

p_1	p_2	p_3	q_1	q_2	r_1	r_2	u_1	u_2	u_3	u_4	v_1	v_2	v_3	v_4	w_1	w_2	w_3	w_4	w_5	w_6	s_1	s_2	s_3	s_4	s_5	s_6	s_7	s_8	s_9	s_{10}	s_{11}	s_{12}
1	1	0	0	0	0	0	−1	0	0	0	0	0	0	−1	0	0	0	0	0	0	0	0	0	0	0	0	0	0	0	0	0	0
1	1	0	0	0	0	0	0	−1	0	0	0	0	−1	0	0	0	0	0	0	0	0	0	0	0	0	0	0	0	0	0	0	0
1	1	0	0	0	0	0	0	0	−1	0	0	−1	0	0	0	0	0	0	0	0	0	0	0	0	0	0	0	0	0	0	0	0
1	0	1	−1	−1	0	0	0	0	0	0	0	0	0	0	0	0	0	0	0	0	0	0	0	0	0	0	0	0	0	0	0	0
1	0	0	−1	0	0	0	0	−1	0	0	0	0	0	0	0	0	0	0	0	0	1	0	0	0	0	0	0	0	0	0	−1	1
1	0	0	−1	0	0	0	0	0	−1	0	0	0	0	0	0	0	0	0	0	0	0	−1	0	0	1	0	0	0	1	0	0	0
1	0	0	0	0	1	0	−1	0	0	0	0	0	0	0	0	0	0	0	0	0	0	0	0	−1	−1	1	0	0	0	0	0	0
1	0	0	0	0	0	0	−1	0	0	−1	0	0	0	0	0	0	0	0	1	0	0	0	0	0	0	0	0	0	0	0	0	0
1	0	0	0	0	0	0	0	−1	0	−1	0	0	0	0	0	0	0	0	0	1	0	0	0	0	0	0	0	0	0	0	0	0
1	0	0	0	0	0	0	0	0	−1	−1	0	0	0	0	0	1	0	0	0	0	0	0	0	0	0	0	0	0	0	0	0	0
1	0	0	0	0	0	0	−1	−1	0	0	0	0	0	0	1	0	0	0	0	0	0	0	0	0	0	0	0	0	0	0	0	0
1	0	0	0	0	0	0	−1	0	−1	0	0	0	0	0	0	0	1	0	0	0	0	0	0	0	0	0	0	0	0	0	0	0
1	0	0	0	0	0	0	0	−1	−1	0	0	0	0	0	0	0	0	1	0	0	0	0	0	0	0	0	0	0	0	0	0	0
1	0	0	0	0	0	0	0	0	−1	0	1	0	0	0	−1	0	0	0	0	0	0	0	0	0	0	0	0	0	0	0	0	0
1	0	0	0	0	0	0	0	0	0	−1	0	1	0	0	−1	0	0	0	0	0	0	0	0	0	0	0	0	0	0	0	0	0
0	1	1	0	0	−1	−1	0	0	0	0	0	0	0	0	0	0	0	0	0	0	0	0	0	0	0	0	0	0	0	0	0	0
0	0	1	−1	0	−1	0	0	0	0	0	0	0	0	0	0	0	0	0	1	0	0	0	0	0	1	0	0	0	0	0	−1	0
0	0	1	0	0	0	0	0	0	0	0	0	0	0	0	1	0	0	0	0	0	−1	−1	0	0	0	0	0	0	0	0	0	0
0	0	1	0	0	0	0	0	0	0	0	0	0	0	0	0	0	0	1	0	0	0	0	0	0	−1	0	0	0	0	−1	0	0
0	0	0	1	0	1	0	0	0	0	0	0	0	0	0	0	0	0	0	0	0	0	0	0	0	−1	0	−1	0	0	0	0	0
0	0	0	1	0	0	1	0	0	0	0	0	0	0	0	0	0	0	0	0	0	−1	0	−1	0	0	0	0	0	0	0	0	0
0	0	0	0	0	0	0	0	0	0	0	0	0	0	0	0	0	0	0	0	0	1	0	0	1	0	−1	0	−1	0	0	0	0
0	0	0	0	0	0	0	0	0	0	0	0	0	0	0	0	0	0	0	0	0	0	0	0	0	1	−1	0	0	0	0	1	−1

The D-term charge matrix is

$$Q_D = \left(\begin{array}{ccc|cc|cc|cccc|cccc|cc|cccccccccc} p_1 & p_2 & p_3 & q_1 & q_2 & r_1 & r_2 & u_1 & u_2 & u_3 & u_4 & v_1 & v_2 & v_3 & v_4 & w_1 & w_2 & w_3 & w_4 & w_5 & w_6 & s_1 & s_2 & s_3 & s_4 & s_5 & s_6 & s_7 & s_8 & s_9 & s_{10} & s_{11} & s_{12} \\ \hline 0 & 0 & 0 & 0 & 0 & 0 & 0 & 0 & 0 & 0 & 0 & 0 & 0 & 0 & 0 & 0 & 0 & 0 & 0 & 0 & 0 & 0 & 1 & -1 & 0 & 0 & 0 & 0 & 0 & 0 & 0 & 0 & 0 \\ 0 & 0 & 0 & 0 & 0 & 0 & 0 & 0 & 0 & 0 & 0 & 0 & 0 & 0 & 0 & 0 & 0 & 0 & 0 & 0 & 0 & 0 & 0 & 1 & -1 & 0 & 0 & 0 & 0 & 0 & 0 & 0 & 0 \\ 0 & 0 & 0 & 0 & 0 & 0 & 0 & 0 & 0 & 0 & 0 & 0 & 0 & 0 & 0 & 0 & 0 & 0 & 0 & 0 & 0 & 0 & 0 & 0 & 1 & -1 & 0 & 0 & 0 & 0 & 0 & 0 & 0 \\ 0 & 0 & 0 & 0 & 0 & 0 & 0 & 0 & 0 & 0 & 0 & 0 & 0 & 0 & 0 & 0 & 0 & 0 & 0 & 0 & 0 & 0 & 0 & 0 & 0 & 1 & -1 & 0 & 0 & 0 & 0 & 0 & 0 \\ 0 & 0 & 0 & 0 & 0 & 0 & 0 & 0 & 0 & 0 & 0 & 0 & 0 & 0 & 0 & 0 & 0 & 0 & 0 & 0 & 0 & 0 & 0 & 0 & 0 & 0 & 1 & -1 & 0 & 0 & 0 & 0 & 0 \\ 0 & 0 & 0 & 0 & 0 & 0 & 0 & 0 & 0 & 0 & 0 & 0 & 0 & 0 & 0 & 0 & 0 & 0 & 0 & 0 & 0 & 0 & 0 & 0 & 0 & 0 & 0 & 1 & -1 & 0 & 0 & 0 & 0 \\ 0 & 0 & 0 & 0 & 0 & 0 & 0 & 0 & 0 & 0 & 0 & 0 & 0 & 0 & 0 & 0 & 0 & 0 & 0 & 0 & 0 & 0 & 0 & 0 & 0 & 0 & 0 & 0 & 1 & -1 & 0 & 0 & 0 \end{array}\right)$$

The total charge matrix Q_t does not exhibit repeated columns. Accordingly, the global symmetry is $U(1)_{f_1} \times U(1)_{f_2} \times U(1)_R$. Following the discussion in §2.3, the flavour and R-charges on the extremal prefect matchings are found as shown in Table 6.

	$U(1)_{f_1}$	$U(1)_{f_2}$	$U(1)_R$	fugacity
p_1	-1/4	1/4	2/3	t_1
p_2	-1/4	-1/4	2/3	t_2
p_3	1/2	0	2/3	t_3

Table 6. The GLSM fields corresponding to extremal points of the toric diagram with their mesonic charges (Model 2).

Products of non-extremal perfect matchings are set to be associated with a single variable as follows,

$$q = q_1 q_2 \ , \ r = r_1 r_2 \ , \ u = u_1 u_2 u_3 u_4 \ , \ v = v_1 v_2 v_3 v_4 \ , \ w = w_1 w_2 w_3 w_4 w_5 w_6 \ , \ s = \prod_{m=1}^{12} s_m \ . \tag{4.2}$$

The fugacities t_α counts extremal perfect matchings p_α with non-zero R-charge. The fugacity y_q counts the product of non-extremal perfect matchings q above.

The mesonic Hilbert series of Model 2 is calculated using the Molien integral formula in (2.9). It is

$$\begin{aligned} g_1(t_\alpha, y_q, y_r, y_u, y_v, y_w, y_s; \mathcal{M}_2^{mes}) &= (1 - y_q^2 y_r^2 y_u^4 y_v^4 y_w^4 y_s^2 \ t_1^4 t_2^4)(1 - y_q^2 y_r^2 y_u^2 y_v^2 y_w^2 y_s^2 \ t_1^2 t_2^2 t_3^2) \\ &\times \frac{1}{(1 - y_q^2 y_u^3 y_v y_w^2 y_s \ t_1^4)(1 - y_r^2 y_u y_v^3 y_w^2 y_s \ t_2^4)(1 - y_q y_r y_s \ t_3^2)} \\ &\times \frac{1}{(1 - y_q y_r y_u^2 y_v^2 y_w^2 y_s \ t_1^2 t_2^2)(1 - y_q y_r y_u y_v y_w y_s \ t_1 t_2 t_3)} \ . \end{aligned} \tag{4.3}$$

The plethystic logarithm of the mesonic Hilbert series is

$$\begin{aligned} PL[g_1(t_\alpha, y_q, y_r, y_u, y_v, y_w, y_s; \mathcal{M}_2^{mes})] &= y_q y_r y_s \ t_3^2 + y_q y_r y_u y_v y_w y_s \ t_1 t_2 t_3 \\ &+ y_q y_r y_u^2 y_v^2 y_w^2 y_s \ t_1^2 t_2^2 + y_q^2 y_u^3 y_v y_w^2 y_s \ t_1^4 + y_r^2 y_u y_v^3 y_w^2 y_s \ t_2^4 \\ &- y_q^2 y_r^2 y_u^2 y_v^2 y_w^2 y_s^2 \ t_1^2 t_2^2 t_3^2 - y_q^2 y_r^2 y_u^4 y_v^4 y_w^4 y_s^2 \ t_1^4 t_2^4 \ . \end{aligned} \tag{4.4}$$

The finite plethystic logarithm indicates that the mesonic moduli space is a complete intersection.

With the fugacity map

$$\begin{aligned} f_1 &= y_q^{1/3} y_r^{1/3} y_u^{-2/3} y_v^{-2/3} y_w^{-2/3} y_s^{-2/3} t_1^{-2/3} t_2^{-2/3} t_3^{4/3} \ , \\ f_2 &= y_q y_r^{-1} y_u y_v^{-1} \ t_1^2 t_2^{-2} \ , \\ t &= y_q^{1/3} y_r^{1/3} y_u^{1/3} y_v^{1/3} y_w^{1/3} y_s^{1/3} t_1^{1/3} t_2^{1/3} t_3^{1/3} \ , \end{aligned} \tag{4.5}$$

where f_1, f_2 and t are the mesonic charge fugacities, the plethystic logarithm becomes

$$PL[g_1(t, f_1, f_2; \mathcal{M}_2^{mes})] = f_1 t^2 + t^3 + \frac{1}{f_1}\left(1 + f_2 + \frac{1}{f_2}\right) t^4 - t^6 - \frac{1}{f_1^2} t^8 \ . \tag{4.6}$$

From the above plethystic logarithm, one can identify the moduli space generators as well as their mesonic charges. They are shown in Table 7. The charge lattice of generators in Table 7 is the dual reflexive polygon of the toric diagram of Model 2. The two relations formed by the generators are

$$A_1 A_3 = A_2^2 \ , \quad B_1 B_2 = A_3^2 \ . \tag{4.7}$$

Generator	$U(1)_{f_1}$	$U(1)_{f_2}$
$A_1 = p_3^2 \ q \ r \ s$	1	0
$A_2 = p_1 p_2 p_3 \ q \ r \ uv \ w \ s$	0	0
$A_3 = p_1^2 p_2^2 \ q \ r \ u^2 v^2 \ w^2 \ s$	-1	0
$B_1 = p_1^4 \ q^2 \ u^3 v \ w^2 \ s$	-1	1
$B_2 = p_2^4 \ r^2 \ uv^3 \ w^2 \ s$	-1	-1

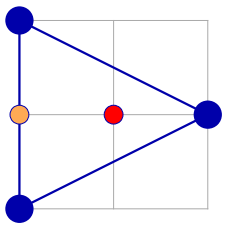


Table 7. The generators and lattice of generators of the mesonic moduli space of Model 2 in terms of GLSM fields with the corresponding flavor charges.

Generator	$U(1)_{f_1}$	$U(1)_{f_2}$
$X_{12}X_{21} = X_{34}X_{43} = X_{56}X_{65} = X_{78}X_{87}$	1	0
$X_{12}X_{23}X_{31} = X_{12}X_{28}X_{81} = X_{14}X_{42}X_{21} = X_{14}X_{43}X_{31} = X_{17}X_{72}X_{21} = X_{17}X_{78}X_{81} = X_{23}X_{34}X_{42} = X_{28}X_{87}X_{72} = X_{34}X_{45}X_{53}$ $= X_{36}X_{64}X_{43} = X_{36}X_{65}X_{53} = X_{45}X_{56}X_{64} = X_{56}X_{67}X_{75} = X_{58}X_{86}X_{65} = X_{58}X_{87}X_{75} = X_{67}X_{78}X_{86}$	0	0
$X_{14}X_{42}X_{23}X_{31} = X_{14}X_{42}X_{28}X_{81} = X_{14}X_{45}X_{53}X_{31} = X_{17}X_{72}X_{23}X_{31} = X_{17}X_{72}X_{28}X_{81} = X_{17}X_{75}X_{58}X_{81} = X_{23}X_{36}X_{64}X_{42}$ $= X_{28}X_{86}X_{67}X_{72} = X_{36}X_{64}X_{45}X_{53} = X_{36}X_{67}X_{75}X_{53} = X_{45}X_{58}X_{86}X_{64} = X_{58}X_{86}X_{67}X_{75}$	-1	0
$X_{14}X_{45}X_{58}X_{81} = X_{23}X_{36}X_{67}X_{72}$	-1	1
$X_{17}X_{75}X_{53}X_{31} = X_{28}X_{86}X_{64}X_{42}$	-1	-1

Table 8. The generators in terms of bifundamental fields (Model 2).

With the fugacity map

$$\begin{aligned} T_1 &= f_1^{-1/4} f_2^{1/4} \ t = y_q^{1/2} y_u^{3/4} y_v^{1/4} y_w^{1/2} y_s^{1/4} \ t_1 \ , \\ T_2 &= f_1^{-1/4} f_2^{-1/4} \ t = y_r^{1/2} y_u^{1/4} y_v^{3/4} y_w^{1/2} y_s^{1/4} \ t_2 \ , \\ T_3 &= f_1^{1/2} \ t = y_q^{1/2} y_r^{1/2} y_s^{1/2} \ t_3 \ , \end{aligned} \tag{4.8}$$

the mesonic Hilbert series takes the form

$$g_1(T_1, T_2, T_3; \mathcal{M}_2^{mes}) = \frac{(1 - T_1^4 T_2^4)(1 - T_1^2 T_2^2 T_3^2)}{(1 - T_1^4)(1 - T_2^4)(1 - T_3^2)(1 - T_1^2 T_2^2)(1 - T_1 T_2 T_3)} \quad , \quad (4.9)$$

with the plethystic logarithm being

$$PL[g_1(T_1, T_2, T_3; \mathcal{M}_2^{mes})] = T_3^2 + T_1 T_2 T_3 + T_1^2 T_2^2 + T_1^4 + T_2^4 - T_1^2 T_2^2 T_3^2 - T_1^4 T_2^4 \ . \quad (4.10)$$

The above refinement of the mesonic Hilbert series emphasises the conical structure of the toric Calabi-Yau space.

5 Model 3: $L_{1,3,1}/\mathbb{Z}_2$ $(0, 1, 1, 1)$

5.1 Model 3 Phase a

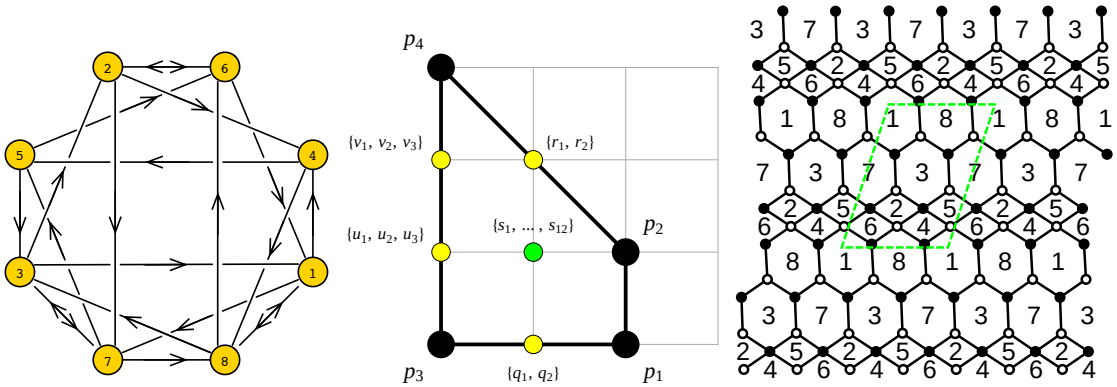


Figure 6. The quiver, toric diagram, and brane tiling of Model 3a.

The superpotential is

$$\begin{aligned} W = &+X_{31}X_{18}X_{83} + X_{32}X_{27}X_{73} + X_{53}X_{37}X_{75} + X_{78}X_{81}X_{17} \\ &-X_{14}X_{48}X_{81} - X_{31}X_{17}X_{73} - X_{78}X_{83}X_{37} - X_{86}X_{61}X_{18} \\ &+X_{14}X_{45}X_{56}X_{61} + X_{62}X_{24}X_{48}X_{86} - X_{32}X_{24}X_{45}X_{53} - X_{62}X_{27}X_{75}X_{56} \ . \end{aligned} \quad (5.1)$$

The perfect matching matrix is

$P =$

	p_1	p_2	p_3	p_4	q_1	q_2	r_1	r_2	u_1	u_2	u_3	v_1	v_2	v_3	s_1	s_2	s_3	s_4	s_5	s_6	s_7	s_8	s_9	s_{10}	s_{11}	s_{12}
X_{81}	1	1	0	0	1	0	1	0	0	0	0	0	0	0	1	0	1	0	1	1	1	1	0	0	0	0
X_{73}	1	1	0	0	1	0	0	1	0	0	0	0	0	0	1	0	1	0	0	0	1	0	1	1	0	1
X_{37}	1	1	0	0	0	1	1	0	0	0	0	0	0	0	0	1	0	1	1	1	0	1	0	0	1	0
X_{18}	1	1	0	0	0	1	0	1	0	0	0	0	0	0	0	1	0	1	0	0	0	0	1	1	1	1
X_{24}	1	0	0	0	1	0	0	0	0	0	0	0	0	0	0	0	0	0	1	0	0	0	0	1	1	0
X_{56}	1	0	0	0	0	1	0	0	0	0	0	0	0	0	1	0	0	0	0	0	0	1	1	0	0	0
X_{45}	0	1	0	0	0	0	1	0	0	0	0	0	0	0	0	1	1	0	0	0	0	0	0	0	0	1
X_{62}	0	1	0	0	0	0	0	1	0	0	0	0	0	0	0	0	0	1	0	1	1	0	0	0	0	0
X_{83}	0	0	1	0	1	0	0	0	1	1	0	0	1	0	1	0	1	0	0	0	1	0	0	0	0	0
X_{61}	0	0	1	0	1	0	0	0	1	0	1	0	0	1	0	0	0	0	1	1	1	0	0	0	0	0
X_{17}	0	0	1	0	0	1	0	0	1	1	0	0	1	0	0	1	0	1	0	0	0	0	0	0	1	0
X_{48}	0	0	1	0	0	1	0	0	1	0	1	0	0	1	0	1	0	0	0	0	0	0	1	0	0	1
X_{75}	0	0	1	0	1	0	0	0	0	1	1	1	0	0	0	0	1	0	0	0	0	0	0	1	0	1
X_{32}	0	0	1	0	0	1	0	0	0	1	1	1	0	0	0	0	0	1	0	1	0	1	0	0	0	0
X_{27}	0	0	0	1	0	0	1	0	1	0	0	0	1	1	0	1	0	0	1	0	0	0	0	0	1	0
X_{86}	0	0	0	1	0	0	1	0	0	1	0	1	1	0	1	0	1	0	0	0	0	1	0	0	0	0
X_{53}	0	0	0	1	0	0	0	1	1	0	0	0	1	1	1	0	0	0	0	0	1	0	1	0	0	0
X_{14}	0	0	0	1	0	0	0	1	0	1	0	1	1	0	0	0	0	1	0	0	0	0	0	1	1	0
X_{31}	0	0	0	1	0	0	1	0	0	0	1	1	0	1	0	0	0	0	1	1	0	1	0	0	0	0
X_{78}	0	0	0	1	0	0	0	1	0	0	1	1	0	1	0	0	0	0	0	0	0	0	1	1	0	1

The F-term charge matrix $Q_F = \ker(P)$ is

$Q_F =$

p_1	p_2	p_3	p_4	q_1	q_2	r_1	r_2	u_1	u_2	u_3	v_1	v_2	v_3	s_1	s_2	s_3	s_4	s_5	s_6	s_7	s_8	s_9	s_{10}	s_{11}	s_{12}
1	0	1	0	−1	−1	0	0	0	0	0	0	0	0	0	0	0	0	0	0	0	0	0	0	0	0
0	1	0	1	0	0	−1	−1	0	0	0	0	0	0	0	0	0	0	0	0	0	0	0	0	0	0
1	0	0	1	0	0	−1	0	0	0	0	0	0	0	−1	0	1	0	0	0	0	0	0	−1	0	0
0	1	1	0	−1	0	0	0	0	0	0	0	0	0	0	−1	0	0	1	−1	0	0	0	0	0	0
1	0	0	0	0	0	0	0	0	0	0	0	1	0	−1	0	0	0	0	0	0	0	0	0	−1	0
0	1	0	0	0	0	0	0	1	0	0	0	0	0	0	−1	0	0	0	0	−1	0	0	0	0	0
1	0	0	0	0	0	1	0	1	0	0	0	0	0	−1	−1	0	0	−1	0	0	0	0	0	0	0
0	1	0	0	0	0	0	0	0	1	0	0	0	0	0	0	−1	−1	0	0	0	0	0	0	0	0
0	0	1	1	0	0	0	0	−1	0	0	−1	0	0	0	0	0	0	0	0	0	0	0	0	0	0
0	0	1	1	0	0	0	0	0	−1	0	0	0	−1	0	0	0	0	0	0	0	0	0	0	0	0
0	0	1	0	0	0	0	0	−1	−1	0	0	1	0	0	0	0	0	0	0	0	0	0	0	0	0
0	0	1	0	0	0	0	0	0	−1	−1	1	0	0	0	0	0	0	0	0	0	0	0	0	0	0
0	0	1	0	−1	0	0	0	0	−1	0	0	0	0	1	0	0	0	0	0	0	0	0	−1	1	0	0
0	0	0	0	1	0	1	0	0	0	0	0	0	0	0	0	−1	0	−1	0	0	0	0	0	0	0
0	0	0	0	0	1	1	0	0	0	0	0	0	0	0	−1	0	0	0	0	0	−1	0	0	0	0
0	0	0	0	0	0	0	0	0	0	0	0	0	0	1	0	−1	0	0	0	0	0	−1	0	0	1

The D-term charge matrix is

$Q_D =$

p_1	p_2	p_3	p_4	q_1	q_2	r_1	r_2	u_1	u_2	u_3	v_1	v_2	v_3	s_1	s_2	s_3	s_4	s_5	s_6	s_7	s_8	s_9	s_{10}	s_{11}	s_{12}
0	0	0	0	0	0	0	0	0	0	0	0	0	0	0	0	0	0	1	−1	0	0	0	0	0	0
0	0	0	0	0	0	0	0	0	0	0	0	0	0	0	0	0	0	0	1	−1	0	0	0	0	0
0	0	0	0	0	0	0	0	0	0	0	0	0	0	0	0	0	0	0	0	1	−1	0	0	0	0
0	0	0	0	0	0	0	0	0	0	0	0	0	0	0	0	0	0	0	0	0	1	−1	0	0	0
0	0	0	0	0	0	0	0	0	0	0	0	0	0	0	0	0	0	0	0	0	0	1	−1	0	0
0	0	0	0	0	0	0	0	0	0	0	0	0	0	0	0	0	0	0	0	0	0	0	1	−1	0
0	0	0	0	0	0	0	0	0	0	0	0	0	0	0	0	0	0	0	0	0	0	0	0	1	−1

The total charge matrix does not exhibit repeated columns. Accordingly, the global symmetry is $U(1)_{f_1} \times U(1)_{f_2} \times U(1)_R$. Following the discussion in §2.3, the mesonic

charges on the extremal perfect matchings are found as shown in Table 9.

	$U(1)_{f_1}$	$U(1)_{f_2}$	$U(1)_R$	fugacity
p_1	1/2	1/2	$R_1 = \frac{1}{6}\left(5-\sqrt{7}\right)$	t_1
p_2	0	-1/2	$R_1 = \frac{1}{6}\left(5-\sqrt{7}\right)$	t_2
p_3	-1/2	-1/2	$R_2 = \frac{1}{6}\left(1+\sqrt{7}\right)$	t_3
p_4	0	1/2	$R_2 = \frac{1}{6}\left(1+\sqrt{7}\right)$	t_4

Table 9. The GLSM fields corresponding to extremal points of the toric diagram with their mesonic charges (Model 3a). The R-charges are obtained using a-maximization.

Products of non-extremal perfect matchings are associated to a single variable as follows

$$q = q_1 q_2 \ , \ r = r_1 r_2 \ , \ u = u_1 u_2 u_3 \ , \ v = v_1 v_2 v_3 \ , \ s = \prod_{m=1}^{12} s_m \quad . \tag{5.2}$$

The fugacity t_α counts extremal perfect matchings. The fugacity y_q counts the product of non-extremal perfect matchings q above.

The mesonic Hilbert series of Model 3a is calculated using the Molien integral formula in (2.9). It is

$$\begin{aligned} g_1(t_\alpha, y_q, y_r, y_u, y_v, y_s; \mathcal{M}_{3a}^{mes}) &= (1 - y_q^2 y_r^2 y_u^2 y_v^2 y_s^2 \ t_1^2 t_2^2 t_3^2 t_4^2)(1 - y_q^2 y_r^2 y_u^3 y_v^3 y_s^2 \ t_1 t_2 t_3^3 t_4^3) \\ &\times \frac{1}{(1 - y_q y_r y_s \ t_1^2 t_2^2)(1 - y_q^2 y_u^2 y_v y_s \ t_1 t_3^3)(1 - y_q y_r y_u^2 y_v^2 y_s \ t_3^2 t_4^2)} \\ &\times \frac{1}{(1 - y_r^2 y_u y_v^2 y_s \ t_2 t_4^3)(1 - y_q y_r y_u y_v y_s \ t_1 t_2 t_3 t_4)} \quad . \end{aligned} \tag{5.3}$$

The plethystic logarithm of the mesonic Hilbert series is

$$\begin{aligned} PL[g_1(t_\alpha, y_q, y_r, y_u, y_v, y_s; \mathcal{M}_{3a}^{mes})] &= y_q y_r y_s \ t_1^2 t_2^2 + y_q y_r y_u y_v y_s \ t_1 t_2 t_3 t_4 + y_q^2 y_u^2 y_v y_s \ t_1 t_3^3 \\ &+ y_r^2 y_u y_v^2 y_s \ t_2 t_4^3 + y_q y_r y_u^2 y_v^2 y_s \ t_3^2 t_4^2 - y_q^2 y_r^2 y_u^2 y_v^2 y_s^2 \ t_1^2 t_2^2 t_3^2 t_4^2 - y_q^2 y_r^2 y_u^3 y_v^3 y_s^2 \ t_1 t_2 t_3^3 t_4^3 \quad . \end{aligned} \tag{5.4}$$

The finite plethystic logarithm indicates that the mesonic moduli space is a complete intersection.

Consider the fugacity map

$$\begin{aligned} f_1 &= \frac{1}{y_u y_v} \ , \\ f_2 &= \frac{y_r y_v \ t_2^{1/2} t_4^{3/2}}{y_q \ t_1^{1/2} t_3^{3/2}} \ , \\ \tilde{t}_1 &= y_q^{1/4} y_r^{1/4} y_u^{1/4} y_v^{1/4} y_s^{1/4} \ t_1^{1/2} t_2^{1/2} \ , \\ \tilde{t}_2 &= y_q^{1/4} y_r^{1/4} y_u^{1/4} y_v^{1/4} y_s^{1/4} \ t_3^{1/2} t_4^{1/2} \ , \end{aligned} \tag{5.5}$$

where f_1 and f_2 are the flavor fugacities, and $\tilde{t}_1$ and $\tilde{t}_2$ are the fugacities for the R-charges R_1 and R_2 in Table 9 respectively. Under the above fugacity map, the plethystic logarithm becomes

$$PL[g_1(t_\alpha, f_1, f_2; \mathcal{M}_{3a}^{mes})] = f_1 \tilde{t}_1^4 + \tilde{t}_1^2 \tilde{t}_2^2 + \left(\frac{1}{f_1 f_2} + f_2 \right) \tilde{t}_1 \tilde{t}_2^3 + \frac{\tilde{t}_2^4}{f_1} - \tilde{t}_1^4 \tilde{t}_2^4 - \frac{\tilde{t}_1^2 \tilde{t}_2^6}{f_1} \ . \tag{5.6}$$

The above plethystic logarithm indicates both the moduli space generators as well as their mesonic charges. They are summarized in Table 11. The generators can be presented on a charge lattice. The convex polygon formed by the generators in Table 11 is the dual reflexive polygon of the toric diagram of Model 3a. The generators satisfy the following relations

$$A_1 A_2 = B^2 \quad , \quad A_2 B = C_1 C_2 \quad . \tag{5.7}$$

Generator	$U(1)_{f_1}$	$U(1)_{f_2}$
$A_1 = p_1^2 p_2^2 \ q \ r \ s$	1	0
$A_2 = p_3^2 p_4^2 \ q \ r \ u^2 v^2 \ s$	-1	0
$B = p_1 p_2 p_3 p_4 \ q \ r \ uv \ s$	0	0
$C_1 = p_1 p_3^3 \ q^2 \ u^2 v \ s$	-1	-1
$C_2 = p_2 p_4^3 \ r^2 \ uv^2 \ s$	0	1

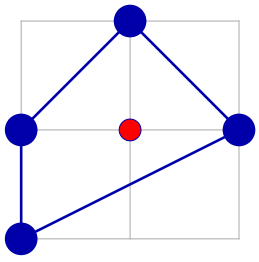


Table 10. The generators and lattice of generators of the mesonic moduli space of Model 3a in terms of GLSM fields with the corresponding flavor charges.

Generator	$U(1)_{f_1}$	$U(1)_{f_2}$
$X_{24}X_{45}X_{56}X_{62} = X_{18}X_{81} = X_{37}X_{73}$	1	0
$X_{14}X_{48}X_{83}X_{31} = X_{14}X_{48}X_{86}X_{61} = X_{17}X_{75}X_{53}X_{31} = X_{17}X_{78}X_{83}X_{31}$ $= X_{17}X_{78}X_{86}X_{61} = X_{27}X_{75}X_{53}X_{32} = X_{27}X_{78}X_{83}X_{32}$	-1	0
$X_{14}X_{45}X_{56}X_{61} = X_{24}X_{45}X_{53}X_{32} = X_{24}X_{48}X_{86}X_{62} = X_{27}X_{75}X_{56}X_{62} = X_{14}X_{48}X_{81}$ $= X_{17}X_{73}X_{31} = X_{17}X_{78}X_{81} = X_{18}X_{83}X_{31} = X_{18}X_{86}X_{61} = X_{27}X_{73}X_{32} = X_{37}X_{75}X_{53} = X_{37}X_{78}X_{83}$	0	0
$X_{17}X_{75}X_{56}X_{61} = X_{24}X_{48}X_{83}X_{32}$	-1	-1
$X_{14}X_{45}X_{53}X_{31} = X_{27}X_{78}X_{86}X_{62}$	0	1

Table 11. The generators in terms of bifundamental fields (Model 3a).

The mesonic Hilbert series and the plethystic logarithm can be re-expressed in terms of the following 3 fugacities,

$$T_1 = \frac{f_2}{\tilde{t}_1^3\tilde{t}_2} = \frac{t_4}{y_q^2 y_u y_s\ t_1^2 t_2 t_3^2}\ ,\ T_2 = \frac{1}{f_1 f_2}\ \tilde{t}_1\tilde{t}_2^3 = y_q^2 y_u^2 y_v y_s\ t_1 t_3^3\ ,\ T_3 = f_1\ \tilde{t}_1^4 = y_q y_r y_s\ t_1^2 t_2^2\ \ , \tag{5.8}$$

such that

$$g_1(T_1, T_2, T_3; \mathcal{M}_{3a}^{mes}) = \frac{(1 - T_1^2T_2^2T_3^2)(1 - T_1^3T_2^3T_3^2)}{(1 - T_3)(1 - T_2)(1 - T_1^2T_2^2T_3)(1 - T_1^3T_2^2T_3^2)(1 - T_1T_2T_3)} \tag{5.9}$$

and

$$\begin{aligned} PL[g_1(T_1, T_2, T_3; \mathcal{M}_{3a}^{mes})] = {} & T_3 + T_1T_2T_3 + T_2 + T_1^2T_2^2T_3 + T_1^3T_2^2T_3^2 \\ & - T_1^2T_2^2T_3^2 - T_1^3T_2^3T_3^2\ \ . \end{aligned} \tag{5.10}$$

The above refinement of the mesonic Hilbert series and the plethystic logarithm illustrates the conical structure of the toric Calalbi-Yau 3-fold.

5.2 Model 3 Phase b

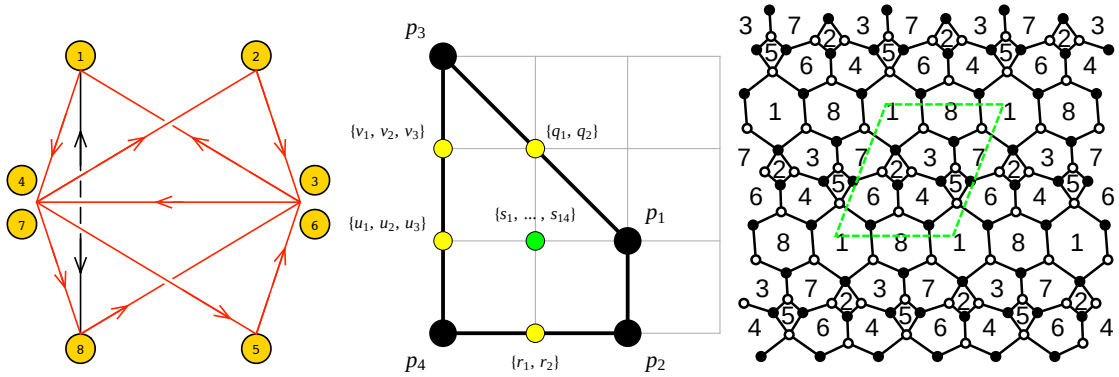


Figure 7. The quiver, toric diagram, and brane tiling of Model 3b. The red arrows in the quiver indicate all possible connections between blocks of nodes.

The superpotential is

$$\begin{aligned} W = &+X_{31}X_{18}X_{83} + X_{42}X_{23}X_{34} + X_{53}X_{37}X_{75} + X_{67}X_{72}X_{26} \\ &-X_{14}X_{48}X_{81} - X_{42}X_{26}X_{64} - X_{53}X_{34}X_{45} - X_{67}X_{75}X_{56} \\ &+X_{78}X_{81}X_{17} + X_{86}X_{64}X_{48} + X_{14}X_{45}X_{56}X_{61} \\ &-X_{78}X_{83}X_{37} - X_{86}X_{61}X_{18} - X_{17}X_{72}X_{23}X_{31} \ . \end{aligned} \tag{5.11}$$

The perfect matching matrix is

$P =$

	p_1	p_2	p_3	p_4	q_1	q_2	r_1	r_2	u_1	u_2	u_3	v_1	v_2	v_3	s_1	s_2	s_3	s_4	s_5	s_6	s_7	s_8	s_9	s_{10}	s_{11}	s_{12}	s_{13}	s_{14}
X_{37}	1	1	0	0	1	0	1	0	0	0	0	0	0	0	1	1	1	1	0	0	0	0	0	0	0	0	0	0
X_{18}	1	1	0	0	0	1	1	0	0	0	0	0	0	0	1	0	1	0	1	0	1	1	1	1	0	0	0	0
X_{81}	1	1	0	0	1	0	0	1	0	0	0	0	0	0	0	1	0	1	0	1	0	0	0	0	1	1	1	1
X_{64}	1	1	0	0	0	1	0	1	0	0	0	0	0	0	1	1	0	0	1	1	0	0	0	0	0	0	0	0
X_{67}	1	0	1	0	1	1	0	0	0	0	1	0	1	1	1	1	1	0	0	1	0	0	0	0	0	0	0	0
X_{34}	0	1	0	1	0	0	1	1	1	1	0	1	0	0	1	1	0	1	1	0	0	0	0	0	0	0	0	0
X_{45}	1	0	0	0	1	0	0	0	0	0	0	0	0	0	0	0	1	0	0	0	1	1	0	0	1	1	0	0
X_{23}	1	0	0	0	0	1	0	0	0	0	0	0	0	0	0	0	0	0	0	1	1	0	1	0	1	0	1	0
X_{56}	0	1	0	0	0	0	1	0	0	0	0	0	0	0	0	0	0	1	0	0	0	0	1	1	0	0	1	1
X_{72}	0	1	0	0	0	0	0	1	0	0	0	0	0	0	0	0	0	0	1	0	0	1	0	1	0	1	0	1
X_{86}	0	0	1	0	1	0	0	0	1	0	0	1	1	0	0	0	0	1	0	0	0	0	0	0	1	1	1	1
X_{31}	0	0	1	0	1	0	0	0	0	1	0	1	0	1	0	1	0	1	0	0	0	0	0	0	0	0	0	0
X_{14}	0	0	1	0	0	1	0	0	1	0	0	1	1	0	1	0	0	0	1	0	0	0	0	0	0	0	0	0
X_{78}	0	0	1	0	0	1	0	0	0	1	0	1	0	1	0	0	0	0	1	0	1	1	1	1	0	0	0	0
X_{42}	0	0	1	0	1	0	0	0	0	0	1	0	1	1	0	0	1	0	0	0	0	1	0	1	0	1	0	1
X_{53}	0	0	1	0	0	1	0	0	0	0	1	0	1	1	0	0	0	0	0	1	0	0	1	1	0	0	1	1
X_{17}	0	0	0	1	0	0	1	0	1	0	1	0	1	0	1	0	1	0	0	0	0	0	0	0	0	0	0	0
X_{48}	0	0	0	1	0	0	1	0	0	1	1	0	0	1	0	0	1	0	0	0	1	1	1	1	0	0	0	0
X_{83}	0	0	0	1	0	0	0	1	1	0	1	0	1	0	0	0	0	0	0	1	0	0	0	0	1	1	1	1
X_{61}	0	0	0	1	0	0	0	1	0	1	1	0	0	1	0	1	0	0	0	1	0	0	0	0	0	0	0	0
X_{26}	0	0	0	1	0	0	1	0	1	1	0	1	0	0	0	0	0	1	0	0	1	0	1	0	1	0	1	0
X_{75}	0	0	0	1	0	0	0	1	1	1	0	1	0	0	0	0	0	0	1	0	1	1	0	0	1	1	0	0

The F-term charge matrix $Q_F = \ker(P)$ is

$$Q_F = \left(\begin{array}{cccc|cc|cc|ccc|ccc|cccccccccccc} p_1 & p_2 & p_3 & p_4 & q_1 & q_2 & r_1 & r_2 & u_1 & u_2 & u_3 & v_1 & v_2 & v_3 & s_1 & s_2 & s_3 & s_4 & s_5 & s_6 & s_7 & s_8 & s_9 & s_{10} & s_{11} & s_{12} & s_{13} & s_{14} \\ \hline 1&0&1&0&-1&-1&0&0&0&0&0&0&0&0&0&0&0&0&0&0&0&0&0&0&0&0&0&0 \\ 0&1&0&1&0&0&-1&-1&0&0&0&0&0&0&0&0&0&0&0&0&0&0&0&0&0&0&0&0 \\ 1&0&0&0&0&0&0&0&1&0&0&0&0&0&-1&0&0&0&0&0&0&0&0&0&-1&0&0&0 \\ 1&0&0&0&0&0&0&0&0&1&0&0&0&0&0&-1&0&0&0&0&-1&0&0&0&0&0&0&0 \\ 0&1&0&0&0&0&0&0&0&0&0&0&1&0&-1&0&0&0&0&0&0&0&0&0&0&0&0&-1 \\ 0&1&0&0&0&0&0&0&0&0&0&0&0&1&0&-1&0&0&0&0&0&0&0&-1&0&0&0&0 \\ 0&1&0&0&0&0&-1&0&0&1&0&0&0&0&1&-1&0&0&-1&0&0&0&0&0&0&0&0 \\ 0&0&1&1&0&0&0&0&-1&0&0&0&0&-1&0&0&0&0&0&0&0&0&0&0&0&0&0 \\ 0&0&1&1&0&0&0&0&0&-1&0&0&-1&0&0&0&0&0&0&0&0&0&0&0&0&0&0 \\ 0&0&0&1&0&0&0&0&-1&0&-1&0&1&0&0&0&0&0&0&0&0&0&0&0&0&0&0 \\ 0&0&0&1&1&0&0&0&-1&0&0&0&0&0&1&-1&-1&0&0&0&0&0&0&0&0&0&0 \\ 0&0&0&1&0&0&0&0&-1&-1&0&1&0&0&0&0&0&0&0&0&0&0&0&0&0&0&0 \\ 0&0&0&1&1&0&0&0&-1&0&0&0&0&0&0&-1&0&0&1&0&0&-1&0&0&0&0&0 \\ 0&0&0&1&0&1&0&0&0&-1&0&0&0&0&-1&1&0&0&0&-1&0&0&0&0&0&0&0 \\ 0&0&0&1&0&0&-1&0&-1&0&0&0&0&0&1&-1&0&1&0&0&0&0&0&0&0&0&0 \\ 0&0&0&0&1&0&0&1&0&0&0&0&0&0&0&-1&0&0&0&0&0&0&0&0&-1&0&0 \\ 0&0&0&0&0&1&1&0&0&0&0&0&0&0&-1&0&0&0&0&0&0&0&-1&0&0&0&0 \\ 0&0&0&0&0&0&0&0&0&0&0&0&0&0&0&1&0&-1&0&-1&0&0&0&0&0&1&0 \end{array}\right)$$

The D-term charge matrix is

$$Q_D = \left(\begin{array}{cccc|cc|cc|ccc|ccc|cccccccccccc} p_1 & p_2 & p_3 & p_4 & q_1 & q_2 & r_1 & r_2 & u_1 & u_2 & u_3 & v_1 & v_2 & v_3 & s_1 & s_2 & s_3 & s_4 & s_5 & s_6 & s_7 & s_8 & s_9 & s_{10} & s_{11} & s_{12} & s_{13} & s_{14} \\ \hline 0&0&0&0&0&0&0&0&0&0&0&0&0&0&0&1&-1&0&0&0&0&0&0&0&0&0&0&0 \\ 0&0&0&0&0&0&0&0&0&0&0&0&0&0&0&0&1&-1&0&0&0&0&0&0&0&0&0&0 \\ 0&0&0&0&0&0&0&0&0&0&0&0&0&0&0&0&0&1&-1&0&0&0&0&0&0&0&0&0 \\ 0&0&0&0&0&0&0&0&0&0&0&0&0&0&0&0&0&0&1&-1&0&0&0&0&0&0&0&0 \\ 0&0&0&0&0&0&0&0&0&0&0&0&0&0&0&0&0&0&0&1&-1&0&0&0&0&0&0&0 \\ 0&0&0&0&0&0&0&0&0&0&0&0&0&0&0&0&0&0&0&0&1&-1&0&0&0&0&0&0 \\ 0&0&0&0&0&0&0&0&0&0&0&0&0&0&0&0&0&0&0&0&0&1&-1&0&0&0&0&0 \end{array}\right)$$

The total charge matrix does not exhibit repeated columns. Accordingly, the global symmetry is $U(1)_{f_1} \times U(1)_{f_2} \times U(1)_R$. The mesonic charges on the GLSM fields with non-zero R-charges are the same as for Model 3a and are shown in Table 9.

Products of non-extremal perfect matchings are expressed in terms of single variables as follows

$$q = q_1 q_2 \ , \ r = r_1 r_2 \ , \ u = u_1 u_2 u_3 \ , \ v = v_1 v_2 v_3 \ , \ s = \prod_{m=1}^{14} s_m \ . \tag{5.12}$$

The fugacity t_α counts GLSM fields corresponding to extremal perfect matchings p_α. The fugacity y_q for instance counts the product of non-extremal perfect matchings q shown above.

The refined mesonic Hilbert series and the corresponding plethystic logarithm are found using the Molien integral formula in (2.9). The Hilbert series is found to be the same as the one for Model 3a given in (5.3), (5.4) and (5.6). Accordingly, the mesonic moduli spaces of Model 3a and 3b are the same, with the corresponding quiver gauge theories being toric (Seiberg) duals.

The generators in terms of all perfect matchings of Model 3b are given in Table 11 with the corresponding mesonic symmetry charges. The corresponding mesonic generators in terms of quiver fields are given in Table 12. The mesonic moduli space is a complete intersection, and the generators satisfy the relation in (5.7).

Generator	$U(1)_{f_1}$	$U(1)_{f_2}$
$X_{18}X_{81} = X_{23}X_{37}X_{72} = X_{45}X_{56}X_{64}$	1	0
$X_{14}X_{42}X_{26}X_{61} = X_{14}X_{48}X_{83}X_{31} = X_{14}X_{48}X_{86}X_{61} = X_{17}X_{75}X_{53}X_{31} = X_{17}X_{78}X_{83}X_{31} = X_{17}X_{78}X_{86}X_{61}$	-1	0
$X_{14}X_{45}X_{56}X_{61} = X_{17}X_{72}X_{23}X_{31} = X_{14}X_{48}X_{81} = X_{17}X_{78}X_{81} = X_{18}X_{83}X_{31} = X_{18}X_{86}X_{61} = X_{23}X_{34}X_{42}$ $= X_{26}X_{64}X_{42} = X_{26}X_{67}X_{72} = X_{34}X_{45}X_{53} = X_{37}X_{75}X_{53} = X_{37}X_{78}X_{83} = X_{48}X_{86}X_{64} = X_{56}X_{67}X_{75}$	0	0
$X_{34}X_{48}X_{83} = X_{17}X_{72}X_{26}X_{61} = X_{17}X_{75}X_{56}X_{61}$	-1	-1
$X_{67}X_{78}X_{86} = X_{14}X_{42}X_{23}X_{31} = X_{14}X_{45}X_{53}X_{31}$	0	1

Table 12. The generators in terms of bifundamental fields (Model 3b).

6 Model 4: $\mathcal{C}/\mathbb{Z}_2 \times \mathbb{Z}_2$ $(1,0,0,1)(0,1,1,0)$, $\mathbf{PdP}_5$

6.1 Model 4 Phase a

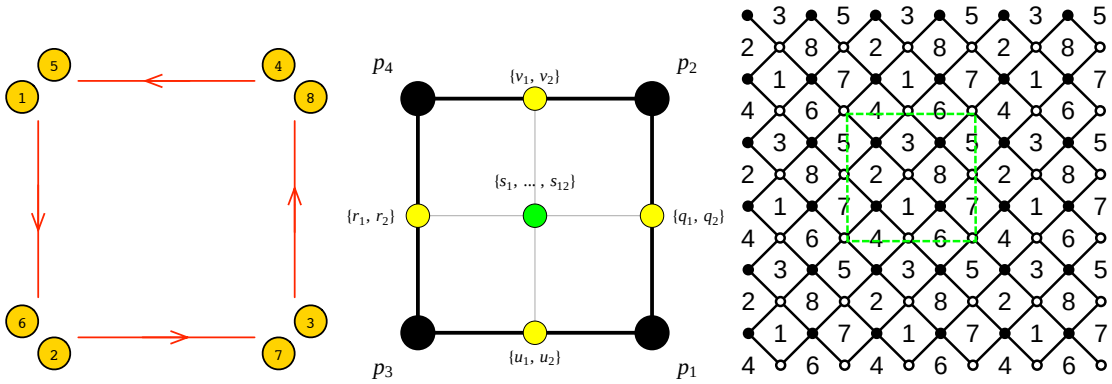


Figure 8. The quiver, toric diagram, and brane tiling of Model 4a. The red arrows in the quiver indicate all possible connections between blocks of nodes.

The superpotential is

$$\begin{aligned} W = &+X_{23}X_{38}X_{81}X_{12} + X_{41}X_{16}X_{63}X_{34} + X_{67}X_{74}X_{45}X_{56} + X_{85}X_{52}X_{27}X_{78} \\ &-X_{27}X_{74}X_{41}X_{12} - X_{45}X_{52}X_{23}X_{34} - X_{63}X_{38}X_{85}X_{56} - X_{81}X_{16}X_{67}X_{78} \end{aligned} \tag{6.1}$$

The perfect matching matrix is

$$P = \left(\begin{array}{c|cccc|cc|cc|cc|cc|cccccccccccc} & p_1 & p_2 & p_3 & p_4 & q_1 & q_2 & r_1 & r_2 & u_1 & u_2 & v_1 & v_2 & s_1 & s_2 & s_3 & s_4 & s_5 & s_6 & s_7 & s_8 & s_9 & s_{10} & s_{11} & s_{12} \\ \hline X_{23} & 1 & 0 & 0 & 0 & 1 & 0 & 0 & 0 & 1 & 0 & 0 & 0 & 1 & 1 & 1 & 0 & 0 & 0 & 0 & 0 & 0 & 0 & 0 & 0 \\ X_{41} & 1 & 0 & 0 & 0 & 1 & 0 & 0 & 0 & 0 & 1 & 0 & 0 & 0 & 0 & 0 & 1 & 1 & 1 & 0 & 0 & 0 & 0 & 0 & 0 \\ X_{85} & 1 & 0 & 0 & 0 & 0 & 1 & 0 & 0 & 1 & 0 & 0 & 0 & 0 & 0 & 0 & 1 & 0 & 0 & 1 & 1 & 0 & 0 & 0 & 0 \\ X_{67} & 1 & 0 & 0 & 0 & 0 & 1 & 0 & 0 & 0 & 1 & 0 & 0 & 1 & 0 & 0 & 0 & 0 & 0 & 0 & 0 & 1 & 1 & 0 & 0 \\ X_{56} & 0 & 1 & 0 & 0 & 1 & 0 & 0 & 0 & 0 & 0 & 1 & 0 & 0 & 1 & 0 & 0 & 1 & 0 & 0 & 0 & 0 & 0 & 1 & 0 \\ X_{78} & 0 & 1 & 0 & 0 & 1 & 0 & 0 & 0 & 0 & 0 & 0 & 1 & 0 & 0 & 1 & 0 & 0 & 1 & 0 & 0 & 0 & 0 & 0 & 1 \\ X_{34} & 0 & 1 & 0 & 0 & 0 & 1 & 0 & 0 & 0 & 0 & 1 & 0 & 0 & 0 & 0 & 0 & 0 & 0 & 1 & 0 & 1 & 0 & 0 & 1 \\ X_{12} & 0 & 1 & 0 & 0 & 0 & 1 & 0 & 0 & 0 & 0 & 0 & 1 & 0 & 0 & 0 & 0 & 0 & 0 & 0 & 1 & 0 & 1 & 1 & 0 \\ X_{74} & 0 & 0 & 1 & 0 & 0 & 0 & 1 & 0 & 1 & 0 & 0 & 0 & 0 & 0 & 1 & 0 & 0 & 0 & 1 & 0 & 0 & 0 & 0 & 1 \\ X_{52} & 0 & 0 & 1 & 0 & 0 & 0 & 1 & 0 & 0 & 1 & 0 & 0 & 0 & 0 & 0 & 0 & 1 & 0 & 0 & 0 & 0 & 1 & 1 & 0 \\ X_{16} & 0 & 0 & 1 & 0 & 0 & 0 & 0 & 1 & 1 & 0 & 0 & 0 & 0 & 1 & 0 & 0 & 0 & 0 & 0 & 1 & 0 & 0 & 1 & 0 \\ X_{38} & 0 & 0 & 1 & 0 & 0 & 0 & 0 & 1 & 0 & 1 & 0 & 0 & 0 & 0 & 0 & 0 & 0 & 1 & 0 & 0 & 1 & 0 & 0 & 1 \\ X_{81} & 0 & 0 & 0 & 1 & 0 & 0 & 1 & 0 & 0 & 0 & 1 & 0 & 0 & 0 & 0 & 1 & 1 & 0 & 1 & 0 & 0 & 0 & 0 & 0 \\ X_{63} & 0 & 0 & 0 & 1 & 0 & 0 & 1 & 0 & 0 & 0 & 0 & 1 & 1 & 0 & 1 & 0 & 0 & 0 & 0 & 0 & 0 & 1 & 0 & 0 \\ X_{27} & 0 & 0 & 0 & 1 & 0 & 0 & 0 & 1 & 0 & 0 & 1 & 0 & 1 & 1 & 0 & 0 & 0 & 0 & 0 & 0 & 1 & 0 & 0 & 0 \\ X_{45} & 0 & 0 & 0 & 1 & 0 & 0 & 0 & 1 & 0 & 0 & 0 & 1 & 0 & 0 & 0 & 1 & 0 & 1 & 0 & 1 & 0 & 0 & 0 & 0 \end{array}\right)$$

The F-term charge matrix $Q_F = \ker(P)$ is

$$Q_F = \left(\begin{array}{cccc|cc|cc|cc|cc|cccccccccccc} p_1 & p_2 & p_3 & p_4 & q_1 & q_2 & r_1 & r_2 & u_1 & u_2 & v_1 & v_2 & s_1 & s_2 & s_3 & s_4 & s_5 & s_6 & s_7 & s_8 & s_9 & s_{10} & s_{11} & s_{12} \\ \hline 1 & 1 & 0 & 0 & -1 & -1 & 0 & 0 & 0 & 0 & 0 & 0 & 0 & 0 & 0 & 0 & 0 & 0 & 0 & 0 & 0 & 0 & 0 & 0 \\ 0 & 0 & 1 & 1 & 0 & 0 & -1 & -1 & 0 & 0 & 0 & 0 & 0 & 0 & 0 & 0 & 0 & 0 & 0 & 0 & 0 & 0 & 0 & 0 \\ 1 & 0 & 1 & 0 & 0 & 0 & 0 & 0 & -1 & -1 & 0 & 0 & 0 & 0 & 0 & 0 & 0 & 0 & 0 & 0 & 0 & 0 & 0 & 0 \\ 0 & 1 & 0 & 1 & 0 & 0 & 0 & 0 & 0 & 0 & -1 & -1 & 0 & 0 & 0 & 0 & 0 & 0 & 0 & 0 & 0 & 0 & 0 & 0 \\ 1 & 0 & 0 & 0 & 0 & 0 & 1 & 0 & 0 & 0 & 1 & 0 & -1 & 0 & 0 & 0 & -1 & 0 & -1 & 0 & 0 & 0 & 0 & 0 \\ 1 & 0 & 0 & 0 & 0 & 0 & 0 & 1 & 0 & 0 & 1 & 0 & 0 & -1 & 0 & -1 & 0 & 0 & 0 & 0 & -1 & 0 & 0 & 0 \\ 1 & 0 & 0 & 0 & 0 & 0 & 0 & 1 & 0 & 0 & 1 & 0 & 0 & -1 & 0 & 0 & 0 & -1 & -1 & 0 & -1 & 0 & 0 & 1 \\ 1 & 0 & 0 & 1 & 0 & 0 & 0 & 0 & 0 & 0 & 0 & 0 & -1 & 0 & 0 & -1 & 0 & 0 & 0 & 0 & 0 & 0 & 0 & 0 \\ 0 & 0 & 1 & 1 & 0 & 1 & -1 & 0 & 0 & 0 & 0 & 0 & 0 & 0 & 0 & 0 & 0 & 0 & 0 & -1 & -1 & 0 & 0 & 0 \\ 0 & 0 & 0 & 0 & 1 & 0 & 0 & 1 & 0 & 0 & 0 & 0 & 0 & -1 & 0 & 0 & 0 & -1 & 0 & 0 & 0 & 0 & 0 & 0 \\ 0 & 0 & 0 & 0 & 0 & 1 & 1 & 0 & 0 & 0 & 0 & 0 & 0 & 0 & 0 & 0 & 0 & 0 & -1 & 0 & 0 & -1 & 0 & 0 \\ 0 & 0 & 0 & 0 & 0 & 0 & 0 & 0 & 1 & 0 & 1 & 0 & 0 & -1 & 0 & 0 & 0 & 0 & -1 & 0 & 0 & 0 & 0 & 0 \\ 0 & 0 & 0 & 0 & 0 & 0 & 0 & 0 & 0 & 0 & 0 & 0 & 1 & -1 & 0 & 0 & 0 & 0 & 0 & 0 & 0 & -1 & 1 & 0 \\ 0 & 0 & 0 & 0 & 0 & 0 & 0 & 0 & 0 & 0 & 0 & 0 & 1 & 0 & -1 & 0 & 0 & 0 & 0 & 0 & -1 & 0 & 0 & 1 \end{array}\right)$$

The D-term charge matrix is

$$Q_D = \left(\begin{array}{cccc|cc|cc|cc|cc|cccccccccccc} p_1 & p_2 & p_3 & p_4 & q_1 & q_2 & r_1 & r_2 & u_1 & u_2 & v_1 & v_2 & s_1 & s_2 & s_3 & s_4 & s_5 & s_6 & s_7 & s_8 & s_9 & s_{10} & s_{11} & s_{12} \\ \hline 0 & 0 & 0 & 0 & 0 & 0 & 0 & 0 & 0 & 0 & 0 & 0 & 0 & 0 & 1 & -1 & 0 & 0 & 0 & 0 & 0 & 0 & 0 & 0 \\ 0 & 0 & 0 & 0 & 0 & 0 & 0 & 0 & 0 & 0 & 0 & 0 & 0 & 0 & 0 & 1 & -1 & 0 & 0 & 0 & 0 & 0 & 0 & 0 \\ 0 & 0 & 0 & 0 & 0 & 0 & 0 & 0 & 0 & 0 & 0 & 0 & 0 & 0 & 0 & 0 & 1 & -1 & 0 & 0 & 0 & 0 & 0 & 0 \\ 0 & 0 & 0 & 0 & 0 & 0 & 0 & 0 & 0 & 0 & 0 & 0 & 0 & 0 & 0 & 0 & 0 & 1 & -1 & 0 & 0 & 0 & 0 & 0 \\ 0 & 0 & 0 & 0 & 0 & 0 & 0 & 0 & 0 & 0 & 0 & 0 & 0 & 0 & 0 & 0 & 0 & 0 & 1 & -1 & 0 & 0 & 0 & 0 \\ 0 & 0 & 0 & 0 & 0 & 0 & 0 & 0 & 0 & 0 & 0 & 0 & 0 & 0 & 0 & 0 & 0 & 0 & 0 & 1 & -1 & 0 & 0 & 0 \\ 0 & 0 & 0 & 0 & 0 & 0 & 0 & 0 & 0 & 0 & 0 & 0 & 0 & 0 & 0 & 0 & 0 & 0 & 0 & 0 & 1 & -1 & 0 & 0 \end{array}\right)$$

The total charge matrix Q_t does not exhibit repeated columns. Accordingly, the global symmetry is $U(1)_{f_1} \times U(1)_{f_2} \times U(1)_R$. The mesonic charges on the extremal perfect matchings are found following the discussion in §2.3. They are shown in Table 13.

	$U(1)_{f_1}$	$U(1)_{f_2}$	$U(1)_R$	fugacity
p_1	1/4	-1/4	1/2	t_1
p_2	1/4	1/4	1/2	t_2
p_3	-1/4	-1/4	1/2	t_3
p_4	-1/4	1/4	1/2	t_4

Table 13. The GLSM fields corresponding to extremal points of the toric diagram with their mesonic charges (Model 4a).

Products of GLSM fields corresponding to non-extremal perfect matchings are called by single variables as follows

$$q = q_1 q_2 \ , \ r = r_1 r_2 \ , \ u = u_1 u_2 \ , \ v = v_1 v_2 \ , \ s = \prod_{m=1}^{12} s_m \ . \tag{6.2}$$

The fugacity t_α counts extremal perfect matchings p_α. The fugacity y_q for instance corresponds to the product of non-extremal perfect matchings q shown above.

The refined mesonic Hilbert series of Model 4a is calculated using the Molien integral formula in (2.9). It is

$$\begin{aligned} g_1(t_\alpha, y_q, y_r, y_u, y_v, y_s; \mathcal{M}_{4a}^{mes}) &= (1 - y_q^2 y_r^2 y_u^2 y_v^2 y_s^2 \ t_1^2 t_2^2 t_3^2 t_4^2)^2 \\ &\times \frac{1}{(1 - y_q^2 y_u y_v y_s \ t_1^2 t_2^2)(1 - y_q y_r y_u^2 y_s \ t_1^2 t_3^2)(1 - y_q y_r y_v^2 y_s \ t_2^2 t_4^2)} \\ &\times \frac{1}{(1 - y_r^2 y_u y_v y_s \ t_3^2 t_4^2)(1 - y_q y_r y_u y_v y_s \ t_1 t_2 t_3 t_4)} \ . \end{aligned} \tag{6.3}$$

The plethystic logarithm of the mesonic Hilbert series is

$$\begin{aligned} PL[g_1(t_\alpha, y_q, y_r, y_u, y_v, y_s; \mathcal{M}_{4a}^{mes})] &= y_q y_r y_u y_v y_s \ t_1 t_2 t_3 t_4 + y_q^2 y_u y_v y_s \ t_1^2 t_2^2 + y_r^2 y_u y_v y_s \ t_3^2 t_4^2 \\ &+ y_q y_r y_v^2 y_s \ t_2^2 t_4^2 + y_q y_r y_u^2 y_s \ t_1^2 t_3^2 - 2 \ y_q^2 y_r^2 y_u^2 y_v^2 y_s^2 \ t_1^2 t_2^2 t_3^2 t_4^2 \ . \end{aligned} \tag{6.4}$$

The finite plethystic logarithm indicates that the mesonic moduli space is a complete intersection.

With the fugacity map

$$f_1 = \frac{y_q\ t_1 t_2}{y_r\ t_3 t_4}\ ,\ f_2 = \frac{y_v\ t_2 t_4}{y_u\ t_1 t_3}\ ,\ t = y_q^{1/4} y_r^{1/4} y_u^{1/4} y_v^{1/4} y_s^{1/4}\ t_1^{1/4} t_2^{1/4} t_3^{1/4} t_4^{1/4}\ , \tag{6.5}$$

where the fugacities f_1, f_2 and t count mesonic charges, the Hilbert series becomes

$$g_1(t, f_1, f_2; \mathcal{M}_{4a}^{mes}) = \frac{(1-t^8)^2}{(1-t^4)(1-\frac{1}{f_1}t^4)(1-f_1 t^4)(1-\frac{1}{f_2}t^4)(1-f_2 t^4)}\ . \tag{6.6}$$

The corresponding plethystic logarithm is

$$PL[g_1(t, f_1, f_2; \mathcal{M}_{4a}^{mes})] = \left(1 + f_1 + \frac{1}{f_1} + f_2 + \frac{1}{f_2}\right) t^4 - 2t^8\ . \tag{6.7}$$

The above plethystic logarithm identifies the moduli space generators with their mesonic charges. They are summarized in Table 14. The charge lattice of generators in Table 14 is the dual reflexive polygon of the toric diagram of Model 4a. The generators satisfy the following relations

$$A_1 A_2 = B_1 B_2 = C^2\ . \tag{6.8}$$

Generator	$U(1)_{f_1}$	$U(1)_{f_2}$
$A_1 = p_1^2 p_3^2\ q\ r\ u^2\ s$	0	-1
$A_2 = p_2^2 p_4^2\ q\ r\ v^2\ s$	0	1
$B_1 = p_1^2 p_2^2\ q^2\ u\ v\ s$	1	0
$B_2 = p_3^2 p_4^2\ r^2\ u\ v\ s$	-1	0
$C = p_1 p_2 p_3 p_4\ q\ r\ u\ v\ s$	0	0

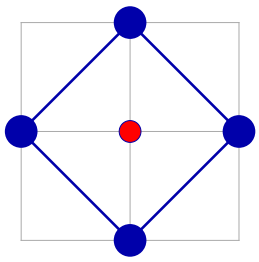


Table 14. The generators and lattice of generators of the mesonic moduli space of Model 4a in terms of GLSM fields with the corresponding flavor charges.

Generator	$U(1)_{f_1}$	$U(1)_{f_2}$
$X_{16}X_{67}X_{74}X_{41} = X_{23}X_{38}X_{85}X_{52}$	0	-1
$X_{12}X_{23}X_{34}X_{41} = X_{56}X_{67}X_{78}X_{85}$	1	0
$X_{12}X_{23}X_{38}X_{81} = X_{12}X_{27}X_{74}X_{41} = X_{16}X_{63}X_{34}X_{41} = X_{16}X_{67}X_{78}X_{81} = X_{23}X_{34}X_{45}X_{52} = X_{27}X_{78}X_{85}X_{52} = X_{38}X_{85}X_{56}X_{63} = X_{45}X_{56}X_{67}X_{74}$	0	0
$X_{16}X_{63}X_{38}X_{81} = X_{27}X_{74}X_{45}X_{52}$	-1	0
$X_{12}X_{27}X_{78}X_{81} = X_{34}X_{45}X_{56}X_{63}$	0	1

Table 15. The generators in terms of bifundamental fields (Model 4a).

The fugacities

$$T_1 = \frac{y_r^2 y_u^2 y_s\ t_1 t_3^3 t_4}{t_2} = \frac{t^4}{f_1 f_2}\ ,\ T_2 = \frac{y_q\ t_1 t_2}{y_r\ t_3 t_4} = f_1\ ,\ T_3 = \frac{y_v\ t_2 t_4}{y_u\ t_1 t_3} = f_2\ , \tag{6.9}$$

can be introduced to rewrite the Hilbert series and plethystic logarithm as

$$g_1(T_1, T_2, T_3; \mathcal{M}_{4a}^{mes}) = \frac{(1 - T_1^2 T_2^2 T_3^2)^2}{(1 - T_1 T_2 T_3)(1 - T_1 T_3)(1 - T_1 T_2^2 T_3)(1 - T_1 T_2)(1 - T_1 T_2 T_3^2)} \tag{6.10}$$

and

$$PL[g_1(T_1, T_2, T_3; \mathcal{M}_{4a}^{mes})] = T_1 T_2 T_3 + T_1 T_2^2 T_3 + T_1 T_3 + T_1 T_2 T_3^2 + T_1 T_2 - T_1^2 T_2^2 T_3^2 \tag{6.11}$$

such that powers of the fugacities in the expressions are positive. This illustrates the cone structure of the variety.

6.2 Model 4 Phase b

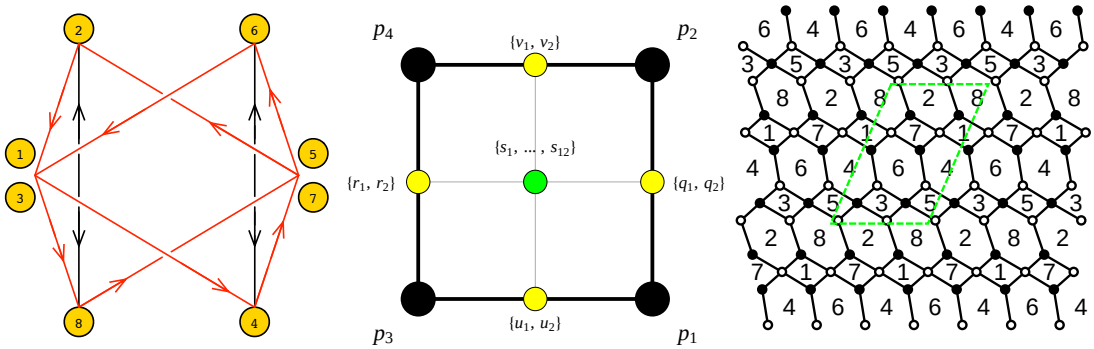


Figure 9. The quiver, toric diagram, and brane tiling of Model 4b. The red arrows in the quiver indicate all possible connections between blocks of nodes.

The superpotential is

$$\begin{aligned} W = &+X_{23}X_{38}X_{82} + X_{45}X_{56}X_{64} + X_{63}X_{34}X_{46} + X_{85}X_{52}X_{28} + X_{21}X_{14}X_{47}X_{72} + X_{61}X_{18}X_{87}X_{76} \\ &-X_{21}X_{18}X_{82} - X_{47}X_{76}X_{64} - X_{87}X_{72}X_{28} - X_{61}X_{14}X_{46} - X_{45}X_{52}X_{23}X_{34} - X_{63}X_{38}X_{85}X_{56} \end{aligned} \tag{6.12}$$

The perfect matching matrix is

$P =$

	p_1	p_2	p_3	p_4	q_1	q_2	r_2		u_1	u_2	v_1	v_2	s_1	s_2	s_3	s_4	s_5	s_6	s_7	s_8	s_9	s_{10}	s_{11}	s_{12}
X_{61}	1	0	0	0	1	0	0	0	1	0	0	0	1	0	1	0	1	0	0	0	0	0	0	0
X_{47}	1	0	0	0	1	0	0	0	0	1	0	0	0	1	0	1	0	1	0	0	0	0	0	0
X_{34}	1	0	0	0	0	1	0	0	1	0	0	0	1	0	0	0	0	0	1	0	1	0	0	0
X_{56}	1	0	0	0	0	1	0	0	0	1	0	0	0	1	0	0	0	0	0	1	0	1	0	0
X_{63}	0	1	0	0	1	0	0	0	0	0	1	0	0	0	1	0	1	0	0	0	0	0	1	0
X_{45}	0	1	0	0	1	0	0	0	0	0	0	1	0	0	0	1	0	1	0	0	0	0	0	1
X_{14}	0	1	0	0	0	1	0	0	0	0	1	0	0	0	0	0	0	0	1	0	1	0	1	0
X_{76}	0	1	0	0	0	1	0	0	0	0	0	1	0	0	0	0	0	0	0	1	0	1	0	1
X_{85}	0	0	1	0	0	0	1	0	1	0	0	0	0	0	0	0	0	1	0	0	1	0	0	1
X_{23}	0	0	1	0	0	0	1	0	0	1	0	0	0	0	0	0	1	0	0	0	0	1	1	0
X_{72}	0	0	1	0	0	0	0	1	1	0	0	0	0	0	1	0	0	0	0	1	0	0	0	1
X_{18}	0	0	1	0	0	0	0	1	0	1	0	0	0	0	0	1	0	0	1	0	0	0	1	0
X_{87}	0	0	0	1	0	0	1	0	0	0	1	0	0	1	0	0	0	1	0	0	1	0	0	0
X_{21}	0	0	0	1	0	0	1	0	0	0	0	1	1	0	0	0	1	0	0	0	0	1	0	0
X_{52}	0	0	0	1	0	0	0	1	0	0	1	0	0	1	1	0	0	0	0	1	0	0	0	0
X_{38}	0	0	0	1	0	0	0	1	0	0	0	1	1	0	0	1	0	0	1	0	0	0	0	0
X_{82}	1	1	0	0	1	1	0	0	1	0	1	0	0	1	1	0	0	1	0	1	1	0	0	1
X_{28}	1	1	0	0	1	1	0	0	0	1	0	1	1	0	0	1	1	0	1	0	0	1	1	0
X_{64}	0	0	1	1	0	0	1	1	1	0	1	0	1	0	1	0	1	0	1	0	1	0	1	0
X_{46}	0	0	1	1	0	0	1	1	0	1	0	1	0	1	0	1	0	1	0	1	0	1	0	1

The F-term charge matrix $Q_F = \ker(P)$ is

$Q_F =$

p_1	p_2	p_3	p_4	q_1	q_2	r_1	r_2	u_1	u_2	v_1	v_2	s_1	s_2	s_3	s_4	s_5	s_6	s_7	s_8	s_9	s_{10}	s_{11}	s_{12}
1	1	0	0	−1	−1	0	0	0	0	0	0	0	0	0	0	0	0	0	0	0	0	0	0
0	0	1	1	0	0	−1	−1	0	0	0	0	0	0	0	0	0	0	0	0	0	0	0	0
1	0	1	0	0	0	0	0	−1	−1	0	0	0	0	0	0	0	0	0	0	0	0	0	0
0	1	0	1	0	0	0	0	0	0	−1	−1	0	0	0	0	0	0	0	0	0	0	0	0
1	0	0	1	0	0	0	0	0	0	0	0	−1	−1	0	0	0	0	0	0	0	0	0	0
0	0	0	0	1	0	0	1	0	0	0	0	0	0	−1	−1	0	0	0	0	0	0	0	0
0	0	0	0	1	0	1	0	0	0	0	0	0	0	0	0	−1	−1	0	0	0	0	0	0
0	0	0	0	0	0	0	0	1	0	1	0	0	0	−1	0	0	0	0	0	−1	0	0	0
0	0	0	0	0	0	0	0	1	0	0	1	−1	0	0	0	0	0	0	0	0	0	0	−1
0	0	1	0	0	0	−1	0	0	0	1	0	0	0	−1	0	1	0	0	0	0	0	−1	0
0	0	1	0	0	0	−1	0	0	0	1	0	1	0	−1	0	0	0	−1	0	0	0	0	0
0	0	0	1	0	1	0	0	0	0	−1	0	−1	0	1	0	0	0	0	−1	0	0	0	0
0	0	0	1	0	0	−1	0	1	0	0	0	−1	0	−1	0	1	0	0	0	0	0	0	0
0	0	0	0	0	0	0	0	0	0	0	0	0	0	1	0	−1	0	0	−1	0	1	0	0

The D-term charge matrix is

$$Q_D = \left(\begin{array}{cccc|cc|cc|cc|cc|cccccccccc} p_1 & p_2 & p_3 & p_4 & q_1 & q_2 & r_1 & r_2 & u_1 & u_2 & v_1 & v_2 & s_1 & s_2 & s_3 & s_4 & s_5 & s_6 & s_7 & s_8 & s_9 & s_{10} & s_{11} & s_{12} \\ \hline 0 & 0 & 0 & 0 & 0 & 0 & 0 & 0 & 0 & 0 & 0 & 0 & 0 & 0 & 0 & 0 & 1 & -1 & 0 & 0 & 0 & 0 & 0 & 0 \\ 0 & 0 & 0 & 0 & 0 & 0 & 0 & 0 & 0 & 0 & 0 & 0 & 0 & 0 & 0 & 0 & 0 & 1 & -1 & 0 & 0 & 0 & 0 & 0 \\ 0 & 0 & 0 & 0 & 0 & 0 & 0 & 0 & 0 & 0 & 0 & 0 & 0 & 0 & 0 & 0 & 0 & 0 & 1 & -1 & 0 & 0 & 0 & 0 \\ 0 & 0 & 0 & 0 & 0 & 0 & 0 & 0 & 0 & 0 & 0 & 0 & 0 & 0 & 0 & 0 & 0 & 0 & 0 & 1 & -1 & 0 & 0 & 0 \\ 0 & 0 & 0 & 0 & 0 & 0 & 0 & 0 & 0 & 0 & 0 & 0 & 0 & 0 & 0 & 0 & 0 & 0 & 0 & 0 & 1 & -1 & 0 & 0 \\ 0 & 0 & 0 & 0 & 0 & 0 & 0 & 0 & 0 & 0 & 0 & 0 & 0 & 0 & 0 & 0 & 0 & 0 & 0 & 0 & 0 & 1 & -1 & 0 \\ 0 & 0 & 0 & 0 & 0 & 0 & 0 & 0 & 0 & 0 & 0 & 0 & 0 & 0 & 0 & 0 & 0 & 0 & 0 & 0 & 0 & 0 & 1 & -1 \end{array}\right)$$

The total charge matrix Q_t does not have repeated columns. Accordingly, the global symmetry is $U(1)_{f_1} \times U(1)_{f_2} \times U(1)_R$. This is the same global symmetry as for Model 4a, and the same mesonic charges on extremal perfect matchings are assigned as for Model 4a, as shown in Table 13.

Let products of non-extremal perfect matchings be associated to a single variable as follows

$$q = q_1 q_2 \ , \ r = r_1 r_2 \ , \ u = u_1 u_2 \ , \ v = v_1 v_2 \ , \ s = \prod_{m=1}^{12} s_m \ . \tag{6.13}$$

The extremal perfect matchings p_α are counted by t_α. The fugacity of the form y_q counts the non-extremal perfect matching product q above.

The refined mesonic Hilbert series is calculated using the Molien integral formula in (2.9). The Hilbert series and the corresponding plethystic logarithm turn out to be the same as for Model 4a. The mesonic Hilbert series and the refined plethystic logarithms are given in (6.3), (6.4) and (6.7). Accordingly, the mesonic moduli spaces of Model 4a and 4b are the same, with the corresponding quiver gauge theories being toric dual.

The generators in terms of perfect matchings of Model 4b are given in Table 14 with the correspoding mesonic symmetry charges. The corresponding generators in terms of quiver fields are shown in Table 16. The mesonic moduli space is a complete intersection, with the generators satisfying the relations in (6.8).

Generator	$U(1)_{f_1}$	$U(1)_{f_2}$
$X_{56}X_{18}X_{85}X_{61} = X_{23}X_{34}X_{47}X_{72}$	0	-1
$X_{28}X_{82} = X_{14}X_{45}X_{56}X_{61} = X_{14}X_{47}X_{76}X_{61} = X_{34}X_{45}X_{56}X_{63} = X_{34}X_{47}X_{76}X_{63}$	1	0
$X_{21}X_{14}X_{47}X_{72} = X_{61}X_{18}X_{87}X_{76} = X_{23}X_{34}X_{45}X_{52} = X_{56}X_{38}X_{85}X_{63} = X_{14}X_{46}X_{61} = X_{21}X_{18}X_{82}$ $= X_{23}X_{38}X_{82} = X_{52}X_{28}X_{85} = X_{72}X_{28}X_{87} = X_{34}X_{46}X_{63} = X_{45}X_{56}X_{64} = X_{64}X_{47}X_{76}$	0	0
$X_{46}X_{64} = X_{21}X_{18}X_{85}X_{52} = X_{21}X_{18}X_{87}X_{72} = X_{23}X_{38}X_{85}X_{52} = X_{23}X_{38}X_{87}X_{72}$	-1	0
$X_{21}X_{14}X_{45}X_{52} = X_{63}X_{38}X_{87}X_{76}$	0	1

Table 16. The generators in terms of bifundamental fields (Model 4b).

6.3 Model 4 Phase c

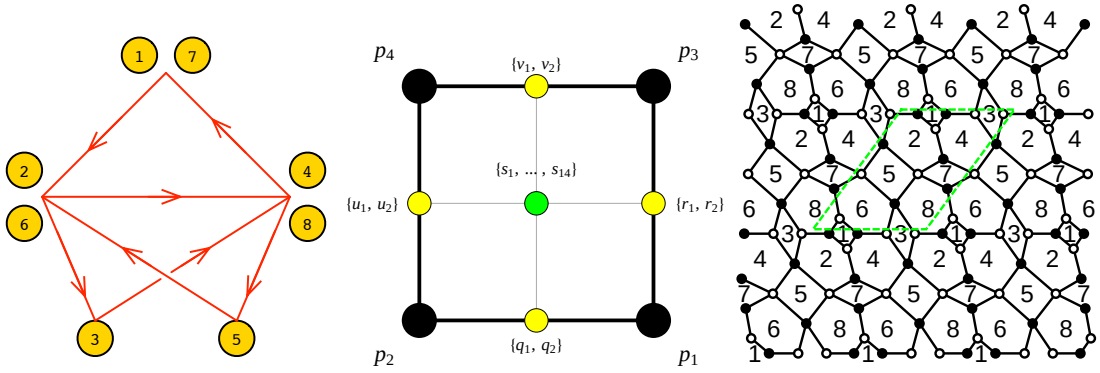


Figure 10. The quiver, toric diagram, and brane tiling of Model 4c. The red arrows in the quiver indicate all possible connections between blocks of nodes.

The superpotential is

$$\begin{aligned} W = &+X_{21}X_{14}X_{42} + X_{23}X_{38}X_{82} + X_{61}X_{18}X_{86} + X_{63}X_{34}X_{46} + X_{67}X_{74}X_{45}X_{56} + X_{85}X_{52}X_{27}X_{78} \\ &-X_{21}X_{18}X_{82} - X_{27}X_{74}X_{42} - X_{61}X_{14}X_{46} - X_{67}X_{78}X_{86} - X_{45}X_{52}X_{23}X_{34} - X_{63}X_{38}X_{85}X_{56} \end{aligned} \tag{6.14}$$

The perfect matching matrix is

$P =$

	p_1	p_2	p_3	p_4	q_1	q_2	r_1	r_2	u_1	u_2	v_1	v_2	s_1	s_2	s_3	s_4	s_5	s_6	s_7	s_8	s_9	s_{10}	s_{11}	s_{12}	s_{13}	s_{14}
X_{61}	1	0	0	0	1	0	1	0	0	0	0	0	0	0	1	1	1	0	1	0	0	0	0	0	1	0
X_{78}	1	0	0	0	1	0	0	1	0	0	0	0	0	0	0	0	1	1	0	0	1	0	1	0	1	0
X_{34}	1	0	0	0	0	1	1	0	0	0	0	0	0	0	1	0	0	1	0	0	0	1	0	1	1	0
X_{56}	1	0	0	0	0	1	0	1	0	0	0	0	1	0	0	0	0	0	0	1	0	0	0	0	0	0
X_{45}	0	1	0	0	1	0	0	0	1	0	0	0	0	1	0	0	0	0	0	0	0	0	1	0	0	0
X_{63}	0	1	0	0	1	0	0	0	0	1	0	0	0	0	0	1	1	0	1	0	1	0	0	0	0	1
X_{27}	0	1	0	0	0	1	0	0	1	0	0	0	0	0	1	1	0	0	0	1	0	1	0	0	0	1
X_{14}	0	1	0	0	0	1	0	0	0	1	0	0	0	0	0	0	0	1	0	0	1	1	0	1	0	1
X_{67}	0	0	1	0	0	0	1	0	0	0	1	0	0	0	1	1	0	0	1	0	0	1	0	0	0	1
X_{85}	0	0	1	0	0	0	1	0	0	0	0	1	0	1	0	0	0	0	0	0	0	0	0	1	0	0
X_{18}	0	0	1	0	0	0	0	1	0	0	1	0	0	0	0	0	0	1	0	0	1	1	1	0	0	1
X_{23}	0	0	1	0	0	0	0	1	0	0	0	1	0	0	0	1	1	0	0	1	1	0	0	0	0	1
X_{38}	0	0	0	1	0	0	0	0	1	0	1	0	0	0	1	0	0	1	0	0	0	1	1	0	1	0
X_{21}	0	0	0	1	0	0	0	0	1	0	0	1	0	0	1	1	1	0	0	1	0	0	0	0	1	0
X_{52}	0	0	0	1	0	0	0	0	0	1	1	0	1	0	0	0	0	0	1	0	0	0	0	0	0	0
X_{74}	0	0	0	1	0	0	0	0	0	1	0	1	0	0	0	0	1	1	0	0	1	0	0	1	1	0
X_{82}	1	1	0	0	1	1	1	0	0	1	0	0	1	1	0	0	0	0	1	0	0	0	0	1	0	0
X_{42}	1	0	1	0	1	0	1	1	0	0	1	0	1	1	0	0	0	0	1	0	0	0	1	0	0	0
X_{86}	0	1	0	1	0	1	0	0	1	1	0	1	1	1	0	0	0	0	0	1	0	0	0	1	0	0
X_{46}	0	0	1	1	0	0	0	1	1	0	1	1	1	1	0	0	0	0	0	1	0	0	1	0	0	0

The F-term charge matrix $Q_F = \ker(P)$ is

$$Q_F = \left(\begin{array}{cccc|cc|cc|cc|cc|cccccccccccc} p_1 & p_2 & p_3 & p_4 & q_1 & q_2 & r_1 & r_2 & u_1 & u_2 & v_1 & v_2 & s_1 & s_2 & s_3 & s_4 & s_5 & s_6 & s_7 & s_8 & s_9 & s_{10} & s_{11} & s_{12} & s_{13} & s_{14} \\ \hline 1 & 1 & 0 & 0 & -1 & -1 & 0 & 0 & 0 & 0 & 0 & 0 & 0 & 0 & 0 & 0 & 0 & 0 & 0 & 0 & 0 & 0 & 0 & 0 & 0 & 0 \\ 1 & 0 & 1 & 0 & 0 & 0 & -1 & -1 & 0 & 0 & 0 & 0 & 0 & 0 & 0 & 0 & 0 & 0 & 0 & 0 & 0 & 0 & 0 & 0 & 0 & 0 \\ 0 & 1 & 0 & 1 & 0 & 0 & 0 & 0 & -1 & -1 & 0 & 0 & 0 & 0 & 0 & 0 & 0 & 0 & 0 & 0 & 0 & 0 & 0 & 0 & 0 & 0 \\ 0 & 0 & 1 & 1 & 0 & 0 & 0 & 0 & 0 & 0 & -1 & -1 & 0 & 0 & 0 & 0 & 0 & 0 & 0 & 0 & 0 & 0 & 0 & 0 & 0 & 0 \\ 1 & 0 & 0 & 1 & 0 & 0 & 0 & 0 & 0 & 0 & 0 & 0 & -1 & 0 & 0 & 0 & 0 & 0 & 0 & 0 & 0 & 0 & 0 & 0 & -1 & 0 \\ 0 & 1 & 1 & 0 & 0 & 0 & 0 & 0 & 0 & 0 & 0 & 0 & 0 & -1 & 0 & 0 & 0 & 0 & 0 & 0 & 0 & 0 & 0 & 0 & 0 & -1 \\ 1 & 0 & 0 & 0 & -1 & 0 & 0 & -1 & 0 & 0 & 0 & 0 & 0 & 0 & 0 & 0 & 0 & -1 & 0 & 0 & 1 & 0 & 1 & 0 & 0 & 0 \\ 1 & 0 & 0 & 0 & -1 & 0 & -1 & 0 & 0 & 0 & 0 & 0 & 0 & 1 & 0 & 1 & 0 & 0 & 0 & -1 & 0 & 0 & 0 & 0 & 0 & 0 \\ 0 & 0 & 1 & 0 & 1 & 0 & -1 & 0 & 0 & 0 & 0 & 0 & 0 & -1 & 0 & 0 & 0 & 0 & 0 & 0 & -1 & 0 & 0 & 1 & 0 & 0 \\ 0 & 0 & 1 & 0 & 0 & 0 & 0 & 0 & 1 & 0 & -1 & 0 & 1 & -1 & 0 & 0 & 0 & 0 & 0 & -1 & 0 & 0 & 0 & 0 & 0 & 0 \\ 0 & 0 & 0 & 0 & 1 & 0 & 0 & 0 & 0 & 0 & 1 & 0 & 0 & 0 & 0 & 0 & 0 & 0 & -1 & 0 & 0 & 0 & -1 & 0 & 0 & 0 \\ 0 & 0 & 0 & 0 & 1 & 0 & 0 & 0 & 0 & 0 & 0 & 1 & 0 & -1 & 0 & 0 & -1 & 0 & 0 & 0 & 0 & 0 & 0 & 0 & 0 & 0 \\ 0 & 0 & 0 & 0 & 0 & 1 & 0 & 0 & 0 & 0 & 1 & 0 & -1 & 0 & 0 & 0 & 0 & 0 & 0 & 0 & 0 & -1 & 0 & 0 & 0 & 0 \\ 0 & 0 & 0 & 0 & 0 & 0 & 1 & 0 & 1 & 0 & 0 & 0 & 0 & -1 & -1 & 0 & 0 & 0 & 0 & 0 & 0 & 0 & 0 & 0 & 0 & 0 \\ 0 & 0 & 0 & 0 & 0 & 0 & 0 & 1 & 0 & 1 & 0 & 0 & -1 & 0 & 0 & 0 & 0 & 0 & 0 & 0 & -1 & 0 & 0 & 0 & 0 & 0 \\ 0 & 0 & 0 & 0 & 0 & 0 & 0 & 0 & 0 & 0 & 0 & 0 & 1 & 0 & 0 & 1 & 0 & 0 & -1 & -1 & 0 & 0 & 0 & 0 & 0 & 0 \end{array}\right)$$

The D-term charge matrix is

$$Q_D = \left(\begin{array}{cccc|cc|cc|cc|cc|cccccccccccc} p_1 & p_2 & p_3 & p_4 & q_1 & q_2 & r_1 & r_2 & u_1 & u_2 & v_1 & v_2 & s_1 & s_2 & s_3 & s_4 & s_5 & s_6 & s_7 & s_8 & s_9 & s_{10} & s_{11} & s_{12} & s_{13} & s_{14} \\ \hline 0 & 0 & 0 & 0 & 0 & 0 & 0 & 0 & 0 & 0 & 0 & 0 & 0 & 0 & 0 & 0 & 0 & 0 & 1 & -1 & 0 & 0 & 0 & 0 & 0 & 0 \\ 0 & 0 & 0 & 0 & 0 & 0 & 0 & 0 & 0 & 0 & 0 & 0 & 0 & 0 & 0 & 0 & 0 & 0 & 0 & 1 & -1 & 0 & 0 & 0 & 0 & 0 \\ 0 & 0 & 0 & 0 & 0 & 0 & 0 & 0 & 0 & 0 & 0 & 0 & 0 & 0 & 0 & 0 & 0 & 0 & 0 & 0 & 1 & -1 & 0 & 0 & 0 & 0 \\ 0 & 0 & 0 & 0 & 0 & 0 & 0 & 0 & 0 & 0 & 0 & 0 & 0 & 0 & 0 & 0 & 0 & 0 & 0 & 0 & 0 & 1 & -1 & 0 & 0 & 0 \\ 0 & 0 & 0 & 0 & 0 & 0 & 0 & 0 & 0 & 0 & 0 & 0 & 0 & 0 & 0 & 0 & 0 & 0 & 0 & 0 & 0 & 0 & 1 & -1 & 0 & 0 \\ 0 & 0 & 0 & 0 & 0 & 0 & 0 & 0 & 0 & 0 & 0 & 0 & 0 & 0 & 0 & 0 & 0 & 0 & 0 & 0 & 0 & 0 & 0 & 1 & -1 & 0 \\ 0 & 0 & 0 & 0 & 0 & 0 & 0 & 0 & 0 & 0 & 0 & 0 & 0 & 0 & 0 & 0 & 0 & 0 & 0 & 0 & 0 & 0 & 0 & 0 & 1 & -1 \end{array}\right)$$

The global symmetry is $U(1)_{f_1} \times U(1)_{f_2} \times U(1)_R$. The global symmetry charge assignment on the GLSM fields with non-zero R-charges is the same as for Model 4a and is shown Table 13.

Products of non-extremal perfect matchings are labelled in terms of single variables as follows

$$q = q_1 q_2 \ , \ r = r_1 r_2 \ , \ u = u_1 u_2 \ , \ v = v_1 v_2 \ , \ s = \prod_{m=1}^{14} s_m \ . \tag{6.15}$$

The fugacity which counts GLSM fields corresponding to extremal perfect matchings p_α is t_α. A product non-extremal perfect matchings, for instance q, is assigned a fugacity of the form y_q.

The mesonic Hilbert series and plethystic logarithm for Model 4c is the same form as for Model 4a. They are given respectively in (6.3), (6.4) and (6.7). Accordingly, the mesonic moduli space of Model 4c is the same as for Model 4a. In other words they are toric (Seiberg) duals.

The generators in terms of the perfect matching variables of Model 4c are given in Table 14 with their mesonic charges. The generators in terms of quiver fields are given in Table 17. The mesonic moduli space is a complete intersection and the generators satisfy the relations given in (6.8).

Generator	$U(1)_{f_1}$	$U(1)_{f_2}$
$X_{27}X_{78}X_{82} = X_{14}X_{45}X_{56}X_{61} = X_{34}X_{45}X_{56}X_{63}$	0	-1
$X_{23}X_{34}X_{42} = X_{56}X_{18}X_{85}X_{61} = X_{56}X_{67}X_{78}X_{85}$	1	0
$X_{23}X_{34}X_{45}X_{52} = X_{52}X_{27}X_{78}X_{85} = X_{56}X_{38}X_{85}X_{63} = X_{45}X_{56}X_{67}X_{74} = X_{21}X_{14}X_{42} = X_{14}X_{46}X_{61}$ $= X_{21}X_{18}X_{82} = X_{61}X_{18}X_{86} = X_{23}X_{38}X_{82} = X_{42}X_{27}X_{74} = X_{34}X_{46}X_{63} = X_{67}X_{78}X_{86}$	0	0
$X_{63}X_{38}X_{86} = X_{21}X_{14}X_{45}X_{52} = X_{45}X_{27}X_{74}X_{52}$	-1	0
$X_{46}X_{67}X_{74} = X_{21}X_{18}X_{85}X_{52} = X_{23}X_{38}X_{85}X_{52}$	0	1

Table 17. The generators in terms of bifundamental fields (Model 4c).

6.4 Model 4 Phase d

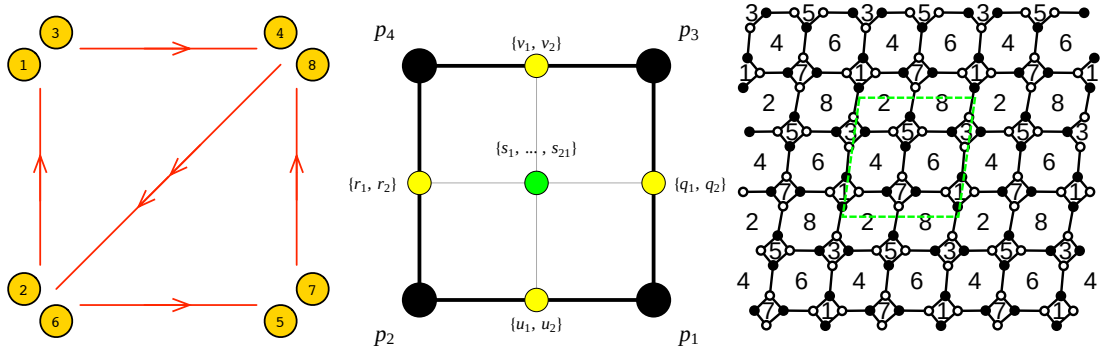


Figure 11. The quiver, toric diagram, and brane tiling of Model 4d. The red arrows in the quiver indicate all possible connections between blocks of nodes.

The superpotential is

$$\begin{aligned} W = &+X_{21}X_{14}X^1_{42} + X_{23}X_{38}X^1_{82} + X_{25}X_{54}X^2_{42} + X_{27}X_{78}X^2_{82} \\ &+X_{61}X_{18}X^1_{86} + X_{63}X_{34}X^1_{46} + X_{65}X_{58}X^2_{86} + X_{67}X_{74}X^2_{46} \\ &-X_{21}X_{18}X^1_{82} - X_{23}X_{34}X^2_{42} - X_{25}X_{58}X^2_{82} - X_{27}X_{74}X^1_{42} \\ &-X_{61}X_{14}X^1_{46} - X_{63}X_{38}X^2_{86} - X_{65}X_{54}X^2_{46} - X_{67}X_{78}X^1_{86} \end{aligned} \tag{6.16}$$

The perfect matching matrix is

$P =$

	p_1	p_2	p_3	p_4	q_1	q_2	r_1	r_2	u_1	u_2	v_1	v_2	s_1	s_2	s_3	s_4	s_5	s_6	s_7	s_8	s_9	s_{10}	s_{11}	s_{12}	s_{13}	s_{14}	s_{15}	s_{16}	s_{17}	s_{18}	s_{19}	s_{20}	s_{21}
X_{42}^1	1	1	0	0	1	0	1	0	1	1	0	0	0	0	0	0	0	0	0	0	0	0	1	0	1	0	0	0	0	0	0	0	1
X_{86}	1	1	0	0	0	1	0	1	1	1	0	0	0	0	0	0	0	0	0	0	0	0	0	1	1	1	0	0	0	0	0	0	0
X_{46}^1	1	0	1	0	1	1	0	0	1	0	1	0	0	0	0	0	0	0	0	0	0	0	0	1	1	0	0	0	0	0	0	0	1
X_{82}	1	0	1	0	1	1	0	0	0	1	0	1	0	0	0	0	0	0	0	0	0	0	1	0	1	1	0	0	0	0	0	0	0
X_{58}	1	0	0	0	1	0	0	0	1	0	0	0	1	1	1	1	1	0	0	0	0	1	0	0	0	0	1	1	0	0	0	0	1
X_{63}	1	0	0	0	1	0	0	0	0	1	0	0	0	0	0	1	1	0	0	1	1	0	1	0	0	0	1	1	0	0	1	1	0
X_{27}	1	0	0	0	0	1	0	0	1	0	0	0	1	0	0	0	0	0	0	0	0	1	0	1	0	0	1	1	1	1	1	1	0
X_{14}	1	0	0	0	0	1	0	0	0	1	0	0	1	1	0	1	0	1	0	1	0	0	0	0	0	1	1	0	1	0	1	0	0
X_{46}	0	1	0	1	0	0	1	1	1	0	1	0	0	0	0	0	0	0	0	0	0	0	0	1	1	0	0	0	0	0	0	0	1
X_{82}^1	0	1	0	1	0	0	1	1	0	1	0	1	0	0	0	0	0	0	0	0	0	0	1	0	1	1	0	0	0	0	0	0	0
X_{38}	0	1	0	0	0	0	1	0	1	0	0	0	1	1	1	0	0	1	1	0	0	1	0	0	0	0	0	0	1	1	0	0	1
X_{65}	0	1	0	0	0	0	1	0	0	1	0	0	0	0	0	0	0	1	1	1	1	0	1	0	0	0	0	0	1	1	1	1	0
X_{21}	0	1	0	0	0	0	0	1	1	0	0	0	0	0	1	0	1	0	1	0	1	1	0	1	0	0	0	1	0	1	0	1	0
X_{74}	0	1	0	0	0	0	0	1	0	1	0	0	0	1	1	1	1	1	1	1	1	0	0	0	0	1	0	0	0	0	0	0	0
X_{42}	0	0	1	1	1	0	1	0	0	0	1	1	0	0	0	0	0	0	0	0	0	0	1	0	1	0	0	0	0	0	0	0	1
X_{86}^1	0	0	1	1	0	1	0	1	0	0	1	1	0	0	0	0	0	0	0	0	0	0	0	1	1	1	0	0	0	0	0	0	0
X_{78}	0	0	1	0	1	0	0	0	0	0	1	0	0	1	1	1	1	1	1	1	1	0	0	0	0	0	0	0	0	0	0	0	1
X_{61}	0	0	1	0	1	0	0	0	0	0	0	1	0	0	1	0	1	0	1	0	1	1	1	0	0	0	0	1	0	1	0	1	0
X_{25}	0	0	1	0	0	1	0	0	0	0	1	0	0	0	0	0	0	1	1	1	1	0	0	1	0	0	0	0	1	1	1	1	0
X_{34}	0	0	1	0	0	1	0	0	0	0	0	1	1	1	1	0	0	1	1	0	0	1	0	0	0	1	0	0	1	1	0	0	0
X_{18}	0	0	0	1	0	0	1	0	0	0	1	0	1	1	0	1	0	1	0	1	0	0	0	0	0	0	1	0	1	0	1	0	1
X_{67}	0	0	0	1	0	0	1	0	0	0	0	1	1	0	0	0	0	0	0	0	0	1	1	0	0	0	1	1	1	1	1	1	0
X_{23}	0	0	0	1	0	0	0	1	0	0	1	0	0	0	0	1	1	0	0	1	1	0	0	1	0	0	1	1	0	0	1	1	0
X_{54}	0	0	0	1	0	0	0	1	0	0	0	1	1	1	1	1	1	0	0	0	0	1	0	0	0	1	1	1	0	0	0	0	0

The F-term charge matrix $Q_F = \ker(P)$ is

$Q_F =$

p_1	p_2	p_3	p_4	q_1	q_2	r_1	r_2	u_1	u_2	v_1	v_2	s_1	s_2	s_3	s_4	s_5	s_6	s_7	s_8	s_9	s_{10}	s_{11}	s_{12}	s_{13}	s_{14}	s_{15}	s_{16}	s_{17}	s_{18}	s_{19}	s_{20}	s_{21}
1	0	1	0	−1	−1	0	0	0	0	0	0	0	0	0	0	0	0	0	0	0	0	0	0	0	0	0	0	0	0	0	0	0
0	1	0	1	0	0	−1	−1	0	0	0	0	0	0	0	0	0	0	0	0	0	0	0	0	0	0	0	0	0	0	0	0	0
1	1	0	0	0	0	0	0	−1	−1	0	0	0	0	0	0	0	0	0	0	0	0	0	0	0	0	0	0	0	0	0	0	0
0	0	1	1	0	0	0	0	0	0	−1	−1	0	0	0	0	0	0	0	0	0	0	0	0	0	0	0	0	0	0	0	0	0
0	0	0	1	0	1	0	0	0	0	−1	0	−1	0	0	0	0	0	0	0	0	0	0	0	−1	0	0	0	0	0	0	0	1
0	0	0	0	0	0	0	0	0	0	0	0	1	−1	1	0	0	0	0	0	0	−1	0	0	0	0	0	0	0	0	0	0	0
0	0	0	0	0	0	0	0	0	0	0	0	0	1	0	0	0	0	0	0	0	0	0	0	1	−1	0	0	0	0	0	0	−1
0	0	0	0	0	0	0	0	0	0	0	0	0	0	1	−1	0	0	0	0	0	−1	0	0	0	0	1	0	0	0	0	0	0
0	0	0	0	0	0	0	0	0	0	0	0	0	0	0	1	−1	−1	1	0	0	0	0	0	0	0	0	0	0	0	0	0	0
0	0	0	0	0	0	0	0	0	0	0	0	0	0	0	1	−1	0	0	−1	1	0	0	0	0	0	0	0	0	0	0	0	0
0	0	0	0	0	0	0	0	0	0	0	0	0	0	0	1	−1	0	0	0	0	0	0	0	0	0	−1	1	0	0	0	0	0
0	0	0	0	0	0	0	0	0	0	0	0	0	0	0	0	1	−1	0	0	0	0	0	0	0	0	0	−1	1	0	0	0	0
0	0	0	0	0	0	0	0	0	0	0	0	0	0	0	0	0	1	−1	0	0	0	0	0	0	0	0	0	−1	1	0	0	0
0	0	0	0	0	0	0	0	0	0	0	0	0	0	0	0	0	0	1	−1	0	0	0	0	0	0	0	0	0	−1	1	0	0
0	0	0	0	0	0	0	0	0	0	0	0	0	0	0	0	0	0	0	1	−1	0	0	0	0	0	0	0	0	0	−1	1	0
1	0	0	0	0	0	1	0	−1	0	0	0	0	0	0	−1	1	0	0	0	0	0	−1	0	0	0	0	0	0	0	0	0	0
0	1	0	0	1	0	0	0	−1	0	0	0	1	−1	0	0	0	0	0	0	0	0	−1	0	0	0	0	0	0	0	0	0	0
1	−1	0	0	−1	0	1	0	0	0	0	0	−1	0	1	0	0	0	0	0	0	0	0	0	0	0	0	0	0	0	0	0	0
1	0	−1	0	0	0	0	0	−1	0	1	0	0	0	0	0	0	0	1	−1	0	0	0	0	0	0	0	0	0	0	0	0	0
0	1	0	0	0	0	−1	0	−1	0	0	0	1	0	0	0	0	0	0	0	0	0	0	0	1	−1	0	0	0	0	0	0	0
0	0	1	0	0	0	1	0	0	0	−1	0	0	−1	0	1	0	0	0	0	0	0	−1	0	0	0	0	0	0	0	0	0	0
0	0	0	1	1	0	0	0	0	0	−1	0	0	−1	0	0	0	1	0	0	0	0	−1	0	0	0	0	0	0	0	0	0	0
0	0	0	0	1	0	1	0	−1	0	−1	0	0	0	0	0	0	0	0	0	0	0	−1	1	0	0	0	0	0	0	0	0	0

The D-term charge matrix is

$$Q_D = \left(\begin{array}{cccc|cc|cc|cc|cc|ccccccccccccccccccc} p_1 & p_2 & p_3 & p_4 & q_1 & q_2 & r_1 & r_2 & u_1 & u_2 & v_1 & v_2 & s_1 & s_2 & s_3 & s_4 & s_5 & s_6 & s_7 & s_8 & s_9 & s_{10} & s_{11} & s_{12} & s_{13} & s_{14} & s_{15} & s_{16} & s_{17} & s_{18} & s_{19} & s_{20} & s_{21} \\ \hline 0&0&0&0&0&0&0&0&0&0&0&0&0&0&0&0&0&0&0&0&1&-1&0&0&0&0&0&0&0&0&0&0&0 \\ 0&0&0&0&0&0&0&0&0&0&0&0&0&0&0&0&0&0&0&0&0&0&1&-1&0&0&0&0&0&0&0&0&0 \\ 0&0&0&0&0&0&0&0&0&0&0&0&0&0&0&0&0&0&0&0&0&0&0&1&-1&0&0&0&0&0&0&0&0 \\ 0&0&0&0&0&0&0&0&0&0&0&0&0&0&0&0&0&0&0&0&0&0&0&0&1&-1&0&0&0&0&0&0&0 \\ 0&0&0&0&0&0&0&0&0&0&0&0&0&0&0&0&0&0&0&0&0&0&0&0&0&1&-1&0&0&0&0&0&0 \\ 0&0&0&0&0&0&0&0&0&0&0&0&0&0&0&0&0&0&0&0&0&0&0&0&0&0&1&-1&0&0&0&0&0 \\ 0&0&0&0&0&0&0&0&0&0&0&0&0&0&0&0&0&0&0&0&0&0&0&0&0&0&0&1&-1&0&0&0&0 \end{array}\right)$$

The global symmetry is $U(1)_{f_1} \times U(1)_{f_2} \times U(1)_R$. The global symmetry charge assignment on perfect matchings with non-zero R-charge is the same as for Model 4a and is shown in Table 13.

Products of non-extremal perfect matchings are expressed in terms of single variables as follows

$$q = q_1 q_2 \ , \ r = r_1 r_2 \ , \ u = u_1 u_2 \ , \ v = v_1 v_2 \ , \ s = \prod_{m=1}^{21} s_m \ . \tag{6.17}$$

The fugacity which counts extremal perfect matchings is t_α. A product of non-extremal perfect matchings such as q is assigned a fugacity of the form y_q.

The mesonic Hilbert series and the plethystic logarithm are the same as for Model 4a. The mesonic Hilbert series and the refined plethystic logarithms are given in (6.3), (6.4) and (6.7) respectively.

The mesonic moduli space generators in terms of perfect matching variables of Model 4d are given in Table 14. In terms of quiver fields, the generators with their mesonic charges are shown in Table 18. The mesonic moduli space is a complete intersection and the generators satisfy the relations in (6.8).

Generator	$U(1)_{f_1}$	$U(1)_{f_2}$
$X_{21}X_{14}X_{42}^2 = X_{42}^2X_{27}X_{74} = X_{63}X_{38}X_{86}^1 = X_{65}X_{58}X_{86}^1$	0	-1
$X_{14}X_{46}^2X_{61} = X_{25}X_{58}X_{82}^1 = X_{27}X_{78}X_{82}^1 = X_{34}X_{46}^2X_{63}$	1	0
$X_{21}X_{14}X_{42}^1 = X_{14}X_{46}^1X_{61} = X_{21}X_{18}X_{82}^1 = X_{61}X_{18}X_{86}^1 = X_{23}X_{34}X_{42}^2 = X_{23}X_{38}X_{82}^1$ $= X_{42}^2X_{25}X_{54} = X_{25}X_{58}X_{82}^2 = X_{42}^1X_{27}X_{74} = X_{27}X_{78}X_{82}^2 = X_{34}X_{46}^1X_{63} = X_{63}X_{38}X_{86}^2$ $= X_{54}X_{46}^2X_{65} = X_{46}^2X_{67}X_{74} = X_{65}X_{58}X_{86}^2 = X_{67}X_{78}X_{86}^1$	0	0
$X_{21}X_{18}X_{82}^2 = X_{23}X_{38}X_{82}^2 = X_{54}X_{46}^1X_{65} = X_{46}^1X_{67}X_{74}$	-1	0
$X_{61}X_{18}X_{86}^2 = X_{23}X_{34}X_{42}^1 = X_{42}^1X_{25}X_{54} = X_{67}X_{78}X_{86}^2$	0	1

Table 18. The generators in terms of bifundamental fields (Model 4d).

7 Model 5: PdP_{4b}

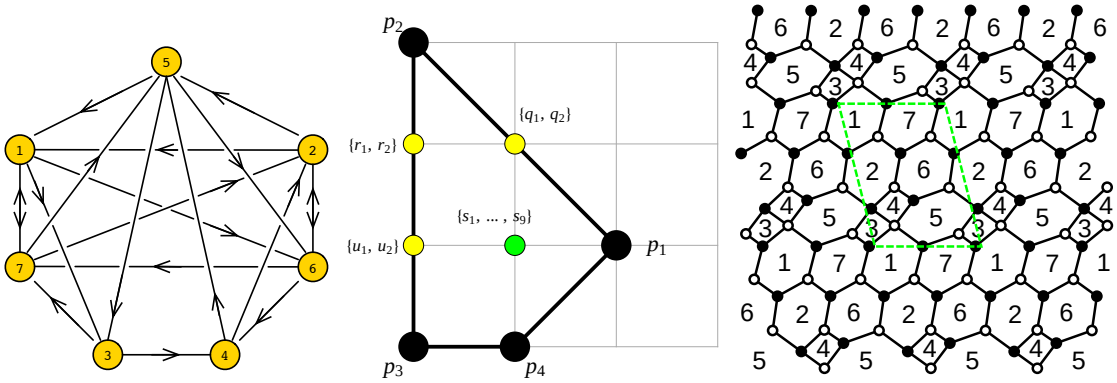


Figure 12. The quiver, toric diagram, and brane tiling of Model 5.

The superpotential is

$$W = +X_{21}X_{17}X_{72} + X_{42}X_{26}X_{64} + X_{56}X_{62}X_{25} + X_{67}X_{71}X_{16} + X_{75}X_{53}X_{37} + X_{13}X_{34}X_{45}X_{51} \\ -X_{13}X_{37}X_{71} - X_{16}X_{62}X_{21} - X_{56}X_{64}X_{45} - X_{67}X_{72}X_{26} - X_{75}X_{51}X_{17} - X_{25}X_{53}X_{34}X_{42} \tag{7.1}$$

The perfect matching matrix is

$$P = \left(\begin{array}{c|cccc|cc|ccc|ccc|ccccccccc} & p_1 & p_2 & p_3 & p_4 & q_1 & q_2 & r_1 & r_2 & r_3 & u_1 & u_2 & u_3 & s_1 & s_2 & s_3 & s_4 & s_5 & s_6 & s_7 & s_8 & s_9 \\ \hline X_{45} & 1 & 0 & 0 & 0 & 1 & 0 & 0 & 0 & 0 & 0 & 0 & 0 & 1 & 1 & 0 & 0 & 0 & 0 & 1 & 0 & 0 \\ X_{53} & 1 & 0 & 0 & 0 & 0 & 1 & 0 & 0 & 0 & 0 & 0 & 0 & 0 & 0 & 1 & 1 & 0 & 0 & 0 & 1 & 0 \\ X_{26} & 1 & 0 & 0 & 1 & 1 & 0 & 0 & 0 & 0 & 0 & 0 & 0 & 0 & 0 & 1 & 0 & 1 & 0 & 1 & 1 & 0 \\ X_{17} & 1 & 0 & 0 & 0 & 1 & 0 & 0 & 0 & 0 & 0 & 0 & 0 & 1 & 0 & 1 & 1 & 1 & 0 & 0 & 0 & 1 \\ X_{62} & 1 & 0 & 0 & 0 & 0 & 1 & 0 & 0 & 0 & 0 & 0 & 0 & 1 & 1 & 0 & 1 & 0 & 1 & 0 & 0 & 1 \\ X_{71} & 1 & 0 & 0 & 1 & 0 & 1 & 0 & 0 & 0 & 0 & 0 & 0 & 0 & 1 & 0 & 0 & 0 & 1 & 1 & 1 & 0 \\ X_{25} & 0 & 1 & 0 & 0 & 1 & 0 & 1 & 0 & 1 & 0 & 1 & 0 & 0 & 0 & 0 & 0 & 0 & 0 & 1 & 0 & 0 \\ X_{75} & 0 & 0 & 1 & 1 & 0 & 0 & 1 & 0 & 0 & 1 & 1 & 0 & 0 & 1 & 0 & 0 & 0 & 1 & 1 & 0 & 0 \\ X_{51} & 0 & 1 & 0 & 0 & 0 & 1 & 0 & 1 & 1 & 0 & 0 & 1 & 0 & 0 & 0 & 0 & 0 & 0 & 0 & 1 & 0 \\ X_{56} & 0 & 0 & 1 & 1 & 0 & 0 & 0 & 1 & 0 & 1 & 0 & 1 & 0 & 0 & 1 & 0 & 1 & 0 & 0 & 1 & 0 \\ X_{37} & 0 & 1 & 0 & 0 & 1 & 0 & 0 & 1 & 1 & 0 & 0 & 1 & 1 & 0 & 0 & 0 & 1 & 0 & 0 & 0 & 1 \\ X_{42} & 0 & 0 & 1 & 0 & 0 & 0 & 0 & 1 & 0 & 1 & 0 & 1 & 1 & 1 & 0 & 0 & 0 & 0 & 0 & 0 & 0 \\ X_{64} & 0 & 1 & 0 & 0 & 0 & 1 & 1 & 0 & 1 & 0 & 1 & 0 & 0 & 0 & 0 & 1 & 0 & 1 & 0 & 0 & 1 \\ X_{13} & 0 & 0 & 1 & 0 & 0 & 0 & 1 & 0 & 0 & 1 & 1 & 0 & 0 & 0 & 1 & 1 & 0 & 0 & 0 & 0 & 0 \\ X_{16} & 0 & 1 & 0 & 0 & 1 & 0 & 1 & 1 & 0 & 1 & 0 & 0 & 0 & 0 & 1 & 0 & 1 & 0 & 0 & 0 & 0 \\ X_{72} & 0 & 1 & 0 & 0 & 0 & 1 & 1 & 1 & 0 & 1 & 0 & 0 & 0 & 1 & 0 & 0 & 0 & 1 & 0 & 0 & 0 \\ X_{21} & 0 & 0 & 1 & 1 & 0 & 0 & 0 & 0 & 1 & 0 & 1 & 1 & 0 & 0 & 0 & 0 & 0 & 0 & 1 & 1 & 0 \\ X_{67} & 0 & 0 & 1 & 0 & 0 & 0 & 0 & 0 & 1 & 0 & 1 & 1 & 1 & 0 & 0 & 1 & 0 & 0 & 0 & 0 & 1 \\ X_{34} & 0 & 0 & 0 & 1 & 0 & 0 & 0 & 0 & 0 & 0 & 0 & 0 & 0 & 0 & 0 & 0 & 1 & 1 & 0 & 0 & 1 \end{array}\right)$$

The F-term charge matrix $Q_F = \ker(P)$ is

$$Q_F = \left(\begin{array}{cccc|cc|ccc|ccc|ccccccccc} p_1 & p_2 & p_3 & p_4 & q_1 & q_2 & r_1 & r_2 & r_3 & u_1 & u_2 & u_3 & s_1 & s_2 & s_3 & s_4 & s_5 & s_6 & s_7 & s_8 & s_9 \\ \hline 1 & 1 & 0 & 0 & -1 & -1 & 0 & 0 & 0 & 0 & 0 & 0 & 0 & 0 & 0 & 0 & 0 & 0 & 0 & 0 & 0 \\ 1 & 0 & 0 & 0 & 0 & 0 & 0 & 0 & 0 & 1 & 0 & 0 & 0 & -1 & -1 & 0 & 0 & 0 & 0 & 0 & 0 \\ 1 & 0 & 0 & 0 & 0 & 0 & 0 & 0 & 0 & 0 & 0 & 1 & -1 & 0 & 0 & 0 & 0 & 0 & 0 & -1 & 0 \\ 1 & 0 & 0 & 0 & -1 & 0 & 1 & 0 & 0 & 0 & 0 & 0 & 1 & -1 & 0 & -1 & 0 & 0 & 0 & 0 & 0 \\ 0 & 1 & 0 & 0 & -1 & 0 & 0 & -1 & 0 & 0 & 0 & 0 & 0 & 1 & 0 & 0 & 1 & -1 & 0 & 0 & 0 \\ 0 & 1 & 0 & 0 & 0 & 0 & -1 & -1 & 0 & 1 & 0 & 0 & 0 & 0 & 0 & 0 & 0 & 0 & 0 & 0 & 0 \\ 0 & 1 & 0 & 0 & 0 & 0 & -1 & 0 & -1 & 0 & 1 & 0 & 0 & 0 & 0 & 0 & 0 & 0 & 0 & 0 & 0 \\ 0 & 1 & 1 & 0 & 0 & 0 & -1 & 0 & 0 & 0 & 0 & -1 & 0 & 0 & 0 & 0 & 0 & 0 & 0 & 0 & 0 \\ 0 & 1 & 1 & 0 & 0 & 0 & 0 & -1 & 0 & 0 & -1 & 0 & 0 & 0 & 0 & 0 & 0 & 0 & 0 & 0 & 0 \\ 0 & 0 & 1 & -1 & 1 & 0 & -1 & 0 & 0 & 0 & 0 & 0 & -1 & 0 & 0 & 0 & 0 & 1 & 0 & 0 & 0 \\ 0 & 0 & 0 & 0 & 1 & 0 & -1 & 0 & 0 & 0 & 1 & 0 & -1 & 1 & 0 & 0 & 0 & 0 & -1 & 0 & 0 \\ 0 & 0 & 0 & 0 & 0 & 0 & 0 & 0 & 0 & 0 & 0 & 0 & 1 & -1 & 0 & 0 & 0 & 1 & 0 & 0 & -1 \end{array}\right)$$

The D-term charge matrix is

$$Q_D = \left(\begin{array}{cccc|cc|ccc|ccc|ccccccccc} p_1 & p_2 & p_3 & p_4 & q_1 & q_2 & r_1 & r_2 & r_3 & u_1 & u_2 & u_3 & s_1 & s_2 & s_3 & s_4 & s_5 & s_6 & s_7 & s_8 & s_9 \\ \hline 0 & 0 & 0 & 0 & 0 & 0 & 0 & 0 & 0 & 0 & 0 & 0 & 0 & 0 & 1 & -1 & 0 & 0 & 0 & 0 & 0 \\ 0 & 0 & 0 & 0 & 0 & 0 & 0 & 0 & 0 & 0 & 0 & 0 & 0 & 0 & 0 & 1 & -1 & 0 & 0 & 0 & 0 \\ 0 & 0 & 0 & 0 & 0 & 0 & 0 & 0 & 0 & 0 & 0 & 0 & 0 & 0 & 0 & 0 & 1 & -1 & 0 & 0 & 0 \\ 0 & 0 & 0 & 0 & 0 & 0 & 0 & 0 & 0 & 0 & 0 & 0 & 0 & 0 & 0 & 0 & 0 & 1 & -1 & 0 & 0 \\ 0 & 0 & 0 & 0 & 0 & 0 & 0 & 0 & 0 & 0 & 0 & 0 & 0 & 0 & 0 & 0 & 0 & 0 & 1 & -1 & 0 \\ 0 & 0 & 0 & 0 & 0 & 0 & 0 & 0 & 0 & 0 & 0 & 0 & 0 & 0 & 0 & 0 & 0 & 0 & 0 & 1 & -1 \end{array}\right)$$

The total charge matrix Q_t does not have repeated columns. Accordingly, the global symmetry is $U(1)_{f_1} \times U(1)_{f_2} \times U(1)_R$. Following the discussion in §2.3, the flavour and R-charges on GLSM fields corresponding to extremal points in the toric diagram in Figure 12 are found. They are shown in Table 19.

	$U(1)_{f_1}$	$U(1)_{f_2}$	$U(1)_R$	fugacity
p_1	0	-1/2	$R_1 \simeq 0.577$	t_1
p_2	0	1/2	$R_2 \simeq 0.640$	t_2
p_3	-1	-1	$R_3 \simeq 0.539$	t_3
p_4	1	1	$R_4 \simeq 0.243$	t_4

Table 19. The GLSM fields corresponding to extremal points of the toric diagram with their mesonic charges (Model 5).

Fine-tuning R-charges. The exact R-charges can be expressed in terms of roots of the

following polynomials

$$\begin{aligned}
0 &= 75 + 110x - 684x^2 + 162x^3 + 81x^4 \\
0 &= -1124565 + 2218649x_0 - 1141683x_0^2 - 16497x_0^3 \\
&\quad +(746100 - 259716x_0 + 4428x_0^2 - 64476x_0^3)y \\
&\quad +(775170 + 520182x_0 - 390258x_0^2 - 70470x_0^3)y^2 \\
&\quad +(14580 + 100764x_0 + 164268x_0^2 + 26244x_0^3)y^3 \\
&\quad +(-110565 - 26487x_0 - 19683x_0^2 - 6561x_0^3)y^4 \\
&\quad +38880y^5 \quad , \qquad (7.2)
\end{aligned}$$

where the roots satisfy the bounds $0 \leq 1 - x_0 \leq \frac{2}{3}$ and $0 \leq 1 - y_0 \leq \frac{2}{3}$. The exact R-charges are

$$\begin{aligned}
R_1 &= \frac{1}{8989575077760}(-443015521905 + 10382230129225x_0 - 1861588105479x_0^2 \\
&\quad -1223569555569x_0^3 + 788576007420y_0 + 7322446656900x_0y_0 - 1514870485020x_0^2y_0 \\
&\quad -803839472100x_0^3y_0 + 105890430210y_0^2 - 45532791090x_0y_0^2 + 616773772782x_0^2y_0^2 \\
&\quad +132554296962x_0^3y_0^2 - 87638359380y_0^3 - 829308203820x_0y_0^3 + 57898633140x_0^2y_0^3 \\
&\quad +57715867980x_0^3y_0^3 + 9044838615y_0^4 + 354606896385x_0y_0^4 - 66414222351x_0^2y_0^4 \\
&\quad -37556288361x_0^3y_0^4) \\
R_2 &= y_0 \ , \ R_3 = x_0 \ , \qquad (7.3)
\end{aligned}$$

$$
\begin{aligned}
R_4 = & \frac{1}{27630249136420257145191668008550400}(443015521905 - 10382230129225x_0 \\
& +1861588105479x_0^2 + 1223569555569x_0^3 - 788576007420y_0 - 7322446656900x_0y_0 \\
& +1514870485020x_0^2y_0 + 803839472100x_0^3y_0 - 105890430210y_0^2 + 45532791090x_0y_0^2 \\
& -616773772782x_0^2y_0^2 - 132554296962x_0^3y_0^2 + 87638359380y_0^3 + 829308203820x_0y_0^3 \\
& -57898633140x_0^2y_0^3 - 57715867980x_0^3y_0^3 - 9044838615y_0^4 - 354606896385x_0y_0^4 \\
& +66414222351x_0^2y_0^4 + 37556288361x_0^3y_0^4)\ (3435680922231398676675 - \\
& 10875934309383304858731x_0 + 2208889158465224949597x_0^2 \\
& +1149691223996073074763x_0^3 + 1308961575315964402860y_0 \\
& -530370354360171863631 6x_0y_0 + 1007391627507047358708x_0^2y_0 \\
& +577767803346582055164x_0^3y_0 - 41445446612526178750y_0^2 \\
& +324345443167855962702x_0y_0^2 - 267480237660960501378x_0^2y_0^2 \\
& -837571295860726812 30x_0^3y_0^2 - 1434022220778297787 40y_0^3 \\
& +581897049297268121604x_0y_0^3 - 73669737309435993132x_0^2y_0^3 \\
& -538608345646998873 96x_0^3y_0^3 + 465549045015915279 55y_0^4 \\
& -286145797904951411547x_0y_0^4 + 582869413953356512 77x_0^2y_0^4 \\
& +316750921798038275 79x_0^3y_0^4)\ .
\end{aligned} \tag{7.4}
$$

Products of non-extremal perfect matchings are expressed in terms of single variables as follows

$$
q = q_1q_2\ ,\ r = r_1r_2\ ,\ u = u_1u_2\ ,\ s = \prod_{m=1}^{9} s_m\ . \tag{7.5}
$$

The fugacity which counts extremal perfect matchings is t_α. The fugacity of the form y_q counts the product of non-extremal perfect matchings q.

The mesonic Hilbert series of Model 5 is found using the Molien integral formula in (2.9). It is

$$
\begin{aligned}
g_1(t_\alpha, y_q, y_r, y_u, y_s; \mathcal{M}_5^{mes}) = & (1 + y_qy_ry_uy_s\ t_1t_2t_3t_4 + y_qy_r^2y_u^2y_s\ t_2^2t_3^2t_4 - y_q^3y_r^3y_u^2y_s^2\ t_1^2t_2^4t_3t_4 \\
& -y_q^3y_r^4y_u^3y_s^2\ t_1t_2^5t_3^2t_4 - y_q^4y_r^5y_u^4y_s^3\ t_1^2t_2^6t_3^3t_4^2) \\
& \times \frac{1}{(1 - y_q^2y_r^2y_uy_s\ t_1t_2^3)(1 - y_q^2y_r^3y_u^2y_s\ t_2^4t_3)(1 - y_qy_s\ t_1^2t_4)(1 - y_ry_u^2y_s\ t_3^3t_4^2)}\ .
\end{aligned} \tag{7.6}
$$

The plethystic logarithm of the mesonic Hilbert series is

$$\begin{aligned}PL[g_1(t_\alpha, y_q, y_r, y_u, y_s; \mathcal{M}_5^{mes})] &= y_q y_r y_u y_s\ t_1 t_2 t_3 t_4 + y_q y_s\ t_1^2 t_4 + y_q^2 y_r^2 y_u y_s\ t_1 t_2^3 \\ &+ y_r y_u^2 y_s\ t_3^3 t_4^2 + y_q y_r^2 y_u^2 y_s\ t_2^2 t_3^2 t_4 + y_q^2 y_r^3 y_u^2 y_s\ t_2^4 t_3 - y_q^2 y_r^2 y_u^2 y_s^2\ t_1^2 t_2^2 t_3^2 t_4^2 \\ &- y_q^3 y_r^3 y_u^2 y_s^2\ t_1^2 t_2^4 t_3 t_4 - y_q^2 y_r^3 y_u^3 y_s^2\ t_1 t_2^3 t_3^3 t_4^2 - y_q^3 y_r^4 y_u^3 y_s^2\ t_1 t_2^5 t_3^2 t_4 - y_q^2 y_r^4 y_u^4 y_s^2\ t_2^4 t_3^4 t_4^2 \\ &+ y_q^4 y_r^4 y_u^3 y_s^3\ t_1^3 t_2^5 t_3^2 t_4^2 + \dots\ . \end{aligned} \tag{7.7}$$

Consider the following fugacity map

$$\begin{aligned} &f_1 = \frac{1}{y_u y_r}\ ,\ f_2 = \frac{1}{y_u y_s}\ , \\ &\tilde{t}_1 = y_q^{1/2} y_r^{1/2} y_u^{1/2} y_s^{1/2} t_1\ ,\ \tilde{t}_2 = y_q^{1/2} y_r^{1/2} y_u^{1/2} y_s^{1/2} t_2\ , \\ &\tilde{t}_3 = t_3\ ,\ \tilde{t}_4 = t_4\ , \end{aligned} \tag{7.8}$$

where f_1 and f_2 are the fugacities for the flavor charges, and $\tilde{t}_i$ is the fugacity for the R-charge R_i in table Table 19. In terms of the fugacity map above, the plethystic logarithm becomes

$$\begin{aligned}PL[g_1(\tilde{t}_\alpha, f_1, f_2; \mathcal{M}_5^{mes})] &= \tilde{t}_1\tilde{t}_2\tilde{t}_3\tilde{t}_4 + f_1\tilde{t}_1^2\tilde{t}_4 + f_2\tilde{t}_1\tilde{t}_2^3 + \frac{1}{f_1 f_2}\tilde{t}_3^3\tilde{t}_4^2 + \frac{1}{f_1}\tilde{t}_2^2\tilde{t}_3^2\tilde{t}_4 + \frac{f_2}{f_1}\tilde{t}_2^4\tilde{t}_3 \\ &- \tilde{t}_1^2\tilde{t}_2^2\tilde{t}_3^2\tilde{t}_4^2 - f_2\tilde{t}_1^2\tilde{t}_2^4\tilde{t}_3\tilde{t}_4 - \frac{1}{f_1}\tilde{t}_1\tilde{t}_2^3\tilde{t}_3^3\tilde{t}_4^2 + \dots\ . \end{aligned} \tag{7.9}$$

The above plethystic logarithm exhibits the moduli space generators with their mesonic charges.

The generators can be presented as points on a $\mathbb{Z}^2$ with the $U(1)_{f_1} \times U(1)_{f_2}$ charges giving the lattice coordinates. The convex polygon formed by the generators on the lattice in Table 20 is the dual reflexive polygon of the toric diagram of Model 5.

Generator	$U(1)_{f_1}$	$U(1)_{f_2}$
$p_1^2 p_4\ q\ s$	1	0
$p_1 p_2 p_3 p_4\ q\ r\ u\ s$	0	0
$p_1 p_2^3\ q^2\ r^2\ u\ s$	0	1
$p_3^3 p_4^2\ r\ u^2\ s$	-1	-1
$p_2^2 p_3^2 p_4\ q\ r^2\ u^2\ s$	-1	0
$p_2^4 p_3\ q^2\ r^3\ u^2\ s$	-1	1

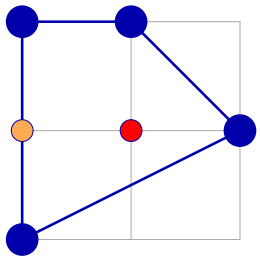


Table 20. The generators and lattice of generators of the mesonic moduli space of Model 5 in terms of GLSM fields with the corresponding flavor charges.

Generator	$U(1)_{f_1}$	$U(1)_{f_2}$
$X_{34}X_{45}X_{53} = X_{17}X_{71} = X_{26}X_{62}$	1	0
$X_{13}X_{34}X_{45}X_{51} = X_{25}X_{53}X_{34}X_{42} = X_{13}X_{37}X_{71} = X_{16}X_{62}X_{21} = X_{16}X_{67}X_{71} = X_{17}X_{72}X_{21}$ $= X_{17}X_{75}X_{51} = X_{25}X_{56}X_{62} = X_{26}X_{64}X_{42} = X_{26}X_{67}X_{72} = X_{37}X_{75}X_{53} = X_{45}X_{56}X_{64}$	0	0
$X_{16}X_{62}X_{25}X_{51} = X_{16}X_{64}X_{45}X_{51} = X_{17}X_{72}X_{25}X_{51} = X_{25}X_{53}X_{37}X_{72}$	0	1
$X_{56}X_{67}X_{75} = X_{13}X_{34}X_{42}X_{21}$	-1	-1
$X_{13}X_{34}X_{42}X_{25}X_{51} = X_{13}X_{37}X_{72}X_{21} = X_{13}X_{37}X_{75}X_{51} = X_{16}X_{64}X_{42}X_{21}$ $= X_{16}X_{67}X_{72}X_{21} = X_{16}X_{67}X_{75}X_{51} = X_{25}X_{56}X_{64}X_{42} = X_{25}X_{56}X_{67}X_{72}$	-1	0
$X_{13}X_{37}X_{72}X_{25}X_{51} = X_{16}X_{64}X_{42}X_{25}X_{51} = X_{16}X_{67}X_{72}X_{25}X_{51}$	-1	1

Table 21. The generators in terms of bifundamental fields (Model 5).

The Hilbert series and the plethystic logarithm can be re-expressed in terms of just 3 fugacities

$$\begin{aligned} T_1 &= \frac{\tilde{t}_3}{f_1 f_2\ \tilde{t}_1^2 \tilde{t}_2^2} = \frac{t_3}{y_q^2 y_r y_s\ t_1^2 t_2^2}\ , \\ T_2 &= f_2\ \tilde{t}_1 \tilde{t}_2^3 = y_q^2 y_r^2 y_u y_s\ t_1 t_2^3\ , \\ T_3 &= f_1\ \tilde{t}_1^2 \tilde{t}_4 = y_q y_s\ t_1^2 t_4\ , \end{aligned} \tag{7.10}$$

such that

$$g_1(T_1, T_2, T_3; \mathcal{M}_5^{mes}) = \frac{1 + T_1T_2T_3 + T_1^2T_2^2T_3 - T_1T_2^2T_3 - T_1^2T_2^3T_3 - T_1^3T_2^4T_3^2}{(1-T_2)(1-T_1T_2^2)(1-T_3)(1-T_1^3T_2^2T_3^2)} \tag{7.11}$$

and

$$\begin{aligned} &PL[g_1(T_1, T_2, T_3; \mathcal{M}_5^{mes})] = T_1T_2T_3 + T_3 + T_2 + T_1^3T_2^2T_3^2 + T_1T_2^2 + T_1^2T_2^2T_3 - T_1T_2^2T_3 \\ &-T_1^2T_2^2T_3^2 - T_1^2T_2^3T_3 - T_1^3T_2^3T_3^2 - T_1^4T_2^4T_3^2 + T_1^2T_2^3T_3^2 + T_1^3T_2^4T_3^2 + T_1^4T_2^4T_3^3 + T_1^4T_2^5T_3^2 \\ &+T_1^5T_2^5T_3^3 - T_1^3T_2^4T_3^3 \ldots \quad . \end{aligned} \tag{7.12}$$

The above mesonic Hilbert series and plethystic logarithm illustrates the conical structure of the toric Calalbi-Yau 3-fold.

8 Model 6: PdP$_{4a}$

8.1 Model 6 Phase a

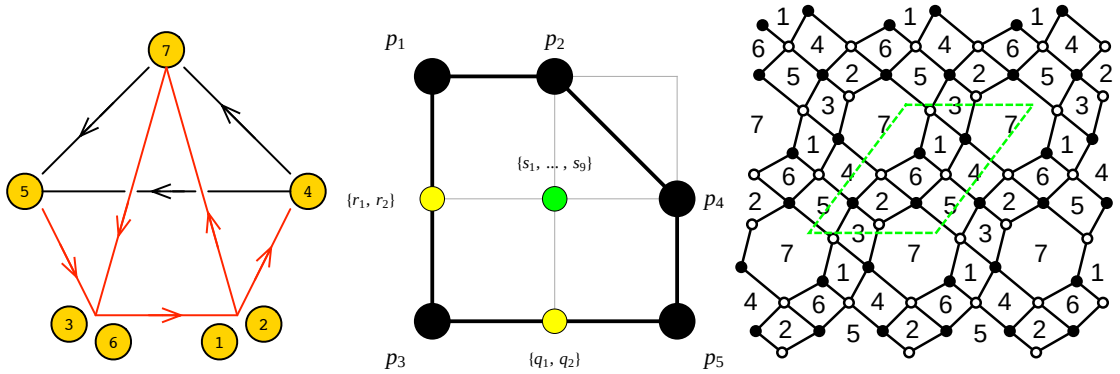


Figure 13. The quiver, toric diagram and brane tiling of Model 6a. The red arrows in the quiver indicate all possible connections between blocks of nodes.

The superpotential is

$$\begin{aligned} W = &+X_{32}X_{27}X_{73} + X_{14}X_{45}X_{56}X_{61} + X_{31}X_{17}X_{75}X_{53} + X_{62}X_{24}X_{47}X_{76} \\ &-X_{76}X_{61}X_{17} - X_{31}X_{14}X_{47}X_{73} - X_{32}X_{24}X_{45}X_{53} - X_{62}X_{27}X_{75}X_{56} \end{aligned} \tag{8.1}$$

The perfect matching matrix is

$$P = \left(\begin{array}{c|ccccc|cc|cc|ccccccccc} & p_1 & p_2 & p_3 & p_4 & p_5 & q_1 & q_2 & r_1 & r_2 & s_1 & s_2 & s_3 & s_4 & s_5 & s_6 & s_7 & s_8 & s_9 \\ \hline X_{17} & 1 & 1 & 0 & 0 & 0 & 0 & 0 & 1 & 0 & 1 & 0 & 1 & 0 & 1 & 0 & 0 & 0 & 0 \\ X_{73} & 1 & 1 & 0 & 0 & 0 & 0 & 0 & 0 & 1 & 0 & 1 & 0 & 1 & 0 & 1 & 0 & 0 & 0 \\ X_{56} & 1 & 0 & 0 & 0 & 0 & 0 & 0 & 1 & 0 & 0 & 1 & 0 & 0 & 0 & 0 & 1 & 0 & 0 \\ X_{24} & 1 & 0 & 0 & 0 & 0 & 0 & 0 & 0 & 1 & 1 & 0 & 0 & 0 & 0 & 0 & 0 & 1 & 0 \\ X_{45} & 0 & 1 & 0 & 1 & 0 & 0 & 0 & 0 & 0 & 0 & 0 & 1 & 0 & 0 & 1 & 0 & 0 & 0 \\ X_{62} & 0 & 1 & 0 & 0 & 0 & 0 & 0 & 0 & 0 & 0 & 0 & 0 & 1 & 1 & 0 & 0 & 0 & 1 \\ X_{32} & 0 & 0 & 1 & 0 & 0 & 1 & 0 & 1 & 0 & 0 & 0 & 0 & 0 & 1 & 0 & 1 & 0 & 1 \\ X_{75} & 0 & 0 & 1 & 0 & 0 & 1 & 0 & 0 & 1 & 0 & 0 & 0 & 0 & 0 & 1 & 0 & 0 & 0 \\ X_{47} & 0 & 0 & 1 & 0 & 0 & 0 & 1 & 1 & 0 & 0 & 0 & 1 & 0 & 0 & 0 & 0 & 0 & 0 \\ X_{61} & 0 & 0 & 1 & 0 & 0 & 0 & 1 & 0 & 1 & 0 & 0 & 0 & 1 & 0 & 0 & 0 & 1 & 1 \\ X_{76} & 0 & 0 & 0 & 1 & 1 & 1 & 0 & 0 & 0 & 0 & 1 & 0 & 0 & 0 & 1 & 1 & 0 & 0 \\ X_{27} & 0 & 0 & 0 & 1 & 1 & 0 & 1 & 0 & 0 & 1 & 0 & 1 & 0 & 0 & 0 & 0 & 1 & 0 \\ X_{31} & 0 & 0 & 0 & 1 & 0 & 0 & 0 & 0 & 0 & 0 & 0 & 0 & 0 & 0 & 0 & 1 & 1 & 1 \\ X_{14} & 0 & 0 & 0 & 0 & 1 & 1 & 0 & 0 & 0 & 1 & 0 & 0 & 0 & 1 & 0 & 0 & 0 & 0 \\ X_{53} & 0 & 0 & 0 & 0 & 1 & 0 & 1 & 0 & 0 & 0 & 1 & 0 & 1 & 0 & 0 & 0 & 0 & 0 \end{array}\right)$$

The F-term charge matrix $Q_F = \ker(P)$ is

$$Q_F = \left(\begin{array}{ccccc|cc|cc|cccccccc} p_1 & p_2 & p_3 & p_4 & p_5 & q_1 & q_2 & r_1 & r_2 & s_1 & s_2 & s_3 & s_4 & s_5 & s_6 & s_7 & s_8 & s_9 \\ \hline 0 & 0 & 1 & 0 & 1 & -1 & -1 & 0 & 0 & 0 & 0 & 0 & 0 & 0 & 0 & 0 & 0 & 0 \\ 1 & 0 & 1 & 0 & 0 & 0 & 0 & -1 & -1 & 0 & 0 & 0 & 0 & 0 & 0 & 0 & 0 & 0 \\ 1 & 0 & 0 & 0 & 1 & 0 & 0 & 0 & 0 & -1 & -1 & 0 & 0 & 0 & 0 & 0 & 0 & 0 \\ 0 & 1 & 0 & 0 & 0 & 0 & 1 & 0 & 0 & 0 & 0 & -1 & -1 & 0 & 0 & 0 & 0 & 0 \\ 0 & 1 & 0 & 0 & 0 & 1 & 0 & 0 & 0 & 0 & 0 & 0 & 0 & -1 & -1 & 0 & 0 & 0 \\ 0 & 0 & 0 & 1 & 0 & 0 & 0 & 1 & 0 & 0 & 0 & -1 & 0 & 0 & 0 & -1 & 0 & 0 \\ 0 & 0 & 0 & 1 & 0 & 0 & 0 & 0 & 1 & 0 & 0 & 0 & 0 & 0 & -1 & 0 & -1 & 0 \\ 0 & 0 & 0 & 0 & 1 & 0 & -1 & 1 & 0 & -1 & 0 & 0 & 0 & 0 & 0 & -1 & 1 & 0 \\ 0 & 0 & 0 & 0 & 0 & 0 & 0 & 0 & 0 & 1 & 0 & 0 & 0 & -1 & 0 & 0 & -1 & 1 \end{array}\right)$$

The D-term charge matrix is

$$Q_D = \left(\begin{array}{ccccc|cc|cc|ccccccc} p_1 & p_2 & p_3 & p_4 & p_5 & q_1 & q_2 & r_1 & r_2 & s_1 & s_2 & s_3 & s_4 & s_5 & s_6 & s_7 & s_8 & s_9 \\ \hline 0 & 0 & 0 & 0 & 0 & 0 & 0 & 0 & 0 & 0 & 0 & 1 & -1 & 0 & 0 & 0 & 0 & 0 \\ 0 & 0 & 0 & 0 & 0 & 0 & 0 & 0 & 0 & 0 & 0 & 0 & 1 & -1 & 0 & 0 & 0 & 0 \\ 0 & 0 & 0 & 0 & 0 & 0 & 0 & 0 & 0 & 0 & 0 & 0 & 0 & 1 & -1 & 0 & 0 & 0 \\ 0 & 0 & 0 & 0 & 0 & 0 & 0 & 0 & 0 & 0 & 0 & 0 & 0 & 0 & 1 & -1 & 0 & 0 \\ 0 & 0 & 0 & 0 & 0 & 0 & 0 & 0 & 0 & 0 & 0 & 0 & 0 & 0 & 0 & 1 & -1 & 0 \\ 0 & 0 & 0 & 0 & 0 & 0 & 0 & 0 & 0 & 0 & 0 & 0 & 0 & 0 & 0 & 0 & 1 & -1 \end{array}\right)$$

The total charge matrix Q_t does not exhibit repeated columns. Accordingly, the global symmetry is $U(1)_{f_1} \times U(1)_{f_2} \times U(1)_R$. The mesonic charges on the GLSM fields corresponding to extremal points in the toric diagram in Figure 13 are found following the discussion in §2.3. They are presented in Table 22.

	$U(1)_{f_1}$	$U(1)_{f_2}$	$U(1)_R$	fugacity
p_1	-1	0	$R_1 \simeq 0.427$	t_1
p_2	1	0	$R_2 \simeq 0.298$	t_2
p_3	0	0	$R_3 \simeq 0.550$	t_3
p_4	0	1	$R_2 \simeq 0.298$	t_4
p_5	0	-1	$R_1 \simeq 0.427$	t_5

Table 22. The GLSM fields corresponding to extremal points of the toric diagram with their mesonic charges (Model 6a).

Fine-tuning R-charges. The exact R-charges on extremal perfect matchings can be expressed in terms of a root x_0 of the following polynomial

$$0 = 289 - 695x + 331x^2 + 3x^3 \quad , \tag{8.2}$$

where the root of interest lies in the range $0 \leq 1 - x_0 \leq \frac{2}{3}$. The exact R-charges are

$$R_1 = R_5 = x_0 \quad ,$$

$$R_2 = R_4 = \frac{1}{24974163079606558247464685479061749334309736698888}(17910391886384784281476836912127220443393525048964-$$
$$1489897938581245099720399561817513883468361262177 6x_0+9465606277116561007612744735839203666371878276840x_0^2$$
$$+8171632306068776293575876125737079492808889002307 4x_0^3-1066227591698018726313508085565489132846725799645 62x_0^4$$
$$-2231293615560338150980050987260867362972606636517 3x_0^5+4762528868015187354760510267495372040181430194304 3x_0^6$$
$$+1743657358426337720401847407318855394624519781774 7x_0^7-1064023366039130910208225662473447784013785856618 9x_0^8$$
$$-5762098668974680244859599181817775913551620378815x_0^9+4201789303547174330940499259459275101797382173 13x_0^{10}$$
$$+7212825052981360329273982686349741119531180244 91x_0^{11}+8469163171024952964469547490466689186720556526 3x_0^{12}$$
$$-2884512717768031282986281138704210153304692279 2x_0^{13}-5936715130045788144646704656470430250253226360x_0^{14}$$
$$-9856820317473776126325732646033745605954981 2x_0^{15}-4278361125883159493660637122162650710849 00x_0^{16})$$

$$R_3 = \frac{1}{16216429359696366564908531394868384321213783660466055544382124418860912527574836681776300074624614 4} \times$$
$$(1169229461732080766319602708065371848435839320818952726286766174485578754720869791380548487029993472$$
$$+2111807782649712902346866891771146614955508474350836097776926084469964891610707635695632005595566 08x_0$$
$$-8045911260354654893884448259742088551904830575685775809252492449742813094597380760696064423664722176x_0^2$$
$$+7868186882915851426335876977581680670251639520854407669554513212398555158000171156489937456815968256x_0^3$$
$$+1061412415136716326837022119308869488382612389978875078709377550354824411184572440342496757041597952x_0^4$$
$$-1653502269547432808110213130155065398558657253926330204747817424734038646912023554904414840355605600x_0^5$$
$$-1803409805355686010966266040602399537481777012614017830538582946961232414356541894961178034998651796x_0^6$$
$$-5497763674675590897309921638784338919541557088407666629751989073298347831546662010682387313724096 8x_0^7$$
$$+1567205800812219625317948680985038429143438706488862950374641790454745258466005289304610895198165728x_0^8$$
$$+1433721411232234278937225795709815998152998730166082929889466098261318411272932929131404259129653584x_0^9$$
$$-6136882330931619036640793227475316505163955291657344172904274083192180668079316628784041862317038 21x_0^{10}$$
$$-1113293590933793106422270537761639133335738086439537494201648209333162655868499870321712814024965074x_0^{11}$$
$$-1020419186525290186845949207351033765174623331594183158929492041140901966475959568078504284124572 23x_0^{12}$$
$$+4239712201647256308830368012372627721035668771432197987938265323979123862245114383980033760835726 68x_0^{13}$$
$$+1807590015263689760932938599001663697551006857811238478827929254165626429014249267867672715988158 11x_0^{14}$$
$$-6407640961270887888491508283155711841546340707225197630370367731027521306826809665741607974661363 0x_0^{15}$$
$$-6551504819136579714820873890716651117283500144325459851304645267888406140527648899700282075382087 9x_0^{16}$$
$$-6673543248212741805371881957906917086875901203329952658459597394917113521671659599449171717221560x_0^{17}$$

$$
\begin{aligned}
&+9783618126417420629286524671582244856923708960297834037315293570385351437452828996816592454899857x_0^{18}\\
&+3743596998189704676218096923916451542387351120245899948167098322376252076440477648997681642932578x_0^{19}\\
&-2759981339778576560489931985485943900316969545177416237377125960729963288010126009352999660170 93x_0^{20}\\
&-4760411523248644433687320137571924693637020441000099811485372315498707248959654478002795560792 04x_0^{21}\\
&-8560927684116465961137542076709719231353834421505121550128767976456638132832351440750414265041 9x_0^{22}\\
&+1736756218281380840704019663440980233984061044275370082133820797625435430996110590672837549597 4x_0^{23}\\
&+8815437949275542972852271440501158360572534817622944767660802051044839059890817853038120935475x_0^{24}\\
&+8108591172311177203810356096440144224269389878048288179765368070395786577436514844028417880 80x_0^{25}\\
&-1920530729096523282105450035700800376217731386109791538123749368072384810836636305353396450 40x_0^{26}\\
&-5365474659169633068556841817393323499347741486358311173950109810271513890823377976715687048 0x_0^{27}\\
&-4633797214013132583423895629091032185087243889634863057878937498434947801893349846356567080x_0^{28}\\
&-1252888490757713861363139507690945073375815948541871969696840844835338178928215289399961 60x_0^{29}\\
&-1502297452596476410349719722105724798487349802028494174267727244065661237915976256430480x_0^{30}\\
&-8418891003214045205392116768323041884281772276495435205984021439684373541279712292000x_0^{31}\\
&-1807984151142524050529861218624808879856545409887321064565329304786923816180045000 0x_0^{32})\quad .
\end{aligned}
\tag{8.3}
$$

Products of non-extremal perfect matchings are expressed in terms of single variables as follows

$$
q = q_1 q_2 \ , \ r = r_1 r_2 \ , \ s = \prod_{m=1}^{9} s_m \ . \tag{8.4}
$$

Extremal perfect matchings are counted by the fugacity t_α. The fugacity y_q is assigned to the product of non-extremal perfect matchings q above.

The refined mesonic Hilbert series of Model 6a is

$$
\begin{aligned}
g_1(t_\alpha, y_q, y_r, y_s; \mathcal{M}_{6a}^{mes}) = &(1 + y_q y_r y_s \ t_1 t_2 t_3 t_4 t_5 - y_q^2 y_r^3 y_s^2 \ t_1^3 t_2^2 t_3^3 t_4 t_5 - y_q^3 y_r^3 y_s^2 \ t_1^2 t_2 t_3^4 t_4 t_5^2\\
&- y_q^2 y_r^2 y_s^2 \ t_1^2 t_2^2 t_3^2 t_4^2 t_5^2 - y_q^3 y_r^2 y_s^2 \ t_1 t_2 t_3^3 t_4^2 t_5^3 + y_q^4 y_r^4 y_s^3 \ t_1^3 t_2^2 t_3^5 t_4^2 t_5^3 + y_q^5 y_r^5 y_s^4 \ t_1^4 t_2^3 t_3^6 t_4^3 t_5^4)\\
&\times \frac{1}{(1 - y_q y_r^2 y_s \ t_1^2 t_2 t_3^2)(1 - y_r y_s \ t_1^2 t_2^2 t_4)(1 - y_q^2 y_r^2 y_s \ t_1 t_3^3 t_5)}\\
&\times \frac{1}{(1 - y_q^2 y_r y_s \ t_3^2 t_4 t_5^2)(1 - y_q y_s \ t_2 t_4^2 t_5^2)} \quad .
\end{aligned}
\tag{8.5}
$$

The plethystic logarithm of the mesonic Hilbert series is

$$\begin{aligned} PL[g_1(t_\alpha, y_q, y_r, y_s; \mathcal{M}^{mes}_{6a})] &= y_q y_s\ t_2 t_4^2 t_5^2 + y_r y_s\ t_1^2 t_2^2 t_4 + y_q y_r y_s\ t_1 t_2 t_3 t_4 t_5 \\ &+ y_q y_r^2 y_s\ t_1^2 t_2 t_3^2 + y_q^2 y_r y_s\ t_3^2 t_4 t_5^2 + y_q^2 y_r^2 y_s\ t_1 t_3^3 t_5 - 2\ y_q^2 y_r^2 y_s^2\ t_1^2 t_2^2 t_3^2 t_4^2 t_5^2 \\ &- y_q^3 y_r^3 y_s^2\ t_1^2 t_2 t_3^4 t_4 t_5^2 + \dots\ . \end{aligned} \tag{8.6}$$

Consider the following fugacity map

$$f_1 = \frac{1}{y_r\ t_1^2 t_2^2 t_4}\ ,\ f_2 = \frac{1}{y_q\ t_2 t_4^2 t_5^2}\ ,\ \tilde{t}_1 = y_q^{1/2} y_r^{1/2} y_s^{1/2}\ t_1 t_5\ ,\ \tilde{t}_2 = t_2 t_4\ ,\ \tilde{t}_3 = \frac{t_3}{t_1 t_2 t_4 t_5}\ , \tag{8.7}$$

where f_1 and f_2 are the flavour charge fugacities, and $\tilde{t}_i$ is the fugacity for the R-charge R_i in Table 22.

In terms of the fugacity map above, the plethystic logarithm becomes

$$\begin{aligned} PL[g_1(\tilde{t}_\alpha, f_1, f_2; \mathcal{M}^{mes}_{6a})] &= (f_1 + f_2)\,\tilde{t}_1^2 \tilde{t}_2^3 + \tilde{t}_1^2 \tilde{t}_2^2 \tilde{t}_3 + \left(\frac{1}{f_1} + \frac{1}{f_2}\right) \tilde{t}_1^2 \tilde{t}_2 \tilde{t}_3^2 + \frac{1}{f_1 f_2} \tilde{t}_1^2 \tilde{t}_3^3 \\ &- 2\tilde{t}_1^4 \tilde{t}_2^4 \tilde{t}_3^2 - \frac{1}{f_1 f_2} \tilde{t}_1^4 \tilde{t}_2^2 \tilde{t}_3^4 + \dots\ . \end{aligned} \tag{8.8}$$

The above plethystic logarithm exhibits the moduli space generators with the corresponding mesonic charges. They are summarized in Table 23. The generators can be presented on a charge lattice. The convex polygon formed by the generators in Table 23 is the dual reflexive polygon of the toric diagram of Model 6a.

Generator	$U(1)_{f_1}$	$U(1)_{f_2}$
$p_2 p_4^2 p_5^2\ q\ s$	1	0
$p_1^2 p_2^2 p_4\ r\ s$	0	1
$p_1 p_2 p_3 p_4 p_5\ q\ r\ s$	0	0
$p_3^2 p_4 p_5^2\ q^2\ r\ s$	0	-1
$p_1^2 p_2 p_3^2\ q\ r^2\ s$	-1	0
$p_1 p_3^3 p_5\ q^2\ r^2\ s$	-1	-1

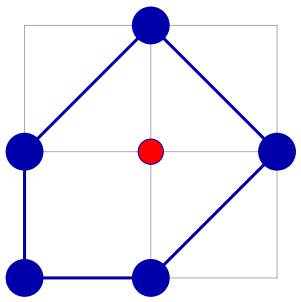


Table 23. The generators and lattice of generators of the mesonic moduli space of Model 6a in terms of GLSM fields with the corresponding flavor charges.

Generator	$U(1)_{f_1}$	$U(1)_{f_2}$
$X_{27}X_{76}X_{62} = X_{14}X_{45}X_{53}X_{31}$	1	0
$X_{17}X_{73}X_{31} = X_{24}X_{45}X_{56}X_{62}$	0	1
$X_{17}X_{76}X_{61} = X_{27}X_{73}X_{32} = X_{14}X_{47}X_{73}X_{31} = X_{14}X_{45}X_{56}X_{61}$	0	0
$= X_{17}X_{75}X_{53}X_{31} = X_{24}X_{45}X_{53}X_{32} = X_{24}X_{47}X_{76}X_{62} = X_{27}X_{75}X_{56}X_{62}$		
$X_{14}X_{47}X_{75}X_{53}X_{31} = X_{14}X_{47}X_{76}X_{61} = X_{27}X_{75}X_{53}X_{32}$	0	-1
$X_{24}X_{47}X_{75}X_{56}X_{62} = X_{17}X_{75}X_{56}X_{61} = X_{24}X_{47}X_{73}X_{32}$	-1	0
$X_{14}X_{47}X_{75}X_{56}X_{61} = X_{24}X_{47}X_{75}X_{53}X_{32}$	-1	-1

Table 24. The generators in terms of bifundamental fields (Model 6a).

The mesonic Hilbert series and plethystic logarithm can be re-expressed in terms of just 3 fugacities

$$T_1 = \frac{f_1}{f_2\ \tilde{t}_1^2\tilde{t}_2^2\tilde{t}_3} = \frac{t_5}{y_r^2 y_s\ t_1^3 t_2^2 t_3}\ ,\ T_2 = \frac{\tilde{t}_1^2\tilde{t}_2\tilde{t}_3^2}{f_1} = y_q y_r^2 y_s\ t_1^2 t_2 t_3^2\ ,\ T_3 = f_2\ \tilde{t}_1^2\tilde{t}_2^3 = y_r y_s\ t_1^2 t_2^2 t_4\ , \tag{8.9}$$

such that

$$g_1(T_1, T_2, T_3; \mathcal{M}_{6a}^{mes}) = \frac{1 + T_1T_2T_3 - T_1T_2^2T_3 - T_1^2T_2^3T_3 - T_1^2T_2^2T_3^2 - T_1^3T_2^3T_3^2 + T_1^3T_2^4T_3^2 + T_1^4T_2^5T_3^3}{(1-T_2)(1-T_3)(1-T_1T_2^2)(1-T_1^2T_2^2T_3)(1-T_1^2T_2T_3^2)} \tag{8.10}$$

and

$$PL[g_1(T_1, T_2, T_3; \mathcal{M}_{6a}^{mes})] = T_1^2T_2T_3^2 + T_3 + T_1T_2T_3 + T_2 + T_1^2T_2^2T_3 + T_1T_2^2 - 2T_1^2T_2^2T_3^2 - T_1^2T_2^3T_3 + \dots\ . \tag{8.11}$$

The Hilbert series and plethystic logarithm above illustrate the conical structure of the toric Calabi-Yau 3-fold.

8.2 Model 6 Phase b

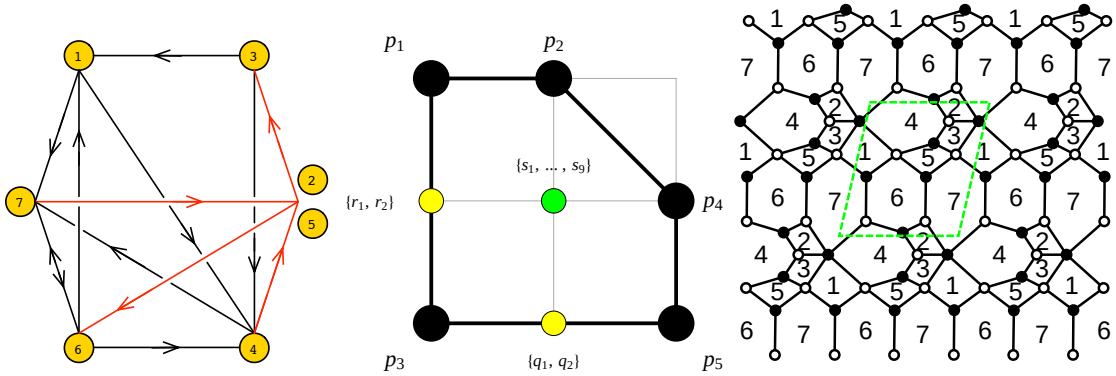


Figure 14. The quiver, toric diagram, and brane tiling of Model 6b. The red arrows in the quiver indicate all possible connections between blocks of nodes.

The superpotential is

$$\begin{aligned} W = &+X_{42}X_{23}X_{34} + X_{67}X_{72}X_{26} + X_{76}X_{64}X_{47} + X_{14}X_{45}X_{56}X_{61} + X_{31}X_{17}X_{75}X_{53} \\ &-X_{67}X_{75}X_{56} - X_{76}X_{61}X_{17} - X_{42}X_{26}X_{64} - X_{53}X_{34}X_{45} - X_{14}X_{47}X_{72}X_{23}X_{31} \end{aligned} \tag{8.12}$$

The perfect matching matrix is

$$P = \left(\begin{array}{c|ccccc|cc|cc|ccccccccc} & p_1 & p_2 & p_3 & p_4 & p_5 & q_1 & q_2 & r_1 & r_2 & s_1 & s_2 & s_3 & s_4 & s_5 & s_6 & s_7 & s_8 & s_9 \\ \hline X_{67} & 1 & 1 & 0 & 1 & 0 & 0 & 0 & 1 & 0 & 1 & 0 & 0 & 0 & 1 & 1 & 1 & 0 & 0 \\ X_{76} & 1 & 1 & 0 & 0 & 0 & 0 & 0 & 0 & 1 & 0 & 1 & 1 & 1 & 0 & 0 & 0 & 1 & 1 \\ X_{42} & 1 & 1 & 0 & 0 & 0 & 0 & 0 & 1 & 0 & 1 & 1 & 0 & 1 & 0 & 0 & 0 & 0 & 0 \\ X_{14} & 1 & 0 & 0 & 0 & 0 & 0 & 0 & 0 & 1 & 0 & 0 & 0 & 0 & 1 & 0 & 0 & 0 & 0 \\ X_{53} & 1 & 0 & 0 & 0 & 0 & 0 & 0 & 1 & 0 & 0 & 1 & 0 & 0 & 0 & 1 & 0 & 1 & 0 \\ X_{31} & 0 & 1 & 0 & 0 & 0 & 0 & 0 & 0 & 0 & 0 & 0 & 0 & 0 & 0 & 0 & 1 & 0 & 1 \\ X_{45} & 0 & 1 & 0 & 1 & 0 & 0 & 0 & 0 & 0 & 1 & 0 & 1 & 1 & 0 & 0 & 0 & 0 & 0 \\ X_{34} & 0 & 0 & 1 & 0 & 1 & 1 & 1 & 0 & 1 & 0 & 0 & 0 & 0 & 1 & 0 & 1 & 0 & 1 \\ X_{17} & 0 & 0 & 0 & 1 & 1 & 1 & 0 & 0 & 0 & 1 & 0 & 0 & 0 & 1 & 0 & 0 & 0 & 0 \\ X_{64} & 0 & 0 & 0 & 1 & 1 & 0 & 1 & 0 & 0 & 0 & 0 & 0 & 0 & 1 & 1 & 1 & 0 & 0 \\ X_{72} & 0 & 0 & 0 & 0 & 1 & 0 & 1 & 0 & 0 & 0 & 1 & 0 & 1 & 0 & 0 & 0 & 0 & 0 \\ X_{23} & 0 & 0 & 0 & 1 & 0 & 0 & 0 & 0 & 0 & 0 & 0 & 1 & 0 & 0 & 1 & 0 & 1 & 0 \\ X_{56} & 0 & 0 & 0 & 0 & 1 & 1 & 0 & 0 & 0 & 0 & 1 & 0 & 0 & 0 & 0 & 0 & 1 & 1 \\ X_{26} & 0 & 0 & 1 & 0 & 0 & 1 & 0 & 0 & 1 & 0 & 0 & 1 & 0 & 0 & 0 & 0 & 1 & 1 \\ X_{47} & 0 & 0 & 1 & 0 & 0 & 1 & 0 & 1 & 0 & 1 & 0 & 0 & 0 & 0 & 0 & 0 & 0 & 0 \\ X_{75} & 0 & 0 & 1 & 0 & 0 & 0 & 1 & 0 & 1 & 0 & 0 & 1 & 1 & 0 & 0 & 0 & 0 & 0 \\ X_{61} & 0 & 0 & 1 & 0 & 0 & 0 & 1 & 1 & 0 & 0 & 0 & 0 & 0 & 0 & 1 & 1 & 0 & 0 \end{array}\right)$$

The F-term charge matrix $Q_F = \ker(P)$ is

$$Q_F = \left(\begin{array}{ccccc|cc|cc|ccccccccc} p_1 & p_2 & p_3 & p_4 & p_5 & q_1 & q_2 & r_1 & r_2 & s_1 & s_2 & s_3 & s_4 & s_5 & s_6 & s_7 & s_8 & s_9 \\ \hline 1 & 0 & 1 & 0 & 0 & 0 & 0 & -1 & -1 & 0 & 0 & 0 & 0 & 0 & 0 & 0 & 0 & 0 \\ 1 & 0 & 0 & 0 & 1 & 0 & 0 & 0 & 0 & 0 & -1 & 0 & 0 & -1 & 0 & 0 & 0 & 0 \\ 0 & 1 & 0 & 0 & 0 & 1 & 0 & 0 & 0 & -1 & 0 & 0 & 0 & 0 & 0 & 0 & 0 & -1 \\ 0 & 1 & 0 & 0 & 0 & 0 & 1 & 0 & 0 & 0 & 0 & 0 & -1 & 0 & 0 & -1 & 0 & 0 \\ 0 & 0 & 1 & 1 & 0 & -1 & 0 & 0 & 0 & 0 & 1 & 0 & -1 & 0 & -1 & 0 & 0 & 0 \\ 0 & 0 & 1 & 0 & 1 & -1 & -1 & 0 & 0 & 0 & 0 & 0 & 0 & 0 & 0 & 0 & 0 & 0 \\ 0 & 0 & 0 & 1 & 0 & 0 & 0 & 1 & 0 & -1 & 0 & 0 & 0 & 0 & -1 & 0 & 0 & 0 \\ 0 & 0 & 0 & 1 & -1 & 1 & 0 & 0 & 0 & -1 & 1 & 0 & 0 & 0 & 0 & 0 & -1 & 0 \\ 0 & 0 & 0 & 0 & 0 & 0 & 0 & 0 & 0 & 0 & 1 & 1 & -1 & 0 & 0 & 0 & -1 & 0 \end{array}\right)$$

The D-term charge matrix is

$$Q_D = \left(\begin{array}{ccccc|cc|cc|ccccccccc} p_1 & p_2 & p_3 & p_4 & p_5 & q_1 & q_2 & r_1 & r_2 & s_1 & s_2 & s_3 & s_4 & s_5 & s_6 & s_7 & s_8 & s_9 \\ \hline 0 & 0 & 0 & 0 & 0 & 0 & 0 & 0 & 0 & 1 & -1 & 0 & 0 & 0 & 0 & 0 & 0 & 0 \\ 0 & 0 & 0 & 0 & 0 & 0 & 0 & 0 & 0 & 0 & 1 & -1 & 0 & 0 & 0 & 0 & 0 & 0 \\ 0 & 0 & 0 & 0 & 0 & 0 & 0 & 0 & 0 & 0 & 0 & 1 & -1 & 0 & 0 & 0 & 0 & 0 \\ 0 & 0 & 0 & 0 & 0 & 0 & 0 & 0 & 0 & 0 & 0 & 0 & 1 & -1 & 0 & 0 & 0 & 0 \\ 0 & 0 & 0 & 0 & 0 & 0 & 0 & 0 & 0 & 0 & 0 & 0 & 0 & 1 & -1 & 0 & 0 & 0 \\ 0 & 0 & 0 & 0 & 0 & 0 & 0 & 0 & 0 & 0 & 0 & 0 & 0 & 0 & 1 & -1 & 0 & 0 \end{array}\right)$$

The global symmetry of Model 6b has the form $U(1)_{f_1} \times U(1)_{f_2} \times U(1)_R$. The charges under the global symmetry on the extremal perfect matchings p_α are the same as for Model 6a. They are shown in Table 22.

Product of non-extremal perfect matchings are expressed in terms of single variables as follows

$$q = q_1 q_2 \ , \ r = r_1 r_2 \ , \ s = \prod_{m=1}^{9} s_m \ . \tag{8.13}$$

The fugacity counting extremal perfect matchings p_α is t_α. The fugacity y_q counts the product of non-extremal perfect matchings q.

The refined mesonic Hilbert series of Model 6b is identical to the mesonic Hilbert series for Model 6a. The mesonic Hilbert series and the corresponding plethystic logarithm is shown in (8.5) and (8.8) respectively. The mesonic Hilbert series for Model 6a and 6b are identical and are not complete intersections.

The generators in terms of perfect matchings of Model 6b are shown in Table 23. The charge lattice of generators forms a reflexive polygon which is the dual of the toric diagram. The generators in terms of quiver fields of Model 6b are shown in Table 25.

Generator	$U(1)_{f_1}$	$U(1)_{f_2}$
$X_{45}X_{56}X_{64} = X_{17}X_{72}X_{23}X_{31}$	0	1
$X_{67}X_{76} = X_{14}X_{42}X_{23}X_{31} = X_{14}X_{45}X_{53}X_{31}$	1	0
$X_{14}X_{47}X_{72}X_{23}X_{31} = X_{14}X_{45}X_{56}X_{61} = X_{17}X_{75}X_{53}X_{31} = X_{17}X_{76}X_{61} = X_{23}X_{34}X_{42}$ $= X_{26}X_{64}X_{42} = X_{26}X_{67}X_{72} = X_{34}X_{45}X_{53} = X_{47}X_{76}X_{64} = X_{56}X_{67}X_{75}$	0	0
$X_{17}X_{72}X_{26}X_{61} = X_{17}X_{75}X_{56}X_{61} = X_{23}X_{34}X_{47}X_{72} = X_{26}X_{64}X_{47}X_{72} = X_{47}X_{75}X_{56}X_{64}$	-1	0
$X_{14}X_{47}X_{75}X_{53}X_{31} = X_{14}X_{42}X_{26}X_{61} = X_{14}X_{47}X_{76}X_{61}$	0	-1
$X_{34}X_{47}X_{75}X_{53} = X_{14}X_{47}X_{72}X_{26}X_{61} = X_{14}X_{47}X_{75}X_{56}X_{61}$	-1	-1

Table 25. The generators in terms of bifundamental fields (Model 6b).

8.3 Model 6 Phase c

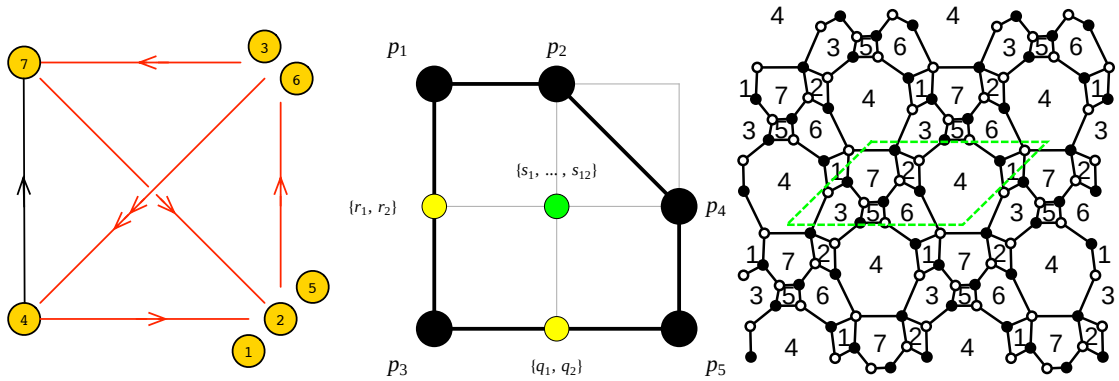


Figure 15. The quiver, toric diagram, and brane tiling of Model 6c. The red arrows in the quiver indicate all possible connections between blocks of nodes.

The superpotential is

$$W = +X_{41}X_{13}X_{34}^2 + X_{42}X_{23}X_{34}^1 + X_{45}X_{56}X_{64}^2 + X_{67}X_{72}X_{26} + X_{75}X_{53}X_{37} + X_{47}X_{71}X_{16}X_{64}^1 - X_{41}X_{16}X_{64}^2 - X_{42}X_{26}X_{64}^1 - X_{45}X_{53}X_{34}^1 - X_{67}X_{75}X_{56} - X_{71}X_{13}X_{37} - X_{47}X_{72}X_{23}X_{34}^2 \tag{8.14}$$

The perfect matching matrix is

$$P = \left(\begin{array}{c|ccccc|cc|cc|cccccccccc} & p_1 & p_2 & p_3 & p_4 & p_5 & q_1 & q_2 & r_1 & r_2 & s_1 & s_2 & s_3 & s_4 & s_5 & s_6 & s_7 & s_8 & s_9 & s_{10} & s_{11} & s_{12} \\ \hline X_{37} & 1 & 1 & 0 & 1 & 0 & 0 & 0 & 0 & 1 & 1 & 1 & 0 & 1 & 0 & 0 & 0 & 0 & 0 & 0 & 0 & 0 \\ X_{64}^1 & 1 & 1 & 0 & 0 & 0 & 0 & 0 & 1 & 0 & 1 & 0 & 1 & 0 & 0 & 0 & 0 & 0 & 0 & 0 & 0 & 0 \\ X_{41} & 1 & 1 & 0 & 0 & 0 & 0 & 0 & 0 & 1 & 0 & 1 & 0 & 0 & 1 & 0 & 1 & 0 & 1 & 0 & 1 & 0 \\ X_{34}^1 & 1 & 0 & 1 & 0 & 0 & 1 & 0 & 1 & 1 & 1 & 0 & 0 & 1 & 0 & 0 & 0 & 0 & 0 & 0 & 0 & 0 \\ X_{72} & 1 & 0 & 0 & 0 & 0 & 0 & 0 & 1 & 0 & 0 & 0 & 0 & 0 & 1 & 1 & 0 & 0 & 1 & 1 & 0 & 0 \\ X_{56} & 1 & 0 & 0 & 0 & 0 & 0 & 0 & 0 & 1 & 0 & 0 & 0 & 1 & 0 & 0 & 0 & 0 & 1 & 1 & 1 & 1 \\ X_{67} & 0 & 1 & 0 & 1 & 1 & 0 & 1 & 0 & 0 & 1 & 1 & 1 & 0 & 0 & 0 & 0 & 0 & 0 & 0 & 0 & 0 \\ X_{45} & 0 & 1 & 0 & 1 & 0 & 0 & 0 & 0 & 0 & 0 & 1 & 0 & 0 & 1 & 1 & 1 & 1 & 0 & 0 & 0 & 0 \\ X_{23} & 0 & 1 & 0 & 0 & 0 & 0 & 0 & 0 & 0 & 0 & 0 & 1 & 0 & 0 & 0 & 1 & 1 & 0 & 0 & 1 & 1 \\ X_{64}^2 & 0 & 0 & 1 & 0 & 1 & 1 & 1 & 1 & 0 & 1 & 0 & 1 & 0 & 0 & 0 & 0 & 0 & 0 & 0 & 0 & 0 \\ X_{75} & 0 & 0 & 1 & 0 & 0 & 1 & 0 & 1 & 0 & 0 & 0 & 0 & 0 & 1 & 1 & 1 & 1 & 0 & 0 & 0 & 0 \\ X_{26} & 0 & 0 & 1 & 0 & 0 & 1 & 0 & 0 & 1 & 0 & 0 & 0 & 1 & 0 & 0 & 1 & 1 & 0 & 0 & 1 & 1 \\ X_{13} & 0 & 0 & 1 & 0 & 0 & 0 & 1 & 1 & 0 & 0 & 0 & 1 & 0 & 0 & 1 & 0 & 1 & 0 & 1 & 0 & 1 \\ X_{47} & 0 & 0 & 1 & 0 & 0 & 0 & 1 & 0 & 1 & 0 & 1 & 0 & 0 & 0 & 0 & 0 & 0 & 0 & 0 & 0 & 0 \\ X_{34}^2 & 0 & 0 & 0 & 1 & 1 & 1 & 0 & 0 & 0 & 1 & 0 & 0 & 1 & 0 & 0 & 0 & 0 & 0 & 0 & 0 & 0 \\ X_{42} & 0 & 0 & 0 & 1 & 1 & 0 & 1 & 0 & 0 & 0 & 1 & 0 & 0 & 1 & 1 & 0 & 0 & 1 & 1 & 0 & 0 \\ X_{16} & 0 & 0 & 0 & 1 & 0 & 0 & 0 & 0 & 0 & 0 & 0 & 0 & 1 & 0 & 1 & 0 & 1 & 0 & 1 & 0 & 1 \\ X_{71} & 0 & 0 & 0 & 0 & 1 & 1 & 0 & 0 & 0 & 0 & 0 & 0 & 0 & 1 & 0 & 1 & 0 & 1 & 0 & 1 & 0 \\ X_{53} & 0 & 0 & 0 & 0 & 1 & 0 & 1 & 0 & 0 & 0 & 0 & 1 & 0 & 0 & 0 & 0 & 0 & 1 & 1 & 1 & 1 \end{array}\right)$$

The F-term charge matrix $Q_F = \ker(P)$ is

$$Q_F = \left(\begin{array}{ccccc|cc|cc|cccccccccc} p_1 & p_2 & p_3 & p_4 & p_5 & q_1 & q_2 & r_1 & r_2 & s_1 & s_2 & s_3 & s_4 & s_5 & s_6 & s_7 & s_8 & s_9 & s_{10} & s_{11} & s_{12} \\ \hline 1 & 0 & 0 & 1 & 0 & 0 & 1 & 0 & 0 & -1 & -1 & 0 & 0 & 0 & 0 & 0 & 0 & 0 & -1 & 0 & 0 \\ 1 & 0 & 0 & 0 & 1 & 0 & 0 & 0 & 0 & -1 & 0 & 0 & 0 & 0 & 0 & 0 & 0 & -1 & 0 & 0 & 0 \\ 0 & 1 & 0 & 0 & 0 & 1 & 0 & 0 & 0 & -1 & 0 & 0 & 0 & 0 & 0 & -1 & 0 & 0 & 0 & 0 & 0 \\ 0 & 1 & 0 & 0 & 0 & 0 & 1 & 0 & 0 & 0 & -1 & -1 & 0 & 0 & 0 & 0 & 0 & 0 & 0 & 0 & 0 \\ 0 & 0 & 1 & 0 & 0 & -1 & 0 & -1 & 0 & 1 & -1 & 0 & 0 & 1 & 0 & 0 & 0 & 0 & 0 & 0 & 0 \\ 0 & 0 & 0 & 1 & 0 & 0 & 0 & 1 & 0 & -1 & 0 & 0 & 0 & 0 & 0 & 0 & -1 & 0 & -1 & 0 & 1 \\ 0 & 0 & 0 & 1 & 0 & 0 & 0 & 1 & 0 & -1 & 0 & 0 & 0 & 0 & 0 & -1 & 0 & 0 & -1 & 1 & 0 \\ 0 & 0 & 0 & 1 & 0 & 0 & 0 & 0 & 1 & 0 & -1 & 0 & -1 & 0 & 0 & 0 & 0 & 0 & 0 & 0 & 0 \\ 0 & 0 & 0 & 0 & 1 & -1 & 0 & 0 & 1 & 0 & -1 & 0 & 0 & 1 & 0 & 0 & 0 & -1 & 0 & 0 & 0 \\ 0 & 0 & 0 & 0 & 1 & 0 & -1 & 1 & 0 & -1 & 1 & 0 & 0 & -1 & 0 & 0 & 0 & 0 & 0 & 0 & 0 \\ 0 & 0 & 0 & 0 & 0 & 0 & 0 & 1 & -1 & -1 & 1 & 0 & 1 & 0 & -1 & 0 & 0 & 0 & 0 & 0 & 0 \\ 0 & 0 & 0 & 0 & 0 & 0 & 0 & 0 & 0 & 0 & 0 & 0 & 0 & -1 & 0 & 1 & 0 & 0 & 1 & 0 & -1 \end{array}\right)$$

The D-term charge matrix is

$$Q_D = \left(\begin{array}{ccccc|cc|cc|cccccccccc} p_1 & p_2 & p_3 & p_4 & p_5 & q_1 & q_2 & r_1 & r_2 & s_1 & s_2 & s_3 & s_4 & s_5 & s_6 & s_7 & s_8 & s_9 & s_{10} & s_{11} & s_{12} \\ \hline 0 & 0 & 0 & 0 & 0 & 0 & 0 & 0 & 0 & 1 & -1 & 0 & 0 & 0 & 0 & 0 & 0 & 0 & 0 & 0 & 0 \\ 0 & 0 & 0 & 0 & 0 & 0 & 0 & 0 & 0 & 0 & 1 & -1 & 0 & 0 & 0 & 0 & 0 & 0 & 0 & 0 & 0 \\ 0 & 0 & 0 & 0 & 0 & 0 & 0 & 0 & 0 & 0 & 0 & 1 & -1 & 0 & 0 & 0 & 0 & 0 & 0 & 0 & 0 \\ 0 & 0 & 0 & 0 & 0 & 0 & 0 & 0 & 0 & 0 & 0 & 0 & 1 & -1 & 0 & 0 & 0 & 0 & 0 & 0 & 0 \\ 0 & 0 & 0 & 0 & 0 & 0 & 0 & 0 & 0 & 0 & 0 & 0 & 0 & 1 & -1 & 0 & 0 & 0 & 0 & 0 & 0 \\ 0 & 0 & 0 & 0 & 0 & 0 & 0 & 0 & 0 & 0 & 0 & 0 & 0 & 0 & 1 & -1 & 0 & 0 & 0 & 0 & 0 \end{array}\right)$$

The global symmetry of Model 6c is $U(1)_{f_1} \times U(1)_{f_2} \times U(1)_R$. The global symmetry is the same as for Model 6a and 6b. The charges on the extremal perfect matchings are shown in Table 22.

Products of non-extremal perfect matchings are chosen to be associated to a single variable as shown below

$$q = q_1 q_2 \ , \ r = r_1 r_2 \ , \ s = \prod_{m=1}^{12} s_m \ . \tag{8.15}$$

Extremal perfect matchings are counted by the fugacity t_α. Products of non-extremal perfect matchings such as q are counted by fugacities of the form y_q.

The refined mesonic Hilbert series of Model 6c computed using the Molien integral formula is identical to the mesonic Hilbert series of Model 6a and 6b in (8.5). Accordingly, the plethystic logarithm are identical as well and hence the mesonic moduli space is a non-complete intersection.

The moduli space generators in terms of perfect matchings of Model 6c are shown in Table 23. The lattice of generators is a reflexive polygon and is the dual of the toric diagram. The generators in terms of quiver fields of Model 6c are shown in Table 26.

Generator	$U(1)_{f_1}$	$U(1)_{f_2}$
$X_{16}X_{67}X_{71} = X_{23}X_{34}^2X_{42} = X_{34}^2X_{45}X_{53}$	1	0
$X_{41}X_{16}X_{64}^1 = X_{23}X_{37}X_{72} = X_{45}X_{56}X_{64}^1$	0	1
$X_{47}X_{71}X_{16}X_{64}^1 = X_{23}X_{34}^2X_{47}X_{72} = X_{13}X_{34}^2X_{41} = X_{13}X_{37}X_{71} = X_{41}X_{16}X_{64}^2 = X_{23}X_{34}^1X_{42}$ $= X_{42}X_{26}X_{64}^1 = X_{26}X_{67}X_{72} = X_{34}^1X_{45}X_{53} = X_{53}X_{37}X_{75} = X_{45}X_{56}X_{64}^2 = X_{56}X_{67}X_{75}$	0	0
$X_{42}X_{26}X_{64}^2 = X_{13}X_{34}^2X_{47}X_{71} = X_{47}X_{71}X_{16}X_{64}^2 = X_{34}^2X_{47}X_{75}X_{53}$	0	-1
$X_{13}X_{34}^1X_{41} = X_{23}X_{34}^1X_{47}X_{72} = X_{47}X_{72}X_{26}X_{64}^1 = X_{56}X_{47}X_{75}X_{64}^1$	-1	0
$X_{13}X_{34}^1X_{47}X_{71} = X_{47}X_{72}X_{26}X_{64}^2 = X_{34}^1X_{47}X_{75}X_{53} = X_{56}X_{47}X_{75}X_{64}^2$	-1	-1

Table 26. The generators in terms of bifundamental fields (Model 6c).

9 Model 7: $\mathbb{C}^3/\mathbb{Z}_6\ (1,2,3)$, $\mathbf{PdP}_{3a}$

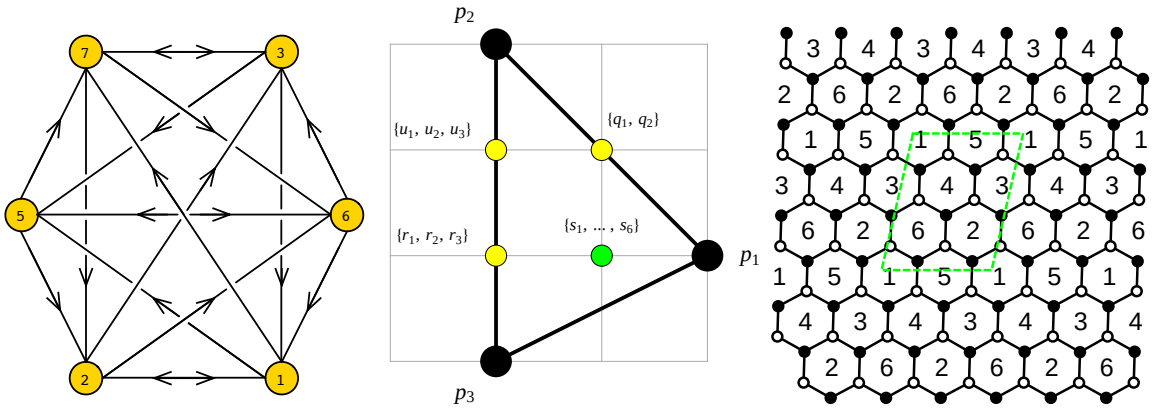


Figure 16. The quiver, toric diagram, and brane tiling of Model 7.

The superpotential is

$$W = +X_{12}X_{26}X_{61} + X_{63}X_{34}X_{46} + X_{24}X_{43}X_{32} + X_{35}X_{51}X_{13} + X_{41}X_{15}X_{54} + X_{56}X_{62}X_{25} \\ -X_{12}X_{25}X_{51} - X_{63}X_{32}X_{26} - X_{24}X_{46}X_{62} - X_{35}X_{54}X_{43} - X_{41}X_{13}X_{34} - X_{56}X_{61}X_{15} \tag{9.1}$$

The perfect matching matrix is

$$P = \left(\begin{array}{c|ccc|cc|ccc|ccc|cccccc} & p_1 & p_2 & p_3 & q_1 & q_2 & r_1 & r_2 & r_3 & u_1 & u_2 & u_3 & s_1 & s_2 & s_3 & s_4 & s_5 & s_6 \\ \hline X_{26} & 1 & 0 & 0 & 1 & 0 & 0 & 0 & 0 & 0 & 0 & 0 & 1 & 0 & 0 & 1 & 1 & 0 \\ X_{62} & 1 & 0 & 0 & 0 & 1 & 0 & 0 & 0 & 0 & 0 & 0 & 0 & 1 & 1 & 0 & 0 & 1 \\ X_{15} & 1 & 0 & 0 & 1 & 0 & 0 & 0 & 0 & 0 & 0 & 0 & 0 & 1 & 1 & 0 & 1 & 0 \\ X_{51} & 1 & 0 & 0 & 0 & 1 & 0 & 0 & 0 & 0 & 0 & 0 & 1 & 0 & 0 & 1 & 0 & 1 \\ X_{43} & 1 & 0 & 0 & 1 & 0 & 0 & 0 & 0 & 0 & 0 & 0 & 1 & 0 & 1 & 0 & 0 & 1 \\ X_{34} & 1 & 0 & 0 & 0 & 1 & 0 & 0 & 0 & 0 & 0 & 0 & 0 & 1 & 0 & 1 & 1 & 0 \\ X_{46} & 0 & 1 & 0 & 1 & 0 & 1 & 0 & 0 & 1 & 1 & 0 & 1 & 0 & 0 & 0 & 0 & 0 \\ X_{32} & 0 & 1 & 0 & 0 & 1 & 1 & 0 & 0 & 1 & 1 & 0 & 0 & 1 & 0 & 0 & 0 & 0 \\ X_{13} & 0 & 1 & 0 & 1 & 0 & 0 & 1 & 0 & 1 & 0 & 1 & 0 & 0 & 1 & 0 & 0 & 0 \\ X_{54} & 0 & 1 & 0 & 0 & 1 & 0 & 1 & 0 & 1 & 0 & 1 & 0 & 0 & 0 & 1 & 0 & 0 \\ X_{25} & 0 & 1 & 0 & 1 & 0 & 0 & 0 & 1 & 0 & 1 & 1 & 0 & 0 & 0 & 0 & 1 & 0 \\ X_{61} & 0 & 1 & 0 & 0 & 1 & 0 & 0 & 1 & 0 & 1 & 1 & 0 & 0 & 0 & 0 & 0 & 1 \\ X_{56} & 0 & 0 & 1 & 0 & 0 & 1 & 1 & 0 & 1 & 0 & 0 & 1 & 0 & 0 & 1 & 0 & 0 \\ X_{12} & 0 & 0 & 1 & 0 & 0 & 1 & 1 & 0 & 1 & 0 & 0 & 0 & 1 & 1 & 0 & 0 & 0 \\ X_{41} & 0 & 0 & 1 & 0 & 0 & 1 & 0 & 1 & 0 & 1 & 0 & 1 & 0 & 0 & 0 & 0 & 1 \\ X_{35} & 0 & 0 & 1 & 0 & 0 & 1 & 0 & 1 & 0 & 1 & 0 & 0 & 1 & 0 & 0 & 1 & 0 \\ X_{24} & 0 & 0 & 1 & 0 & 0 & 0 & 1 & 1 & 0 & 0 & 1 & 0 & 0 & 0 & 1 & 1 & 0 \\ X_{63} & 0 & 0 & 1 & 0 & 0 & 0 & 1 & 1 & 0 & 0 & 1 & 0 & 0 & 1 & 0 & 0 & 1 \end{array}\right)$$

The F-term charge matrix $Q_F = \ker(P)$ is

$$Q_F = \left(\begin{array}{ccc|cc|ccc|ccc|cccccc} p_1 & p_2 & p_3 & q_1 & q_2 & r_1 & r_2 & r_3 & u_1 & u_2 & u_3 & s_1 & s_2 & s_3 & s_4 & s_5 & s_6 \\ \hline 1 & 1 & 0 & -1 & -1 & 0 & 0 & 0 & 0 & 0 & 0 & 0 & 0 & 0 & 0 & 0 & 0 \\ 1 & 0 & 0 & 0 & 0 & 1 & 0 & 0 & 0 & 0 & 0 & -1 & -1 & 0 & 0 & 0 & 0 \\ 1 & 0 & 0 & 0 & 0 & 0 & 1 & 0 & 0 & 0 & 0 & 0 & 0 & -1 & -1 & 0 & 0 \\ 1 & 0 & 0 & 0 & 0 & 0 & 0 & 1 & 0 & 0 & 0 & 0 & 0 & 0 & 0 & -1 & -1 \\ 1 & 0 & 0 & 0 & -1 & 0 & 0 & 0 & 1 & 0 & 0 & -1 & 0 & -1 & 0 & 0 & 1 \\ 0 & 1 & 1 & 0 & 0 & -1 & 0 & 0 & 0 & 0 & -1 & 0 & 0 & 0 & 0 & 0 & 0 \\ 0 & 1 & 1 & 0 & 0 & 0 & -1 & 0 & 0 & -1 & 0 & 0 & 0 & 0 & 0 & 0 & 0 \\ 0 & 1 & 1 & 0 & 0 & 0 & 0 & -1 & -1 & 0 & 0 & 0 & 0 & 0 & 0 & 0 & 0 \\ 0 & 0 & 1 & 0 & 0 & -1 & -1 & 0 & 1 & 0 & 0 & 0 & 0 & 0 & 0 & 0 & 0 \end{array}\right)$$

The D-term charge matrix is

$$Q_D = \left(\begin{array}{ccc|cc|ccc|ccc|cccccc} p_1 & p_2 & p_3 & q_1 & q_2 & r_1 & r_2 & r_3 & u_1 & u_2 & u_3 & s_1 & s_2 & s_3 & s_4 & s_5 & s_6 \\ \hline 0 & 0 & 0 & 0 & 0 & 0 & 0 & 0 & 0 & 0 & 0 & 1 & -1 & 0 & 0 & 0 & 0 \\ 0 & 0 & 0 & 0 & 0 & 0 & 0 & 0 & 0 & 0 & 0 & 0 & 1 & -1 & 0 & 0 & 0 \\ 0 & 0 & 0 & 0 & 0 & 0 & 0 & 0 & 0 & 0 & 0 & 0 & 0 & 1 & -1 & 0 & 0 \\ 0 & 0 & 0 & 0 & 0 & 0 & 0 & 0 & 0 & 0 & 0 & 0 & 0 & 0 & 1 & -1 & 0 \\ 0 & 0 & 0 & 0 & 0 & 0 & 0 & 0 & 0 & 0 & 0 & 0 & 0 & 0 & 0 & 1 & -1 \end{array}\right)$$

The total charge matrix Q_t does not exhibit repeated columns. Accordingly, the global symmetry is $U(1)_{f_1} \times U(1)_{f_2} \times U(1)_R$. The flavour and R-charges on the GLSM fields corresponding to extremal points in the toric diagram in Figure 16 are found as shown in Table 27 following the discussion in §2.3.

	$U(1)_{f_1}$	$U(1)_{f_2}$	$U(1)_R$	fugacity
p_1	1/2	0	2/3	t_1
p_2	-1/6	1/3	2/3	t_2
p_3	-1/3	-1/3	2/3	t_3

Table 27. The GLSM fields corresponding to extremal points of the toric diagram with their mesonic charges (Model 7).

Products of non-extremal perfect matchings are expressed in terms of single variables as follows

$$q = q_1 q_2 \ , \ r = r_1 r_2 r_3 \ , \ u = u_1 u_2 u_3 \ , \ s = \prod_{m=1}^{6} s_m \ . \tag{9.2}$$

Extremal perfect matchings are counted by the fugacity t_α. Products of non-extremal perfect matchings such as q are counted by fugacities of the form y_q.

The mesonic Hilbert series of Model 7 is

$$g_1(t_\alpha, y_q, y_r, y_u, y_s; \mathcal{M}_7^{mes}) = \frac{1 + y_q^2 y_r y_u^2 y_s \; t_1 t_2^3 + y_q y_r y_u y_s \; t_1 t_2 t_3 + y_q^2 y_r^2 y_u^3 y_s \; t_2^4 t_3 + y_q y_r^2 y_u^2 y_s \; t_2^2 t_3^2 + y_q^3 y_r^3 y_u^4 y_s^2 \; t_1 t_2^5 t_3^2}{(1 - y_q y_s \; t_1^2)(1 - y_q^3 y_r^2 y_u^4 y_s \; t_2^6)(1 - y_r^2 y_u y_s \; t_3^3)} \; . \tag{9.3}$$

The plethystic logarithm of the mesonic Hilbert series is

$$\begin{aligned} PL[g_1(t_\alpha, y_q, y_r, y_u, y_s; \mathcal{M}_7^{mes})] &= y_q y_s \; t_1^2 + y_q y_r y_u y_s \; t_1 t_2 t_3 + y_r^2 y_u y_s \; t_3^3 \\ &+ y_q y_r^2 y_u^2 y_s \; t_2^2 t_3^2 + y_q^2 y_r y_u^2 y_s \; t_1 t_2^3 + y_q^2 y_r^2 y_u^3 y_s \; t_2^4 t_3 - y_q^2 y_r^2 y_u^2 y_s^2 \; t_1^2 t_2^2 t_3^2 \\ &+ y_q^3 y_r^2 y_u^4 y_s \; t_2^6 - y_q^2 y_r^3 y_u^3 y_s^2 \; t_1 t_2^3 t_3^3 - y_q^3 y_r^2 y_u^3 y_s^2 \; t_1^2 t_2^4 t_3 + \dots \; . \end{aligned} \tag{9.4}$$

With the following fugacity map

$$\begin{aligned} f_1 &= y_q^{1/3} y_r^{-2/3} y_u^{-2/3} y s^{1/3} \; t_1^{4/3} t_2^{-2/3} t_3^{-2/3} \; , \\ f_2 &= y_q^{2/3} y_r^{-1/3} y_u^{2/3} y_s^{-1/3} \; t_1^{-1/3} t_2^{5/3} t_3^{-4/3} \; , \\ t &= y_q^{1/3} y_r^{1/3} y_u^{1/3} y_s^{1/3} t_1^{1/3} t_2^{1/3} t_3^{1/3} \; , \end{aligned} \tag{9.5}$$

where the fugacities f_1, f_2 and t count the mesonic symmetry charges. Under the fugacity map above, the above plethystic logarithm becomes

$$\begin{aligned} PL[g_1(t, f_1, f_2; \mathcal{M}_7^{mes})] &= f_1 t^2 + \left(1 + \frac{1}{f_1 f_2}\right) t^3 + \left(\frac{1}{f_1} + f_2\right) t^4 + \frac{f_2}{f_1} t^5 - t^6 + \frac{f_2^2}{f_1} t^6 \\ &- \left(\frac{1}{f_1} + f_2\right) t^7 + \dots \; . \end{aligned} \tag{9.6}$$

The plethystic logarithm above exhibits the moduli space generators with their mesonic charges. They are summarized in Table 28. The mesonic generators can be presented on a charge lattice. The convex polygon formed by the generators in Table 28 is the dual reflexive polygon of the toric diagram of Model 7. For the case of Model 7, the toric diagram is self-dual, and the charge lattice of the generators forms again the toric diagram of Model 7.

Generator	$U(1)_{f_1}$	$U(1)_{f_2}$
$p_1^2\ q\ s$	1	0
$p_1p_2p_3\ q\ r\ u\ s$	0	0
$p_1p_2^3\ q^2\ r\ u^2\ s$	0	1
$p_3^3\ r^2\ u\ s$	-1	-1
$p_2^2p_3^2\ q\ r^2\ u^2\ s$	-1	0
$p_2^4p_3\ q^2\ r^2\ u^3\ s$	-1	1
$p_2^6\ q^3\ r^2\ u^4\ s$	-1	2

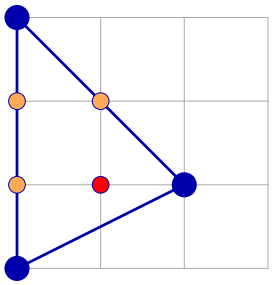


Table 28. The generators and lattice of generators of the mesonic moduli space of Model 7 in terms of GLSM fields with the corresponding flavor charges.

Generator	$U(1)_{f_1}$	$U(1)_{f_2}$
$X_{15}X_{51} = X_{26}X_{62} = X_{34}X_{43}$	1	0
$X_{12}X_{25}X_{51} = X_{12}X_{26}X_{61} = X_{13}X_{34}X_{41} = X_{13}X_{35}X_{51} = X_{15}X_{54}X_{41} = X_{15}X_{56}X_{61}$ $= X_{24}X_{43}X_{32} = X_{24}X_{46}X_{62} = X_{25}X_{56}X_{62} = X_{26}X_{63}X_{32} = X_{34}X_{46}X_{63} = X_{35}X_{54}X_{43}$	0	0
$X_{13}X_{32}X_{25}X_{51} = X_{13}X_{32}X_{26}X_{61} = X_{13}X_{34}X_{46}X_{61} = X_{15}X_{54}X_{46}X_{61} = X_{25}X_{54}X_{43}X_{32} = X_{25}X_{54}X_{46}X_{62}$	0	1
$X_{12}X_{24}X_{41} = X_{35}X_{56}X_{63}$	-1	-1
$X_{12}X_{24}X_{46}X_{61} = X_{12}X_{25}X_{54}X_{41} = X_{12}X_{25}X_{56}X_{61} = X_{13}X_{32}X_{24}X_{41} = X_{13}X_{35}X_{54}X_{41}$ $= X_{13}X_{35}X_{56}X_{61} = X_{24}X_{46}X_{63}X_{32} = X_{25}X_{56}X_{63}X_{32} = X_{35}X_{54}X_{46}X_{63}$	-1	0
$X_{12}X_{25}X_{54}X_{46}X_{61} = X_{13}X_{32}X_{24}X_{46}X_{61} = X_{13}X_{32}X_{25}X_{54}X_{41}$ $= X_{13}X_{32}X_{25}X_{56}X_{61} = X_{13}X_{35}X_{54}X_{46}X_{61} = X_{25}X_{54}X_{46}X_{63}X_{32}$	-1	1
$X_{13}X_{32}X_{25}X_{54}X_{46}X_{61}$	-1	2

Table 29. The generators in terms of bifundamental fields (Model 7).

With the fugacity map

$$\begin{aligned} T_1 &= f_1^{1/2}\ t = y_q^{1/2}y_s^{1/2}\ t_1\ , \\ T_2 &= \frac{f_2^{1/3}\ t}{f_1^{1/6}} = y_q^{1/2}y_r^{1/3}y_u^{2/3}y_s^{1/6}\ t_2\ , \\ T_3 &= \frac{t}{f_1^{1/3}f_2^{1/3}} = y_r^{2/3}y_u^{1/3}y_s^{1/3}\ t_3 \end{aligned} \tag{9.7}$$

the mesonic Hilbert series becomes

$$g_1(T_1,T_2,T_3;\mathcal{M}_7^{mes}) = \frac{1+T_1T_2^3+T_1T_2T_3+T_2^4T_3+T_2^2T_3^2+T_1T_2^5T_3^2}{(1-T_1^2)(1-T_2^6)(1-T_3^2)} \tag{9.8}$$

with the plethystic logarithm being

$$\begin{aligned} PL[g_1(T_1,T_2,T_3;\mathcal{M}_7^{mes})] &= T_1^2+T_1T_2T_3+T_3^3+T_2T_3+T_1T_2^3 \\ &+T_2^4T_3-T_1^2T_2^2T_3^2+T_2^6-T_1T_2^3T_3^3-T_1^2T_2^4T_3+\dots \end{aligned} \tag{9.9}$$

The above Hilbert series and plethystic logarithm illustrate the conical structure of the toric Calabi-Yau 3-fold.

10 Model 8: SPP/$\mathbb{Z}_2$ $(0,1,1,1)$, $\mathbf{PdP}_{3c}$

10.1 Model 8 Phase a

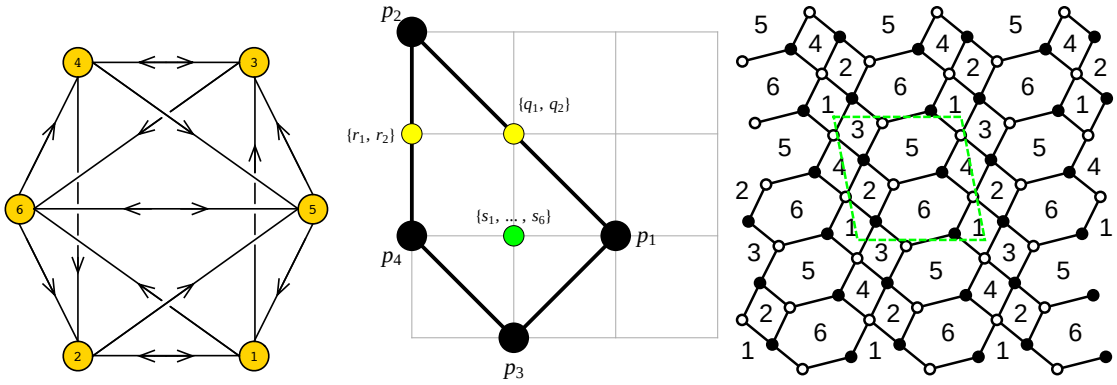


Figure 17. The quiver, toric diagram, and brane tiling of Model 8a.

The superpotential is

$$\begin{aligned} W = &+X_{56}X_{62}X_{25} + X_{65}X_{53}X_{36} + X_{13}X_{34}X_{45}X_{51} + X_{21}X_{16}X_{64}X_{42} \\ &-X_{56}X_{64}X_{45} - X_{65}X_{51}X_{16} - X_{13}X_{36}X_{62}X_{21} - X_{25}X_{53}X_{34}X_{42} \end{aligned} \tag{10.1}$$

The perfect matching matrix is

$$P = \left(\begin{array}{c|cccc|cc|cc|cccccc} & p_1 & p_2 & p_3 & p_4 & q_1 & q_2 & r_1 & r_2 & s_1 & s_2 & s_3 & s_4 & s_5 & s_6 \\ \hline X_{16} & 1 & 0 & 0 & 0 & 1 & 0 & 0 & 0 & 0 & 1 & 1 & 0 & 0 & 0 \\ X_{45} & 1 & 0 & 0 & 0 & 1 & 0 & 0 & 0 & 0 & 0 & 0 & 0 & 1 & 1 \\ X_{62} & 1 & 0 & 0 & 0 & 0 & 1 & 0 & 0 & 1 & 0 & 0 & 0 & 0 & 1 \\ X_{53} & 1 & 0 & 0 & 0 & 0 & 1 & 0 & 0 & 0 & 0 & 1 & 1 & 0 & 0 \\ X_{36} & 0 & 1 & 0 & 0 & 1 & 0 & 1 & 0 & 0 & 1 & 0 & 0 & 0 & 0 \\ X_{25} & 0 & 1 & 0 & 0 & 1 & 0 & 0 & 1 & 0 & 0 & 0 & 0 & 1 & 0 \\ X_{51} & 0 & 1 & 0 & 0 & 0 & 1 & 1 & 0 & 0 & 0 & 0 & 1 & 0 & 0 \\ X_{64} & 0 & 1 & 0 & 0 & 0 & 1 & 0 & 1 & 1 & 0 & 0 & 0 & 0 & 0 \\ X_{56} & 0 & 0 & 1 & 1 & 0 & 0 & 1 & 0 & 0 & 1 & 1 & 1 & 0 & 0 \\ X_{65} & 0 & 0 & 1 & 1 & 0 & 0 & 0 & 1 & 1 & 0 & 0 & 0 & 1 & 1 \\ X_{34} & 0 & 0 & 1 & 0 & 0 & 0 & 0 & 0 & 1 & 1 & 0 & 0 & 0 & 0 \\ X_{21} & 0 & 0 & 1 & 0 & 0 & 0 & 0 & 0 & 0 & 0 & 0 & 1 & 1 & 0 \\ X_{42} & 0 & 0 & 0 & 1 & 0 & 0 & 1 & 0 & 0 & 0 & 0 & 0 & 0 & 1 \\ X_{13} & 0 & 0 & 0 & 1 & 0 & 0 & 0 & 1 & 0 & 0 & 1 & 0 & 0 & 0 \end{array}\right)$$

The F-term charge matrix $Q_F = \ker(P)$ is

$$Q_F = \left(\begin{array}{cccc|cc|cc|cccccc} p_1 & p_2 & p_3 & p_4 & q_1 & q_2 & r_1 & r_2 & s_1 & s_2 & s_3 & s_4 & s_5 & s_6 \\ \hline 1 & 1 & 0 & 0 & -1 & -1 & 0 & 0 & 0 & 0 & 0 & 0 & 0 & 0 \\ 1 & 0 & 0 & 0 & -1 & 0 & 0 & 1 & -1 & 1 & -1 & 0 & 0 & 0 \\ 0 & 1 & 0 & 0 & -1 & 0 & -1 & 0 & -1 & 1 & 0 & 0 & 0 & 1 \\ 0 & 1 & 0 & 1 & 0 & 0 & -1 & -1 & 0 & 0 & 0 & 0 & 0 & 0 \\ 0 & 0 & 1 & 0 & 1 & 0 & 0 & 0 & 0 & -1 & 0 & 0 & -1 & 0 \\ 0 & 0 & 1 & 0 & 0 & 1 & 0 & 0 & -1 & 0 & 0 & -1 & 0 & 0 \end{array}\right)$$

The D-term charge matrix is

$$Q_D = \left(\begin{array}{cccc|cc|cc|cccccc} p_1 & p_2 & p_3 & p_4 & q_1 & q_2 & r_1 & r_2 & s_1 & s_2 & s_3 & s_4 & s_5 & s_6 \\ \hline 0 & 0 & 0 & 0 & 0 & 0 & 0 & 0 & 1 & -1 & 0 & 0 & 0 & 0 \\ 0 & 0 & 0 & 0 & 0 & 0 & 0 & 0 & 0 & 1 & -1 & 0 & 0 & 0 \\ 0 & 0 & 0 & 0 & 0 & 0 & 0 & 0 & 0 & 0 & 1 & -1 & 0 & 0 \\ 0 & 0 & 0 & 0 & 0 & 0 & 0 & 0 & 0 & 0 & 0 & 1 & -1 & 0 \\ 0 & 0 & 0 & 0 & 0 & 0 & 0 & 0 & 0 & 0 & 0 & 0 & 1 & -1 \end{array}\right)$$

The total charge matrix Q_t does not have repeated columns. Accordingly, the global symmetry is $U(1)_{f_1} \times U(1)_{f_2} \times U(1)_R$. The mesonic charges on the GLSM fields corresponding to extremal points in the toric diagram in Figure 17 are presented in Table 30. The charges have been found using the constraints discussed in §2.3.

	$U(1)_{f_1}$	$U(1)_{f_2}$	$U(1)_R$	fugacity
p_1	1	0	$R_1 = 1/\sqrt{3}$	t_1
p_2	-1/2	1/2	$R_1 = 1/\sqrt{3}$	t_2
p_3	-1	0	$R_2 = 1 - 1/\sqrt{3}$	t_3
p_4	1/2	-1/2	$R_2 = 1 - 1/\sqrt{3}$	t_4

Table 30. The GLSM fields corresponding to extremal points of the toric diagram with their mesonic charges (Model 8a). The R-charges are obtained using a-maximization.

Products of non-extremal perfect matchings are labelled in terms of single variables as follows

$$q = q_1 q_2 \ , \ r = r_1 r_2 \ , \ s = \prod_{m=1}^{6} s_m \ . \tag{10.2}$$

The fugacity which counts extremal perfect matchings p_α is t_α. A product of non-extremal perfect matchings such as q above is associated to the fugacity of the form y_q.

The mesonic Hilbert series of Model 8a is calculated using the Molien integral formula in (2.9). It is

$$\begin{aligned} g_1(t_\alpha, y_q, y_r, y_s; \mathcal{M}_{8a}^{mes}) = & (1 + y_q^2 y_r^2 y_s \ t_1 t_2^3 t_4 + y_q y_r y_s \ t_1 t_2 t_3 t_4 - y_q^3 y_r^2 y_s^2 \ t_1^3 t_2^3 t_3 t_4 \\ & + y_q y_r^2 y_s \ t_2^2 t_3 t_4^2 - y_q^3 y_r^3 y_s^2 \ t_1^2 t_2^4 t_3 t_4^2 - y_q^2 y_r^2 y_s^2 \ t_1^2 t_2^2 t_3^2 t_4^2 - y_q^4 y_r^4 y_s^3 \ t_1^3 t_2^5 t_3^2 t_4^3) \\ & \times \frac{1}{(1 - y_q^2 y_r y_s \ t_1^2 t_2^2)(1 - y_q y_s \ t_1^2 t_3)(1 - y_q^2 y_r^3 y_s \ t_2^4 t_4^2)(1 - y_r y_s \ t_3^2 t_4^2)} \ . \end{aligned} \tag{10.3}$$

The plethystic logarithm of the mesonic Hilbert series is

$$\begin{aligned} PL[g_1(t_\alpha, y_q, y_r, y_s; \mathcal{M}_{8a}^{mes})] = & y_q^2 y_r y_s \ t_1^2 t_2^2 + y_q y_s \ t_1^2 t_3 + y_q^2 y_r^2 y_s \ t_1 t_2^3 t_4 + y_q y_r y_s \ t_1 t_2 t_3 t_4 \\ & + y_q^2 y_r^3 y_s \ t_2^4 t_4^2 - y_q^3 y_r^2 y_s^2 \ t_1^3 t_2^3 t_3 t_4 - y_q^4 y_r^4 y_s^2 \ t_1^2 t_2^6 t_4^2 + y_q y_r^2 y_s \ t_2^2 t_3 t_4^2 - 2 \ y_q^3 y_r^3 y_s^2 \ t_1^2 t_2^4 t_3 t_4^2 \\ & + \dots \ . \end{aligned} \tag{10.4}$$

Consider the following fugacity map

$$f_1 = \frac{t_1 t_3^{1/2}}{y_r \ t_2 t_4^{1/2}} \ , \ f_2 = \frac{t_2 t_4^{1/2}}{y_s \ t_1 t_3^{1/2}} \ , \ \tilde{t}_1 = y_q^{1/2} y_r^{1/2} y_s^{1/2} \ t_1^{1/2} t_2^{1/2} \ , \ \tilde{t}_2 = t_3^{1/2} t_4^{1/2} \ , \tag{10.5}$$

where the fugacities f_1 and f_2 count flavour charges, and the fugacities $\tilde{t}_1$ and $\tilde{t}_2$ count R-charges R_1 and R_2 in Table 30 respectively. Under the fugacity map above, the plethystic logarithm becomes

$$\begin{aligned} PL[g_1(\tilde{t}_\alpha, f_1, f_2; \mathcal{M}_{8a}^{mes})] = & f_1 f_2 \tilde{t}_1^4 + f_1 \tilde{t}_1^2 \tilde{t}_2 + f_2 \tilde{t}_1^4 \tilde{t}_2 + \tilde{t}_1^2 \tilde{t}_2^2 + \frac{f_2}{f_1} \tilde{t}_1^4 \tilde{t}_2^2 - f_1 f_2 \tilde{t}_1^6 \tilde{t}_2^2 \\ & - f_2^2 \tilde{t}_1^8 \tilde{t}_2^2 + \frac{1}{f_1} \tilde{t}_1^2 \tilde{t}_2^3 - 2 f_2 \tilde{t}_1^6 \tilde{t}_2^3 \dots \ . \end{aligned} \tag{10.6}$$

The above plethystic logarithm exhibits the moduli space generators with their corresponding mesonic charges. They are summarized in Table 31. The generators can be presented on a charge lattice. The convex polygon formed by the generators in Table 31 is the dual reflexive polygon of the toric diagram of Model 8a. For the case of Model 8a, the toric diagram is self-dual, and the charge lattice of the generators forms again the toric diagram of Model 8a.

Generator	$U(1)_{f_1}$	$U(1)_{f_2}$
$p_1^2 p_3\ q\ s$	1	0
$p_3^2 p_4^2\ r\ s$	-1	-1
$p_1 p_2 p_3 p_4\ q\ r\ s$	0	0
$p_1^2 p_2^2\ q^2\ r\ s$	1	1
$p_2^2 p_3 p_4^2\ q\ r^2\ s$	-1	0
$p_1 p_2^3 p_4\ q^2\ r^2\ s$	0	1
$p_2^4 p_4^2\ q^2\ r^3\ s$	-1	1

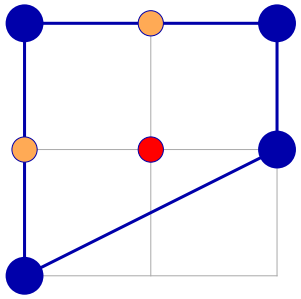


Table 31. The generators and lattice of generators of the mesonic moduli space of Model 8a in terms of GLSM fields with the corresponding flavor charges.

Generator	$U(1)_{f_1}$	$U(1)_{f_2}$
$X_{16}X_{62}X_{21} = X_{34}X_{45}X_{53}$	1	0
$X_{56}X_{65} = X_{13}X_{34}X_{42}X_{21}$	-1	-1
$X_{16}X_{65}X_{51} = X_{25}X_{56}X_{62} = X_{36}X_{65}X_{53} = X_{45}X_{56}X_{64}$	0	0
$= X_{13}X_{36}X_{62}X_{21} = X_{13}X_{34}X_{45}X_{51} = X_{16}X_{64}X_{42}X_{21} = X_{25}X_{53}X_{34}X_{42}$		
$X_{16}X_{62}X_{25}X_{51} = X_{16}X_{64}X_{45}X_{51} = X_{25}X_{53}X_{36}X_{62} = X_{36}X_{64}X_{45}X_{53}$	1	1
$X_{13}X_{36}X_{65}X_{51} = X_{25}X_{56}X_{64}X_{42} = X_{13}X_{36}X_{64}X_{42}X_{21} = X_{13}X_{34}X_{42}X_{25}X_{51}$	-1	0
$X_{13}X_{36}X_{62}X_{25}X_{51} = X_{13}X_{36}X_{64}X_{45}X_{51} = X_{16}X_{64}X_{42}X_{25}X_{51} = X_{25}X_{53}X_{36}X_{64}X_{42}$	0	1
$X_{13}X_{36}X_{64}X_{42}X_{25}X_{51}$	-1	1

Table 32. The generators in terms of bifundamental fields (Model 8a).

The mesonic Hilbert series and the plethystic logarithm can be re-expressed in terms of just 3 fugacities

$$T_1 = \frac{\tilde{t}_2}{f_1^2 f_2\ \tilde{t}_1^4} = \frac{t_4}{y_q^2 y_s\ t_1^3 t_2}\ ,\ T_2 = f_1 f_2\ \tilde{t}_1^4 = y_q^2 y_r y_s\ t_1^2 t_2^2\ ,\ T_3 = f_1\ \tilde{t}_1^2 \tilde{t}_2 = y_q y_s\ t_1^2 t_3\ , \tag{10.7}$$

such that

$$g_1(T_1, T_2, T_3; \mathcal{M}_{8a}^{mes}) = \frac{1 + T_1 T_2^2 + T_1 T_2 T_3 - T_1 T_2^2 T_3 + T_1^2 T_2^2 T_3 - T_1^2 T_2^3 T_3 - T_1^2 T_2^2 T_3^2 - T_1^3 T_2^4 T_3^2}{(1 - T_2)(1 - T_3)(1 - T_1^2 T_2^3)(1 - T_1^2 T_2 T_3^2)} \tag{10.8}$$

and

$$PL[g_1(T_1, T_2, T_3; \mathcal{M}_{8a}^{mes})] = T_2 + T_3 + T_1 T_2^2 + T_1 T_2 T_3 + T_1^2 T_2^3 - T_1 T_2^2 T_3 - T_1^2 T_2^4 + T_1^2 T_2^2 T_3 - 2 T_1^2 T_2^3 T_3 + \dots\ . \tag{10.9}$$

The above Hilbert series and plethystic logarithm in terms of just three fugacities with positive powers illustrate the conical structure of the toric Calabi-Yau 3-fold.

10.2 Model 8 Phase b

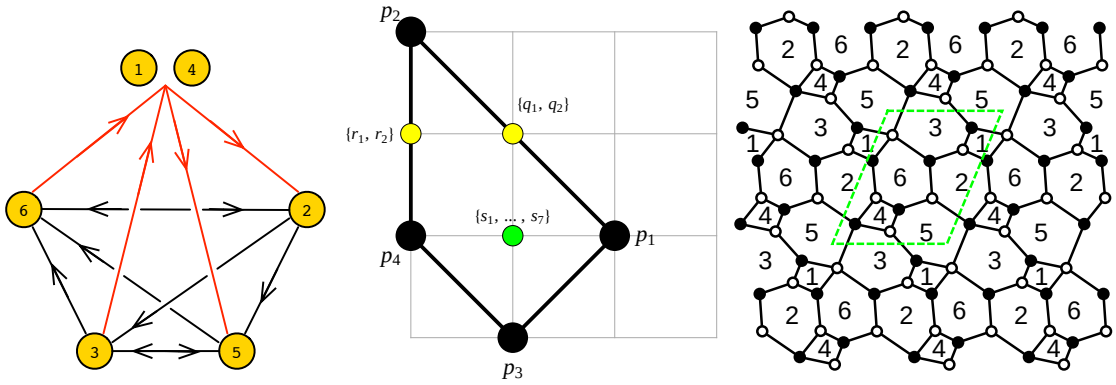


Figure 18. The quiver, toric diagram, and brane tiling of Model 8b. The red arrows in the quiver indicate all possible connections between blocks of nodes.

The superpotential is

$$\begin{aligned} W = &+X_{31}X_{12}X_{23} + X_{56}X_{62}X_{25} + X_{64}X_{42}X_{26} + X_{61}X_{15}X_{53}^{1}X_{36} + X_{34}X_{45}X_{53}^{2} \\ &-X_{31}X_{15}X_{53}^{2} - X_{36}X_{62}X_{23} - X_{56}X_{64}X_{45} - X_{61}X_{12}X_{26} - X_{25}X_{53}^{1}X_{34}X_{42} \quad . \end{aligned} \tag{10.10}$$

The perfect matching matrix is

$$P = \left(\begin{array}{c|cccc|cc|cc|ccccccc} & p_1 & p_2 & p_3 & p_4 & q_1 & q_2 & r_1 & r_2 & s_1 & s_2 & s_3 & s_4 & s_5 & s_6 & s_7 \\ \hline X_{560} & 1 & 1 & 0 & 0 & 0 & 0 & 1 & 0 & 0 & 0 & 1 & 1 & 0 & 0 & 0 \\ X_{23} & 1 & 1 & 0 & 0 & 0 & 0 & 0 & 1 & 1 & 0 & 0 & 1 & 0 & 0 & 0 \\ X_{26} & 1 & 0 & 1 & 0 & 0 & 1 & 0 & 0 & 1 & 0 & 1 & 1 & 0 & 0 & 0 \\ X_{15} & 1 & 0 & 0 & 0 & 0 & 0 & 0 & 0 & 1 & 0 & 0 & 0 & 1 & 0 & 1 \\ X_{34} & 1 & 0 & 0 & 0 & 0 & 0 & 0 & 0 & 0 & 1 & 1 & 0 & 0 & 0 & 1 \\ X_{53}^2 & 0 & 1 & 0 & 1 & 1 & 0 & 1 & 1 & 0 & 0 & 0 & 1 & 0 & 0 & 0 \\ X_{42} & 0 & 1 & 0 & 0 & 0 & 0 & 1 & 0 & 0 & 0 & 0 & 0 & 1 & 1 & 0 \\ X_{61} & 0 & 1 & 0 & 0 & 0 & 0 & 0 & 1 & 0 & 1 & 0 & 0 & 0 & 1 & 0 \\ X_{62} & 0 & 0 & 1 & 0 & 1 & 0 & 0 & 0 & 0 & 1 & 0 & 0 & 1 & 1 & 1 \\ X_{53}^1 & 0 & 0 & 1 & 0 & 1 & 0 & 0 & 0 & 0 & 0 & 0 & 1 & 0 & 0 & 0 \\ X_{45} & 0 & 0 & 1 & 0 & 0 & 1 & 0 & 0 & 1 & 0 & 0 & 0 & 1 & 1 & 0 \\ X_{31} & 0 & 0 & 1 & 0 & 0 & 1 & 0 & 0 & 0 & 1 & 1 & 0 & 0 & 1 & 0 \\ X_{12} & 0 & 0 & 0 & 1 & 1 & 0 & 1 & 0 & 0 & 0 & 0 & 0 & 1 & 0 & 1 \\ X_{64} & 0 & 0 & 0 & 1 & 1 & 0 & 0 & 1 & 0 & 1 & 0 & 0 & 0 & 0 & 1 \\ X_{36} & 0 & 0 & 0 & 1 & 0 & 1 & 1 & 0 & 0 & 0 & 1 & 0 & 0 & 0 & 0 \\ X_{25} & 0 & 0 & 0 & 1 & 0 & 1 & 0 & 1 & 1 & 0 & 0 & 0 & 0 & 0 & 0 \end{array}\right)$$

The F-term charge matrix $Q_F = \ker(P)$ is

$$Q_F = \left(\begin{array}{cccc|cc|cc|ccccccc} p_1 & p_2 & p_3 & p_4 & q_1 & q_2 & r_1 & r_2 & s_1 & s_2 & s_3 & s_4 & s_5 & s_6 & s_7 \\ \hline 1 & 1 & 1 & 1 & 0 & 0 & -1 & 0 & 0 & -1 & 0 & 0 & -1 & -1 & 0 \\ 1 & 1 & 0 & 0 & -1 & -1 & 0 & 0 & 0 & 0 & 0 & 0 & 0 & 0 & 0 \\ 0 & 1 & 1 & 0 & 0 & 0 & -1 & 0 & 1 & 0 & -1 & 0 & 0 & -1 & 0 \\ 0 & 0 & 1 & 0 & 1 & 0 & 0 & 0 & 0 & 0 & 0 & 0 & 0 & -1 & -1 \\ 0 & 0 & 0 & 1 & 1 & 0 & -1 & 0 & 0 & -1 & 1 & 0 & 0 & -1 & 0 \\ 0 & 0 & 0 & 1 & 1 & 0 & -1 & 0 & 1 & 0 & 0 & -1 & 0 & -1 & 0 \\ 0 & 0 & 0 & 1 & 1 & 0 & 0 & -1 & -1 & 0 & 1 & 0 & 0 & 0 & -1 \end{array}\right)$$

The D-term charge matrix is

$$Q_D = \left(\begin{array}{cccc|cc|cc|ccccccc} p_1 & p_2 & p_3 & p_4 & q_1 & q_2 & r_1 & r_2 & s_1 & s_2 & s_3 & s_4 & s_5 & s_6 & s_7 \\ \hline 0 & 0 & 0 & 0 & 0 & 0 & 0 & 0 & 0 & 1 & -1 & 0 & 0 & 0 & 0 \\ 0 & 0 & 0 & 0 & 0 & 0 & 0 & 0 & 0 & 0 & 1 & -1 & 0 & 0 & 0 \\ 0 & 0 & 0 & 0 & 0 & 0 & 0 & 0 & 0 & 0 & 0 & 1 & -1 & 0 & 0 \\ 0 & 0 & 0 & 0 & 0 & 0 & 0 & 0 & 0 & 0 & 0 & 0 & 1 & -1 & 0 \\ 0 & 0 & 0 & 0 & 0 & 0 & 0 & 0 & 0 & 0 & 0 & 0 & 0 & 1 & -1 \end{array}\right)$$

The total charge matrix Q_t does not have repeated columns. Accordingly, the global symmetry is $U(1)_{f_1} \times U(1)_{f_2} \times U(1)_R$. The flavour and R-charges on the GLSM fields corresponding to extremal points in the toric diagram are the same as in Model 8a, and are given in Table 30.

Products of non-extremal perfect matchings are expressed as

$$q = q_1 q_2 \ , \ r = r_1 r_2 \ , \ s = \prod_{m=1}^{7} s_m \ . \tag{10.11}$$

The extremal perfect matchings are counted by t_α. Products of non-extremal perfect matchings such as q are associated to a fugacity of the form y_q.

The mesonic Hilbert series and the plethystic logarithm are identical to the ones for Model 8a and are given in (10.3) and (10.6) respectively. As a result, the mesonic moduli spaces for Models 8a and 8b are the same.

The generators of the mesonic moduli space in terms of all perfect matchings of Model 8b are shown in Table 31. In terms of Model 8b quiver fields, the generators are shown in Table 33. From the plethystic logarithm in (10.6) one observes that the mesonic moduli space is not a complete intersection.

Generator	$U(1)_{f_1}$	$U(1)_{f_2}$
$X_{26}X_{62} = X_{15}X^1_{53}X_{31} = X_{34}X_{45}X^1_{53}$	1	0
$X_{15}X_{56}X_{61} = X_{23}X_{34}X_{42}$	-1	-1
$X_{15}X^1_{53}X_{36}X_{61} = X_{25}X^1_{53}X_{34}X_{42} = X_{12}X_{23}X_{31} = X_{12}X_{26}X_{61} = X_{15}X^2_{53}X_{31}$ $= X_{23}X_{36}X_{62} = X_{25}X_{56}X_{62} = X_{26}X_{64}X_{42} = X_{34}X_{45}X^2_{53} = X_{45}X_{56}X_{64}$	0	0
$X_{12}X_{25}X^1_{53}X_{31} = X_{25}X^1_{53}X_{36}X_{62} = X_{36}X_{64}X_{45}X^1_{53}$	1	1
$X_{12}X_{23}X_{36}X_{61} = X_{12}X_{25}X_{56}X_{61} = X_{15}X^2_{53}X_{36}X_{61}$ $= X_{23}X_{36}X_{64}X_{42} = X_{25}X^2_{53}X_{34}X_{42} = X_{25}X_{56}X_{64}X_{42}$	-1	0
$X_{12}X_{25}X^1_{53}X_{36}X_{61} = X_{25}X^1_{53}X_{36}X_{64}X_{42} = X_{12}X_{25}X^2_{53}X_{31} = X_{25}X^2_{53}X_{36}X_{62} = X_{36}X_{64}X_{45}X^2_{53}$	0	1
$X_{12}X_{25}X^2_{53}X_{36}X_{61} = X_{25}X^2_{53}X_{36}X_{64}X_{42}$	-1	1

Table 33. The generators in terms of bifundamental fields (Model 8b).

11 Model 9: PdP_{3b}

11.1 Model 9 Phase a

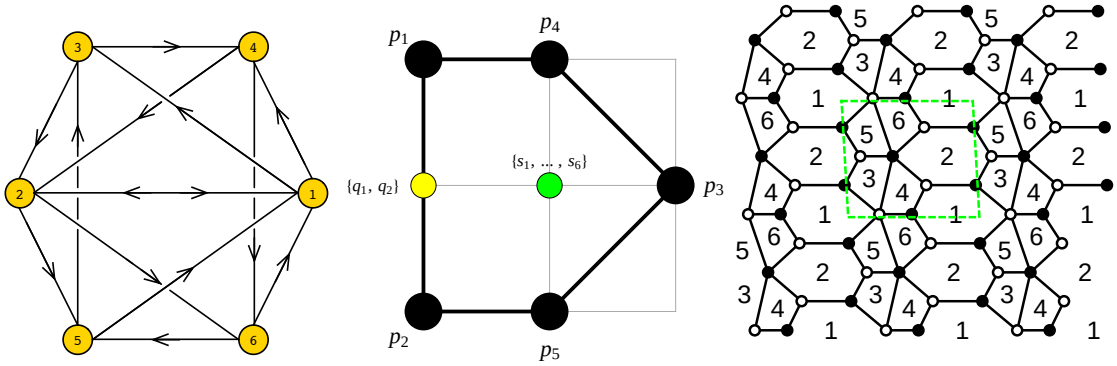


Figure 19. The quiver, toric diagram, and brane tiling of Model 9a.

The superpotential is

$$\begin{aligned} W = &+X_{12}X_{26}X_{61} + X_{25}X_{53}X_{32} + X_{42}X_{21}X_{14} + X_{13}X_{34}X_{46}X_{65}X_{51} \\ &-X_{13}X_{32}X_{21} - X_{25}X_{51}X_{12} - X_{46}X_{61}X_{14} - X_{26}X_{65}X_{53}X_{34}X_{42} \end{aligned} \tag{11.1}$$

The perfect matching matrix is

$$P = \left(\begin{array}{c|cccccc|cc|cccccc} & p_1 & p_2 & p_3 & p_4 & p_5 & q_1 & q_2 & s_1 & s_2 & s_3 & s_4 & s_5 & s_6 \\ \hline X_{26} & 1 & 0 & 0 & 0 & 0 & 1 & 0 & 1 & 0 & 0 & 0 & 0 & 0 \\ X_{51} & 1 & 0 & 0 & 0 & 0 & 0 & 1 & 0 & 1 & 0 & 0 & 0 & 0 \\ X_{13} & 0 & 1 & 0 & 0 & 0 & 1 & 0 & 0 & 0 & 1 & 0 & 0 & 0 \\ X_{42} & 0 & 1 & 0 & 0 & 0 & 0 & 1 & 0 & 0 & 0 & 1 & 0 & 0 \\ X_{46} & 0 & 0 & 1 & 0 & 0 & 0 & 0 & 1 & 0 & 0 & 1 & 0 & 0 \\ X_{53} & 0 & 0 & 1 & 0 & 0 & 0 & 0 & 0 & 1 & 1 & 0 & 0 & 0 \\ X_{14} & 1 & 0 & 0 & 1 & 0 & 1 & 0 & 0 & 0 & 1 & 0 & 1 & 0 \\ X_{32} & 1 & 0 & 0 & 1 & 0 & 0 & 1 & 0 & 0 & 0 & 1 & 1 & 0 \\ X_{25} & 0 & 1 & 0 & 0 & 1 & 1 & 0 & 1 & 0 & 0 & 0 & 0 & 1 \\ X_{61} & 0 & 1 & 0 & 0 & 1 & 0 & 1 & 0 & 1 & 0 & 0 & 0 & 1 \\ X_{12} & 0 & 0 & 1 & 1 & 0 & 0 & 0 & 0 & 0 & 1 & 1 & 1 & 0 \\ X_{21} & 0 & 0 & 1 & 0 & 1 & 0 & 0 & 1 & 1 & 0 & 0 & 0 & 1 \\ X_{65} & 0 & 0 & 0 & 1 & 0 & 0 & 0 & 0 & 0 & 0 & 0 & 0 & 1 \\ X_{34} & 0 & 0 & 0 & 0 & 1 & 0 & 0 & 0 & 0 & 0 & 0 & 1 & 0 \end{array}\right)$$

The F-term charge matrix $Q_F = \ker(P)$ is

$$Q_F = \left(\begin{array}{cccccc|cc|cccccc} p_1 & p_2 & p_3 & p_4 & p_5 & q_1 & q_2 & s_1 & s_2 & s_3 & s_4 & s_5 & s_6 \\ \hline 1 & 1 & 0 & 0 & 0 & -1 & -1 & 0 & 0 & 0 & 0 & 0 & 0 \\ 0 & 0 & 0 & 1 & 1 & 0 & 0 & 0 & 0 & 0 & 0 & -1 & -1 \\ 1 & 0 & 1 & 0 & 1 & 0 & 0 & -1 & -1 & 0 & 0 & -1 & 0 \\ 0 & 0 & 1 & 0 & 0 & 1 & 0 & -1 & 0 & -1 & 0 & 0 & 0 \\ 0 & 0 & 1 & 0 & 0 & 0 & 1 & 0 & -1 & 0 & -1 & 0 & 0 \end{array}\right)$$

The D-term charge matrix is

$$Q_D = \left(\begin{array}{cccccc|cc|cccccc} p_1 & p_2 & p_3 & p_4 & p_5 & q_1 & q_2 & s_1 & s_2 & s_3 & s_4 & s_5 & s_6 \\ \hline 0 & 0 & 0 & 0 & 0 & 0 & 0 & 1 & -1 & 0 & 0 & 0 & 0 \\ 0 & 0 & 0 & 0 & 0 & 0 & 0 & 0 & 1 & -1 & 0 & 0 & 0 \\ 0 & 0 & 0 & 0 & 0 & 0 & 0 & 0 & 0 & 1 & -1 & 0 & 0 \\ 0 & 0 & 0 & 0 & 0 & 0 & 0 & 0 & 0 & 0 & 1 & -1 & 0 \\ 0 & 0 & 0 & 0 & 0 & 0 & 0 & 0 & 0 & 0 & 0 & 1 & -1 \end{array}\right)$$

The total charge matrix does not exhibit repeated columns. Accordingly, the global symmetry is $U(1)_{f_1} \times U(1)_{f_2} \times U(1)_R$. Following the discussion in §2.3, the mesonic charges on extremal perfect matchings are found. They are shown in Table 34.

	$U(1)_{f_1}$	$U(1)_{f_2}$	$U(1)_R$	fugacity
p_1	-2/5	1/2	$R_1 = 2\left(-2+\sqrt{5}\right)$	t_1
p_2	-1/5	-1/2	$R_1 = 2\left(-2+\sqrt{5}\right)$	t_2
p_3	2/5	0	$R_1 = 2\left(-2+\sqrt{5}\right)$	t_3
p_4	1/5	0	$R_2 = 7-3\sqrt{5}$	t_4
p_5	0	0	$R_2 = 7-3\sqrt{5}$	t_5

Table 34. The GLSM fields corresponding to extremal points of the toric diagram with their mesonic charges (Model 9a). The R-charges are obtained using a-maximization.

Products of non-extremal perfect matchings are expressed as

$$q = q_1 q_2 \ , \ s = \prod_{m=1}^{6} s_m \ . \tag{11.2}$$

Extremal perfect matchings are counted by t_α. Products of non-extremal perfect matchings such as q are counted by a fugacity of the form y_q.

The mesonic Hilbert series of Model 9a is found using the Molien integral formula

in (2.3). It is

$$g_1(t_\alpha, y_q, y_s; \mathcal{M}_{9a}^{mes}) = \frac{P(t_\alpha)}{(1-y_q^2 y_s\ t_1^3 t_2 t_4^2)(1-y_q y_s\ t_1^2 t_3 t_4^2)(1-y_s\ t_3^2 t_4 t_5)(1-y_q^2 y_s\ t_1 t_2^3 t_5^2)(1-y_q y_s\ t_2^2 t_3 t_5^2)} \ . \tag{11.3}$$

The numerator is given by the polynomial

$$\begin{aligned} P(t_\alpha) = 1 &+ y_q^2 y_s\ t_1^2 t_2^2 t_4 t_5 + y_q y_s\ t_1 t_2 t_3 t_4 t_5 - y_q^3 y_s^2\ t_1^4 t_2^2 t_3 t_4^3 t_5 - y_q^2 y_s^2\ t_1^3 t_2 t_3^2 t_4^3 t_5 \\ &- y_q^3 y_s^2\ t_1^3 t_2^3 t_3 t_4^2 t_5^2 - y_q^2 y_s^2\ t_1^2 t_2^2 t_3^2 t_4^2 t_5^2 - y_q^3 y_s^2\ t_1^2 t_2^4 t_3 t_4 t_5^3 - y_q^2 y_s^2\ t_1 t_2^3 t_3^2 t_4 t_5^3 \\ &+ y_q^4 y_s^3\ t_1^4 t_2^4 t_3^2 t_4^3 t_5^3 + y_q^3 y_s^3\ t_1^3 t_2^3 t_3^3 t_4^3 t_5^3 + y_q^5 y_s^4\ t_1^5 t_2^5 t_3^3 t_4^4 t_5^4 \ . \end{aligned} \tag{11.4}$$

The plethystic logarithm of the mesonic Hilbert series is

$$\begin{aligned} PL[g_1(t_\alpha, y_q, y_s; \mathcal{M}_{9a}^{mes})] = &\ y_s\ t_3^2 t_4 t_5 + y_q y_s\ t_1 t_2 t_3 t_4 t_5 + y_q y_s\ t_1^2 t_3 t_4^2 + y_q y_s\ t_2^2 t_3 t_5^2 \\ &+ y_q^2 y_s\ t_1^2 t_2^2 t_4 t_5 + y_q^2 y_s\ t_1 t_2^3 t_5^2 + y_q^2 y_s\ t_1^3 t_2 t_4^2 - 2\ y_q^2 y_s^2\ t_1^2 t_2^2 t_3^2 t_4^2 t_5^2 - y_q^2 y_s^2\ t_1^3 t_2 t_3^2 t_4^3 t_5 \\ &- y_q^2 y_s^2\ t_1 t_2^3 t_3^2 t_4 t_5^3 + \dots \ . \end{aligned} \tag{11.5}$$

Consider the following fugacity map

$$f_1 = y_q^{-2/3} y_s^{1/3}\ t_1^{-2/3} t_2^{2/3} t_3^{4/3}\ ,\ f_2 = \frac{t_1 t_4}{t_2 t_5}\ ,\ \tilde{t}_1 = y_q^{1/3} y_s^{1/3}\ t_1^{1/3} t_2^{1/3} t_3^{1/3}\ ,\ \tilde{t}_2 = t_4^{1/2} t_5^{1/2}\ , \tag{11.6}$$

where the fugacities f_1 and f_2 count flavour charges, and the fugacities $\tilde{t}_1$ and $\tilde{t}_2$ count the R-charges R_1 and R_2 in Table 34 respectively. Under the fugacity map above, the plethystic logarithm becomes

$$\begin{aligned} PL[g_1(\tilde{t}_\alpha, f_1, f_2; \mathcal{M}_{9a}^{mes})] = &\ f_1 \tilde{t}_1^2 \tilde{t}_2^2 + \left(1 + f_2 + \frac{1}{f_2}\right) \tilde{t}_1^3 \tilde{t}_2^2 + \left(\frac{1}{f_1} + \frac{1}{f_1 f_2} + \frac{f_2}{f_1}\right) \tilde{t}_1^4 \tilde{t}_2^2 \\ &- \left(2 + f_2 + \frac{1}{f_2}\right) \tilde{t}_1^6 \tilde{t}_2^4 + \dots \ . \end{aligned} \tag{11.7}$$

This plethystic logarithm exhibits the moduli space generators with their mesonic charges. They are summarized in Table 35. The generators can be presented on a charge lattice. The convex polygon formed by the generators in Table 35 is the dual reflexive polygon of the toric diagram of Model 9a. For the case of Model 9a, the toric diagram is self-dual, and the charge lattice of the generators forms again the toric diagram of Model 9a.

Generator	$U(1)_{f_1}$	$U(1)_{f_2}$
$p_3^2 p_4 p_5\ s$	1	0
$p_1^2 p_3 p_4^2\ q\ s$	0	1
$p_1 p_2 p_3 p_4 p_5\ q\ s$	0	0
$p_2^2 p_3 p_5^2\ q\ s$	0	-1
$p_1^3 p_2 p_4^2\ q^2\ s$	-1	1
$p_1^2 p_2^2 p_4 p_5\ q^2\ s$	-1	0
$p_1 p_2^3 p_5^2\ q^2\ s$	-1	-1

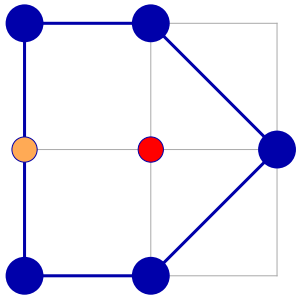


Table 35. The generators and lattice of generators of the mesonic moduli space of Model 9a in terms of GLSM fields with the corresponding flavor charges.

Generator	$U(1)_{f_1}$	$U(1)_{f_2}$
$X_{12}X_{21} = X_{34}X_{46}X_{65}X_{53}$	1	0
$X_{12}X_{26}X_{65}X_{51} = X_{14}X_{46}X_{65}X_{51} = X_{26}X_{65}X_{53}X_{32}$	0	1
$X_{13}X_{34}X_{46}X_{65}X_{51} = X_{26}X_{65}X_{53}X_{34}X_{42} = X_{12}X_{25}X_{51} = X_{12}X_{26}X_{61}$ $= X_{13}X_{32}X_{21} = X_{14}X_{42}X_{21} = X_{14}X_{46}X_{61} = X_{25}X_{53}X_{32}$	0	0
$X_{13}X_{34}X_{42}X_{21} = X_{13}X_{34}X_{46}X_{61} = X_{25}X_{53}X_{34}X_{42}$	0	-1
$X_{13}X_{32}X_{26}X_{65}X_{51} = X_{14}X_{42}X_{26}X_{65}X_{51}$	-1	1
$X_{13}X_{34}X_{42}X_{26}X_{65}X_{51} = X_{13}X_{32}X_{25}X_{51} = X_{13}X_{32}X_{26}X_{61} = X_{14}X_{42}X_{25}X_{51} = X_{14}X_{42}X_{26}X_{61}$	-1	0
$X_{13}X_{34}X_{42}X_{25}X_{51} = X_{13}X_{34}X_{42}X_{26}X_{61}$	-1	-1

Table 36. The generators in terms of bifundamental fields (Model 9a).

The mesonic Hilbert series and the plethystic logarithm can be re-expressed in terms of 3 fugacities

$$T_1 = \frac{t_5}{y_q^2 y_s\ t_1^4 t_4^3}\ ,\ T_2 = y_q^2 y_s\ t_1^3 t_2 t_4^2\ ,\ T_3 = y_q y_s\ t_1^2 t_3 t_4^2\ , \tag{11.8}$$

such that

$$\begin{aligned} &g_1(T_1, T_2, T_3; \mathcal{M}_{9a}^{mes}) = \\ &(1 + T_1 T_2^2 + T_1 T_2 T_3 - T_1 T_2^2 T_3 - T_1 T_2 T_3^2 - T_1^2 T_2^3 T_3 - T_1^2 T_2^2 T_3^2 - T_1^3 T_2^4 T_3 - T_1^3 T_2^3 T_3^2 \\ &+ T_1^3 T_2^4 T_3^2 + T_1^3 T_2^3 T_3^3 + T_1^4 T_2^5 T_3^3) \times \frac{1}{(1-T_2)(1-T_3)(1-T_1^2 T_2^3)(1-T_1 T_3^2)(1-T_1^2 T_2^2 T_3)} \end{aligned} \tag{11.9}$$

and

$$\begin{aligned} PL[g_1(T_1, T_2, T_3; \mathcal{M}_{9a}^{mes})] = T_1 T_3^2 + T_1 T_2 T_3 + T_3 + T_1^2 T_2^2 T_3 + T_1 T_2^2 + T_1^2 T_2^3 + T_2 \\ -2 T_1^2 T_2^2 T_3^2 - T_1 T_2 T_3^2 - T_1^3 T_2^3 T_3^2 + \dots \quad . \end{aligned} \tag{11.10}$$

The above Hilbert series and plethystic logarithm illustrate the conical structure of the toric Calabi-Yau 3-fold.

11.2 Model 9 Phase b

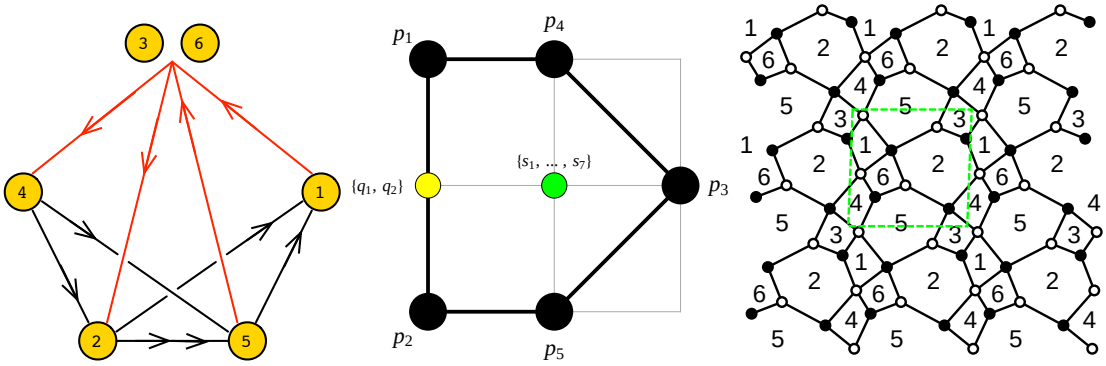


Figure 20. The quiver, toric diagram, and brane tiling of Model 9b. The red arrows in the quiver indicate all possible connections between blocks of nodes.

The superpotential is

$$\begin{aligned} W = &+X_{25}^2 X_{53} X_{32} + X_{56} X_{62} X_{25}^1 + X_{13} X_{34} X_{45} X_{51} + X_{21} X_{16} X_{64} X_{42} \\ &- X_{13} X_{32} X_{21} - X_{56} X_{64} X_{45} - X_{16} X_{62} X_{25}^2 X_{51} - X_{25}^1 X_{53} X_{34} X_{42} \end{aligned} \tag{11.11}$$

The perfect matching matrix is

$$P = \left(\begin{array}{c|ccccc|cc|ccccccc} 0 & p_1 & p_2 & p_3 & p_4 & p_5 & q_1 & q_2 & s_1 & s_2 & s_3 & s_4 & s_5 & s_6 & s_7 \\ \hline X_{32} & 1 & 0 & 0 & 1 & 0 & 1 & 0 & 0 & 1 & 0 & 1 & 0 & 1 & 0 \\ X_{25}^1 & 1 & 0 & 0 & 1 & 0 & 0 & 1 & 1 & 0 & 0 & 0 & 0 & 0 & 0 \\ X_{51} & 1 & 0 & 0 & 0 & 0 & 1 & 0 & 0 & 0 & 0 & 0 & 0 & 0 & 1 \\ X_{64} & 1 & 0 & 0 & 0 & 0 & 0 & 1 & 0 & 0 & 1 & 0 & 0 & 1 & 0 \\ X_{56} & 0 & 1 & 0 & 0 & 1 & 1 & 0 & 0 & 1 & 0 & 0 & 1 & 0 & 1 \\ X_{25}^2 & 0 & 1 & 0 & 0 & 1 & 0 & 1 & 1 & 0 & 0 & 0 & 0 & 0 & 0 \\ X_{42} & 0 & 1 & 0 & 0 & 0 & 1 & 0 & 0 & 0 & 0 & 1 & 0 & 0 & 0 \\ X_{13} & 0 & 1 & 0 & 0 & 0 & 0 & 1 & 0 & 0 & 1 & 0 & 1 & 0 & 0 \\ X_{45} & 0 & 0 & 1 & 1 & 0 & 0 & 0 & 1 & 0 & 0 & 1 & 0 & 0 & 0 \\ X_{21} & 0 & 0 & 1 & 0 & 1 & 0 & 0 & 1 & 0 & 0 & 0 & 0 & 0 & 1 \\ X_{62} & 0 & 0 & 1 & 0 & 0 & 0 & 0 & 0 & 0 & 1 & 1 & 0 & 1 & 0 \\ X_{53} & 0 & 0 & 1 & 0 & 0 & 0 & 0 & 0 & 0 & 1 & 0 & 1 & 0 & 1 \\ X_{16} & 0 & 0 & 0 & 1 & 0 & 0 & 0 & 0 & 1 & 0 & 0 & 1 & 0 & 0 \\ X_{34} & 0 & 0 & 0 & 0 & 1 & 0 & 0 & 0 & 1 & 0 & 0 & 0 & 1 & 0 \end{array}\right)$$

The F-term charge matrix $Q_F = \ker(P)$ is

$$Q_F = \left(\begin{array}{ccccc|cc|ccccccc} p_1 & p_2 & p_3 & p_4 & p_5 & q_1 & q_2 & s_1 & s_2 & s_3 & s_4 & s_5 & s_6 & s_7 \\ \hline 1 & 1 & 0 & 0 & 0 & -1 & -1 & 0 & 0 & 0 & 0 & 0 & 0 & 0 \\ 0 & 0 & 0 & 1 & 1 & 0 & 0 & -1 & -1 & 0 & 0 & 0 & 0 & 0 \\ 1 & 0 & 0 & 0 & 1 & -1 & 0 & -1 & 0 & 0 & 1 & 0 & -1 & 0 \\ 1 & 0 & 0 & 0 & 1 & 0 & -1 & 0 & 0 & 1 & 0 & 0 & -1 & -1 \\ 0 & 1 & 1 & 1 & 0 & 0 & 0 & -1 & 0 & 0 & -1 & -1 & 0 & 0 \\ 0 & 0 & 1 & 0 & 0 & 1 & 0 & 0 & 0 & 0 & -1 & 0 & 0 & -1 \end{array}\right)$$

The D-term charge matrix is

$$Q_D = \left(\begin{array}{ccccc|cc|ccccccc} p_1 & p_2 & p_3 & p_4 & p_5 & q_1 & q_2 & s_1 & s_2 & s_3 & s_4 & s_5 & s_6 & s_7 \\ \hline 0 & 0 & 0 & 0 & 0 & 0 & 0 & 1 & -1 & 0 & 0 & 0 & 0 & 0 \\ 0 & 0 & 0 & 0 & 0 & 0 & 0 & 0 & 1 & -1 & 0 & 0 & 0 & 0 \\ 0 & 0 & 0 & 0 & 0 & 0 & 0 & 0 & 0 & 1 & -1 & 0 & 0 & 0 \\ 0 & 0 & 0 & 0 & 0 & 0 & 0 & 0 & 0 & 0 & 1 & -1 & 0 & 0 \\ 0 & 0 & 0 & 0 & 0 & 0 & 0 & 0 & 0 & 0 & 0 & 0 & 1 & -1 \end{array}\right)$$

The total charge matrix Q_t does not have repeated columns. Accordingly, the global symmetry group for the Model 9b theory is $U(1)_{f_1} \times U(1)_{f_2} \times U(1)_R$. The flavour and R-charges on the extremal perfect matchings p_α are the same as for Model 9a, and are summarised in Table 34. They are found following the discussion in §2.3.

Products of non-extremal perfect matchings are expressed as

$$q = q_1 q_2 \ , \ s = \prod_{m=1}^{7} s_m \ . \tag{11.12}$$

The fugacity counting extremal perfect matchings p_α is t_α. The fugacity y_q counts the product of non-extremal perfect matchings q above.

The mesonic Hilbert series for Model 9b is identical to the one for Model 9a. The mesonic Hilbert series is shown in (11.3). The corresponding plethystic logarithm in (11.7) indicates that the mesonic moduli space is not a complete intersection. As a summary, both Model 9a and 9b mesonic moduli spaces are identical.

The generators of the mesonic moduli space in terms of the perfect matching fields of Model 9b are presented in Table 35. The charge lattice of mesonic generators forms a convex polygon which is another reflexive polygon precisely being the dual of the toric diagram. The generators of the mesonic moduli space in terms of quiver fields of Model 9b are shown in Table 37.

Generator	$U(1)_{f_1}$	$U(1)_{f_2}$
$X_{16}X_{62}X_{21} = X_{34}X_{45}X_{53}$	1	0
$X^1_{25}X_{53}X_{32} = X_{16}X_{62}X^1_{25}X_{51} = X_{16}X_{64}X_{45}X_{51}$	0	1
$X_{13}X_{32}X_{21} = X^1_{25}X_{56}X_{62} = X^2_{25}X_{53}X_{32} = X_{45}X_{56}X_{64}$ $= X_{13}X_{34}X_{45}X_{51} = X_{16}X_{64}X_{42}X_{21} = X_{16}X_{62}X^2_{25}X_{51} = X^1_{25}X_{53}X_{34}X_{42}$	0	0
$X^2_{25}X_{56}X_{62} = X_{13}X_{34}X_{42}X_{21} = X^2_{25}X_{53}X_{34}X_{42}$	0	-1
$X_{13}X_{32}X^1_{25}X_{51} = X_{16}X_{64}X_{42}X^1_{25}X_{51}$	-1	1
$X_{13}X_{32}X^2_{25}X_{51} = X^1_{25}X_{56}X_{64}X_{42} = X_{13}X_{34}X_{42}X^1_{25}X_{51} = X_{16}X_{64}X_{42}X^2_{25}X_{51}$	-1	0
$X^2_{25}X_{56}X_{64}X_{42} = X_{13}X_{34}X_{42}X^2_{25}X_{51}$	-1	-1

Table 37. The generators in terms of bifundamental fields (Model 9b).

11.3 Model 9 Phase c

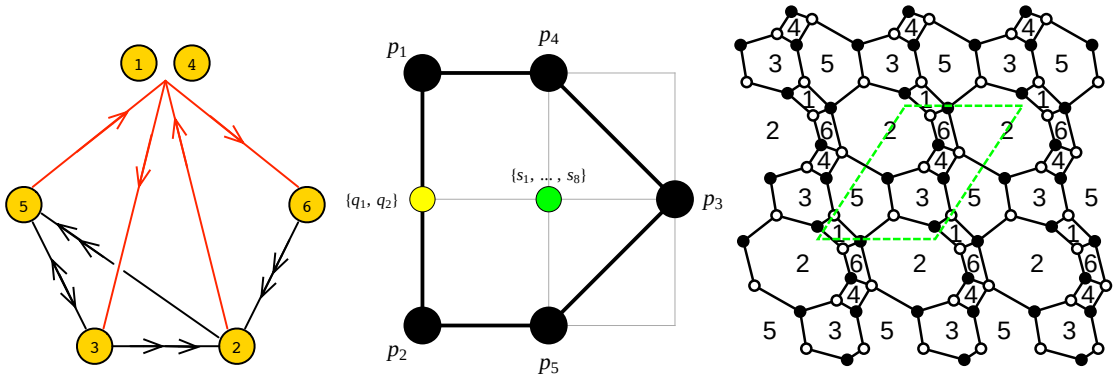


Figure 21. The quiver, toric diagram, and brane tiling of Model 9c. The red arrows in the quiver indicate all possible connections between blocks of nodes.

The superpotential is

$$\begin{aligned} W = &+X_{21}X_{16}X^2_{62} + X_{24}X_{43}X^2_{32} + X^2_{25}X_{53}X^1_{32} + X_{51}X_{13}X_{35} + X_{54}X_{46}X^1_{62}X^1_{25} \\ &-X_{13}X^1_{32}X_{21} - X_{24}X_{46}X^2_{62} - X^1_{25}X_{53}X^2_{32} - X_{54}X_{43}X_{35} - X_{16}X^1_{62}X^2_{25}X_{51} \end{aligned} \tag{11.13}$$

The perfect matching matrix is

$$P = \left(\begin{array}{c|ccccc|cc|cccccccc} & p_1 & p_2 & p_3 & p_4 & p_5 & q_1 & q_2 & s_1 & s_2 & s_3 & s_4 & s_5 & s_6 & s_7 & s_8 \\ \hline X^1_{25} & 1 & 0 & 0 & 1 & 0 & 1 & 0 & 0 & 1 & 0 & 0 & 0 & 0 & 0 & 0 \\ X^1_{32} & 1 & 0 & 0 & 1 & 0 & 0 & 1 & 1 & 0 & 0 & 0 & 0 & 0 & 0 & 1 \\ X^2_{25} & 0 & 1 & 0 & 0 & 1 & 1 & 0 & 0 & 1 & 0 & 0 & 0 & 0 & 0 & 0 \\ X^2_{32} & 0 & 1 & 0 & 0 & 1 & 0 & 1 & 1 & 0 & 0 & 0 & 0 & 0 & 0 & 1 \\ X_{43} & 1 & 0 & 0 & 0 & 0 & 1 & 0 & 0 & 0 & 1 & 1 & 0 & 1 & 0 & 0 \\ X_{51} & 1 & 0 & 0 & 0 & 0 & 0 & 1 & 0 & 0 & 0 & 0 & 0 & 1 & 1 & 0 \\ X_{13} & 0 & 1 & 0 & 0 & 0 & 1 & 0 & 0 & 0 & 1 & 1 & 1 & 0 & 0 & 0 \\ X_{54} & 0 & 1 & 0 & 0 & 0 & 0 & 1 & 0 & 0 & 0 & 0 & 1 & 0 & 1 & 0 \\ X_{53} & 0 & 0 & 1 & 0 & 0 & 0 & 0 & 0 & 0 & 1 & 1 & 1 & 1 & 1 & 0 \\ X^1_{62} & 0 & 0 & 1 & 0 & 0 & 0 & 0 & 0 & 0 & 0 & 1 & 0 & 0 & 0 & 1 \\ X^2_{62} & 1 & 1 & 0 & 0 & 0 & 1 & 1 & 0 & 0 & 0 & 1 & 0 & 0 & 0 & 1 \\ X_{24} & 0 & 0 & 1 & 1 & 0 & 0 & 0 & 0 & 1 & 0 & 0 & 1 & 0 & 1 & 0 \\ X_{21} & 0 & 0 & 1 & 0 & 1 & 0 & 0 & 0 & 1 & 0 & 0 & 0 & 1 & 1 & 0 \\ X_{16} & 0 & 0 & 0 & 1 & 0 & 0 & 0 & 1 & 0 & 1 & 0 & 1 & 0 & 0 & 0 \\ X_{46} & 0 & 0 & 0 & 0 & 1 & 0 & 0 & 1 & 0 & 1 & 0 & 0 & 1 & 0 & 0 \\ X_{35} & 0 & 0 & 1 & 1 & 1 & 0 & 0 & 1 & 1 & 0 & 0 & 0 & 0 & 0 & 1 \end{array}\right)$$

The F-term charge matrix $Q_F = \ker(P)$ is

$$Q_F = \left(\begin{array}{ccccc|cc|cccccccc} p_1 & p_2 & p_3 & p_4 & p_5 & q_1 & q_2 & s_1 & s_2 & s_3 & s_4 & s_5 & s_6 & s_7 & s_8 \\ \hline 1 & 1 & 0 & 0 & 0 & -1 & -1 & 0 & 0 & 0 & 0 & 0 & 0 & 0 & 0 \\ 0 & 0 & 0 & 1 & 1 & 0 & 0 & -1 & -1 & 0 & 0 & 0 & 0 & 0 & 0 \\ 1 & 0 & 0 & 0 & 1 & -1 & 0 & -1 & 0 & 0 & 0 & 1 & 0 & -1 & 0 \\ 1 & 0 & 0 & 0 & 1 & -1 & 0 & -1 & 0 & 1 & 0 & 0 & -1 & 0 & 0 \\ 0 & 1 & 0 & 1 & 0 & -1 & 0 & -1 & 0 & 1 & 0 & -1 & 0 & 0 & 0 \\ 0 & 0 & 1 & 0 & 0 & 1 & 0 & 0 & -1 & 0 & -1 & 0 & 0 & 0 & 0 \\ 0 & 0 & 0 & 0 & 0 & 0 & 0 & -1 & 0 & 1 & -1 & 0 & 0 & 0 & 1 \end{array}\right)$$

The D-term charge matrix is

$$Q_D = \left(\begin{array}{ccccc|cc|cccccccc} p_1 & p_2 & p_3 & p_4 & p_5 & q_1 & q_2 & s_1 & s_2 & s_3 & s_4 & s_5 & s_6 & s_7 & s_8 \\ \hline 0 & 0 & 0 & 0 & 0 & 0 & 0 & 0 & 1 & -1 & 0 & 0 & 0 & 0 & 0 \\ 0 & 0 & 0 & 0 & 0 & 0 & 0 & 0 & 0 & 1 & -1 & 0 & 0 & 0 & 0 \\ 0 & 0 & 0 & 0 & 0 & 0 & 0 & 0 & 0 & 0 & 1 & -1 & 0 & 0 & 0 \\ 0 & 0 & 0 & 0 & 0 & 0 & 0 & 0 & 0 & 0 & 0 & 1 & -1 & 0 & 0 \\ 0 & 0 & 0 & 0 & 0 & 0 & 0 & 0 & 0 & 0 & 0 & 0 & 1 & -1 & 0 \\ 0 & 0 & 0 & 0 & 0 & 0 & 0 & 0 & 0 & 0 & 0 & 0 & 0 & 1 & -1 \end{array}\right)$$

The total charge matrix Q_t does not have repeated columns. Accordingly, the global symmetry of Model 9c is the same as for Model 9a and 9b above and takes the form $U(1)_{f_1} \times U(1)_{f_2} \times U(1)_R$. The mesonic charges on the extremal perfect matchings are summarised in Table 34.

The following products of non-extremal perfect matchings are assigned single vari-

ables

$$q = q_1 q_2 \ , \ s = \prod_{m=1}^{8} s_m \ . \tag{11.14}$$

The extremal perfect matchings are counted by the fugacity t_α. Products of non-extremal perfect matchings such as q above are associated to fugacities of the form y_q.

The mesonic Hilbert series is identical to the mesonic Hilbert series of Model 9a and 9b. The mesonic Hilbert series is given in (11.3) with the corresponding plethystic logarithm in (11.7). The mesonic Hilbert series of Models 9a, 9b and 9c are identical and are not complete intersections.

The generators of the mesonic moduli space in terms of Model 9c GLSM fields are shown in Table 35. The mesonic charges of the generators correspond to lattice coordinates of points which form a reflexive polygon being the dual of the toric diagram. The generators in terms of quiver fields of Model 9c are shown in Table 38.

Generator	$U(1)_{f_1}$	$U(1)_{f_2}$
$X_{35}X_{53} = X_{16}X^1_{62}X_{21} = X_{24}X_{46}X^1_{62}$	1	0
$X_{16}X^1_{62}X^1_{25}X_{51} = X_{24}X_{43}X^1_{32} = X^1_{25}X_{53}X^1_{32}$	0	1
$X_{16}X^1_{62}X^2_{25}X_{51} = X^1_{25}X_{54}X_{46}X^1_{62} = X_{13}X^1_{32}X_{21} = X_{13}X_{35}X_{51} =$ $X_{16}X^2_{62}X_{21} = X_{24}X_{43}X^2_{32} = X_{24}X_{46}X^2_{62} = X^1_{25}X_{53}X^2_{32} = X^2_{25}X_{53}X^1_{32} = X_{35}X_{54}X_{43}$	0	0
$X^2_{25}X_{54}X_{46}X^1_{62} = X_{13}X^2_{32}X_{21} = X^2_{25}X_{53}X^2_{32}$	0	-1
$X_{13}X^1_{32}X^1_{25}X_{51} = X_{16}X^2_{62}X^1_{25}X_{51} = X^1_{25}X_{54}X_{43}X^1_{32}$	-1	1
$X_{13}X^2_{32}X^1_{25}X_{51} = X_{13}X^1_{32}X^2_{25}X_{51} = X_{16}X^2_{62}X^2_{25}X_{51} = X^1_{25}X_{54}X_{43}X^2_{32} = X^1_{25}X_{54}X_{46}X^2_{62} = X^2_{25}X_{54}X_{43}X^1_{32}$	-1	0
$X_{13}X^2_{32}X^2_{25}X_{51} = X^2_{25}X_{54}X_{43}X^2_{32} = X^2_{25}X_{54}X_{46}X^2_{62}$	-1	-1

Table 38. The generators in terms of bifundamental fields (Model 9c).

12 Model 10: dP_3

12.1 Model 10 Phase a

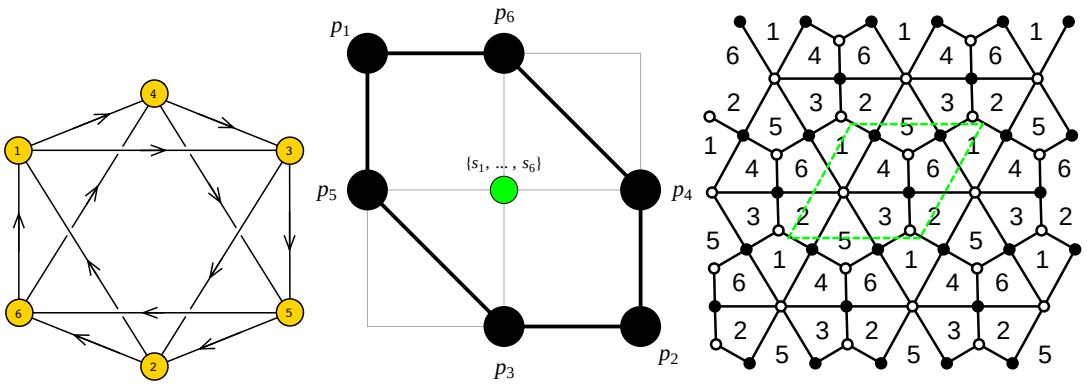


Figure 22. The quiver, toric diagram, and brane tiling of Model 10a.

The superpotential is

$$\begin{aligned} W = &+X_{13}X_{32}X_{21} + X_{56}X_{64}X_{45} + X_{43}X_{35}X_{52}X_{26}X_{61}X_{14} \\ &-X_{13}X_{35}X_{56}X_{61} - X_{14}X_{45}X_{52}X_{21} - X_{26}X_{64}X_{43}X_{32} \end{aligned} \tag{12.1}$$

The perfect matching matrix is

$$P = \left(\begin{array}{c|cccccc|cccccc} & p_1 & p_2 & p_3 & p_4 & p_5 & p_6 & s_1 & s_2 & s_3 & s_4 & s_5 & s_6 \\ \hline X_{45} & 1 & 0 & 0 & 0 & 1 & 0 & 1 & 0 & 0 & 0 & 1 & 0 \\ X_{13} & 1 & 0 & 0 & 0 & 0 & 1 & 1 & 0 & 0 & 0 & 0 & 1 \\ X_{56} & 0 & 1 & 1 & 0 & 0 & 0 & 0 & 1 & 1 & 0 & 0 & 0 \\ X_{21} & 0 & 1 & 0 & 1 & 0 & 0 & 0 & 1 & 0 & 1 & 0 & 0 \\ X_{32} & 0 & 0 & 1 & 0 & 1 & 0 & 0 & 0 & 1 & 0 & 1 & 0 \\ X_{64} & 0 & 0 & 0 & 1 & 0 & 1 & 0 & 0 & 0 & 1 & 0 & 1 \\ X_{26} & 1 & 0 & 0 & 0 & 0 & 0 & 0 & 1 & 0 & 0 & 0 & 0 \\ X_{43} & 0 & 1 & 0 & 0 & 0 & 0 & 1 & 0 & 0 & 0 & 0 & 0 \\ X_{14} & 0 & 0 & 1 & 0 & 0 & 0 & 0 & 0 & 0 & 0 & 0 & 1 \\ X_{35} & 0 & 0 & 0 & 1 & 0 & 0 & 0 & 0 & 0 & 0 & 1 & 0 \\ X_{61} & 0 & 0 & 0 & 0 & 1 & 0 & 0 & 0 & 0 & 1 & 0 & 0 \\ X_{52} & 0 & 0 & 0 & 0 & 0 & 1 & 0 & 0 & 1 & 0 & 0 & 0 \end{array}\right)$$

The F-term charge matrix $Q_F = \ker(P)$ is

$$Q_F = \left(\begin{array}{cccccc|cccccc} p_1 & p_2 & p_3 & p_4 & p_5 & p_6 & s_1 & s_2 & s_3 & s_4 & s_5 & s_6 \\ \hline 1 & 1 & 0 & 0 & 0 & 0 & -1 & -1 & 0 & 0 & 0 & 0 \\ 0 & 0 & 0 & 1 & 1 & 0 & 0 & 0 & 0 & -1 & -1 & 0 \\ 0 & 1 & 0 & 0 & 1 & 1 & -1 & 0 & -1 & -1 & 0 & 0 \\ 0 & 0 & 1 & 0 & 0 & 1 & 0 & 0 & -1 & 0 & 0 & -1 \end{array}\right)$$

The D-term charge matrix is

$$Q_D = \left(\begin{array}{cccccc|cccccc} p_1 & p_2 & p_3 & p_4 & p_5 & p_6 & s_1 & s_2 & s_3 & s_4 & s_5 & s_6 \\ \hline 0 & 0 & 0 & 0 & 0 & 0 & 1 & -1 & 0 & 0 & 0 & 0 \\ 0 & 0 & 0 & 0 & 0 & 0 & 0 & 1 & -1 & 0 & 0 & 0 \\ 0 & 0 & 0 & 0 & 0 & 0 & 0 & 0 & 1 & -1 & 0 & 0 \\ 0 & 0 & 0 & 0 & 0 & 0 & 0 & 0 & 0 & 1 & -1 & 0 \\ 0 & 0 & 0 & 0 & 0 & 0 & 0 & 0 & 0 & 0 & 1 & -1 \end{array}\right)$$

The total charge matrix Q_t does not exhibit repeated columns. Accordingly, the global symmetry is $U(1)_{f_1} \times U(1)_{f_2} \times U(1)_R$. The mesonic charges on the GLSM fields corresponding to extremal points in the toric diagram in Figure 22 are found following the discussion in §2.3. They are presented in Table 39.

	$U(1)_{f_1}$	$U(1)_{f_2}$	$U(1)_R$	fugacity
p_1	-1	0	1/3	t_1
p_2	-1	1	1/3	t_2
p_3	1	0	1/3	t_3
p_4	1	-1	1/3	t_4
p_5	0	0	1/3	t_5
p_6	0	0	1/3	t_6

Table 39. The GLSM fields corresponding to extremal points of the toric diagram with their mesonic charges (Model 10a).

The product of all internal perfect matchings is labelled as follows

$$s = \prod_{m=1}^{6} s_m \ . \tag{12.2}$$

The fugacity counting extremal perfect matchings is t_α. The product of internal perfect matchings is associated to the fugacity y_s.

The refined mesonic Hilbert series of Model 10a is found using the Molien integral

formula in (2.9). It is

$$g_1(t_\alpha, y_s; \mathcal{M}^{mes}_{10a}) = \frac{P(t_\alpha)}{(1-y_s\ t_2^2t_3^2t_4t_5)(1-y_s\ t_1t_2t_3^2t_5^2)(1-y_s\ t_2^2t_3t_4^2t_6)} \times \frac{1}{(1-y_s\ t_1^2t_3t_5^2t_6)(1-y_s\ t_1t_2t_4^2t_6^2)(1-y_s\ t_1^2t_4t_5t_6^2)} \ . \tag{12.3}$$

The numerator is given by the polynomial

$$\begin{aligned} P(t_\alpha) = 1 &+ y_s\ t_1t_2t_3t_4t_5t_6 - y_s^2\ t_1t_2^3t_3^3t_4^2t_5^2t_6 - y_s^2\ t_1^2t_2^2t_3^3t_4t_5^3t_6 - y_s^2\ t_1t_2^3t_3^2t_4^3t_5t_6^2 \\ &-2\ y_s^2\ t_1^2t_2^2t_3^2t_4^2t_5^2t_6^2 - y_s^2\ t_1^3t_2t_3^2t_4t_5^3t_6^2 + y_s^3\ t_1^2t_2^4t_3^4t_4^3t_5^3t_6^2 + y_s^3\ t_1^3t_2^3t_3^4t_4^2t_5^4t_6^2 \\ &-y_s^2\ t_1^2t_2^2t_3t_4^3t_5t_6^3 - y_s^2\ t_1^3t_2t_3t_4^2t_5^2t_6^3 + y_s^3\ t_1^2t_2^4t_3^3t_4^4t_5^2t_6^3 + 2\ y_s^3\ t_1^3t_2^3t_3^3t_4^3t_5^3t_6^3 \\ &+y_s^3\ t_1^4t_2^2t_3^3t_4^2t_5^4t_6^3 + y_s^3\ t_1^3t_2^3t_3^2t_4^4t_5^2t_6^4 + y_s^3\ t_1^4t_2^2t_3^2t_4^3t_5^3t_6^4 - y_s^4\ t_1^4t_2^4t_3^4t_4^4t_5^4t_6^4 \\ &-y_s^5\ t_1^5t_2^5t_3^5t_4^5t_5^5t_6^5 \ . \end{aligned} \tag{12.4}$$

The plethystic logarithm of the mesonic Hilbert series is

$$\begin{aligned} PL[g_1(t_\alpha, y_s; \mathcal{M}^{mes}_{10a})] = &\ y_s\ t_1t_2t_3t_4t_5t_6 + y_s\ t_1^2t_3t_5^2t_6 + y_s\ t_2^2t_3t_4^2t_6 + y_s\ t_1t_2t_4^2t_6^2 + y_s\ t_1t_2t_3^2t_5^2 \\ &+y_s\ t_1^2t_4t_5t_6^2 + y_s\ t_2^2t_3^2t_4t_5 - 3\ y_s^2\ t_1^2t_2^2t_3^2t_4^2t_5^2t_6^2 - y_s^2\ t_1^3t_2t_3^2t_4t_5^3t_6^2 - y_s^2\ t_1t_2^3t_3^2t_4^3t_5t_6^2 \\ &-y_s^2\ t_1^2t_2^2t_3t_4^3t_5t_6^3 - y_s^2\ t_1^2t_2^2t_3^3t_4t_5^3t_6 - y_s^2\ t_1^3t_2t_3t_4^2t_5^2t_6^3 - y_s^2\ t_1t_2^3t_3^3t_4^2t_5^2t_6 + \dots \ . \end{aligned} \tag{12.5}$$

Under the following fugacity map

$$f_1 = \frac{t_2t_4}{t_1t_5}\ ,\ f_2 = \frac{t_3t_5}{t_4t_6}\ ,\ t = y_s^{1/6}\ t_1^{1/6}t_2^{1/6}t_3^{1/6}t_4^{1/6}t_5^{1/6}t_6^{1/6}\ , \tag{12.6}$$

where f_1, f_2 and t are the mesonic charge fugacities, the mesonic Hilbert series and the plethystic logarithm are expressed as

$$\begin{aligned} g_1(t, f_1, f_2; \mathcal{M}^{mes}_{10a}) = &\left(1 + t^6 - \left(2 + \frac{1}{f_1} + f_1 + \frac{1}{f_2} + \frac{1}{f_1f_2} + f_2 + f_1f_2\right) t^{12}\right. \\ &\left. + \left(2 + \frac{1}{f_1} + f_1 + \frac{1}{f_2} + \frac{1}{f_1f_2} + f_2 + f_1f_2\right) t^{18} - t^{24} - t^{30}\right) \times \\ &\frac{1}{\left(1-\frac{1}{f_1}t^6\right)(1-f_1t^6)\left(1-\frac{1}{f_2}t^6\right)\left(1-\frac{1}{f_1f_2}t^6\right)(1-f_2t^6)(1-f_1f_2t^6)} \end{aligned} \tag{12.7}$$

and

$$\begin{aligned} PL[g_1(t, f_1, f_2; \mathcal{M}^{mes}_{10a})] = &\left(1 + \frac{1}{f_1} + f_1 + \frac{1}{f_2} + f_2 + \frac{1}{f_1f_2} + f_1f_2\right)t^6 - \left(3 + \frac{1}{f_1} + f_1 + \frac{1}{f_2}\right. \\ &\left. + f_2 + \frac{1}{f_1f_2} + f_1f_2\right)t^{12} + 2\left(2 + \frac{1}{f_1} + f_1 + \frac{1}{f_2} + f_2 + \frac{1}{f_1f_2} + f_1f_2\right)t^{18} + \dots \ . \end{aligned} \tag{12.8}$$

The above plethystic logarithm exhibits both the moduli space generators and the corresponding mesonic charges. They are summarized in Table 23. The generators can be presented on a charge lattice. The convex polygon formed by the generators in Table 23 is the dual reflexive polygon of the toric diagram of Model 10a.

Generator	$U(1)_{f_1}$	$U(1)_{f_2}$
$p_2^2p_3^2p_4p_5$ s	1	1
$p_1p_2p_3^2p_5^2$ s	0	1
$p_2^2p_3p_4^2p_6$ s	1	0
$p_1p_2p_3p_4p_5p_6$ s	0	0
$p_1^2p_3p_5^2p_6$ s	-1	0
$p_1p_2p_4^2p_6^2$ s	0	-1
$p_1^2p_4p_5p_6^2$ s	-1	-1

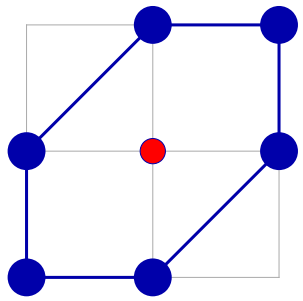


Figure 23. The generators and lattice of generators of the mesonic moduli space of Model 10a in terms of GLSM fields with the corresponding flavor charges.

Generator	$U(1)_{f_1}$	$U(1)_{f_2}$
$X_{14}X_{43}X_{32}X_{21} = X_{14}X_{43}X_{35}X_{56}X_{61}$	1	1
$X_{14}X_{45}X_{56}X_{61} = X_{14}X_{43}X_{32}X_{26}X_{61}$	0	1
$X_{35}X_{56}X_{64}X_{43} = X_{14}X_{43}X_{35}X_{52}X_{21}$	1	0
$X_{14}X_{43}X_{35}X_{52}X_{26}X_{61} = X_{13}X_{32}X_{21} = X_{45}X_{56}X_{64} = X_{13}X_{35}X_{56}X_{61} = X_{14}X_{45}X_{52}X_{21} = X_{26}X_{64}X_{43}X_{32}$	0	0
$X_{13}X_{32}X_{26}X_{61} = X_{14}X_{45}X_{52}X_{26}X_{61}$	-1	0
$X_{13}X_{35}X_{52}X_{21} = X_{26}X_{64}X_{43}X_{35}X_{52}$	0	-1
$X_{26}X_{64}X_{45}X_{52} = X_{13}X_{35}X_{52}X_{26}X_{61}$	-1	-1

Figure 24. The generators in terms of bifundamental fields (Model 10a).

Under the following fugacity map

$$T_1 = \frac{t^6}{f_1 f_2} = y_s\, t_1^2 t_4 t_5 t_6^2\ ,\ T_2 = f_1 = \frac{t_2 t_4}{t_1 t_5}\ ,\ T_3 = f_2 = \frac{t_3 t_5}{t_4 t_6}\ , \tag{12.9}$$

the mesonic Hilbert series and the plethystic logarithm can be rewritten as

$$\begin{aligned} g_1(T_1,T_2,T_3;\mathcal{M}_{10a}^{mes}) = \big(1 + T_1T_2T_3 - (2T_1^2T_2^2T_3^2 + T_1^2T_2T_3^2 + T_1^2T_2^3T_3^2 + T_1^2T_2^2T_3 \\ + T_1^2T_2T_3 + T_1^2T_2^2T_3^3 + T_1^2T_2^3T_3^3) + (2T_1^3T_2^3T_3^3 + T_1^3T_2^2T_3^3 + T_1^3T_2^4T_3^3 + T_1^3T_2^3T_3^2 \\ + T_1^3T_2^2T_3^2 + T_1^3T_2^3T_3^4 + T_1^3T_2^4T_3^4) - T_1^4T_2^4T_3^4 - T_1^5T_2^5T_3^5\big) \times \\ \frac{1}{(1-T_1T_3)(1-T_1T_2^2T_3)(1-T_1T_2)(1-T_1)(1-T_1T_2T_3^2)(1-T_1T_2^2T_3^2)} \end{aligned} \tag{12.10}$$

and

$$PL[g_1(t,f_1,f_2;\mathcal{M}^{mes}_{10a})] = T_1T_2T_3 + T_1T_3 + T_1T_2^2T_3 + T_1T_2 + T_1T_2T_3^2 + T_1 + T_1T_2^2T_3^2$$
$$-(3T_1^2T_2^2T_3^2 + T_1^2T_2T_3^2 + T_1^2T_2^3T_3^2 + T_1^2T_2^2T_3 + T_1^2T_2^2T_3^3 + T_1^2T_2T_3 + T_1^2T_2^3T_3^3)$$
$$+4T_1^3T_2^3T_3^3 + T_1^3T_2^2T_3^3 + T_1^3T_2^4T_3^3 + T_1^3T_2^3T_3^2 + T_1^3T_2^3T_3^4 + T_1^3T_2^2T_3^2 + T_1^3T_2^4T_3^4 + \ldots \tag{12.11}$$

such that the powers of the fugacities are all positive indicating the cone structure of the variety.

12.2 Model 10 Phase b

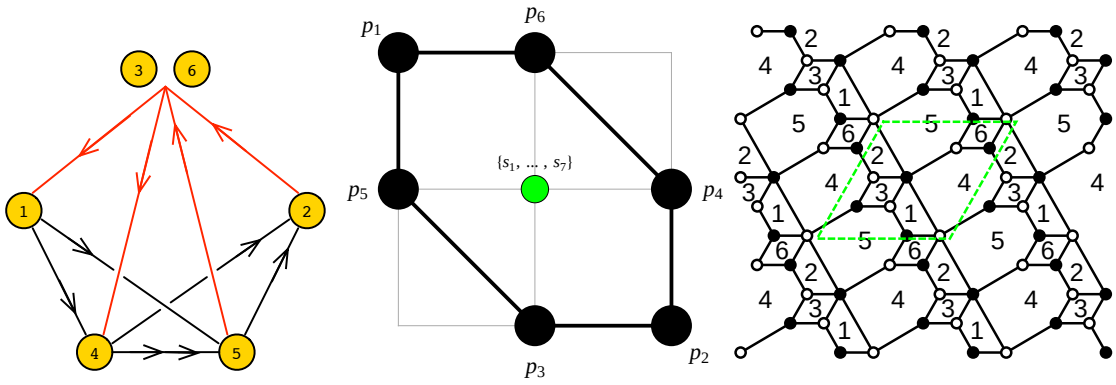


Figure 25. The quiver, toric diagram and brane tiling of Model 10b. The red arrows in the quiver indicate all possible connections between blocks of nodes.

The superpotential is

$$W = +X_{31}X_{15}X_{53} + X_{42}X_{23}X_{34} + X_{56}X_{64}X_{45}^2 + X_{52}X_{26}X_{61}X_{14}X_{45}^1$$
$$-X_{42}X_{26}X_{64} - X_{53}X_{34}X_{45}^1 - X_{56}X_{61}X_{15} - X_{14}X_{45}^2X_{52}X_{23}X_{31} \tag{12.12}$$

The perfect matching matrix is

$$P = \left(\begin{array}{c|cccccc|ccccccc} & p_1 & p_2 & p_3 & p_4 & p_5 & p_6 & s_1 & s_2 & s_3 & s_4 & s_5 & s_6 & s_7 \\ \hline X_{45}^2 & 1 & 0 & 0 & 0 & 0 & 1 & 0 & 0 & 0 & 0 & 1 & 0 & 0 \\ X_{15} & 1 & 0 & 1 & 0 & 1 & 0 & 0 & 0 & 0 & 0 & 1 & 1 & 0 \\ X_{34} & 1 & 0 & 0 & 0 & 1 & 0 & 1 & 0 & 1 & 0 & 0 & 1 & 0 \\ X_{26} & 1 & 0 & 0 & 0 & 0 & 0 & 1 & 0 & 0 & 1 & 0 & 0 & 0 \\ X_{42} & 0 & 1 & 0 & 1 & 0 & 1 & 0 & 0 & 0 & 0 & 1 & 0 & 1 \\ X_{56} & 0 & 1 & 0 & 1 & 0 & 0 & 1 & 0 & 0 & 1 & 0 & 0 & 1 \\ X_{45}^1 & 0 & 1 & 1 & 0 & 0 & 0 & 0 & 0 & 0 & 0 & 1 & 0 & 0 \\ X_{31} & 0 & 1 & 0 & 0 & 0 & 0 & 1 & 0 & 1 & 0 & 0 & 0 & 0 \\ X_{64} & 0 & 0 & 1 & 0 & 1 & 0 & 0 & 1 & 1 & 0 & 0 & 1 & 0 \\ X_{23} & 0 & 0 & 1 & 0 & 0 & 0 & 0 & 1 & 0 & 1 & 0 & 0 & 0 \\ X_{53} & 0 & 0 & 0 & 1 & 0 & 1 & 0 & 1 & 0 & 1 & 0 & 0 & 1 \\ X_{14} & 0 & 0 & 0 & 1 & 0 & 0 & 0 & 0 & 0 & 0 & 0 & 1 & 0 \\ X_{52} & 0 & 0 & 0 & 0 & 1 & 0 & 0 & 0 & 0 & 0 & 0 & 0 & 1 \\ X_{61} & 0 & 0 & 0 & 0 & 0 & 1 & 0 & 1 & 1 & 0 & 0 & 0 & 0 \end{array}\right)$$

The F-term charge matrix $Q_F = \ker(P)$ is

$$Q_F = \left(\begin{array}{cccccc|ccccccc} p_1 & p_2 & p_3 & p_4 & p_5 & p_6 & s_1 & s_2 & s_3 & s_4 & s_5 & s_6 & s_7 \\ \hline 1 & 1 & 0 & 0 & 0 & 0 & -1 & 0 & 0 & 0 & -1 & 0 & 0 \\ 1 & 0 & 1 & 0 & -1 & 0 & 0 & 0 & 0 & -1 & -1 & 0 & 1 \\ 1 & 0 & 0 & 1 & 0 & -1 & -1 & 0 & 1 & 0 & 0 & -1 & 0 \\ 0 & 0 & 0 & 1 & 1 & 0 & 0 & 0 & 0 & 0 & 0 & -1 & -1 \\ 0 & 0 & 0 & 0 & 0 & 0 & 1 & 1 & -1 & -1 & 0 & 0 & 0 \end{array}\right)$$

The D-term charge matrix is

$$Q_D = \left(\begin{array}{cccccc|ccccccc} p_1 & p_2 & p_3 & p_4 & p_5 & p_6 & s_1 & s_2 & s_3 & s_4 & s_5 & s_6 & s_7 \\ \hline 0 & 0 & 0 & 0 & 0 & 0 & 0 & 1 & -1 & 0 & 0 & 0 & 0 \\ 0 & 0 & 0 & 0 & 0 & 0 & 0 & 0 & 1 & -1 & 0 & 0 & 0 \\ 0 & 0 & 0 & 0 & 0 & 0 & 0 & 0 & 0 & 1 & -1 & 0 & 0 \\ 0 & 0 & 0 & 0 & 0 & 0 & 0 & 0 & 0 & 0 & 1 & -1 & 0 \\ 0 & 0 & 0 & 0 & 0 & 0 & 0 & 0 & 0 & 0 & 0 & 1 & -1 \end{array}\right)$$

The total charge matrix Q_t does not exhibit repeated columns. Accordingly, the global symmetry of Model 10b is identical to the one for Model 10a, $U(1)_{f_1} \times U(1)_{f_2} \times U(1)_R$. The flavour and R-charges on the extremal perfect matchings are found following the discussion in §2.3. They are identical to Model 10a, and are shown in Table 39.

The product of all internal perfect matchings is given by the variable

$$s = \prod_{m=1}^{7} s_m \ . \tag{12.13}$$

The fugacity for extremal perfect matchings p_α is t_α and the fugacity for the above product of internal perfect matchings is y_s.

The mesonic Hilbert series of Model 10a and 10b are identical. They are called phases of the same toric moduli space. The Hilbert series is found in (12.4) with the plethystic logarithm in (12.8). The moduli space is not a complete intersection.

The generators of the mesonic moduli space in terms of the perfect matchings of Model 10b are shown in Table 23. The generators in terms of quiver fields of Model 10b are shown in Table 24. The charge lattice of generators is the dual reflexive polygon of the toric diagram of Model 10b.

Generator	$U(1)_{f_1}$	$U(1)_{f_2}$
$X_{15}X_{52}X_{23}X_{31} = X_{23}X_{34}X^1_{45}X_{52} = X_{26}X_{64}X^1_{45}X_{52}$	1	1
$X_{15}X_{52}X_{26}X_{61} = X_{23}X_{34}X^2_{45}X_{52} = X_{26}X_{64}X^2_{45}X_{52}$	0	1
$X^1_{45}X_{56}X_{64} = X_{14}X^1_{45}X_{52}X_{23}X_{31}$	1	0
$X_{14}X^2_{45}X_{52}X_{23}X_{31} = X_{14}X^1_{45}X_{52}X_{26}X_{61} = X_{15}X_{53}X_{31} = X_{15}X_{56}X_{61} = X_{23}X_{34}X_{42} = X_{26}X_{64}X_{42} = X_{34}X^1_{45}X_{53} = X^2_{45}X_{56}X_{64}$	0	0
$X_{34}X^2_{45}X_{53} = X_{14}X^2_{45}X_{52}X_{26}X_{61}$	-1	0
$X_{14}X_{42}X_{23}X_{31} = X_{14}X^1_{45}X_{53}X_{31} = X_{14}X^1_{45}X_{56}X_{61}$	0	-1
$X_{14}X_{42}X_{26}X_{61} = X_{14}X^2_{45}X_{53}X_{31} = X_{14}X^2_{45}X_{56}X_{61}$	-1	-1

Table 40. The generators in terms of bifundamental fields (Model 10b).

12.3 Model 10 Phase c

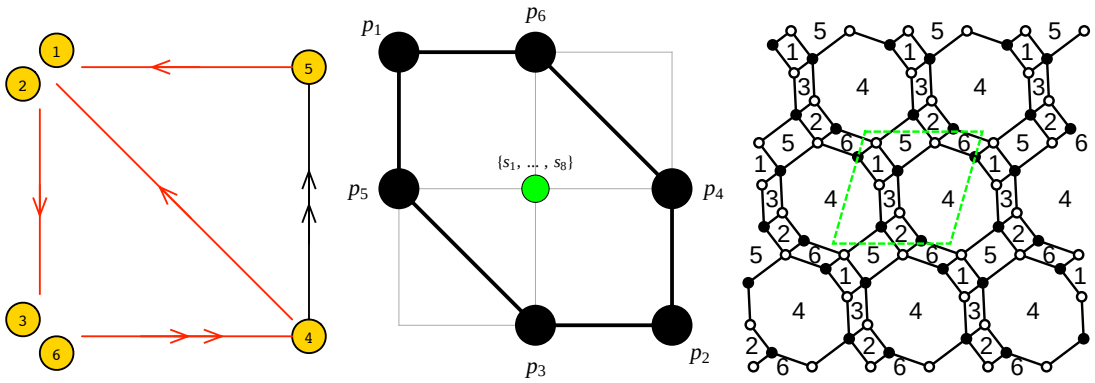


Figure 26. The quiver, toric diagram, and brane tiling of Model 10c. The red arrows in the quiver indicate all possible connections between blocks of nodes.

The superpotential is

$$\begin{aligned} W = &+X_{41}X_{13}X^2_{34} + X_{42}X_{23}X^1_{34} + X^1_{45}X_{52}X_{26}X^2_{64} + X_{51}X_{16}X^1_{64}X^2_{45} \\ &-X_{41}X_{16}X^2_{64} - X_{42}X_{26}X^1_{64} - X^2_{45}X_{52}X_{23}X^2_{34} - X_{51}X_{13}X^1_{34}X^1_{45} \end{aligned} \quad (12.14)$$

The perfect matching matrix is

$$P = \left(\begin{array}{c|cccccc|cccccccc} & p_1 & p_2 & p_3 & p_4 & p_5 & p_6 & s_1 & s_2 & s_3 & s_4 & s_5 & s_6 & s_7 & s_8 \\ \hline X_{42} & 1 & 0 & 0 & 0 & 1 & 1 & 0 & 0 & 1 & 0 & 1 & 1 & 0 & 0 \\ X_{34}^2 & 1 & 0 & 0 & 0 & 1 & 0 & 0 & 1 & 0 & 0 & 0 & 0 & 0 & 1 \\ X_{64}^2 & 1 & 0 & 0 & 0 & 0 & 1 & 0 & 0 & 0 & 0 & 0 & 0 & 1 & 1 \\ X_{51} & 1 & 0 & 0 & 0 & 0 & 0 & 0 & 0 & 0 & 1 & 0 & 1 & 0 & 0 \\ X_{41} & 0 & 1 & 1 & 1 & 0 & 0 & 0 & 0 & 1 & 1 & 0 & 1 & 0 & 0 \\ X_{64}^1 & 0 & 1 & 1 & 0 & 0 & 0 & 0 & 0 & 0 & 0 & 0 & 0 & 1 & 1 \\ X_{34}^1 & 0 & 1 & 0 & 1 & 0 & 0 & 0 & 1 & 0 & 0 & 0 & 0 & 0 & 1 \\ X_{52} & 0 & 1 & 0 & 0 & 0 & 0 & 0 & 0 & 0 & 0 & 1 & 1 & 0 & 0 \\ X_{45}^1 & 0 & 0 & 1 & 0 & 1 & 0 & 0 & 0 & 1 & 0 & 0 & 0 & 0 & 0 \\ X_{23} & 0 & 0 & 1 & 0 & 0 & 0 & 1 & 0 & 0 & 1 & 0 & 0 & 1 & 0 \\ X_{45}^2 & 0 & 0 & 0 & 1 & 0 & 1 & 0 & 0 & 1 & 0 & 0 & 0 & 0 & 0 \\ X_{26} & 0 & 0 & 0 & 1 & 0 & 0 & 1 & 1 & 0 & 1 & 0 & 0 & 0 & 0 \\ X_{16} & 0 & 0 & 0 & 0 & 1 & 0 & 1 & 1 & 0 & 0 & 1 & 0 & 0 & 0 \\ X_{13} & 0 & 0 & 0 & 0 & 0 & 1 & 1 & 0 & 0 & 0 & 1 & 0 & 1 & 0 \end{array}\right)$$

The F-term charge matrix $Q_F = \ker(P)$ is

$$Q_F = \left(\begin{array}{cccccc|cccccccc} p_1 & p_2 & p_3 & p_4 & p_5 & p_6 & s_1 & s_2 & s_3 & s_4 & s_5 & s_6 & s_7 & s_8 \\ \hline 1 & 1 & 0 & 0 & 0 & 0 & 0 & 0 & 0 & 0 & 0 & -1 & 0 & -1 \\ 1 & 0 & 0 & 1 & 0 & -1 & 0 & -1 & 0 & 0 & 1 & -1 & 0 & 0 \\ 0 & 0 & 1 & 0 & 0 & 1 & 0 & 0 & -1 & 0 & 0 & 0 & -1 & 0 \\ 0 & 0 & 0 & 1 & 1 & 0 & 0 & -1 & -1 & 0 & 0 & 0 & 0 & 0 \\ 0 & 0 & 0 & 0 & 0 & 0 & 1 & -1 & 0 & 0 & 0 & 0 & -1 & 1 \\ 0 & 0 & 0 & 0 & 0 & 0 & 1 & 0 & 0 & -1 & -1 & 1 & 0 & 0 \end{array}\right)$$

The D-term charge matrix is

$$Q_D = \left(\begin{array}{cccccc|cccccccc} p_1 & p_2 & p_3 & p_4 & p_5 & p_6 & s_1 & s_2 & s_3 & s_4 & s_5 & s_6 & s_7 & s_8 \\ \hline 0 & 0 & 0 & 0 & 0 & 0 & 0 & 0 & 1 & -1 & 0 & 0 & 0 & 0 \\ 0 & 0 & 0 & 0 & 0 & 0 & 0 & 0 & 0 & 1 & -1 & 0 & 0 & 0 \\ 0 & 0 & 0 & 0 & 0 & 0 & 0 & 0 & 0 & 0 & 1 & -1 & 0 & 0 \\ 0 & 0 & 0 & 0 & 0 & 0 & 0 & 0 & 0 & 0 & 0 & 1 & -1 & 0 \\ 0 & 0 & 0 & 0 & 0 & 0 & 0 & 0 & 0 & 0 & 0 & 0 & 1 & -1 \end{array}\right)$$

The global symmetry for Model 10c is identical to the global symmetries of Model 10a and Model 10b, $U(1)_{f_1} \times U(1)_{f_2} \times U(1)_R$. The mesonic charges on the extremal perfect matchings with non-zero R-charge are shown in Table 39.

The product of all internal perfect matchings is expressed as

$$s = \prod_{m=1}^{8} s_m \ . \tag{12.15}$$

The fugacity t_α counts extremal perfect matchings and the fugacity y_s counts the above product of internal perfect matchings.

The mesonic Hilbert series is identical to the Hilbert series for Models 10a and 10b in (12.3).

The moduli space generators in terms of all perfect matchings of Model 10c are shown in Table 23, with the corresponding lattice of generators being the dual reflexive polygon of the toric diagram. The generators in terms of quiver fields of Model 10c are shown in Table 41.

Generator	$U(1)_{f_1}$	$U(1)_{f_2}$
$X_{16}X^1_{64}X_{41} = X_{23}X^1_{34}X^1_{45}X_{52} = X_{26}X^1_{64}X^1_{45}X_{52}$	1	1
$X_{13}X^1_{34}X_{41} = X_{23}X^1_{34}X^2_{45}X_{52} = X_{26}X^1_{64}X^2_{45}X_{52}$	0	1
$X_{16}X^1_{64}X^1_{45}X_{51} = X_{23}X^2_{34}X^1_{45}X_{52}$	1	0
$X_{13}X^2_{34}X_{41} = X_{16}X^2_{64}X_{41} = X_{23}X^1_{34}X_{42} = X_{26}X^1_{64}X_{42}$ $= X_{13}X^1_{34}X^1_{45}X_{51} = X_{16}X^1_{64}X^2_{45}X_{51} = X_{23}X^2_{34}X^2_{45}X_{52} = X_{26}X^2_{64}X^1_{45}X_{52}$	0	0
$X_{13}X^1_{34}X^2_{45}X_{51} = X_{26}X^2_{64}X^2_{45}X_{52}$	-1	0
$X_{23}X^2_{34}X_{42} = X_{13}X^2_{34}X^1_{45}X_{51} = X_{16}X^2_{64}X^1_{45}X_{51}$	0	-1
$X_{26}X^2_{64}X_{42} = X_{13}X^2_{34}X^2_{45}X_{51} = X_{16}X^2_{64}X^2_{45}X_{51}$	-1	-1

Table 41. The generators in terms of bifundamental fields (Model 10c).

12.4 Model 10 Phase d

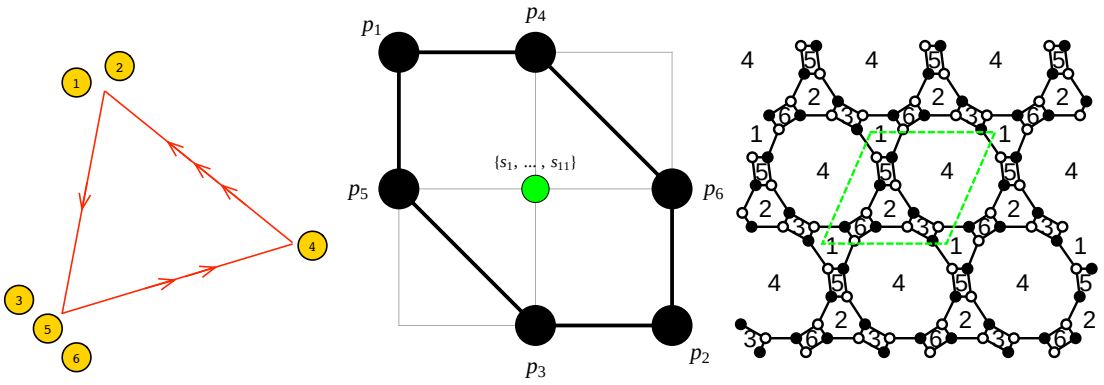


Figure 27. The quiver, toric diagram, and brane tiling of Model 10d. The red arrows in the quiver indicate all possible connections between blocks of nodes.

The superpotential is

$$W = +X_{15}X^1_{54}X^2_{41} + X_{25}X^2_{54}X^2_{42} + X_{26}X^2_{64}X^3_{42} + X^1_{41}X_{13}X^2_{34} + X_{16}X^1_{64}X^3_{41} + X^1_{42}X_{23}X^1_{34} \\ -X_{15}X^2_{54}X^3_{41} - X_{13}X^1_{34}X^2_{41} - X_{23}X^2_{34}X^2_{42} - X_{25}X^1_{54}X^3_{42} - X^1_{41}X_{16}X^2_{64} - X^1_{42}X_{26}X^1_{64} \ . \tag{12.16}$$

The perfect matching matrix is

$$P = \left(\begin{array}{c|cccccc|ccccccccccc} & p_1 & p_2 & p_3 & p_4 & p_5 & p_6 & s_1 & s_2 & s_3 & s_4 & s_5 & s_6 & s_7 & s_8 & s_9 & s_{10} & s_{11} \\ \hline X^2_{42} & 1 & 0 & 1 & 0 & 1 & 0 & 0 & 0 & 0 & 0 & 0 & 1 & 1 & 0 & 0 & 0 & 0 \\ X^3_{42} & 1 & 0 & 0 & 1 & 0 & 1 & 0 & 0 & 0 & 0 & 0 & 1 & 1 & 0 & 0 & 0 & 0 \\ X^1_{41} & 1 & 0 & 0 & 0 & 1 & 1 & 0 & 0 & 0 & 0 & 1 & 0 & 1 & 0 & 0 & 0 & 0 \\ X_{34} & 1 & 0 & 0 & 0 & 1 & 0 & 0 & 0 & 1 & 1 & 0 & 0 & 0 & 0 & 1 & 0 & 1 \\ X_{64} & 1 & 0 & 0 & 0 & 0 & 1 & 0 & 1 & 1 & 0 & 0 & 0 & 0 & 0 & 0 & 1 & 1 \\ X_{15} & 1 & 0 & 0 & 0 & 0 & 0 & 1 & 0 & 0 & 1 & 0 & 1 & 0 & 0 & 0 & 1 & 1 \\ X^3_{41} & 0 & 1 & 1 & 0 & 1 & 0 & 0 & 0 & 0 & 0 & 1 & 0 & 1 & 0 & 0 & 0 & 0 \\ X^2_{64} & 0 & 1 & 1 & 0 & 0 & 0 & 0 & 1 & 1 & 0 & 0 & 0 & 0 & 0 & 0 & 1 & 1 \\ X^1_{42} & 0 & 1 & 1 & 1 & 0 & 0 & 0 & 0 & 0 & 0 & 0 & 1 & 1 & 0 & 0 & 0 & 0 \\ X^2_{41} & 0 & 1 & 0 & 1 & 0 & 1 & 0 & 0 & 0 & 0 & 1 & 0 & 1 & 0 & 0 & 0 & 0 \\ X^2_{34} & 0 & 1 & 0 & 1 & 0 & 0 & 0 & 0 & 1 & 1 & 0 & 0 & 0 & 0 & 1 & 0 & 1 \\ X_{25} & 0 & 1 & 0 & 0 & 0 & 0 & 1 & 0 & 0 & 1 & 1 & 0 & 0 & 0 & 0 & 1 & 1 \\ X_{54} & 0 & 0 & 1 & 0 & 1 & 0 & 0 & 1 & 1 & 0 & 0 & 0 & 0 & 1 & 1 & 0 & 0 \\ X_{13} & 0 & 0 & 1 & 0 & 0 & 0 & 1 & 1 & 0 & 0 & 0 & 1 & 0 & 1 & 0 & 1 & 0 \\ X^2_{54} & 0 & 0 & 0 & 1 & 0 & 1 & 0 & 1 & 1 & 0 & 0 & 0 & 0 & 1 & 1 & 0 & 0 \\ X_{16} & 0 & 0 & 0 & 1 & 0 & 0 & 1 & 0 & 0 & 1 & 0 & 1 & 0 & 1 & 1 & 0 & 0 \\ X_{26} & 0 & 0 & 0 & 0 & 1 & 0 & 1 & 0 & 0 & 1 & 1 & 0 & 0 & 1 & 1 & 0 & 0 \\ X_{23} & 0 & 0 & 0 & 0 & 0 & 1 & 1 & 1 & 0 & 0 & 1 & 0 & 0 & 1 & 0 & 1 & 0 \end{array}\right)$$

The F-term charge matrix $Q_F = \ker(P)$ is

$$Q_F = \left(\begin{array}{cccccc|ccccccccccc} p_1 & p_2 & p_3 & p_4 & p_5 & p_6 & s_1 & s_2 & s_3 & s_4 & s_5 & s_6 & s_7 & s_8 & s_9 & s_{10} & s_{11} \\ \hline 1 & 1 & 0 & -1 & -1 & 0 & 0 & 0 & 0 & 0 & 0 & 0 & 0 & 1 & 0 & -1 & 0 \\ 1 & 0 & 0 & 1 & 0 & -1 & 0 & 0 & 0 & 0 & 0 & -1 & 0 & 1 & -1 & 0 & 0 \\ 1 & 0 & 0 & 1 & 0 & -1 & 0 & 0 & 0 & 0 & 0 & -1 & 0 & 0 & 0 & 1 & -1 \\ 0 & 1 & 0 & -1 & 0 & 1 & 0 & 0 & 0 & 1 & -1 & 0 & 0 & 0 & 0 & 0 & -1 \\ 0 & 1 & 0 & -1 & 0 & 1 & 0 & 0 & 0 & 0 & 0 & 1 & -1 & 0 & 0 & -1 & 0 \\ 0 & 0 & 1 & 0 & 0 & 1 & 0 & -1 & 0 & 0 & 0 & 0 & -1 & 0 & 0 & 0 & 0 \\ 0 & 0 & 0 & 0 & 0 & 0 & 1 & 0 & 1 & 0 & 0 & 0 & 0 & 0 & -1 & -1 & 0 \\ 0 & 0 & 0 & 0 & 0 & 0 & 0 & 1 & 0 & 1 & 0 & 0 & 0 & 0 & -1 & -1 & 0 \\ 0 & 0 & 0 & 0 & 0 & 0 & 0 & 1 & -1 & 0 & 0 & 0 & 0 & 0 & 0 & -1 & 1 \end{array}\right)$$

The D-term charge matrix is

$$Q_D = \left(\begin{array}{cccccc|ccccccccccc} p_1 & p_2 & p_3 & p_4 & p_5 & p_6 & s_1 & s_2 & s_3 & s_4 & s_5 & s_6 & s_7 & s_8 & s_9 & s_{10} & s_{11} \\ \hline 0 & 0 & 0 & 0 & 0 & 0 & 0 & 0 & 0 & 0 & 1 & -1 & 0 & 0 & 0 & 0 & 0 \\ 0 & 0 & 0 & 0 & 0 & 0 & 0 & 0 & 0 & 0 & 0 & 1 & -1 & 0 & 0 & 0 & 0 \\ 0 & 0 & 0 & 0 & 0 & 0 & 0 & 0 & 0 & 0 & 0 & 0 & 1 & -1 & 0 & 0 & 0 \\ 0 & 0 & 0 & 0 & 0 & 0 & 0 & 0 & 0 & 0 & 0 & 0 & 0 & 1 & -1 & 0 & 0 \\ 0 & 0 & 0 & 0 & 0 & 0 & 0 & 0 & 0 & 0 & 0 & 0 & 0 & 0 & 1 & -1 & 0 \end{array}\right)$$

The symmetry $U(1)_{f_1} \times U(1)_{f_2} \times U(1)_R$ of Model 10d is identical to Models 10a to 10c discussed above. The symmetry charges on the extremal perfect matchings with non-zero R-charges are shown in Table 39.

The product of all internal perfect matchings is

$$s = \prod_{m=1}^{11} s_m \ . \tag{12.17}$$

The fugacity y_s counts the above product of internal perfect matchings whereas the fugacity t_α counts the external perfect matchings p_α.

The mesonic Hilbert series of Model 10d is identical to Models 10a, 10b and 10c. This indicates that the mesonic moduli spaces are identical, and given the corresponding plethystic logarithm in (12.8), the mesonic moduli spaces are not complete intersections.

The moduli space generators in terms of all perfect matchings of Model 10d are shown in Table 23 with the corresponding charge lattice of generators forming a reflexive polygon which is the dual polygon of the toric diagram. The generators in terms of quiver fields of Model 10d are shown in Table 28.

Generator	$U(1)_{f_1}$	$U(1)_{f_2}$
$X_{13}X^2_{34}X^3_{41} = X^3_{41}X_{16}X^2_{64} = X^1_{42}X_{25}X^1_{54} = X^1_{42}X_{26}X^2_{64}$	1	1
$X_{13}X^1_{34}X^3_{41} = X^3_{41}X_{15}X^1_{54} = X^2_{42}X_{25}X^1_{54} = X^2_{42}X_{26}X^2_{64}$	0	1
$X_{13}X^2_{34}X^2_{41} = X^2_{41}X_{16}X^2_{64} = X_{23}X^2_{34}X^1_{42} = X^1_{42}X_{25}X^2_{54}$	1	0
$X_{13}X^1_{34}X^2_{41} = X_{13}X^2_{34}X^1_{41} = X^2_{41}X_{15}X^1_{54} = X^3_{41}X_{15}X^2_{54} = X^1_{41}X_{16}X^2_{64} = X^3_{41}X_{16}X^1_{64} = X_{23}X^1_{34}X^1_{42}$ $= X_{23}X^2_{34}X^2_{42} = X^2_{42}X_{25}X^2_{54} = X^3_{42}X_{25}X^1_{54} = X^1_{42}X_{26}X^1_{64} = X^3_{42}X_{26}X^2_{64}$	0	0
$X_{13}X^1_{34}X^1_{41} = X^1_{41}X_{15}X^1_{54} = X_{23}X^1_{34}X^2_{42} = X^2_{42}X_{26}X^1_{64}$	-1	0
$X^2_{41}X_{15}X^2_{54} = X^2_{41}X_{16}X^1_{64} = X_{23}X^2_{34}X^3_{42} = X^3_{42}X_{25}X^2_{54}$	0	-1
$X^1_{41}X_{15}X^2_{54} = X^1_{41}X_{16}X^1_{64} = X_{23}X^1_{34}X^3_{42} = X^3_{42}X_{26}X^1_{64}$	-1	-1

Figure 28. The generators in terms of bifundamental fields (Model 10d).

13 Model 11: PdP_2

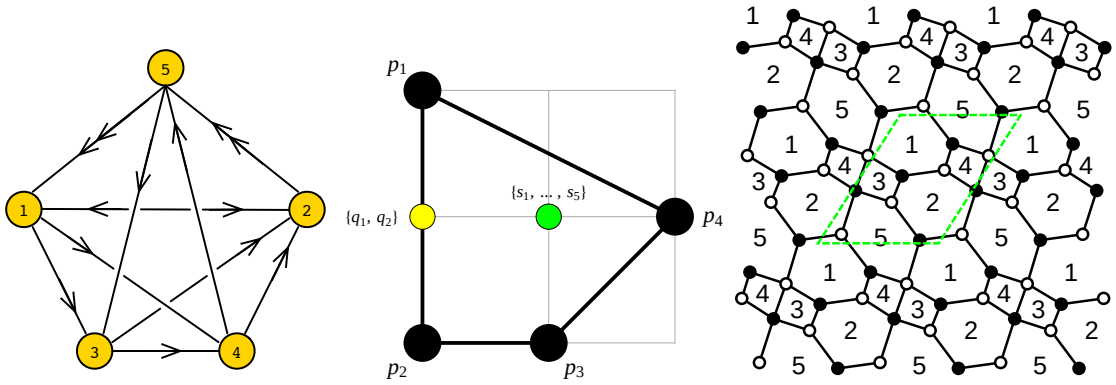


Figure 29. The quiver, toric diagram, and brane tiling of Model 11.

The superpotential is

$$\begin{aligned} W = &+X_{21}X_{14}X_{42} + X_{53}X_{32}X_{25}^2 + X_{51}^2X_{12}X_{25}^1 + X_{13}X_{34}X_{45}X_{51}^1 \\ &-X_{13}X_{32}X_{21} - X_{14}X_{45}X_{51}^2 - X_{51}^1X_{12}X_{25}^2 - X_{53}X_{34}X_{42}X_{25}^1 \end{aligned} \tag{13.1}$$

The perfect matching matrix is

$$P = \left(\begin{array}{c|cccc|cc|ccccc} & p_1 & p_2 & p_3 & p_4 & q_1 & q_2 & s_1 & s_2 & s_3 & s_4 & s_5 \\ \hline X_{14} & 1 & 0 & 0 & 0 & 1 & 0 & 1 & 0 & 0 & 1 & 0 \\ X_{32} & 1 & 0 & 0 & 0 & 0 & 1 & 1 & 0 & 0 & 0 & 1 \\ X_{25}^1 & 1 & 0 & 0 & 0 & 1 & 0 & 0 & 1 & 0 & 0 & 0 \\ X_{25}^2 & 0 & 1 & 1 & 0 & 1 & 0 & 0 & 1 & 0 & 0 & 0 \\ X_{51}^1 & 1 & 0 & 0 & 0 & 0 & 1 & 0 & 0 & 1 & 0 & 0 \\ X_{51}^2 & 0 & 1 & 1 & 0 & 0 & 1 & 0 & 0 & 1 & 0 & 0 \\ X_{13} & 0 & 1 & 0 & 0 & 1 & 0 & 0 & 0 & 0 & 1 & 0 \\ X_{42} & 0 & 1 & 0 & 0 & 0 & 1 & 0 & 0 & 0 & 0 & 1 \\ X_{21} & 0 & 0 & 1 & 1 & 0 & 0 & 0 & 1 & 1 & 0 & 0 \\ X_{12} & 0 & 0 & 0 & 1 & 0 & 0 & 1 & 0 & 0 & 1 & 1 \\ X_{34} & 0 & 0 & 1 & 0 & 0 & 0 & 1 & 0 & 0 & 0 & 0 \\ X_{45} & 0 & 0 & 0 & 1 & 0 & 0 & 0 & 1 & 0 & 0 & 1 \\ X_{53} & 0 & 0 & 0 & 1 & 0 & 0 & 0 & 0 & 1 & 1 & 0 \end{array}\right)$$

The F-term charge matrix $Q_F = \ker(P)$ is

$$Q_F = \left(\begin{array}{cccc|cc|ccccc} p_1 & p_2 & p_3 & p_4 & q_1 & q_2 & s_1 & s_2 & s_3 & s_4 & s_5 \\ \hline 1 & 1 & 0 & 0 & -1 & -1 & 0 & 0 & 0 & 0 & 0 \\ 1 & 1 & 0 & 1 & -1 & 0 & 0 & 0 & -1 & 0 & -1 \\ 0 & 1 & -1 & 0 & -1 & 0 & 1 & 1 & 0 & 0 & -1 \\ 0 & 0 & 0 & 1 & 1 & 0 & 0 & -1 & 0 & -1 & 0 \end{array}\right)$$

The D-term charge matrix is

$$Q_D = \left(\begin{array}{cccc|cc|ccccc} p_1 & p_2 & p_3 & p_4 & q_1 & q_2 & s_1 & s_2 & s_3 & s_4 & s_5 \\ \hline 0 & 0 & 0 & 0 & 0 & 0 & 1 & -1 & 0 & 0 & 0 \\ 0 & 0 & 0 & 0 & 0 & 0 & 0 & 1 & -1 & 0 & 0 \\ 0 & 0 & 0 & 0 & 0 & 0 & 0 & 0 & 1 & -1 & 0 \\ 0 & 0 & 0 & 0 & 0 & 0 & 0 & 0 & 0 & 1 & -1 \end{array}\right)$$

The total charge matrix Q_t does not exhibit repeated columns. Accordingly, the global symmetry is $U(1)_{f_1} \times U(1)_{f_2} \times U(1)_R$. The flavour and R-charges on the GLSM fields corresponding to extremal points in the toric diagram in Figure 29 are found following the discussion in §2.3. They are presented in Table 42.

	$U(1)_{f_1}$	$U(1)_{f_2}$	$U(1)_R$	fugacity
p_1	-1/4	-1/3	$R_1 \simeq 0.622$	t_1
p_2	-1/4	0	$R_2 \simeq 0.502$	t_2
p_3	0	2/3	$R_3 \simeq 0.306$	t_3
p_4	1/2	-1/3	$R_4 \simeq 0.570$	t_4

Table 42. The GLSM fields corresponding to extremal points of the toric diagram with their mesonic charges (Model 11).

Fine-tuning R-charges. The exact R-charges are expressed in terms of the root x_0 in the range $0 \leq 1 - x_0 \leq \frac{2}{3}$ of the polynomial

$$27 - 42x - 68x^2 + 42x^3 + 9x^4 = 0, \tag{13.2}$$

where

$$\begin{aligned} R_1 &= 1 + \frac{1}{144}\left(-63 + 250x_0 - 422x_0^2 - 384x_0^3 + 261x_0^4 + 54x_0^5\right) \\ R_2 &= 1 + \frac{1}{72}\left(-189 + 281x_0 + 257x_0^2 - 177x_0^3 - 36x_0^4\right) \\ R_3 &= 1 + \frac{1}{288}\left(333 - 1351x_0 - 294x_0^2 + 1450x_0^3 - 327x_0^4 - 99x_0^5\right) \\ R_4 &= 1 - x_0 \quad . \end{aligned} \tag{13.3}$$

Products of non-extremal perfect matchings are assigned the following variables

$$q = q_1 q_2 \ , \ s = \prod_{m=1}^{5} s_m \ . \tag{13.4}$$

The fugacities y_q and y_s count respectively the above products of internal perfect matchings. The fugacity t_α counts all other extremal perfect matchings p_α.

The mesonic Hilbert series of Model 11 is found using the Molien integral formula in (2.9). It is

$$\begin{aligned} g_1(t_\alpha, y_q, y_s; \mathcal{M}_{11}^{mes}) = & (1 + y_q y_s\ t_1 t_2 t_3 t_4 + y_q^2 y_s\ t_1 t_2^3 t_3^2 + y_q^2 y_s\ t_1^2 t_2^2 t_3 - y_q^2 y_s^2\ t_1^2 t_2^2 t_3^2 t_4^2 \\ & - y_q^2 y_s^2\ t_1^3 t_2 t_3 t_4^2 - y_q^3 y_s^2\ t_1^3 t_2^3 t_3^2 t_4 - y_q^3 y_s^2\ t_1^4 t_2^2 t_3 t_4 - y_q^3 y_s^3\ t_1^4 t_2^4 t_3^3 t_4^2 + y_q y_s\ t_2^2 t_3^2 t_4) \\ & \times \frac{1}{(1 - y_q^2 y_s\ t_1^3 t_2)(1 - y_q^2 y_s\ t_2^4 t_3^3)(1 - y_q y_s\ t_1^2 t_4)(1 - y_s\ t_3 t_4^2)} \ . \end{aligned} \tag{13.5}$$

The plethystic logarithm of the mesonic Hilbert series is

$$\begin{aligned} PL[g_1(t_\alpha, y_q, y_s; \mathcal{M}_{11}^{mes})] = & \ y_q y_s\ t_1^2 t_4 + y_s\ t_3 t_4^2 + y_q^2 y_s\ t_1^3 t_2 + y_q y_s\ t_1 t_2 t_3 t_4 + y_q^2 y_s\ t_1^2 t_2^2 t_3 \\ & + y_q y_s\ t_2^2 t_3^2 t_4 + y_q^2 y_s\ t_1 t_2^3 t_3^2 + y_q^2 y_s\ t_2^4 t_3^3 - y_q^2 y_s^2\ t_1^3 t_2 t_3 t_4^2 - y_q^3 y_s^2\ t_1^4 t_2^2 t_3 t_4 - 2\ y_q^2 y_s^2\ t_1^2 t_2^2 t_3^2 t_4^2 \\ & + \dots \ . \end{aligned} \tag{13.6}$$

Consider the following fugacity map

$$\begin{aligned} & f_1 = y_q^{-3/4} y_s^{1/4}\ ,\ \ f_2 = y_q^{-1/4} y_s^{-1/4}\ , \\ & \tilde{t}_1 = y_q^{1/4} y_s^{1/4}\ t_1\ ,\ \tilde{t}_2 = y_q^{1/4} y_s^{1/4}\ t_2\ ,\ \tilde{t}_3 = y_q^{1/4} y_s^{1/4}\ t_3\ ,\ \tilde{t}_4 = y_q^{1/4} y_s^{1/4}\ t_4\ , \end{aligned} \tag{13.7}$$

where the fugacities f_1 and f_2 count flavour charges, and the fugacity $\tilde{t}_i$ counts the R-charge R_i in Table 42.

Under the fugacity map above, the plethystic logarithm becomes

$$\begin{aligned} PL[g_1(\tilde{t}_\alpha, f_1, f_2; \mathcal{M}_{11}^{mes})] = & \frac{1}{f_2}\tilde{t}_1^2\tilde{t}_4 + f_1\tilde{t}_3\tilde{t}_4^2 + \frac{1}{f_1 f_2}\tilde{t}_1^3\tilde{t}_2 + \tilde{t}_1\tilde{t}_2\tilde{t}_3\tilde{t}_4 + \frac{1}{f_1}\tilde{t}_1^2\tilde{t}_2^2\tilde{t}_3 \\ & + f_2\tilde{t}_2^2\tilde{t}_3^2\tilde{t}_4 + \frac{f_2}{f_1}\tilde{t}_1\tilde{t}_2^3\tilde{t}_3^2 + \frac{f_2^2}{f_1}\tilde{t}_2^4\tilde{t}_3^3 - \frac{1}{f_2}\tilde{t}_1^3\tilde{t}_2\tilde{t}_3\tilde{t}_4^2 - \frac{1}{f_1 f_2}\tilde{t}_1^4\tilde{t}_2^2\tilde{t}_3\tilde{t}_4 - 2\tilde{t}_1^2\tilde{t}_2^2\tilde{t}_3^2\tilde{t}_4^2 + \dots \ . \end{aligned} \tag{13.8}$$

The plethsytic logarithm above exhibits the moduli space generators with the corresponding mesonic charges. They are summarized in Table 43. The generators can be presented on a charge lattice. The convex polygon formed by the generators in Table 43 is the dual reflexive polygon of the toric diagram of Model 11.

Generator	$U(1)_{f_1}$	$U(1)_{f_2}$
$p_3 p_4^2\ s$	1	0
$p_1^2 p_4\ q\ s$	0	-1
$p_1 p_2 p_3 p_4\ q\ s$	0	0
$p_2^2 p_3^2 p_4\ q\ s$	0	1
$p_1^3 p_2\ q^2\ s$	-1	-1
$p_1^2 p_2^2 p_3\ q^2\ s$	-1	0
$p_1 p_2^3 p_3^2\ q^2\ s$	-1	1
$p_2^4 p_3^3\ q^2\ s$	-1	2

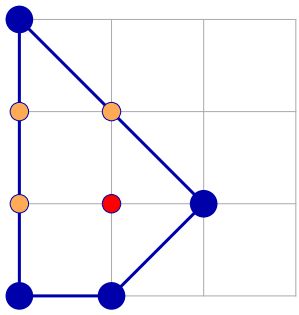


Table 43. The generators and lattice of generators of the mesonic moduli space of Model 11 in terms of GLSM fields with the corresponding flavor charges.

Generator	$U(1)_{f_1}$	$U(1)_{f_2}$
$X_{12}X_{21} = X_{34}X_{45}X_{53}$	1	0
$X_{12}X_{25}^1X_{51}^1 = X_{14}X_{45}X_{51}^1 = X_{32}X_{25}^1X_{53}$	0	-1
$X_{13}X_{34}X_{45}X_{51}^1 = X_{34}X_{25}^1X_{53}X_{42} = X_{12}X_{25}^1X_{51}^2 = X_{12}X_{25}^2X_{51}^1$ $= X_{21}X_{13}X_{32} = X_{21}X_{14}X_{42} = X_{14}X_{45}X_{51}^2 = X_{32}X_{25}^2X_{53}$	0	0
$X_{12}X_{25}^2X_{51}^2 = X_{21}X_{13}X_{34}X_{42} = X_{13}X_{34}X_{45}X_{51}^2 = X_{34}X_{25}^2X_{53}X_{42}$	0	1
$X_{25}^1X_{51}^1X_{13}X_{32} = X_{25}^1X_{51}^1X_{14}X_{42}$	-1	-1
$X_{25}^1X_{51}^1X_{13}X_{34}X_{42} = X_{25}^1X_{51}^2X_{13}X_{32} = X_{25}^2X_{51}^1X_{13}X_{32} = X_{25}^1X_{51}^2X_{14}X_{42} = X_{25}^2X_{51}^1X_{14}X_{42}$	-1	0
$X_{25}^2X_{51}^2X_{13}X_{32} = X_{25}^2X_{51}^2X_{14}X_{42} = X_{25}^1X_{51}^2X_{13}X_{34}X_{42} = X_{25}^2X_{51}^1X_{13}X_{34}X_{42}$	-1	1
$X_{25}^2X_{51}^2X_{13}X_{34}X_{42}$	-1	2

Table 44. The generators in terms of bifundamental fields (Model 11).

The mesonic Hilbert series and the plethystic logarithm can be re-expressed in terms of just 3 fugacities

$$T_1 = \frac{f_2\ \tilde{t}_2}{f_1\ \tilde{t}_1\tilde{t}_4^2} = \frac{t_2}{y_s\ t_1 t_4^2}\ ,\ T_2 = \frac{1}{f_2}\ \tilde{t}_1^2\tilde{t}_4 = y_q y_s\ t_1^2 t_4\ ,\ T_3 = f_1\ \tilde{t}_3\tilde{t}_4^2 = y_s\ t_3 t_4^2\ , \quad (13.9)$$

such that

$$\begin{aligned} &g_1(T_1, T_2, T_3; \mathcal{M}_{11}^{mes}) = \\ &\quad (1 + T_1T_2T_3 + T_1^3T_2^2T_3^2 + T_1^2T_2^2T_3 - T_1^2T_2^2T_3^2 - T_1T_2^2T_3 - T_1^3T_2^3T_3^2 - T_1^2T_2^3T_3 \\ &\quad -T_1^4T_2^4T_3^3 + T_1^2T_2T_3^2) \times \frac{1}{(1 - T_1T_2^2)(1 - T_1^4T_2^2T_3^3)(1 - T_2)(1 - T_3)} \end{aligned} \quad (13.10)$$

and

$$PL[g_1(T_1,T_2,T_3;\mathcal{M}_{11}^{mes})] = T_2+T_3+T_1T_2^2+T_1T_2T_3+T_1^2T_2^2T_3+T_1^2T_2T_3^2 \\ +T_1^3T_2^2T_3^2+T_1^4T_2^2T_3^3-T_1^2T_2^3T_3-T_1T_2^2T_3+2T_1^2T_2^2T_3^2+\dots \quad . \tag{13.11}$$

The powers of the fugacities in the Hilbert series and plethystic logarithm above are all positive. This illustrates the conical structure of the toric Calabi-Yau 3-fold.

14 Model 12: dP_2

14.1 Model 12 Phase a

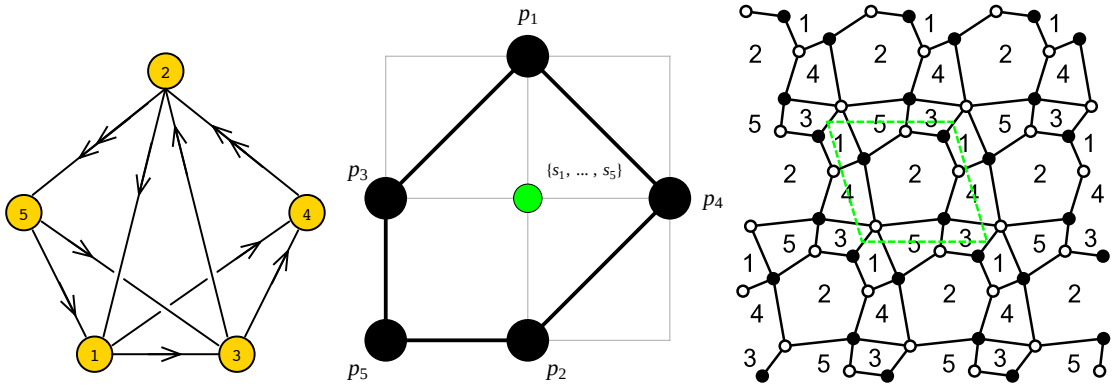


Figure 30. The quiver, toric diagram, and brane tiling of Model 12a.

The superpotential is

$$W = +X_{21}X_{14}X_{42}^1+X_{25}^2X_{53}X_{32}+X_{42}^2X_{25}^1X_{51}X_{13}X_{34} \\ -X_{13}X_{32}X_{21}-X_{14}X_{42}^2X_{25}^2X_{51}-X_{25}^1X_{53}X_{34}X_{42}^1 \quad . \tag{14.1}$$

The perfect matching matrix is

$$P = \left(\begin{array}{c|ccccc|ccccc} & p_1 & p_2 & p_3 & p_4 & p_5 & s_1 & s_2 & s_3 & s_4 & s_5 \\ \hline X_{14} & 1 & 0 & 0 & 0 & 0 & 1 & 0 & 0 & 0 & 1 \\ X_{34} & 0 & 1 & 0 & 0 & 0 & 1 & 0 & 0 & 0 & 0 \\ X^1_{25} & 1 & 0 & 0 & 0 & 0 & 0 & 1 & 0 & 0 & 0 \\ X^2_{25} & 0 & 1 & 0 & 0 & 1 & 0 & 1 & 0 & 0 & 0 \\ X^1_{42} & 0 & 0 & 1 & 0 & 1 & 0 & 0 & 1 & 0 & 0 \\ X^2_{42} & 0 & 0 & 0 & 1 & 0 & 0 & 0 & 1 & 0 & 0 \\ X_{32} & 1 & 0 & 1 & 0 & 0 & 1 & 0 & 1 & 0 & 0 \\ X_{21} & 0 & 1 & 0 & 1 & 0 & 0 & 1 & 0 & 1 & 0 \\ X_{51} & 0 & 0 & 1 & 0 & 0 & 0 & 0 & 0 & 1 & 0 \\ X_{53} & 0 & 0 & 0 & 1 & 0 & 0 & 0 & 0 & 1 & 1 \\ X_{13} & 0 & 0 & 0 & 0 & 1 & 0 & 0 & 0 & 0 & 1 \end{array}\right)$$

The F-term charge matrix $Q_F = \ker(P)$ is

$$Q_F = \left(\begin{array}{ccccc|ccccc} p_1 & p_2 & p_3 & p_4 & p_5 & s_1 & s_2 & s_3 & s_4 & s_5 \\ \hline 1 & 1 & 0 & 0 & 0 & -1 & -1 & 0 & 0 & 0 \\ 0 & 0 & 1 & 1 & 0 & 0 & 0 & -1 & -1 & 0 \\ 0 & 1 & 0 & -1 & -1 & -1 & 0 & 1 & 0 & 1 \end{array}\right)$$

The D-term charge matrix is

$$Q_D = \left(\begin{array}{ccccc|ccccc} p_1 & p_2 & p_3 & p_4 & p_5 & s_1 & s_2 & s_3 & s_4 & s_5 \\ \hline 0 & 0 & 0 & 0 & 0 & 1 & -1 & 0 & 0 & 0 \\ 0 & 0 & 0 & 0 & 0 & 0 & 1 & -1 & 0 & 0 \\ 0 & 0 & 0 & 0 & 0 & 0 & 0 & 1 & -1 & 0 \\ 0 & 0 & 0 & 0 & 0 & 0 & 0 & 0 & 1 & -1 \end{array}\right)$$

The total charge matrix Q_t does not exhibit repeated columns. Accordingly, the global symmetry is $U(1)_{f_1} \times U(1)_{f_2} \times U(1)_R$. The mesonic charges on the extremal perfect matchings are found following the discussion in §2.3. They are presented in Table 45.

	$U(1)_{f_1}$	$U(1)_{f_2}$	$U(1)_R$	fugacity
p_1	1/2	0	$R_1 = \frac{1}{16}\left(-21+5\sqrt{33}\right)$	t_1
p_2	-1/2	0	$R_2 = \frac{3}{16}\left(19-3\sqrt{33}\right)$	t_2
p_3	0	-1/2	$R_2 = \frac{3}{16}\left(19-3\sqrt{33}\right)$	t_3
p_4	0	1/2	$R_1 = \frac{1}{16}\left(-21+5\sqrt{33}\right)$	t_4
p_5	0	0	$R_3 = \frac{1}{2}\left(-5+\sqrt{33}\right)$	t_5

Table 45. The GLSM fields corresponding to extremal points of the toric diagram with their mesonic charges (Model 12a). The R-charges are obtained using a-maximization [69].

The product of all internal perfect matchings is

$$s = \prod_{m=1}^{5} s_m \ . \tag{14.2}$$

The above product is counted by the fugacity y_s. The extremal perfect matchings p_α are counted by t_α.

The mesonic Hilbert series of Model 12a is calculated using the Molien integral formula in (2.9). It is

$$g_1(t_\alpha, y_s; \mathcal{M}^{mes}_{12a}) = \frac{P(t_\alpha)}{(1-y_s\ t_1^2t_3t_4)(1-y_s\ t_1t_2t_4^2)(1-y_s\ t_1^2t_3^2t_5)(1-y_s\ t_2^2t_4^2t_5)(1-y_s\ t_2^2t_3^2t_5^3)} \ , \tag{14.3}$$

where the numerator is the polynomial

$$\begin{aligned} P(t_\alpha) = 1 &+ y_s\ t_1t_2t_3t_4t_5 - y_s^2\ t_1^3t_2t_3^2t_4^2t_5 - y_s^2\ t_1^2t_2^2t_3t_4^3t_5 + y_s\ t_1t_2t_3^2t_5^2 + y_s\ t_2^2t_3t_4t_5^2 \\ &- y_s^2\ t_1^3t_2t_3^3t_4t_5^2 - 2\ y_s^2\ t_1^2t_2^2t_3^2t_4^2t_5^2 - y_s^2\ t_1t_2^3t_3t_4^3t_5^2 + y_s^3\ t_1^4t_2^2t_3^3t_4^3t_5^2 + y_s^3\ t_1^3t_2^3t_3^2t_4^4t_5^2 \\ &- y_s^2\ t_1^2t_2^2t_3^3t_4t_5^3 - y_s^2\ t_1t_2^3t_3^2t_4^2t_5^3 + y_s^3\ t_1^3t_2^3t_3^3t_4^3t_5^3 + y_s^4\ t_1^4t_2^4t_3^4t_4^4t_5^4 \ . \end{aligned} \tag{14.4}$$

The mesonic moduli space of Model 12a is not a complete intersection. The plethystic logarithm of the mesonic Hilbert series is

$$\begin{aligned} PL[g_1(t_\alpha, y_s; \mathcal{M}^{mes}_{12a})] = {} & y_s\ t_1^2t_3t_4 + y_s\ t_1t_2t_4^2 + y_s\ t_1t_2t_3t_4t_5 + y_s\ t_1^2t_3^2t_5 + y_s\ t_2^2t_4^2t_5 \\ & + y_s\ t_2^2t_3t_4t_5^2 + y_s\ t_1t_2t_3^2t_5^2 + y_s\ t_2^2t_3^2t_5^3 - y_s^2\ t_1^3t_2t_3^2t_4^2t_5 - y_s^2\ t_1^2t_2^2t_3t_4^3t_5 - 3\ y_s^2\ t_1^2t_2^2t_3^2t_4^2t_5^2 \\ & - y_s^2\ t_1^3t_2t_3^3t_4t_5^2 - y_s^2\ t_1t_2^3t_3^3t_4^2t_5^2 + \dots \ . \end{aligned} \tag{14.5}$$

Consider the following fugacity map

$$f_1 = t_3t_4 \ , \ f_2 = \frac{t_2t_4^2}{t_1} \ , \ \tilde{t}_1 = y_s^{1/4}\ t_1^{1/2} \ , \ \tilde{t}_2 = y_s^{1/4}\ t_1^{1/2} \ , \ \tilde{t}_3 = \frac{t_2t_3t_4t_5}{t_1} \ , \tag{14.6}$$

where f_1 and f_2 are flavour charge fugacities, and $\tilde{t}_i$ is the fugacity for R-charge R_i in Table 45. Under the fugacity map above, the above plethystic logarithm becomes

$$\begin{aligned} PL[g_1(\tilde{t}_\alpha, f_1, f_2; \mathcal{M}^{mes}_{12a})] = {} & (f_1+f_2)\,\tilde{t}_1^3\tilde{t}_2 + \left(1 + \frac{f_1}{f_2} + \frac{f_2}{f_1}\right)\tilde{t}_1^2\tilde{t}_2^2\tilde{t}_3 \\ & + \left(\frac{1}{f_1} + \frac{1}{f_2}\right)\tilde{t}_1\tilde{t}_2^3\tilde{t}_3^2 + \frac{1}{f_1f_2}\tilde{t}_2^4\tilde{t}_3^3 - (f_1+f_2)\,\tilde{t}_1^5\tilde{t}_2^3\tilde{t}_3 - \left(3 - \frac{f_1}{f_2} - \frac{f_2}{f_1}\right)\tilde{t}_1^4\tilde{t}_2^4\tilde{t}_3^2 + \dots \ . \end{aligned} \tag{14.7}$$

The above plethystic logarithm with its refinement exhibits all the moduli space generators with their mesonic charges. They are summarized in Table 46. The generators can be presented on a charge lattice. The convex polygon formed by the generators in Table 46 is the dual reflexive polygon of the toric diagram of Model 12a.

Generator	$U(1)_{f_1}$	$U(1)_{f_2}$
$p_1^2 p_3 p_4\ s$	1	0
$p_1 p_2 p_4^2\ s$	0	1
$p_1^2 p_3^2 p_5\ s$	1	-1
$p_1 p_2 p_3 p_4 p_5\ s$	0	0
$p_2^2 p_4^2 p_5\ s$	-1	1
$p_1 p_2 p_3^2 p_5^2\ s$	0	-1
$p_2^2 p_3 p_4 p_5^2\ s$	-1	0
$p_2^2 p_3^2 p_5^3\ s$	-1	-1

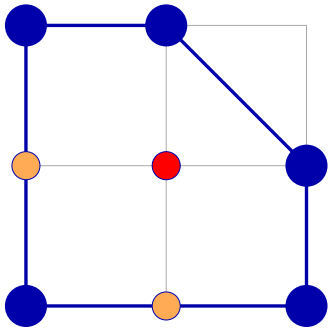


Table 46. The generators and lattice of generators of the mesonic moduli space of Model 12a in terms of GLSM fields with the corresponding flavor charges.

Generator	$U(1)_{f_1}$	$U(1)_{f_2}$
$X_{25}^1 X_{53} X_{32} = X_{14} X_{42}^2 X_{25}^1 X_{51}$	1	0
$X_{14} X_{42}^2 X_{21} = X_{25}^1 X_{53} X_{34} X_{42}^2$	0	1
$X_{13} X_{32} X_{25}^1 X_{51} = X_{14} X_{42}^1 X_{25}^1 X_{51}$	1	-1
$X_{13} X_{34} X_{42}^2 X_{25}^1 X_{51} = X_{14} X_{42}^2 X_{25}^2 X_{51} = X_{25}^1 X_{53} X_{34} X_{42}^1 = X_{13} X_{32} X_{21} = X_{14} X_{42}^1 X_{21} = X_{25}^2 X_{53} X_{32}$	0	0
$X_{13} X_{34} X_{42}^2 X_{21} = X_{25}^2 X_{53} X_{34} X_{42}^2$	-1	1
$X_{13} X_{34} X_{42}^1 X_{25}^1 X_{51} = X_{13} X_{32} X_{25}^2 X_{51} = X_{14} X_{42}^1 X_{25}^2 X_{51}$	0	1
$X_{13} X_{34} X_{42}^2 X_{25}^2 X_{51} = X_{13} X_{34} X_{42}^1 X_{21} = X_{25}^2 X_{53} X_{34} X_{42}^1$	-1	0
$X_{13} X_{34} X_{42}^1 X_{25}^2 X_{51}$	-1	-1

Table 47. The generators in terms of bifundamental fields (Model 12a).

The mesonic Hilbert series and the plethystic logarithm can be re-expressed in terms of just 3 fugacities

$$T_1 = \frac{\tilde{t}_3}{f_1 f_2\ \tilde{t}_1^4} = \frac{t_5}{y_s\ t_1^2 t_4^2}\ ,\ T_2 = f_1\ \tilde{t}_1^3 \tilde{t}_2 = y_s\ t_1^2 t_3 t_4\ ,\ T_3 = f_2\ \tilde{t}_1^3 \tilde{t}_2 = y_s\ t_1 t_2 t_4^2\ , \quad (14.8)$$

such that

$$g_1(T_1,T_2,T_3;\mathcal{M}^{mes}_{12a}) = \\ (1+T_1T_2T_3-T_1T_2^2T_3-T_1T_2T_3^2+T_1^2T_2^2T_3+T_1^2T_2T_3^2-T_1^2T_2^3T_3-2T_1^2T_2^2T_3^2 \\ -T_1^2T_2T_3^3+T_1^2T_2^3T_3^2+T_1^2T_2^2T_3^3-T_1^3T_2^3T_3^2-T_1^3T_2^2T_3^3+T_1^3T_2^3T_3^3+T_1^4T_2^4T_3^4) \\ \times\frac{1}{(1-T_2)(1-T_3)(1-T_1T_2^2)(1-T_1T_3^2)(1-T_1^3T_2^2T_3^2)} \tag{14.9}$$

and

$$PL[g_1(T_1,T_2,T_3;\mathcal{M}^{mes}_{12a})] = T_2+T_3+T_1T_2T_3+T_1T_2^2+T_1T_3^2+T_1^2T_2T_3^2+T_1^2T_2^2T_3 \\ +T_1^3T_2^2T_3^2-T_1T_2^2T_3-T_1T_2T_3^2-T_1^2T_2^3T_3-3T_1^2T_2^2T_3^2-T_1^2T_2^3T_3-T_1^2T_2T_3^3 \\ +\dots \quad . \tag{14.10}$$

The above Hilbert series and plethystic logarithm illustrate the conical structure of the toric Calabi-Yau 3-fold.

14.2 Model 12 Phase b

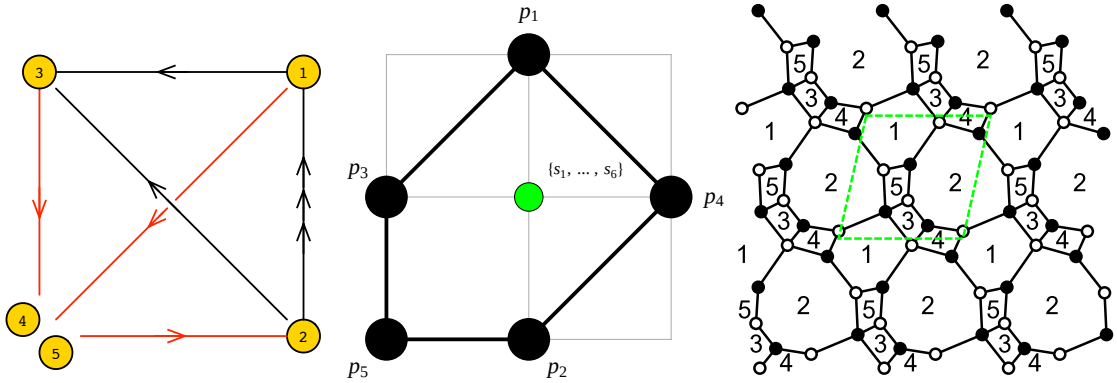


Figure 31. The quiver, toric diagram, and brane tiling of Model 12b. The red arrows in the quiver indicate all possible connections between blocks of nodes.

The superpotential is

$$W = +X_{15}X_{52}^2X_{21}^2+X_{21}^1X_{14}X_{42}^1+X_{35}X_{52}^1X_{23}+X_{13}X_{34}X_{42}^2X_{21}^3 \\ -X_{14}X_{42}^2X_{21}^2-X_{15}X_{52}^1X_{21}^3-X_{34}X_{42}^1X_{23}-X_{21}^1X_{13}X_{35}X_{52}^2 \quad . \tag{14.11}$$

The perfect matching matrix is

$$P = \left(\begin{array}{c|cccccc|cccccc} & p_1 & p_2 & p_3 & p_4 & p_5 & s_1 & s_2 & s_3 & s_4 & s_5 & s_6 \\ \hline X^1_{21} & 1 & 0 & 1 & 0 & 0 & 1 & 0 & 0 & 0 & 0 & 0 \\ X^2_{42} & 1 & 0 & 0 & 0 & 0 & 0 & 1 & 1 & 0 & 0 & 0 \\ X^2_{21} & 0 & 1 & 1 & 0 & 1 & 1 & 0 & 0 & 0 & 0 & 0 \\ X^3_{21} & 0 & 1 & 0 & 1 & 0 & 1 & 0 & 0 & 0 & 0 & 0 \\ X_{23} & 1 & 0 & 0 & 1 & 0 & 1 & 0 & 0 & 0 & 0 & 1 \\ X^1_{42} & 0 & 1 & 0 & 0 & 1 & 0 & 1 & 1 & 0 & 0 & 0 \\ X^1_{52} & 0 & 0 & 1 & 0 & 1 & 0 & 1 & 0 & 1 & 0 & 0 \\ X^2_{52} & 0 & 0 & 0 & 1 & 0 & 0 & 1 & 0 & 1 & 0 & 0 \\ X_{15} & 1 & 0 & 0 & 0 & 0 & 0 & 0 & 1 & 0 & 1 & 1 \\ X_{35} & 0 & 1 & 0 & 0 & 0 & 0 & 0 & 1 & 0 & 1 & 0 \\ X_{34} & 0 & 0 & 1 & 0 & 0 & 0 & 0 & 0 & 1 & 1 & 0 \\ X_{14} & 0 & 0 & 0 & 1 & 0 & 0 & 0 & 0 & 1 & 1 & 1 \\ X_{13} & 0 & 0 & 0 & 0 & 1 & 0 & 0 & 0 & 0 & 0 & 1 \end{array}\right)$$

The F-term charge matrix $Q_F = \ker(P)$ is

$$Q_F = \left(\begin{array}{ccccc|cccccc} p_1 & p_2 & p_3 & p_4 & p_5 & s_1 & s_2 & s_3 & s_4 & s_5 & s_6 \\ \hline 1 & 1 & 0 & 0 & 0 & -1 & 0 & -1 & 0 & 0 & 0 \\ 0 & 0 & 1 & 1 & 0 & -1 & 0 & 0 & -1 & 0 & 0 \\ 0 & 1 & 1 & 0 & -1 & -1 & 0 & 0 & 0 & -1 & 1 \\ 0 & 0 & 0 & 0 & 0 & 0 & 1 & -1 & -1 & 1 & 0 \end{array}\right)$$

The D-term charge matrix is

$$Q_D = \left(\begin{array}{ccccc|cccccc} p_1 & p_2 & p_3 & p_4 & p_5 & s_1 & s_2 & s_3 & s_4 & s_5 & s_6 \\ \hline 0 & 0 & 0 & 0 & 0 & 1 & -1 & 0 & 0 & 0 & 0 \\ 0 & 0 & 0 & 0 & 0 & 0 & 0 & 1 & -1 & 0 & 0 \\ 0 & 0 & 0 & 0 & 0 & 0 & 0 & 0 & 1 & -1 & 0 \\ 0 & 0 & 0 & 0 & 0 & 0 & 0 & 0 & 0 & 1 & -1 \end{array}\right)$$

The total charge matrix Q_t does not have repeated columns. Accordingly, the global symmetry is $U(1)_{f_1} \times U(1)_{f_2} \times U(1)_R$. The charge assignment on the extremal perfect matchings with non-zero R-charge is the the same as for Model 12a in Table 45.

The product of all internal perfect matchings is expressed as

$$s = \prod_{m=1}^{6} s_m \ . \tag{14.12}$$

The product is counted by the fugacity y_s. The remaining extremal perfect matchings p_α are counted by the fugacity t_α.

The mesonic Hilbert series and the plethystic logarithm of the Hilbert series is the same as for Model 12a. They are shown respectively in (14.3), (14.5) and (14.7).

Accordingly, the mesonic moduli spaces of Model 12a and 12b are toric duals.

The moduli space generators in terms of perfect matching variables of Model 12b are shown in Table 46 with their corresponding mesonic charges. The generators in terms of quiver fields are shown in Table 48.

Generator	$U(1)_{f_1}$	$U(1)_{f_2}$
$X_{14}X_{42}^2X_{21}^1 = X_{15}X_{52}^2X_{21}^1 = X_{23}X_{34}X_{42}^2$	1	0
$X_{14}X_{42}^2X_{21}^3 = X_{15}X_{52}^2X_{21}^3 = X_{23}X_{35}X_{52}^2$	0	1
$X_{15}X_{52}^1X_{21}^1 = X_{13}X_{34}X_{42}^2X_{21}^1$	1	-1
$X_{13}X_{35}X_{52}^2X_{21}^1 = X_{13}X_{34}X_{42}^2X_{21}^3 = X_{14}X_{42}^1X_{21}^1 = X_{14}X_{42}^2X_{21}^2 = X_{15}X_{52}^2X_{21}^2 = X_{15}X_{52}^1X_{21}^3 = X_{23}X_{34}X_{42}^1 = X_{23}X_{35}X_{52}^1$	0	0
$X_{14}X_{42}^1X_{21}^3 = X_{13}X_{35}X_{52}^2X_{21}^3$	-1	1
$X_{15}X_{52}^1X_{21}^2 = X_{13}X_{34}X_{42}^1X_{21}^1 = X_{13}X_{35}X_{52}^1X_{21}^1 = X_{13}X_{34}X_{42}^2X_{21}^2$	0	-1
$X_{14}X_{42}^1X_{21}^2 = X_{13}X_{35}X_{52}^2X_{21}^2 = X_{13}X_{34}X_{42}^1X_{21}^3 = X_{13}X_{35}X_{52}^1X_{21}^3$	-1	0
$X_{13}X_{34}X_{42}^1X_{21}^2 = X_{13}X_{35}X_{52}^1X_{21}^2$	-1	-1

Table 48. The generators in terms of bifundamental fields (Model 12b).

15 Model 13: $\mathbb{C}^3/\mathbb{Z}_{4,(1,1,2)}$, $Y^{2,2}$

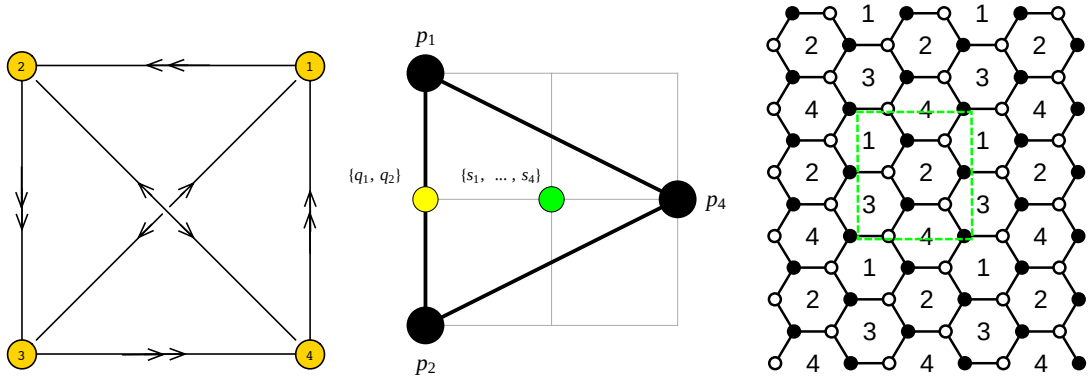


Figure 32. The quiver, toric diagram, and brane tiling Model 13.

The superpotential is

$$W = +X_{12}X_{24}X_{41}^1 + X_{31}X_{12}^2X_{23}^2 + X_{41}^2X_{13}X_{34}^1 + X_{34}^2X_{42}X_{23}^1 \\ -X_{12}X_{23}X_{31} - X_{13}X_{34}^2X_{41}^1 - X_{41}^2X_{12}^2X_{24} - X_{34}^1X_{42}X_{23}^2 \quad . \tag{15.1}$$

The perfect matching matrix is

$$P = \left(\begin{array}{c|ccc|cc|cccc} & p_1 & p_2 & p_3 & q_1 & q_2 & s_1 & s_2 & s_3 & s_4 \\ \hline X^1_{34} & 1 & 0 & 0 & 1 & 0 & 1 & 0 & 0 & 0 \\ X^2_{34} & 0 & 1 & 0 & 1 & 0 & 1 & 0 & 0 & 0 \\ X^2_{12} & 1 & 0 & 0 & 1 & 0 & 0 & 1 & 0 & 0 \\ X^1_{12} & 0 & 1 & 0 & 1 & 0 & 0 & 1 & 0 & 0 \\ X^1_{23} & 1 & 0 & 0 & 0 & 1 & 0 & 0 & 1 & 0 \\ X^2_{23} & 0 & 1 & 0 & 0 & 1 & 0 & 0 & 1 & 0 \\ X^1_{41} & 1 & 0 & 0 & 0 & 1 & 0 & 0 & 0 & 1 \\ X^2_{41} & 0 & 1 & 0 & 0 & 1 & 0 & 0 & 0 & 1 \\ X_{24} & 0 & 0 & 1 & 0 & 0 & 1 & 0 & 1 & 0 \\ X_{31} & 0 & 0 & 1 & 0 & 0 & 1 & 0 & 0 & 1 \\ X_{13} & 0 & 0 & 1 & 0 & 0 & 0 & 1 & 1 & 0 \\ X_{42} & 0 & 0 & 1 & 0 & 0 & 0 & 1 & 0 & 1 \end{array}\right)$$

The F-term charge matrix $Q_F = \ker(P)$ is

$$Q_F = \left(\begin{array}{ccc|cc|cccc} p_1 & p_2 & p_3 & q_1 & q_2 & s_1 & s_2 & s_3 & s_4 \\ \hline 1 & 1 & 0 & -1 & -1 & 0 & 0 & 0 & 0 \\ 0 & 0 & 1 & 1 & 0 & -1 & -1 & 0 & 0 \\ 0 & 0 & 1 & 0 & 1 & 0 & 0 & -1 & -1 \end{array}\right)$$

The D-term charge matrix is

$$Q_D = \left(\begin{array}{ccc|cc|cccc} p_1 & p_2 & p_3 & q_1 & q_2 & s_1 & s_2 & s_3 & s_4 \\ \hline 0 & 0 & 0 & 0 & 0 & 1 & -1 & 0 & 0 \\ 0 & 0 & 0 & 0 & 0 & 0 & 1 & -1 & 0 \\ 0 & 0 & 0 & 0 & 0 & 0 & 0 & 1 & -1 \end{array}\right)$$

The GLSM fields p_1 and p_2 are equally charged under the F-term and D-term constraints. This is shown by the corresponding columns in the total charge matrix Q_t which are identical. Accordingly, the global symmetry is enhanced from $U(1)^3$ to $SU(2)_x \times U(1)_f \times U(1)_R$ with $U(1)_R$ being the R-symmetry. The mesonic charges on the GLSM fields corresponding to extremal points in the toric diagram in Figure 32 are found following the discussion in §2.3. They are presented in Table 49.

	$U(1)_f$	$SU(2)_x$	$U(1)_R$	fugacity
p_1	-1/4	1/2	2/3	t_1
p_2	-1/4	-1/2	2/3	t_2
p_3	1/2	0	2/3	t_3

Table 49. The GLSM fields corresponding to extremal points of the toric diagram with their mesonic charges (Model 13).

Products of non-extremal perfect matchings are expressed as follows

$$q = q_1 q_2 \ , \ s = \prod_{m=1}^{4} s_m \ . \tag{15.2}$$

The fugacities counting the above products are respectively y_q and y_s. The fugacity which counts extremal perfect matchings is t_α.

The mesonic Hilbert series of Model 13 is computed using the Molien integral formula in (2.9). It is

$$g_1(t_\alpha, y_q, y_s; \mathcal{M}_{13}^{mes}) = \frac{1 + y_q^2 y_s \ t_1^3 t_2 + y_q^2 y_s \ t_1^2 t_2^2 + y_q^2 y_s \ t_1 t_2^3 + y_q y_s \ t_1^2 t_3 + y_q y_s \ t_1 t_2 t_3 + y_q y_s \ t_2^2 t_3 + y_q^3 y_s^2 \ t_1^3 t_2^3 t_3}{(1 - y_q^2 y_s \ t_1^4)(1 - y_q^2 y_s \ t_2^4)(1 - y_s \ t_3^2)} \ . \tag{15.3}$$

The mesonic moduli space of Model 13 is not a complete intersection. The plethystic logarithm of the mesonic Hilbert series is

$$\begin{aligned} PL[g_1(t_\alpha, y_q, y_s; \mathcal{M}_{13}^{mes})] = & \ y_s \ t_3^2 + y_q y_s \ t_1 t_2 t_3 + y_q y_s \ t_1^2 t_3 + y_q y_s \ t_2^2 t_3 + y_q^2 y_s \ t_1^4 \\ & + y_q^2 y_s \ t_1^3 t_2 + y_q^2 y_s \ t_1^2 t_2^2 + y_q^2 y_s \ t_1 t_2^3 + y_q^2 y_s \ t_2^4 - 2 \ y_q^2 y_s^2 \ t_1^2 t_2^2 t_3^2 + \dots \ . \end{aligned} \tag{15.4}$$

Consider the following fugacity map

$$f = y_q^{-2/3} y_s^{1/3} \ t_1^{-2/3} t_2^{-2/3} t_3^{4/3} \ , \ \tilde{x}^2 = x = \frac{t_1}{t_2} \ , \ t = y_q^{1/3} y_s^{1/3} \ t_1^{1/3} t_2^{1/3} t_3^{1/3} \ , \tag{15.5}$$

where the fugacities f, x and t are mesonic charge fugacities. x is the charge fugacity for the enhanced symmetry $SU(2)_x$. Using the redefinition of this fugacity to $\tilde{x} = \sqrt{x}$ and the fugacities f and t, one can rewrite the expansion of the Hilbert series in terms of characters of irreducible representations of $SU(2)$ as follows

$$g_1(t, \tilde{x}, f; \mathcal{M}_{13}^{mes}) = \sum_{m=0}^{\infty} \sum_{n=0}^{\infty} \ \left([2m]_{\tilde{x}} f^n t^{2n+3m} + [4(n+1) + 2m]_{\tilde{x}} f^{-(n+1)} t^{4(n+1)+3m} \right) \ . \tag{15.6}$$

The corresponding plethystic logarithm is

$$\begin{aligned} PL[g_1(t, \tilde{x}, f; \mathcal{M}_{13}^{mes})] = & \ f t^2 + [2]_{\tilde{x}} t^3 + [4]_{\tilde{x}} \frac{1}{f} t^4 - (1 + [4]_{\tilde{x}}) t^6 - ([2]_{\tilde{x}} + [4]_{\tilde{x}}) \frac{1}{f} t^7 \\ & - (1 + [4]_{\tilde{x}}) \frac{1}{f^2} t^8 + ([2]_{\tilde{x}} + [4]_{\tilde{x}}) t^9 + (1 + 2[2]_{\tilde{x}} + 2[4]_{\tilde{x}} + [6]_{\tilde{x}}) \frac{1}{f} t^{10} + \dots \ . \end{aligned} \tag{15.7}$$

In terms of the mesonic charge fugacities f, x and t, the above plethystic logarithm exhibits the moduli space generators and their mesonic charges. They are summarized in Table 50. The flavour charges of generators are integers using f and x. They can be presented on a charge lattice. The convex polygon formed by the generators is the dual reflexive polygon of the toric diagram.

As indicated in (15.7), the generators fall into irreducible representation of $SU(2)$ with the characters

$$ft^2 + [2]_{\tilde{x}}t^3 + [4]_{\tilde{x}}\frac{1}{f}t^4 = ft^2 + \left(\tilde{x}^2 + 1 + \frac{1}{\tilde{x}^2}\right)t^3 + \left(\tilde{x}^4 + \tilde{x}^2 + 1 + \frac{1}{\tilde{x}^2} + \frac{1}{\tilde{x}^4}\right)\frac{1}{f}t^4 \quad . \tag{15.8}$$

The above three terms correspond to the three columns of points in the lattice of generators in Table 50. The generators in terms of quiver fields are shown in Table 51.

Generator	$U(1)_f$	$SU(2)_x$
$p_3^2\ s$	1	0
$p_1^2 p_3\ q\ s$	0	1
$p_1 p_2 p_3\ q\ s$	0	0
$p_2^2 p_3\ q\ s$	0	-1
$p_1^4\ q^2\ s$	-1	2
$p_1^3 p_2\ q^2\ s$	-1	1
$p_1^2 p_2^2\ q^2\ s$	-1	0
$p_1 p_2^3\ q^2\ s$	-1	-1
$p_2^4\ q^2\ s$	-1	-2

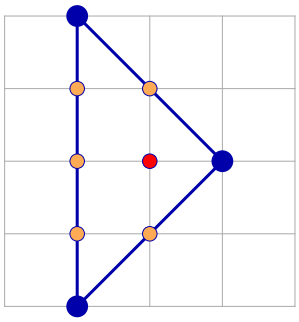


Table 50. The generators and lattice of generators of the mesonic moduli space of Model 13 in terms of GLSM fields with the corresponding flavor charges.

Generator	$U(1)_f$	$SU(2)_x$
$X_{13}X_{31} = X_{24}X_{42}$	1	0
$X_{12}^2X_{23}^1X_{31} = X_{12}^2X_{24}X_{41}^1 = X_{13}X_{34}^1X_{41}^1 = X_{23}^1X_{34}^1X_{42}$	0	1
$X_{12}^1X_{23}^1X_{31} = X_{12}^1X_{24}X_{41}^1 = X_{12}^2X_{23}^2X_{31} = X_{12}^2X_{24}X_{41}^2 = X_{13}X_{34}^1X_{41}^2 = X_{13}X_{34}^2X_{41}^1 = X_{23}^1X_{34}^2X_{42} = X_{23}^2X_{34}^1X_{42}$	0	0
$X_{12}^1X_{23}^2X_{31} = X_{12}^1X_{24}X_{41}^2 = X_{13}X_{34}^2X_{41}^2 = X_{23}^2X_{34}^2X_{42}$	0	-1
$X_{12}^2X_{23}^1X_{34}^1X_{41}^1$	-1	2
$X_{12}^1X_{23}^1X_{34}^1X_{41}^1 = X_{12}^2X_{23}^1X_{34}^1X_{41}^2 = X_{12}^2X_{23}^1X_{34}^2X_{41}^1 = X_{12}^2X_{23}^2X_{34}^1X_{41}^1$	1	-1
$X_{12}^1X_{23}^1X_{34}^1X_{41}^2 = X_{12}^1X_{23}^1X_{34}^2X_{41}^1 = X_{12}^1X_{23}^2X_{34}^1X_{41}^1 = X_{12}^2X_{23}^1X_{34}^1X_{41}^2 = X_{12}^2X_{23}^1X_{34}^2X_{41}^1 = X_{12}^2X_{23}^2X_{34}^1X_{41}^1$	-1	0
$X_{12}^1X_{23}^1X_{34}^2X_{41}^2 = X_{12}^1X_{23}^2X_{34}^1X_{41}^2 = X_{12}^1X_{23}^2X_{34}^2X_{41}^1 = X_{12}^2X_{23}^1X_{34}^2X_{41}^2 = X_{12}^2X_{23}^2X_{34}^1X_{41}^2 = X_{12}^2X_{23}^2X_{34}^2X_{41}^1$	-1	-1
$X_{12}^1X_{23}^2X_{34}^2X_{41}^2$	-1	-2

Table 51. The generators in terms of bifundamental fields (Model 13).

With the fugacity map

$$T_1 = f^{-1/4}x^{1/2}\ t = y_q^{1/2}y_s^{1/4}t_1\ ,\ T_2 = f^{-1/4}x^{-1/2}\ t = y_q^{1/2}y_s^{1/4}t_2\ ,\ T_3 = f^{1/2}\ t = y_s^{1/2}t_3\ , \tag{15.9}$$

the mesonic Hilbert series takes the form

$$g_1(T_1,T_2,T_3;\mathcal{M}_{13}^{mes}) = \frac{1+T_1^3T_2+T_1^2T_2^2+T_1T_2^3+T_1^2T_3+T_1T_2T_3+T_2^2T_3+T_1^3T_2^3T_3}{(1-T_1^4)(1-T_2^4)(1-T_3^2)}\ , \tag{15.10}$$

with the plethystic logarithm becoming

$$\begin{aligned} PL[g_1(T_1,T_2,T_3;\mathcal{M}_{13}^{mes})] &= T_3^2+T_1T_2T_3+T_1^2T_3+T_2^2T_3+T_1^4+T_1^3T_2+T_1^2T_2^2 \\ &+T_1T_2^3+T_2^4-2T_1^2T_2^2T_3^2+\dots\ . \end{aligned} \tag{15.11}$$

The above Hilbert series and plethystic logarithm is written in terms of just three fugacities with positive powers. This illustrates the conical structure of the toric Calabi-Yau 3-fold.

16 Model 14: dP_1

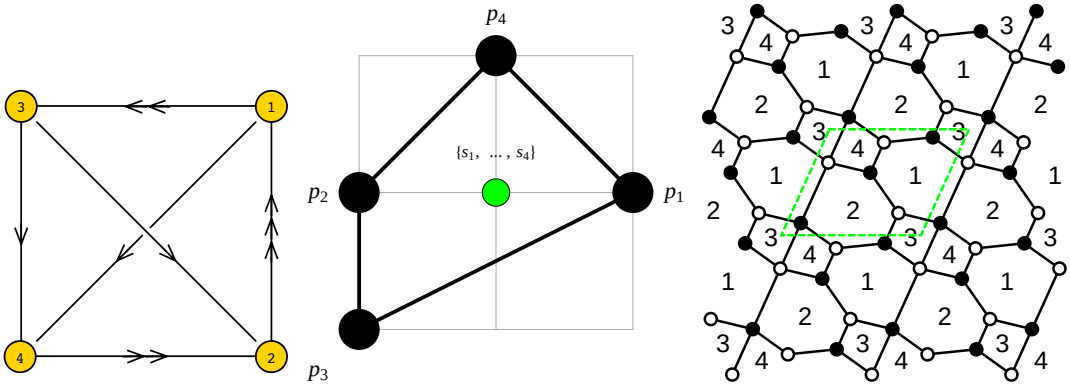


Figure 33. The quiver, toric diagram, and brane tiling of Model 14.

The superpotential is

$$\begin{aligned} W = &+X_{21}^1X_{14}X_{42}^1+X_{21}^3X_{13}^2X_{32}+X_{42}^2X_{21}^2X_{13}^1X_{34} \\ &-X_{13}^1X_{32}X_{21}^1-X_{14}X_{42}^2X_{21}^3-X_{21}^2X_{13}^2X_{34}X_{42}^1 \end{aligned} \tag{16.1}$$

The perfect matching matrix is

$$P = \left(\begin{array}{c|cccc|cccc} & p_1 & p_2 & p_3 & p_4 & s_1 & s_2 & s_3 & s_4 \\ \hline X_{21}^2 & 1 & 0 & 0 & 0 & 1 & 0 & 0 & 0 \\ X_{32} & 1 & 0 & 0 & 0 & 0 & 1 & 0 & 1 \\ X_{21}^3 & 0 & 1 & 1 & 0 & 1 & 0 & 0 & 0 \\ X_{21}^1 & 0 & 1 & 0 & 1 & 1 & 0 & 0 & 0 \\ X_{42}^1 & 0 & 0 & 1 & 0 & 0 & 1 & 0 & 0 \\ X_{42}^2 & 0 & 0 & 0 & 1 & 0 & 1 & 0 & 0 \\ X_{13}^1 & 0 & 0 & 1 & 0 & 0 & 0 & 1 & 0 \\ X_{13}^2 & 0 & 0 & 0 & 1 & 0 & 0 & 1 & 0 \\ X_{14} & 1 & 0 & 0 & 0 & 0 & 0 & 1 & 1 \\ X_{34} & 0 & 1 & 0 & 0 & 0 & 0 & 0 & 1 \end{array}\right)$$

The F-term charge matrix $Q_F = \ker(P)$ is

$$Q_F = \left(\begin{array}{cccc|cccc} p_1 & p_2 & p_3 & p_4 & s_1 & s_2 & s_3 & s_4 \\ \hline 1 & 1 & 0 & 0 & -1 & 0 & 0 & -1 \\ 1 & 0 & 1 & 1 & -1 & -1 & -1 & 0 \end{array}\right)$$

The D-term charge matrix is

$$Q_D = \left(\begin{array}{cccc|cccc} p_1 & p_2 & p_3 & p_4 & s_1 & s_2 & s_3 & s_4 \\ \hline 0 & 0 & 0 & 0 & 1 & -1 & 0 & 0 \\ 0 & 0 & 0 & 0 & 0 & 1 & -1 & 0 \\ 0 & 0 & 0 & 0 & 0 & 0 & 1 & -1 \end{array}\right)$$

The total charge matrix Q_t does not have repeated columns. Accordingly, the global symmetry is $U(1)_{f_1} \times U(1)_{f_2} \times U(1)_R$. The flavour and R-charges on the GLSM fields corresponding to extremal points in the toric diagram in Figure 33 are found following the discussion in §2.3. They are presented in Table 52.

	$U(1)_{f_1}$	$U(1)_{f_2}$	$U(1)_R$	fugacity
p_1	1	0	$R_1 = \sqrt{13} - 3$	t_1
p_2	1	1	$R_2 = (5\sqrt{13} - 17)/3$	t_2
p_3	-1	-1	$R_3 = 4(4 - \sqrt{13})/3$	t_3
p_4	-1	0	$R_3 = 4(4 - \sqrt{13})/3$	t_4

Table 52. The GLSM fields corresponding to extremal points of the toric diagram with their mesonic charges (Model 14). The R-charges are obtained using a-maximization [69].

The product of all internal perfect matchings is

$$s = \prod_{m=1}^{4} s_m \ . \tag{16.2}$$

The fugacity counting the above product is y_s. The fugacity which counts the remaining extremal perfect matchings p_α is t_α.

The mesonic Hilbert series of Model 14 is found using the Molien integral formula in (2.9). It is

$$g_1(t_\alpha, y_s; \mathcal{M}_{14}^{mes}) = \frac{P(t_\alpha)}{(1-y_s\ t_1^2t_3)(1-y_s\ t_2^2t_3^3)(1-y_s\ t_1^2t_4)(1-y_s\ t_2^2t_4^3)} \quad , \tag{16.3}$$

where the numerator is given by the polynomial

$$\begin{aligned} P(t_\alpha) = 1 &+ y_s\ t_1t_2t_3^2 + y_s\ t_1t_2t_3t_4 - y_s^2\ t_1^3t_2t_3^2t_4 + y_s\ t_2^2t_3^2t_4 - y_s^2\ t_1^2t_2^2t_3^3t_4 \\ &+ y_s\ t_1t_2t_4^2 - y_s^2\ t_1^3t_2t_3t_4^2 + y_s\ t_2^2t_3t_4^2 - y_s^2\ t_1^2t_2^2t_3^2t_4^2 - y_s^2\ t_1^2t_2^2t_3t_4^3 - y_s^3\ t_1^3t_2^3t_3^3t_4^3 \quad . \end{aligned} \tag{16.4}$$

The plethystic logarithm of the mesonic Hilbert series is

$$\begin{aligned} PL[g_1(t_\alpha, y_s; \mathcal{M}_{14}^{mes})] &= y_s\ t_1^2t_4 + y_s\ t_1^2t_3 + y_s\ t_1t_2t_3t_4 + y_s\ t_1t_2t_4^2 + y_s\ t_1t_2t_3^2 \\ &+ y_s\ t_2^2t_3^2t_4 + y_s\ t_2^2t_3^3 + y_s\ t_2^2t_3t_4^2 + y_s\ t_2^2t_4^3 - y_s^2\ t_1^3t_2t_3t_4^2 - y_s^2\ t_1^3t_2t_3^2t_4 + \dots \quad . \end{aligned} \tag{16.5}$$

Consider the following fugacity map

$$f_1 = t_3^{-1/2}t_4^{1/2} \ , \ f_2 = \frac{t_4}{t_3} \ , \ \tilde{t}_1 = y_s^{1/2}\ t_1 \ , \ \tilde{t}_2 = y_s^{1/2}\ t_2 \ , \ \tilde{t}_3 = t_3^{1/2}t_4^{1/2} \ , \tag{16.6}$$

where the fugacities f_1 and f_2 count flavour charges, and the fugacity $\tilde{t}_i$ count the R-charge R_i in Table 52. Accordingly, the plethystic logarithm becomes

$$\begin{aligned} PL[g_1(\tilde{t}_\alpha, f_1, f_2; \mathcal{M}_{14}^{mes})] &= \left(f_1 + \frac{f_1}{f_2}\right)\tilde{t}_1^2\tilde{t}_3 + \left(1 + f_2 + \frac{1}{f_2}\right)\tilde{t}_1\tilde{t}_2\tilde{t}_3^2 \\ &+ \left(\frac{1}{f_1} + \frac{1}{f_1f_2} + \frac{f_2}{f_1} + \frac{f_2^2}{f_1}\right)\tilde{t}_2^2\tilde{t}_3^3 - \left(f_1 + \frac{f_1}{f_2}\right)\tilde{t}_1^3\tilde{t}_2\tilde{t}_3^3 + \dots \quad . \end{aligned} \tag{16.7}$$

The first positive terms in the above plethystic logarithm correspond to moduli space generators with the corresponding flavour charge counted by the fugacities f_1 and f_2. The generators and the corresponding mesonic charges are shown in Table 53. The generators can be presented on a charge lattice. The convex polygon formed by the generators in Table 53 is the dual reflexive polygon of the toric diagram of Model 14.

Generator	$U(1)_{f_1}$	$U(1)_{f_2}$
$p_1^2 p_3$ s	1	-1
$p_1 p_2 p_3^2$ s	0	-1
$p_2^2 p_3^3$ s	-1	-1
$p_1^2 p_4$ s	1	0
$p_1 p_2 p_3 p_4$ s	0	0
$p_2^2 p_3^2 p_4$ s	-1	0
$p_1 p_2 p_4^2$ s	0	1
$p_2^2 p_3 p_4^2$ s	-1	1
$p_2^2 p_4^3$ s	-1	2

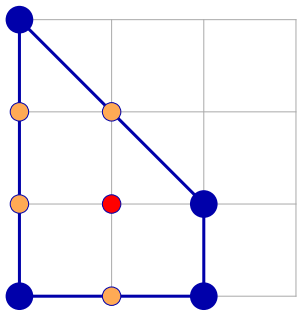


Table 53. The generators and lattice of generators of the mesonic moduli space of Model 14 in terms of GLSM fields with the corresponding flavor charges. The lattice of generators is the toric diagram of Model 3.

Generator	$U(1)_{f_1}$	$U(1)_{f_2}$
$X_{13}^1 X_{32} X_{21}^2 = X_{14} X_{42}^1 X_{21}^2$	1	-1
$X_{13}^1 X_{34} X_{42}^1 X_{21}^2 = X_{13}^1 X_{32} X_{21}^3 = X_{14} X_{42}^1 X_{21}^3$	0	-1
$X_{13}^1 X_{34} X_{42}^1 X_{21}^3$	-1	-1
$X_{13}^2 X_{32} X_{21}^2 = X_{14} X_{42}^2 X_{21}^2$	1	0
$X_{13}^1 X_{34} X_{42}^2 X_{21}^2 = X_{13}^2 X_{34} X_{42}^1 X_{21}^2 = X_{13}^1 X_{32} X_{21}^1 = X_{13}^2 X_{32} X_{21}^3 = X_{14} X_{42}^1 X_{21}^1 = X_{14} X_{42}^2 X_{21}^3$	0	0
$X_{13}^1 X_{34} X_{42}^1 X_{21}^1 = X_{13}^1 X_{34} X_{42}^2 X_{21}^3 = X_{13}^2 X_{34} X_{42}^1 X_{21}^3$	-1	0
$X_{13}^2 X_{34} X_{42}^2 X_{21}^2 = X_{13}^2 X_{32} X_{21}^1 = X_{14} X_{42}^2 X_{21}^1$	0	1
$X_{13}^1 X_{34} X_{42}^2 X_{21}^1 = X_{13}^2 X_{34} X_{42}^1 X_{21}^1 = X_{13}^2 X_{34} X_{42}^2 X_{21}^3$	-1	1
$X_{13}^2 X_{34} X_{42}^2 X_{21}^1$	-1	2

Table 54. The generators in terms of bifundamental fields (Model 14).

The mesonic Hilbert series and the plethystic logarithm can be re-expressed in terms of just 3 fugacities

$$T_1 = \frac{f_2\ \tilde{t}_2}{f_1^2\ \tilde{t}_1^3} = \frac{t_2}{y_s\ t_1^3}\ ,\ T_2 = \frac{f_1}{f_2}\ \tilde{t}_1^2 \tilde{t}_3 = y_s\ t_1^2 t_3\ ,\ T_3 = f_1\ \tilde{t}_1^2 \tilde{t}_3 = y_s\ t_1^2 t_4\ , \tag{16.8}$$

such that

$$\begin{aligned} &g_1(T_1, T_2, T_3; \mathcal{M}_{14}^{mes}) = \\ &\quad (1 + T_1 T_2^2 + T_1 T_2 T_3 - T_1 T_2^2 T_3 + T_1^2 T_2^2 T_3 - T_1^2 T_2^3 T_3 + T_1 T_3^2 - T_1 T_2 T_3^2 + T_1^2 T_2 T_3^2 \\ &\quad - T_1^2 T_2^2 T_3^2 - T_1^2 T_2 T_3^3 - T_1^3 T_2^3 T_3^3) \times \frac{1}{(1 - T_2)(1 - T_1^2 T_2^3)(1 - T_3)(1 - T_1^2 T_3^3)} \end{aligned} \tag{16.9}$$

and

$$PL[g_1(T_1,T_2,T_3;\mathcal{M}_{14}^{mes})] = T_3 + T_2 + T_1T_2T_3 + T_1T_3^2 + T_1T_2^2 + T_1^2T_2^2T_3 + T_1^2T_2^3 + T_1^2T_2T_3^2 + T_1^2T_3^3 - T_1T_2T_3^2 - T_1T_2^2T_3 + \dots \quad . \tag{16.10}$$

The above Hilbert series and plethystic logarithm illustrate the conical structure of the toric Calabi-Yau 3-fold.

17 Model 15: $\mathcal{C}/\mathbb{Z}_2\ (1,1,1,1),\ \mathbb{F}_0$

17.1 Model 15 Phase a

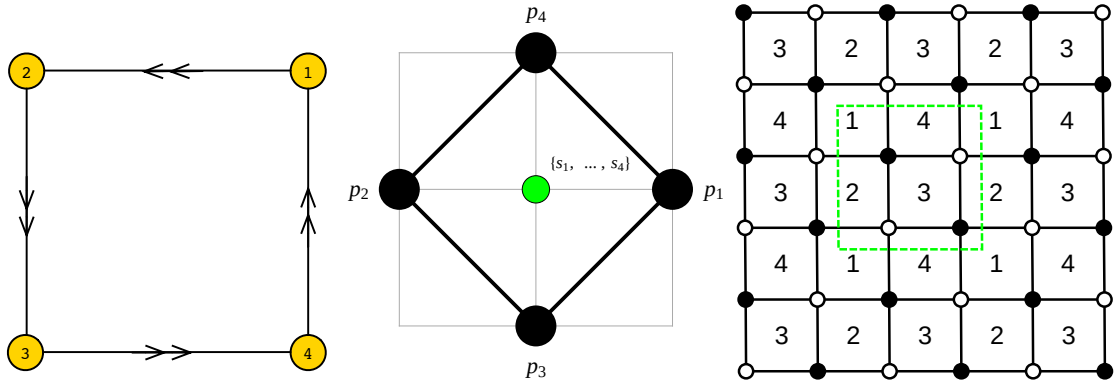


Figure 34. The quiver, toric diagram, and brane tiling of Model 15a.

The superpotential is

$$W = +X_{12}^1X_{23}^1X_{34}^2X_{41}^2 + X_{12}^2X_{23}^2X_{34}^1X_{41}^1 - X_{12}^1X_{23}^2X_{34}^2X_{41}^1 - X_{12}^2X_{23}^1X_{34}^1X_{41}^2 \quad . \tag{17.1}$$

The perfect matching matrix is

$$P = \left(\begin{array}{c|cccc|cccc} & p_1 & p_2 & p_3 & p_4 & s_1 & s_2 & s_3 & s_4 \\ \hline X_{12}^1 & 1 & 0 & 0 & 0 & 1 & 0 & 0 & 0 \\ X_{12}^2 & 0 & 1 & 0 & 0 & 1 & 0 & 0 & 0 \\ X_{34}^1 & 1 & 0 & 0 & 0 & 0 & 1 & 0 & 0 \\ X_{34}^2 & 0 & 1 & 0 & 0 & 0 & 1 & 0 & 0 \\ X_{23}^1 & 0 & 0 & 1 & 0 & 0 & 0 & 1 & 0 \\ X_{23}^2 & 0 & 0 & 0 & 1 & 0 & 0 & 1 & 0 \\ X_{41}^1 & 0 & 0 & 1 & 0 & 0 & 0 & 0 & 1 \\ X_{41}^2 & 0 & 0 & 0 & 1 & 0 & 0 & 0 & 1 \end{array}\right)$$

The F-term charge matrix $Q_F = \ker(P)$ is

$$Q_F = \left(\begin{array}{cccc|cccc} p_1 & p_2 & p_3 & p_4 & s_1 & s_2 & s_3 & s_4 \\ \hline 1 & 1 & 0 & 0 & -1 & -1 & 0 & 0 \\ 0 & 0 & 1 & 1 & 0 & 0 & -1 & -1 \end{array}\right)$$

The D-term charge matrix is

$$Q_D = \left(\begin{array}{cccc|cccc} p_1 & p_2 & p_3 & p_4 & s_1 & s_2 & s_3 & s_4 \\ \hline 0 & 0 & 0 & 0 & 1 & -1 & 0 & 0 \\ 0 & 0 & 0 & 0 & 0 & 1 & -1 & 0 \\ 0 & 0 & 0 & 0 & 0 & 0 & 1 & -1 \end{array}\right)$$

The pairs of GLSM fields $\{p_1, p_2\}$ and $\{p_3, p_4\}$ have the same charge under the F-term and D-term constraints. This is shown by the identical columns in the total charge matrix Q_t. Accordingly, the global symmetry is enhanced from $U(1)^2 \times U(1)_R$ to $SU(1)_{x_1} \times SU(2)_{x_2} \times U(1)_R$. The mesonic charges on the GLSM fields corresponding to extremal points in the toric diagram in Figure 34 are found following the discussion in §2.3. They are presented in Table 55.

	$SU(2)_{x_1}$	$SU(2)_{x_2}$	$U(1)_R$	fugacity
p_1	1/2	0	1/2	t_1
p_2	-1/2	0	1/2	t_2
p_3	0	1/2	1/2	t_3
p_4	0	-1/2	1/2	t_4

Table 55. The GLSM fields corresponding to extremal points of the toric diagram with their mesonic charges (Model 15a).

The product of all internal perfect matchings labelled by

$$s = \prod_{m=1}^{4} s_m \ . \tag{17.2}$$

The above product is counted by the fugacity y_s. All remaining extremal perfect matchings p_α are counted by the fugacity t_α.

The mesonic Hilbert series of Model 15a is calculated using the Molien integral formula in (2.9). It is

$$g_1(t_\alpha, y_s; \mathcal{M}^{mes}_{15a}) = \frac{P(t_\alpha)}{(1 - y_s\ t_1^2 t_3^2)(1 - y_s\ t_2^2 t_3^2)(1 - y_s\ t_1^2 t_4^2)(1 - y_s\ t_2^2 t_4^2)} \ , \tag{17.3}$$

where the numerator is given by the polynomial

$$P(t_\alpha) = 1 + y_s\ t_1t_2t_3^2 + y_s\ t_1^2t_3t_4 + y_s\ t_1t_2t_3t_4 + y_s\ t_2^2t_3t_4 - y_s^2\ t_1^2t_2^2t_3^3t_4 \\ +y_s\ t_1t_2t_4^2 - y_s^2\ t_1^3t_2t_3^2t_4^2 - y_s^2\ t_1^2t_2^2t_3^2t_4^2 - y_s^2\ t_1t_2^3t_3^2t_4^2 - y_s^2\ t_1^2t_2^2t_3t_4^3 - y_s^3\ t_1^3t_2^3t_3^3t_4^3 \quad . \tag{17.4}$$

The plethystic logarithm of the mesonic Hilbert series is

$$PL[g_1(t_\alpha, y_s; \mathcal{M}_{15a}^{mes})] = y_s\ t_1^2t_3^2 + y_s\ t_1t_2t_3^2 + y_s\ t_2^2t_3^2 + y_s\ t_1^2t_3t_4 + y_s\ t_1t_2t_3t_4 + y_s\ t_2^2t_3t_4 \\ +y_s\ t_1^2t_4^2 + y_s\ t_1t_2t_4^2 + y_s\ t_2^2t_4^2 - y_s^2\ t_1^2t_2^2t_3^4 - y_s^2\ t_1^3t_2t_3^3t_4 - 2\ y_s^2\ t_1^2t_2^2t_3^3t_4 - y_s^2\ t_1t_2^3t_3^3t_4 \\ -y_s^2\ t_1^4t_3^2t_4^2 - 2\ y_s^2\ t_1^3t_2t_3^2t_4^2 - 4\ y_s^2\ t_1^2t_2^2t_3^2t_4^2 - 2\ y_s^2\ t_1t_2^3t_3^2t_4^2 - y_s^2\ t_2^4t_3^2t_4^2 - y_s^2\ t_1^3t_2t_3t_4^3 \\ -2\ y_s^2\ t_1^2t_2^2t_3t_4^3 - y_s^2\ t_1t_2^3t_3t_4^3 - y_s^2\ t_1^2t_2^2t_4^4 + \dots \ . \tag{17.5}$$

From the infinite plethystic logarithm one concludes that the moduli space is not a complete intersection.

Consider the following fugacity map

$$\tilde{x}_1^2 = x_1 = \frac{t_1}{t_2}\ ,\ \tilde{x}_2^2 = x_2 = \frac{t_3}{t_4}\ ,\ t = y_s^{1/4}\ t_1^{1/4}t_2^{1/4}t_3^{1/4}t_4^{1/4}\ , \tag{17.6}$$

where x_1, x_2 and t are mesonic charge fugacities. In terms of $\tilde{x}_1$ and $\tilde{x}_2$ both the Hilbert series and the plethystic logarithm can be expressed in terms of characters of irreducible representations of $SU(2) \times SU(2)$. The Taylor expansion of the Hilbert series takes the form

$$g_1(t, \tilde{x}_1, \tilde{x}_2; \mathcal{M}_{15a}^{mes}) = \sum_{n=0}^{\infty}\ [2n; 2n]_{\tilde{x}_1, \tilde{x}_2}\ t^{4n} \quad . \tag{17.7}$$

The plethystic logarithm in terms of characters of irreducible representations of $SU(2) \times SU(2)$ is

$$PL[g_1(t, \tilde{x}_1, \tilde{x}_2; \mathcal{M}_{15a}^{mes})] = [2;2]_{\tilde{x}_1,\tilde{x}_2}t^4 - (1 + [4;0]_{\tilde{x}_1,\tilde{x}_2} + [2;2]_{\tilde{x}_1,\tilde{x}_2} + [0;4]_{\tilde{x}_1,\tilde{x}_2})t^8 \\ +([2;0]_{\tilde{x}_1,\tilde{x}_2} + [4;0]_{\tilde{x}_1,\tilde{x}_2} + [0;2]_{\tilde{x}_1,\tilde{x}_2} + 2[2;2]_{\tilde{x}_1,\tilde{x}_2} + [4;2]_{\tilde{x}_1,\tilde{x}_2} + [0;4]_{\tilde{x}_1,\tilde{x}_2} + [2;4]_{\tilde{x}_1,\tilde{x}_2})t^{12} \\ -(4[2;0]_{\tilde{x}_1,\tilde{x}_2} + [4;0]_{\tilde{x}_1,\tilde{x}_2} + [6;0]_{\tilde{x}_1,\tilde{x}_2} + 4[0;2]_{\tilde{x}_1,\tilde{x}_2} + 5[2;2]_{\tilde{x}_1,\tilde{x}_2} + 4[4;2]_{\tilde{x}_1,\tilde{x}_2} + [6;2]_{\tilde{x}_1,\tilde{x}_2} \\ +[0;4]_{\tilde{x}_1,\tilde{x}_2} + 4[2;4]_{\tilde{x}_1,\tilde{x}_2} + [4;4]_{\tilde{x}_1,\tilde{x}_2} + [0;6]_{\tilde{x}_1,\tilde{x}_2} + [2;6]_{\tilde{x}_1,\tilde{x}_2})t^{16} + \dots \ . \tag{17.8}$$

In terms of the fugacities x_1 and x_2 the above plethystic logarithm exhibits the moduli space generators with their mesonic charges, where the flavour charges as powers of x_1 and x_2 take integer values. They are summarized in Table 56. The generators can be presented on a charge lattice. The generators form a convex polygon on the charge lattice which is the dual of the toric diagram of Model 15a.

As indicated in (17.8), the generators fall into an irreducible representation of $SU(2) \times SU(2)$ with the character

$$[2;2]_{\tilde{x}_1,\tilde{x}_2} t^4 = \left(\tilde{x}_1^2 + 1 + \frac{1}{\tilde{x}_1^2}\right)\left(\tilde{x}_2^2 + 1 + \frac{1}{\tilde{x}_2^2}\right) \quad . \tag{17.9}$$

The generators in terms of quiver fields are shown in Table 57.

Generator	$SU(2)_{x_1}$	$SU(2)_{x_2}$
$p_1^2 p_3^2\ s$	1	1
$p_1 p_2 p_3^2\ s$	0	1
$p_2^2 p_3^2\ s$	-1	1
$p_1^2 p_3 p_4\ s$	1	0
$p_1 p_2 p_3 p_4\ s$	0	0
$p_2^2 p_3 p_4\ s$	-1	0
$p_1^2 p_4^2\ s$	1	-1
$p_1 p_2 p_4^2\ s$	0	-1
$p_2^2 p_4^2\ s$	-1	-1

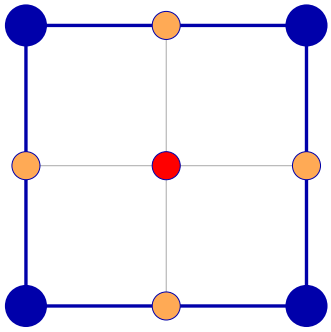


Table 56. The generators and lattice of generators of the mesonic moduli space of Model 15a in terms of GLSM fields with the corresponding flavor charges.

Generator	$SU(2)_{x_1}$	$SU(2)_{x_2}$
$X_{12}^1 X_{23}^1 X_{34}^1 X_{41}^1$	1	1
$X_{12}^1 X_{23}^1 X_{34}^2 X_{41}^1 = X_{12}^2 X_{23}^1 X_{34}^1 X_{41}^1$	0	1
$X_{12}^2 X_{23}^1 X_{34}^2 X_{41}^1$	-1	1
$X_{12}^1 X_{23}^1 X_{34}^1 X_{41}^2 = X_{12}^1 X_{23}^2 X_{34}^1 X_{41}^1$	1	0
$X_{12}^1 X_{23}^1 X_{34}^2 X_{41}^2 = X_{12}^1 X_{23}^2 X_{34}^2 X_{41}^1 = X_{12}^2 X_{23}^1 X_{34}^1 X_{41}^2 = X_{12}^2 X_{23}^2 X_{34}^1 X_{41}^1$	0	0
$X_{12}^2 X_{23}^1 X_{34}^2 X_{41}^2 = X_{12}^2 X_{23}^2 X_{34}^2 X_{41}^1$	-1	0
$X_{12}^1 X_{23}^2 X_{34}^1 X_{41}^2$	1	-1
$X_{12}^1 X_{23}^2 X_{34}^2 X_{41}^2 = X_{12}^2 X_{23}^2 X_{34}^1 X_{41}^2$	0	-1
$X_{12}^2 X_{23}^2 X_{34}^2 X_{41}^2$	-1	-1

Table 57. The generators in terms of bifundamental fields (Model 15a).

By introducing the fugacity map

$$T_1 = \frac{t^4}{x_1 x_2} = y_s\ t_2^2 t_4^2\ ,\ T_2 = x_1 = \frac{t_1}{t_2}\ ,\ T_3 = x_2 = \frac{t_3}{t_4}\ , \tag{17.10}$$

the mesonic Hilbert series can be expressed as

$$g_1(T_1,T_2,T_3;\mathcal{M}^{mes}_{15a}) = \big(1+T_1T_2T_3+T_1T_3+T_1T_2^2T_3+T_1T_2+T_1T_2T_3^2 \\ -(T_1^2T_2^2T_3^2+T_1^2T_2T_3^2+T_1^2T_2^3T_3^2+T_1^2T_2^2T_3+T_1^2T_2^2T_3^3)-T_1^3T_2^3T_3^3\big)\times \\ \frac{1}{(1-T_1)(1-T_1T_2^2)(1-T_1T_3^2)(1-T_1T_2^2T_3^2)} \quad . \tag{17.11}$$

The corresponding plethystic logarithm has the form

$$PL[g_1(T_1,T_2,T_3;\mathcal{M}^{mes}_{15a})] = T_1T_2^2T_3^2+T_1T_2T_3^2+T_1T_3^2+T_1T_2^2T_3+T_1T_2T_3+T_1T_3 \\ +T_1T_2^2+T_1T_2+T_1-T_1^2T_2^2-T_1^2T_2^3T_3^3+\ldots \quad . \tag{17.12}$$

The above Hilbert series and plethystic logarithm are in terms of three fugacities which carry only positive powers. This illustrates the conical structure of the toric Calabi-Yau 3-fold.

17.2 Model 15 Phase b

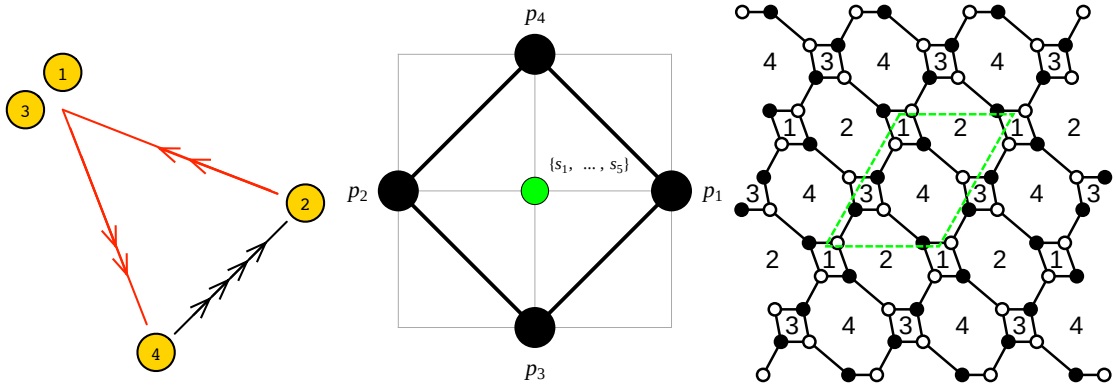


Figure 35. The quiver, toric diagram, and brane tiling of Model 15b. The red arrows in the quiver indicate all possible connections between blocks of nodes.

The superpotential is

$$W = +X^1_{21}X^1_{14}X^1_{42}+X^2_{21}X^2_{14}X^2_{42}+X^1_{23}X^2_{34}X^3_{42}+X^2_{23}X^1_{34}X^4_{42} \\ -X^1_{21}X^2_{14}X^3_{42}-X^2_{21}X^1_{14}X^4_{42}-X^1_{23}X^1_{34}X^2_{42}-X^2_{23}X^2_{34}X^1_{42} \tag{17.13}$$

The perfect matching matrix is

$$P = \left(\begin{array}{c|cccc|ccccc} & p_1 & p_2 & p_3 & p_4 & s_1 & s_2 & s_3 & s_4 & s_5 \\ \hline X^2_{42} & 1 & 0 & 1 & 0 & 0 & 0 & 1 & 0 & 0 \\ X^3_{42} & 0 & 1 & 1 & 0 & 0 & 0 & 1 & 0 & 0 \\ X^4_{42} & 1 & 0 & 0 & 1 & 0 & 0 & 1 & 0 & 0 \\ X^1_{42} & 0 & 1 & 0 & 1 & 0 & 0 & 1 & 0 & 0 \\ X^1_{21} & 1 & 0 & 0 & 0 & 1 & 0 & 0 & 1 & 0 \\ X^2_{21} & 0 & 1 & 0 & 0 & 1 & 0 & 0 & 1 & 0 \\ X^2_{34} & 1 & 0 & 0 & 0 & 0 & 1 & 0 & 1 & 0 \\ X^1_{34} & 0 & 1 & 0 & 0 & 0 & 1 & 0 & 1 & 0 \\ X^2_{23} & 0 & 0 & 1 & 0 & 1 & 0 & 0 & 0 & 1 \\ X^1_{23} & 0 & 0 & 0 & 1 & 1 & 0 & 0 & 0 & 1 \\ X^1_{14} & 0 & 0 & 1 & 0 & 0 & 1 & 0 & 0 & 1 \\ X^2_{14} & 0 & 0 & 0 & 1 & 0 & 1 & 0 & 0 & 1 \end{array}\right)$$

The F-term charge matrix $Q_F = \ker(P)$ is

$$Q_F = \left(\begin{array}{cccc|ccccc} p_1 & p_2 & p_3 & p_4 & s_1 & s_2 & s_3 & s_4 & s_5 \\ \hline 1 & 1 & 0 & 0 & 0 & 0 & -1 & -1 & 0 \\ 0 & 0 & 1 & 1 & 0 & 0 & -1 & 0 & -1 \\ 0 & 0 & 0 & 0 & 1 & 1 & 0 & -1 & -1 \end{array}\right)$$

The D-term charge matrix is

$$Q_D = \left(\begin{array}{cccc|ccccc} p_1 & p_2 & p_3 & p_4 & s_1 & s_2 & s_3 & s_4 & s_5 \\ \hline 0 & 0 & 0 & 0 & 0 & 1 & -1 & 0 & 0 \\ 0 & 0 & 0 & 0 & 0 & 0 & 1 & -1 & 0 \\ 0 & 0 & 0 & 0 & 0 & 0 & 0 & 1 & -1 \end{array}\right)$$

The total charge matrix Q_t exhibits two pairs of identical columns. Accordingly, the global symmetry is enhanced to $SU(2)_{x_1} \times SU(2)_{x_2} \times U(1)_R$. The mesonic charges on extremal perfect matchings are found following the discussion in §2.3. They are identical to the ones for Model 15a and are presented in Table 55.

The product of all internal perfect matchings is expressed as

$$s = \prod_{m=1}^{5} s_m \ . \tag{17.14}$$

The fugacity which counts the above product is y_s. The fugacity which counts the remaining extremal perfect matchings p_α is t_α.

The mesonic Hilbert series for Model 15b is found using the Molien integral formula in (2.9). The mesonic Hilbert series of Model 15b is identical to the one for Model 15a in (17.3).

The moduli space generators in terms of perfect matchings of Model 15b are shown in Table 56. In terms of quiver fields of Model 15b, they are presented in Table 58. The lattice of generators is a reflexive polygon and the dual of the toric diagram.

Generator	$SU(2)_{x_1}$	$SU(2)_{x_2}$
$X^1_{14}X^2_{42}X^1_{21} = X^2_{23}X^2_{34}X^2_{42}$	1	1
$X^1_{14}X^3_{42}X^1_{21} = X^1_{14}X^2_{42}X^2_{21} = X^2_{23}X^1_{34}X^2_{42} = X^2_{23}X^2_{34}X^3_{42}$	0	1
$X^1_{14}X^3_{42}X^2_{21} = X^2_{23}X^1_{34}X^3_{42}$	-1	1
$X^1_{14}X^4_{42}X^1_{21} = X^2_{14}X^2_{42}X^1_{21} = X^1_{23}X^2_{34}X^2_{42} = X^2_{23}X^2_{34}X^4_{42}$	1	0
$X^1_{14}X^1_{42}X^1_{21} = X^1_{14}X^4_{42}X^2_{21} = X^2_{14}X^3_{42}X^1_{21} = X^2_{14}X^2_{42}X^2_{21} = X^1_{23}X^1_{34}X^2_{42} = X^1_{23}X^2_{34}X^3_{42} = X^2_{23}X^1_{34}X^4_{42} = X^2_{23}X^2_{34}X^1_{42}$	0	0
$X^1_{14}X^1_{42}X^2_{21} = X^2_{14}X^3_{42}X^2_{21} = X^1_{23}X^1_{34}X^3_{42} = X^2_{23}X^1_{34}X^1_{42}$	-1	0
$X^2_{14}X^4_{42}X^1_{21} = X^1_{23}X^2_{34}X^4_{42}$	1	-1
$X^2_{14}X^1_{42}X^1_{21} = X^2_{14}X^4_{42}X^2_{21} = X^1_{23}X^1_{34}X^4_{42} = X^1_{23}X^2_{34}X^1_{42}$	0	-1
$X^2_{14}X^1_{42}X^2_{21} = X^1_{23}X^1_{34}X^1_{42}$	-1	-1

Table 58. The generators in terms of bifundamental fields (Model 15b).

18 Model 16: $\mathbb{C}^3/\mathbb{Z}_3$ $(1,1,1)$, $\mathbf{dP}_0$

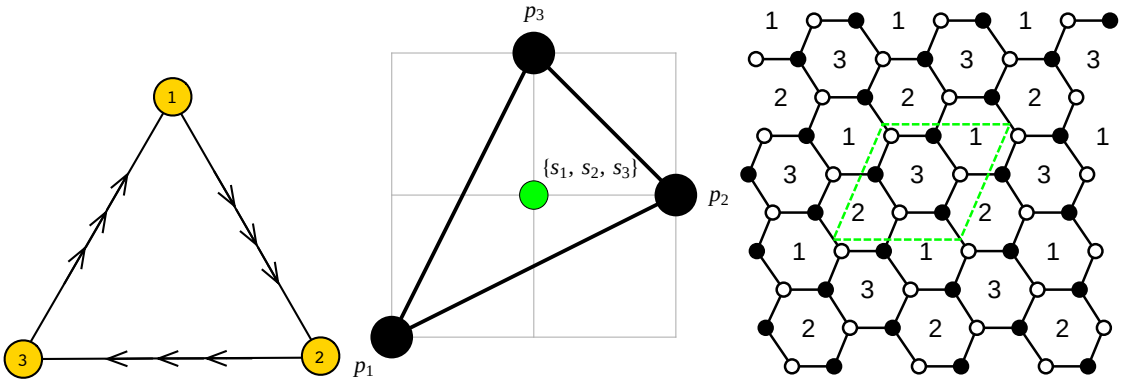


Figure 36. The quiver, toric diagram, and brane tiling of Model 16.

The superpotential is

$$\begin{aligned} W = &+X^1_{12}X^3_{23}X^2_{31} + X^2_{12}X^1_{23}X^3_{31} + X^3_{12}X^2_{23}X^1_{31} \\ &-X^1_{12}X^1_{23}X^1_{31} - X^3_{12}X^3_{23}X^3_{31} - X^2_{12}X^2_{23}X^2_{31} \end{aligned} \tag{18.1}$$

The perfect matching matrix is

$$P = \left(\begin{array}{c|ccc|ccc} & p_1 & p_2 & p_3 & s_1 & s_2 & s_3 \\ \hline X^3_{12} & 1 & 0 & 0 & 1 & 0 & 0 \\ X^2_{31} & 1 & 0 & 0 & 0 & 1 & 0 \\ X^1_{23} & 1 & 0 & 0 & 0 & 0 & 1 \\ X^1_{12} & 0 & 1 & 0 & 1 & 0 & 0 \\ X^3_{31} & 0 & 1 & 0 & 0 & 1 & 0 \\ X^2_{23} & 0 & 1 & 0 & 0 & 0 & 1 \\ X^2_{12} & 0 & 0 & 1 & 1 & 0 & 0 \\ X^1_{31} & 0 & 0 & 1 & 0 & 1 & 0 \\ X^3_{23} & 0 & 0 & 1 & 0 & 0 & 1 \end{array}\right)$$

The F-term charge matrix $Q_F = \ker(P)$ is

$$Q_F = \left(\begin{array}{ccc|ccc} p_1 & p_2 & p_3 & s_1 & s_2 & s_3 \\ \hline 1 & 1 & 1 & -1 & -1 & -1 \end{array}\right)$$

The D-term charge matrix is

$$Q_D = \left(\begin{array}{ccc|ccc} p_1 & p_2 & p_3 & s_1 & s_2 & s_3 \\ \hline 0 & 0 & 0 & 1 & -1 & 0 \\ 0 & 0 & 0 & 0 & 1 & -1 \end{array}\right)$$

One observes that the GLSM fields corresponding to the extremal points of the toric diagram in Figure 36 are equally charged under the F- and D-term constraints. This is shown by three identical columns of the total charge matrix Q_t. This leads to the enhancement of the global symmetry from $U(1)^3$ to $SU(3)_{(x_1,x_2)} \times U(1)_R$. Accordingly, the mesonic charges on the GLSM fields corresponding to extremal points in the toric diagram in Figure 36 can be found following the discussion in §2.3. They are presented in Table 59.

	$SU(3)_{(x_1,x_2)}$	$U(1)_R$	fugacity
p_1	(-1/3, -1/3)	2/3	t_1
p_2	(+2/3, -1/3)	2/3	t_2
p_3	(-1/3, +2/3)	2/3	t_3

Table 59. The GLSM fields corresponding to extremal points of the toric diagram with their mesonic charges (Model 16).

The product of all internal perfect matchings expressed as

$$s = \prod_{m=1}^{3} s_m \ . \tag{18.2}$$

The above product is counted by the fugacity y_s. The remaining extremal perfect matchings p_α are counted by t_α.

The mesonic Hilbert series of Model 16 is calculated using the Molien integral formula in (2.9). It is

$$g_1(t_\alpha, y_s; \mathcal{M}_{16}^{mes}) = \frac{1 + y_s\ t_1^2 t_2 + y_s\ t_1 t_2^2 + y_s\ t_1^2 t_3 + y_s\ t_1 t_2 t_3 + y_s\ t_2^2 t_3 + y_s\ t_1 t_3^2 + y_s\ t_2 t_3^2 + y_s^2\ t_1^2 t_2^2 t_3^2}{(1 - y_s\ t_1^3)(1 - y_s\ t_2^3)(1 - y_s\ t_3^3)} \ . \tag{18.3}$$

The plethystic logarithm of the mesonic Hilbert series is

$$\begin{aligned} PL[g_1(t_\alpha, y_s; \mathcal{M}_{16}^{mes})] = {} & y_s\ t_1^3 + y_s\ t_1^2 t_2 + y_s\ t_1 t_2^2 + y_s\ t_2^3 + y_s\ t_1^2 t_3 + y_s\ t_1 t_2 t_3 + y_s\ t_2^2 t_3 \\ & + y_s\ t_1 t_3^2 + y_s\ t_2 t_3^2 + y_s\ t_3^3 - y_s^2\ t_1^4 t_2^2 - y_s^2\ t_1^3 t_2^3 - y_s^2\ t_1^2 t_2^4 - y_s^2\ t_1^4 t_2 t_3 - 2\ y_s^2\ t_1^3 t_2^2 t_3 \\ & - 2\ y_s^2\ t_1^2 t_2^3 t_3 - y_s^2\ t_1 t_2^4 t_3 - y_s^2\ t_1^4 t_3^2 - 2\ y_s^2\ t_1^3 t_2 t_3^2 - 3\ y_s^2\ t_1^2 t_2^2 t_3^2 - 2\ y_s^2\ t_1 t_2^3 t_3^2 - y_s^2\ t_2^4 t_3^2 \\ & - y_s^2\ t_1^3 t_3^3 - 2\ y_s^2\ t_1^2 t_2 t_3^3 - 2\ y_s^2\ t_1 t_2^2 t_3^3 - y_s^2\ t_2^3 t_3^3 - y_s^2\ t_1^2 t_3^4 - y_s^2\ t_1 t_2 t_3^4 - y_s^2\ t_2^2 t_3^4 + \dots \ . \end{aligned} \tag{18.4}$$

Consider the following fugacity map

$$x_1 = \frac{t_2}{t_1}\ ,\ x_2 = \frac{t_3}{t_1}\ ,\ t = y_s^{1/3}\ t_1^{1/3} t_2^{1/3} t_3^{1/3}\ , \tag{18.5}$$

where x_1, x_2 and t count the mesonic charges. The fugacities x_1 and x_2 with their powers being integers count integer flavour charges. With a further redefinition of fugacities,

$$\tilde{x}_1 = \frac{1}{x_1^{1/3} x_2^{1/3}}\ ,\ \tilde{x}_2 = \frac{x_1^{1/3}}{x_2^{2/3}} \tag{18.6}$$

the Hilbert series and plethystic logarithm can be expressed in terms of characters of irreducible representations of $SU(3)$. The expansion of the Hilbert series takes the form

$$g_1(t, \tilde{x}_1, \tilde{x}_2; \mathcal{M}_{16}^{mes}) = \sum_{n=0}^{\infty} [3n, 0]_{(\tilde{x}_1, \tilde{x}_2)}\ t^{3n} \ . \tag{18.7}$$

The plethystic logarithm is

$$\begin{aligned} PL[g_1(t, \tilde{x}_1, \tilde{x}_2; \mathcal{M}_{16}^{mes})] = {} & [3,0]_{(\tilde{x}_1,\tilde{x}_2)} t^3 - [2,2]_{(\tilde{x}_1,\tilde{x}_2)} t^6 + ([1,1]_{(\tilde{x}_1,\tilde{x}_2)} + [1,4]_{(\tilde{x}_1,\tilde{x}_2)} \\ & + [2,2]_{(\tilde{x}_1,\tilde{x}_2)} + [4,1]_{(\tilde{x}_1,\tilde{x}_2)}) t^9 - (2[0,3]_{(\tilde{x}_1,\tilde{x}_2)} + 2[1,1]_{(\tilde{x}_1,\tilde{x}_2)} + 2[1,4]_{(\tilde{x}_1,\tilde{x}_2)} \\ & + 2[2,2]_{(\tilde{x}_1,\tilde{x}_2)} + [2,5]_{(\tilde{x}_1,\tilde{x}_2)} + 2[3,0]_{(\tilde{x}_1,\tilde{x}_2)} + 2[3,3]_{(\tilde{x}_1,\tilde{x}_2)} + 2[4,1]_{(\tilde{x}_1,\tilde{x}_2)} \\ & + [5,2]_{(\tilde{x}_1,\tilde{x}_2)}) t^{12} + \dots \ . \end{aligned} \tag{18.8}$$

In terms of fugacities x_1 and x_2 the above plethystic logarithm exhibits the moduli space generators with their integer flavour charges and R-charges. They are summarized in Table 60. The generators can be presented on a charge lattice. The lattice of generators is the dual polygon of the toric diagram. As indicated in (18.8), the generators fall into an irreducible representation of $SU(3)$ with the character being

$$[3,0]_{(\tilde{x}_1,\tilde{x}_2)}t^3 = \left(\tilde{x}_1^3 + \tilde{x}_1\tilde{x}_2 + \frac{\tilde{x}_1^2}{\tilde{x}_2} + \frac{\tilde{x}_2^2}{\tilde{x}_1} + 1 + \frac{\tilde{x}_2^3}{\tilde{x}_1^3} + \frac{\tilde{x}_1}{\tilde{x}_2^2} + \frac{\tilde{x}_2}{\tilde{x}_1^2} + \frac{1}{\tilde{x}_1\tilde{x}_2} + \frac{1}{\tilde{x}_2^3}\right) t^3 \quad . \tag{18.9}$$

The generators of the mesonic moduli space in terms of quiver fields of Model 16 are shown in Table 61.

Generator	$SU(3)_{(x_1,x_2)}$
$p_1^3\ s$	(-1, -1)
$p_1^2p_2\ s$	(0, -1)
$p_1p_2^2\ s$	(1, -1)
$p_2^3\ s$	(2, -1)
$p_1^2p_3\ s$	(-1, 0)
$p_1p_2p_3\ s$	(0, 0)
$p_2^2p_3\ s$	(1, 0)
$p_1p_3^2\ s$	(-1, 1)
$p_2p_3^2\ s$	(0, 1)
$p_3^3\ s$	(-1, 2)

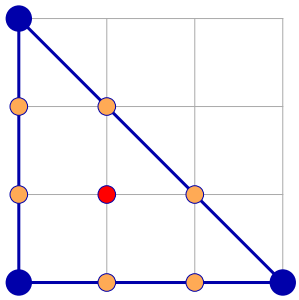


Table 60. The generators and lattice of generators of the mesonic moduli space of Model 16 in terms of GLSM fields with the corresponding flavor charges.

Generator	$SU(3)_{(x_1,x_2)}$
$X^3_{12}X^1_{23}X^2_{31}$	(-1, -1)
$X^1_{12}X^1_{23}X^2_{31} = X^3_{12}X^1_{23}X^3_{31} = X^3_{12}X^2_{23}X^2_{31}$	(0, -1)
$X^1_{12}X^1_{23}X^3_{31} = X^1_{12}X^2_{23}X^2_{31} = X^3_{12}X^2_{23}X^3_{31}$	(1, -1)
$X^1_{12}X^2_{23}X^3_{31}$	(2, -1)
$X^2_{12}X^1_{23}X^2_{31} = X^3_{12}X^1_{23}X^1_{31} = X^3_{12}X^3_{23}X^2_{31}$	(-1, 0)
$X^1_{12}X^1_{23}X^1_{31} = X^1_{12}X^3_{23}X^2_{31} = X^2_{12}X^1_{23}X^3_{31} = X^2_{12}X^2_{23}X^2_{31} = X^3_{12}X^2_{23}X^1_{31} = X^3_{12}X^3_{23}X^3_{31}$	(0, 0)
$X^1_{12}X^2_{23}X^1_{31} = X^1_{12}X^3_{23}X^3_{31} = X^2_{12}X^2_{23}X^3_{31}$	(1, 0)
$X^2_{12}X^1_{23}X^1_{31} = X^2_{12}X^3_{23}X^2_{31} = X^3_{12}X^3_{23}X^1_{31}$	(-1, 1)
$X^1_{12}X^3_{23}X^1_{31} = X^2_{12}X^2_{23}X^1_{31} = X^2_{12}X^3_{23}X^3_{31}$	(0, 1)
$X^2_{12}X^3_{23}X^1_{31}$	(-1, 2)

Table 61. The generators in terms of bifundamental fields (Model 16).

With the fugacity map

$$T_1 = \frac{t}{x_1^{1/3}x_2^{1/3}} = y_s^{1/3}t_1 \ , \ T_2 = \frac{x_1^{2/3}t}{x_2^{1/3}} = y_s^{1/3}t_2 \ , \ T_3 = \frac{x_2^{2/3}t}{x_1^{1/3}} = y_s^{1/3}t_3 \ , \tag{18.10}$$

the mesonic Hilbert series becomes

$$g_1(T_1,T_2,T_3;\mathcal{M}_{16}^{mes}) = \frac{1+T_1^2T_2+T_1T_2^2+T_1^2T_3+T_1T_2T_3+T_2^2T_3+T_1T_3^2+T_2T_3^2+T_1^2T_2^2T_3^2}{(1-T_1^3)(1-T_2^3)(1-T_3^3)} \ , \tag{18.11}$$

with the plethystic logarithm becoming

$$\begin{aligned} PL[g_1(T_1,T_2,T_3;\mathcal{M}_{16}^{mes})] = {} & T_1^3+T_1^2T_2+T_1T_2^2+T_2^3+T_1^2T_3+T_1T_2T_3+T_2^2T_3+T_1T_3^2 \\ & +T_2T_3^2+T_3^3-T_1^4T_2^2-T_1^3T_2^3-T_1^2T_2^4-T_1^4T_2T_3-2\ T_1^3T_2^2T_3-2\ T_1^2T_2^3T_3 \\ & -T_1T_2^4T_3-T_1^4T_3^2-2\ T_1^3T_2T_3^2-3\ T_1^2T_2^2T_3^2-2\ T_1T_2^3T_3^2-T_2^4T_3^2-T_1^3T_3^3 \\ & -2\ T_1^2T_2T_3^3-2\ T_1T_2^2T_3^3-T_2^3T_3^3-T_1^2T_3^4-T_1T_2T_3^4-T_2^2T_3^4+\dots \ . \end{aligned} \tag{18.12}$$

The above Hilbert series and plethystic logarithm are in terms of three fugacities with positive powers. This illustrates the conical structure of the toric Calabi-Yau 3-fold.

19 Seiberg Duality Trees

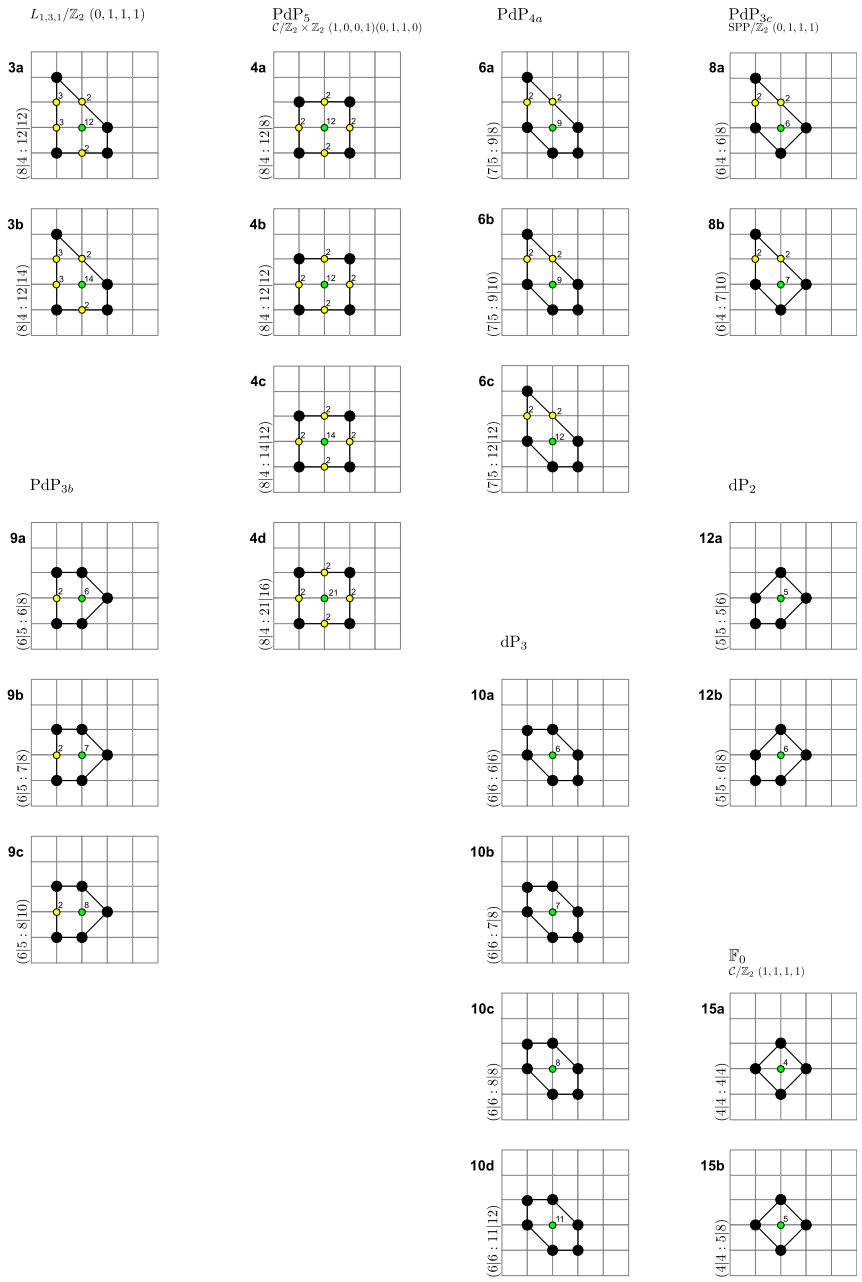


Figure 37. Toric Diagrams of toric (Seiberg) dual phases of quiver gauge theories with brane tilings. The label $(G|n_p : n_i|n_w)$ is used, where G, n_p, n_i and n_w are the number of $U(n)$ gauge groups, GLSM fields with non-zero R-charge, internal toric points and superpotential terms respectively.

The above sections have identified all 30 supersymmetric gauge theories with brane tilings corresponding to the 16 reflexive polygons. 8 reflexive polygons are associated to multiple quiver gauge theories as summarized in Figure 37. These are called phases of the corresponding toric variety. For a given toric variety, the phases are so called *toric (Seiberg) dual* and are related under toric (Seiberg) duality as discussed in appendix §B.1. Multiple toric duality actions on various $U(n)$ gauge groups corresponding to 4-sided faces in the brane tiling create closed orbits among the phases.

In Figure 38 to Figure 45, a summary of the orbits presented as *duality trees* is shown, where nodes represent the brane tiling of the phase, and arrows are labelled with the index of the gauge group on which one acts under toric (Seiberg) duality to obtain the phase at the head of the arrow.

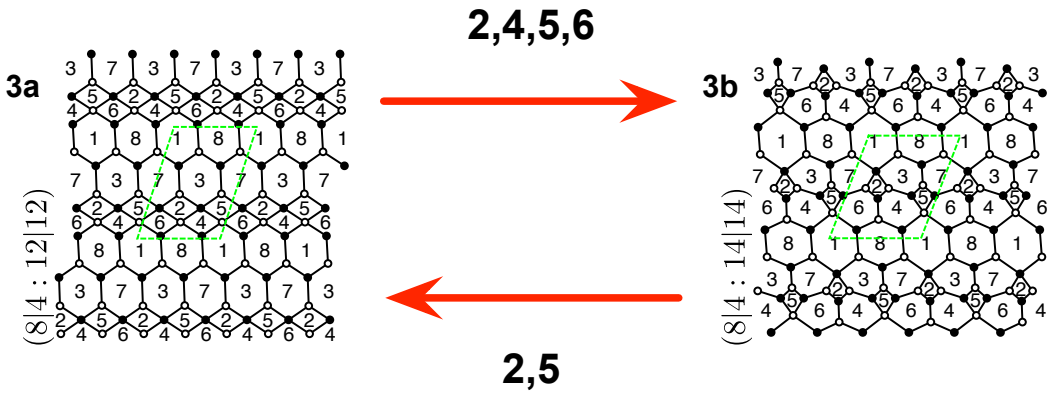


Figure 38. The duality tree for $L_{131}/\mathbb{Z}_2$ with orbifold action $(0, 1, 1, 1)$ [Model 3].

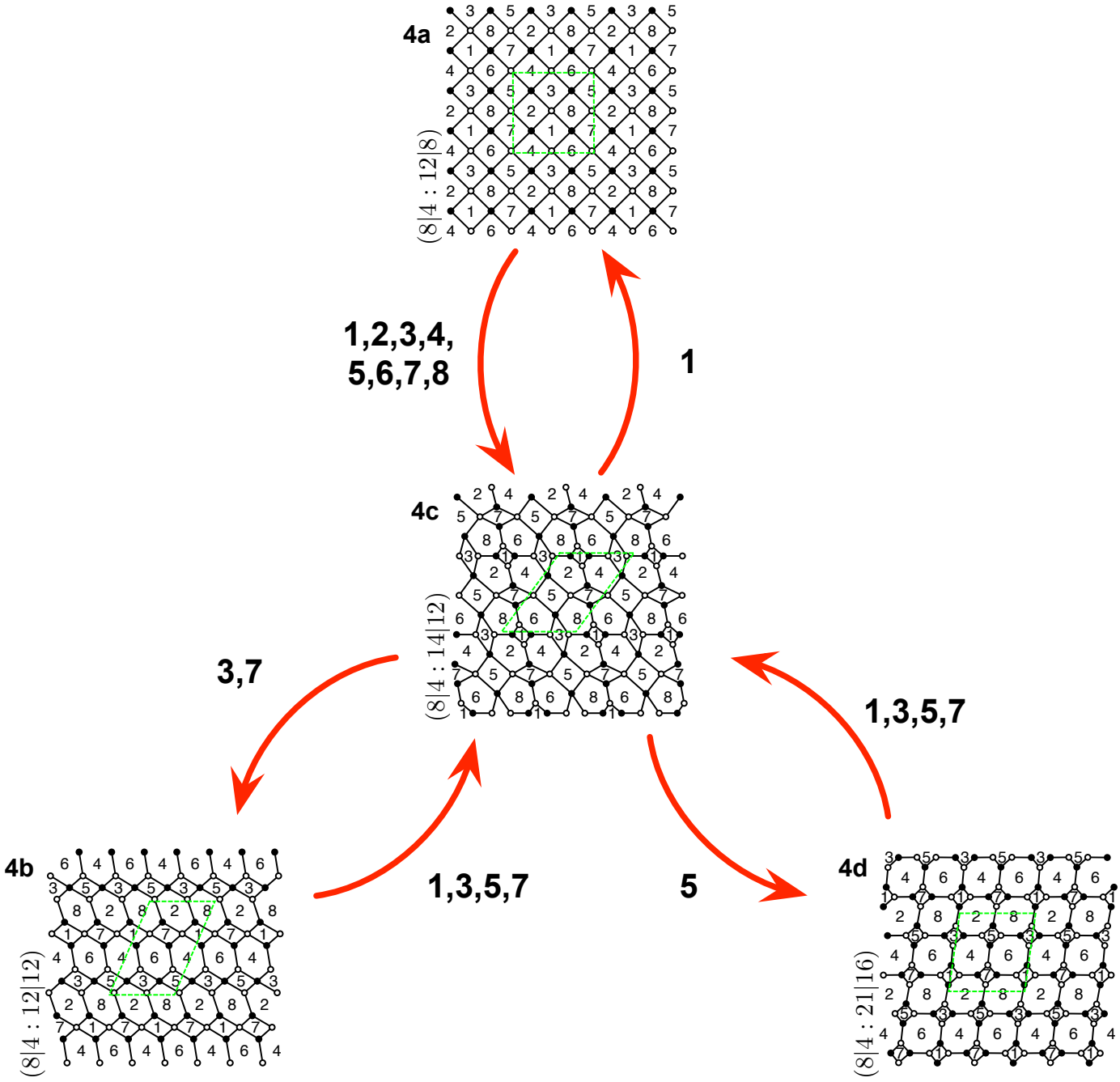


Figure 39. The duality tree for $\mathcal{C}/\mathbb{Z}_2 \times \mathbb{Z}_2$ with orbifold action $(0,1,1,0)(1,0,0,1)$ [Model 4].

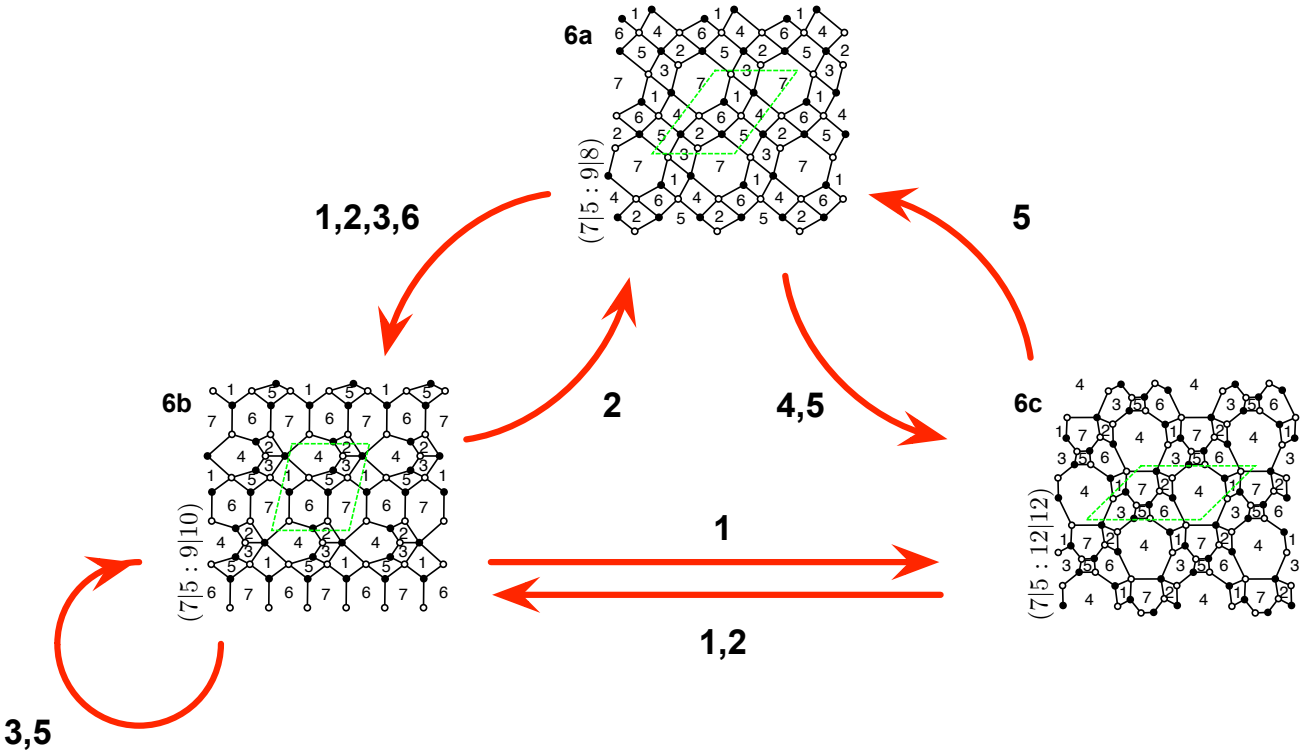


Figure 40. The duality tree for PdP_{4a} [Model 6].

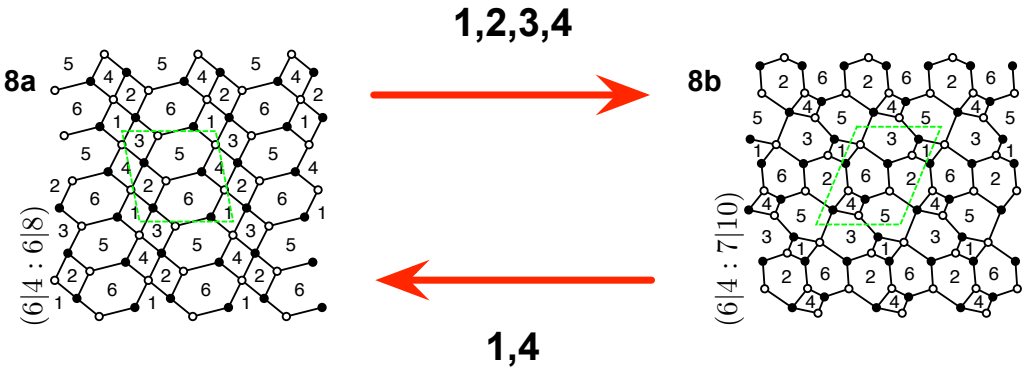


Figure 41. The duality tree for $\mathrm{SPP}/\mathbb{Z}_2$ with orbifold action $(0, 1, 1, 1)$ [Model 8].

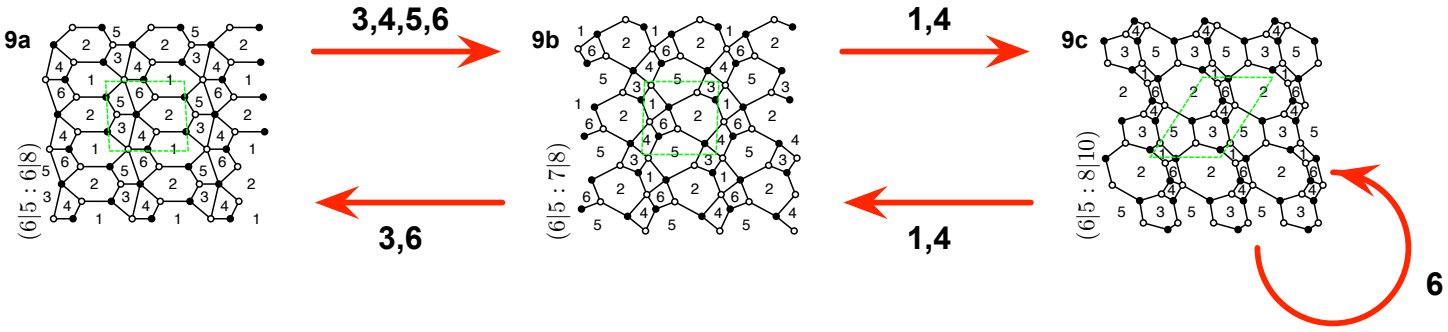


Figure 42. The duality tree for $\mathrm{PdP}_{3(b)}$ [Model 9].

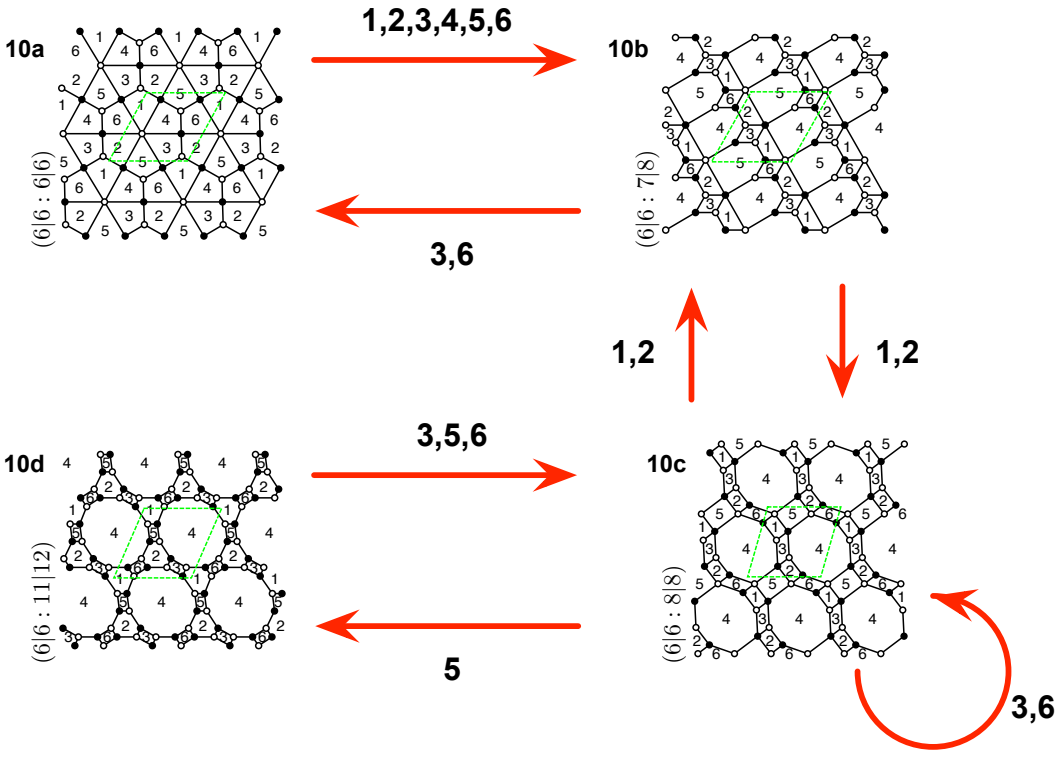


Figure 43. The duality tree for dP_3 [Model 10].

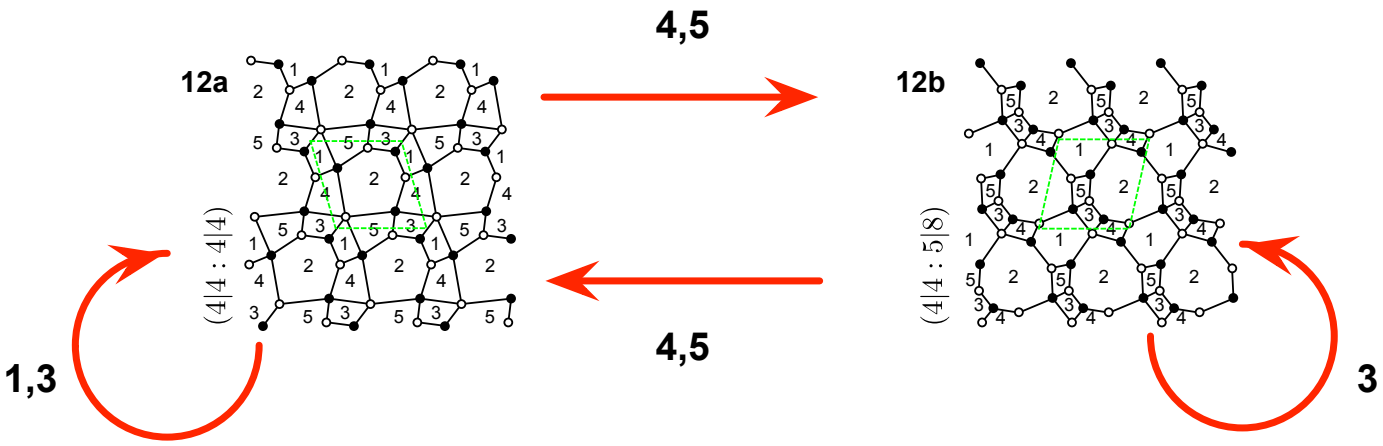


Figure 44. The duality tree for dP_2 [Model 12].

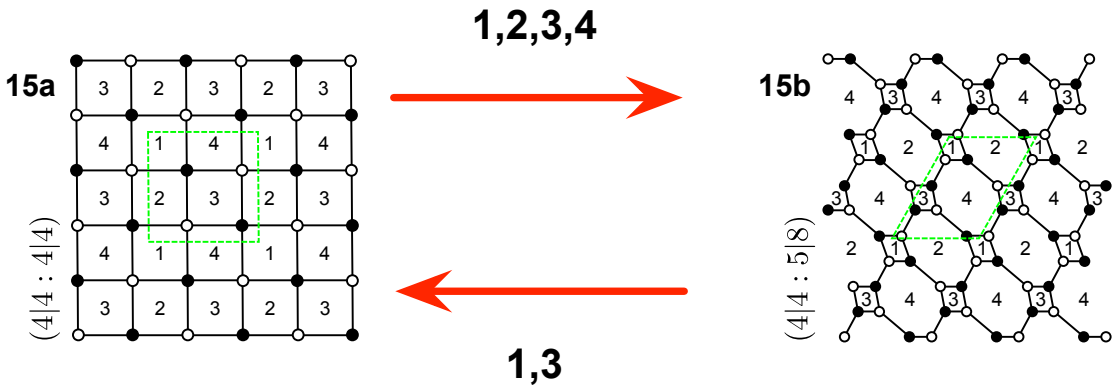


Figure 45. The duality tree for $\mathcal{C}/\mathbb{Z}_2$ with orbifold action $(1,1,1,1)$ or the cone over F_0 [Model 15].

20 Specular Duality and Conclusions

The work above uses the 16 reflexive polygons in Figure 1 as toric diagrams of Calabi-Yau moduli spaces of $3+1$ dimensional $\mathcal{N}=1$ supersymmetric gauge theories. These quiver gauge theories are represented by brane tilings. A natural question to ask from this setup is to identify all brane tilings corresponding to the 16 reflexive polygons. Motivated by this line of thought, the following comprehensive results have been presented in this paper:

- There are exactly 30 brane tilings encoding supersymmetric quiver gauge theories whose mesonic moduli spaces are represented by reflexive polygons. All gauge theories are related by a cascade of Higgs mechanisms. In addition, toric (Seiberg) duality maps multiple gauge theories to the same reflexive polygon.

- The generating function of mesonic gauge invariant operators known as the mesonic Hilbert series is computed using the Molien integral formula for each of the 30 quiver theories. Fugacities of the Hilbert series are related both to perfect matchings and hence points in the toric diagram as well as charges under the global symmetry of the gauge theory. Hilbert series of toric dual phases have been shown to be identical.

- The generators of the mesonic moduli space of all 30 quiver gauge theories have been found both in terms of chiral fields of the gauge theory as well as the perfect matchings of the brane tiling.

- The mesonic charges on the moduli space generators have been found such that they form for each generator a point on $\mathbb{Z}^2$. The convex hull of all such points is a reflexive polygon. For all 30 quiver gauge theories, these reflexive polygons known as lattice of generators are exactly the polar duals to the toric diagrams.

The above observations made by classifying all brane tilings corresponding to reflexive polygons lead to a comprehensive overview of a special set of quiver gauge theories. This overview is the precursor to a discovery of a new duality of quiver gauge theories. This **specular duality** is best observed in the context of toric diagrams with points labelled by perfect matchings of the brane tiling. Recall that extremal perfect matchings correspond to the corner points coloured black in the toric diagrams in Figure 2, whereas internal perfect matchings are points lying strictly within the perimeter of the polygon. External perfect matchings are all points on the perimeter of the polygon including the extremal ones. All except extremal perfect matchings correspond to GLSM fields with zero R-charge.

The new duality we propose exchanges the internal perfect matchings with the external perfect matchings. For the set of brane tilings corresponding to reflexive polygons, the duality map is unique by forming duality pairs between models as follows

$$\begin{gathered}
1 \leftrightarrow 1 \\
2 \leftrightarrow 4d\ ,\ 3a \leftrightarrow 4c\ ,\ 3b \leftrightarrow 3b\ ,\ 4a \leftrightarrow 4a\ ,\ 4b \leftrightarrow 4b \\
5 \leftrightarrow 6c\ ,\ 6a \leftrightarrow 6a\ ,\ 6b \leftrightarrow 6b \\
7 \leftrightarrow 10d\ ,\ 8a \leftrightarrow 10c\ ,\ 8b \leftrightarrow 9c\ ,\ 9a \leftrightarrow 10b\ ,\ 9b \leftrightarrow 9b\ ,\ 10a \leftrightarrow 10a \\
11 \leftrightarrow 12b\ ,\ 12a \leftrightarrow 12a \\
13 \leftrightarrow 15b\ ,\ 14 \leftrightarrow 14\ ,\ 15a \leftrightarrow 15a \\
16 \leftrightarrow 16 \qquad .
\end{gathered} \tag{20.1}$$

For instance, the dual pair $13 \leftrightarrow 15b$ in Figure 46 is exact under the indicated swap between external and internal perfect matchings.

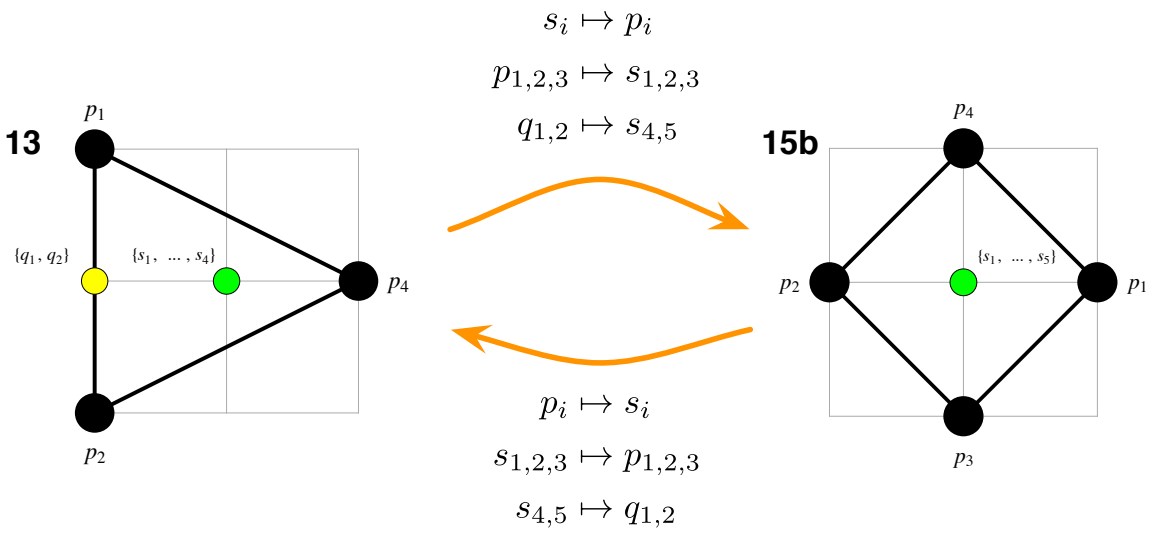


Figure 46. Specular duality between Model 13 ($\mathbb{C}^3/\mathbb{Z}_4(1,1,2)$) and Model 15b ($\mathbb{F}_0$, phase b). The exchange of internal and external perfect matchings map between the two models.

Accordingly, specular duality maps between brane tilings whose corresponding quiver gauge theories have different mesonic moduli spaces. In [87], it is illustrated how specular duality maps not the mesonic moduli spaces but the master spaces [65, 68, 75, 76, 80, 81] of the dual pairs in (20.1). The master space is the complete moduli space including both the mesonic and baryonic branches. It is shown that

the master spaces of the dual pairs in (20.1) are *identical* under a translation of fields given by the mapping of perfect matchings of the corresponding brane tilings. Further study of this duality is of great interest and some interpretations are reported in [87].

Acknowledgements

We would like to thank Alastair D. King for very interesting discussions that eventually led to the creation of this project. R.-K. S. likes to thank the Yukawa Institute of Theoretical Physics at Kyoto University, the Simons Center for Geometry and Physics at Stony Brook University and the Hebrew University of Jerusalem for hospitality during various stages of this work. He also likes to thank Tohru Eguchi and Kazuo Hosomichi for hospitality in Kyoto, as well as Stefano Cremonesi, Masato Taki and Giuseppe Torri for valuable discussions. He is also grateful to his parents.

A The theory for $\mathbb{C}^3/\mathbb{Z}_4 \times \mathbb{Z}_4$ $(1,0,3)(0,1,3)$

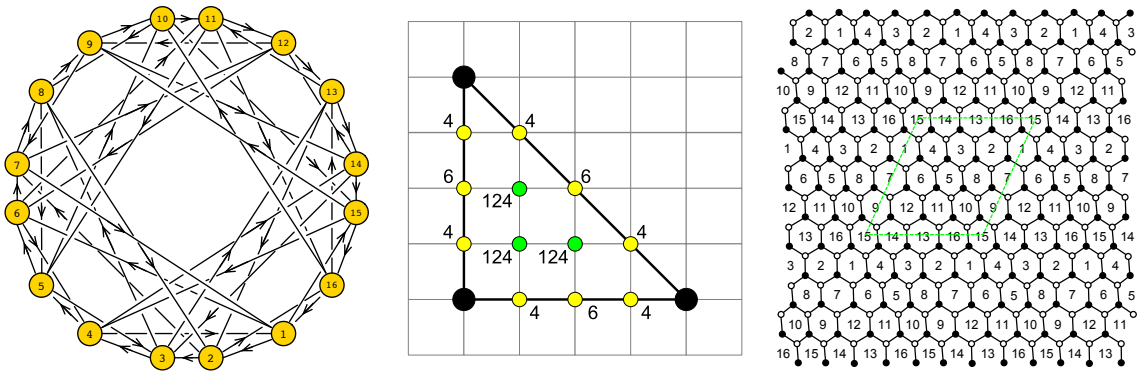


Figure 47. The quiver, toric diagram, and brane tiling of the abelian orbifold of the form $\mathbb{C}^3/\mathbb{Z}_4 \times \mathbb{Z}_4$ with orbifold action $(1,0,3)(0,1,3)$.

The quiver, toric diagram and brane tiling of $\mathbb{C}^3/\mathbb{Z}_4 \times \mathbb{Z}_4$ $(1,0,3)(0,1,3)$ theory are shown in Figure 47 with the superpotential[8] having the form

$$\begin{aligned} W = &+X_{7\,8}\,X_{8\,2}\,X_{2\,7} + X_{12\,9}\,X_{9\,7}\,X_{7\,12} + X_{13\,14}\,X_{14\,12}\,X_{12\,13} + X_{2\,3}\,X_{3\,13}\,X_{13\,2} \\ &+X_{8\,5}\,X_{5\,3}\,X_{3\,8} + X_{9\,10}\,X_{10\,8}\,X_{8\,9} + X_{14\,15}\,X_{15\,9}\,X_{9\,14} + X_{3\,4}\,X_{4\,14}\,X_{14\,3} \\ &+X_{5\,6}\,X_{6\,4}\,X_{4\,5} + X_{10\,11}\,X_{11\,5}\,X_{5\,10} + X_{15\,16}\,X_{16\,10}\,X_{10\,15} + X_{4\,1}\,X_{1\,15}\,X_{15\,4} \\ &+X_{6\,7}\,X_{7\,1}\,X_{1\,6} + X_{11\,12}\,X_{12\,6}\,X_{6\,11} + X_{16\,13}\,X_{13\,11}\,X_{11\,16} + X_{1\,2}\,X_{2\,16}\,X_{16\,1} \\ &-X_{7\,8}\,X_{8\,9}\,X_{9\,7} - X_{12\,9}\,X_{9\,14}\,X_{14\,12} - X_{13\,14}\,X_{14\,3}\,X_{3\,13} - X_{2\,3}\,X_{3\,8}\,X_{8\,2} \\ &-X_{8\,5}\,X_{5\,10}\,X_{10\,8} - X_{9\,10}\,X_{10\,15}\,X_{15\,9} - X_{14\,15}\,X_{15\,4}\,X_{4\,14} - X_{3\,4}\,X_{4\,5}\,X_{5\,3} \\ &-X_{5\,6}\,X_{6\,11}\,X_{11\,5} - X_{10\,11}\,X_{11\,16}\,X_{16\,10} - X_{15\,16}\,X_{16\,1}\,X_{1\,15} - X_{4\,1}\,X_{1\,6}\,X_{6\,4} \\ &-X_{6\,7}\,X_{7\,12}\,X_{12\,6} - X_{11\,12}\,X_{12\,13}\,X_{13\,11} - X_{16\,13}\,X_{13\,2}\,X_{2\,16} - X_{1\,2}\,X_{2\,7}\,X_{7\,1} \quad . \end{aligned} \tag{A.1}$$

B Review: Seiberg Duality, Integrating out Mass Terms, and the Higgs Mechanism

B.1 Seiberg Duality

Two $3+1$ dimensional worldvolume theories are called **toric (Seiberg) dual** if in the UV they have different Lagrangians with a different field content and superpotential, but flow to the same universality class in the IR. The mesonic moduli spaces of toric (Seiberg) dual theories are toric Calabi-Yau 3-folds which are identical. The corresponding toric diagrams are $GL(2,\mathbb{Z})$ equivalent, however multiplicities of internal toric points and hence GLSM fields with zero R-charge can differ.

The relationship between two toric (Seiberg) dual theories is best illustrated with an example using brane tilings. Dualizing on a given gauge group $U(n)$ has a natural interpretation in the brane tiling picture. Let us consider the Hirzebruch $\mathbb{F}_0$ model. The corresponding gauge theory has a superpotential of the form

$$W_I = \underbrace{X^1_{14}X^1_{42}X^1_{23}X^1_{31}}_{A} + \underbrace{X^2_{14}X^2_{42}X^2_{23}X^2_{31}}_{B} - \underbrace{X^2_{14}X^1_{42}X^2_{23}X^1_{31}}_{C} - \underbrace{X^1_{14}X^2_{42}X^1_{23}X^2_{31}}_{D} \quad , \tag{B.1}$$

[8]Note: The superpotential features an overall trace which is not explicitly written down in the following discussion.

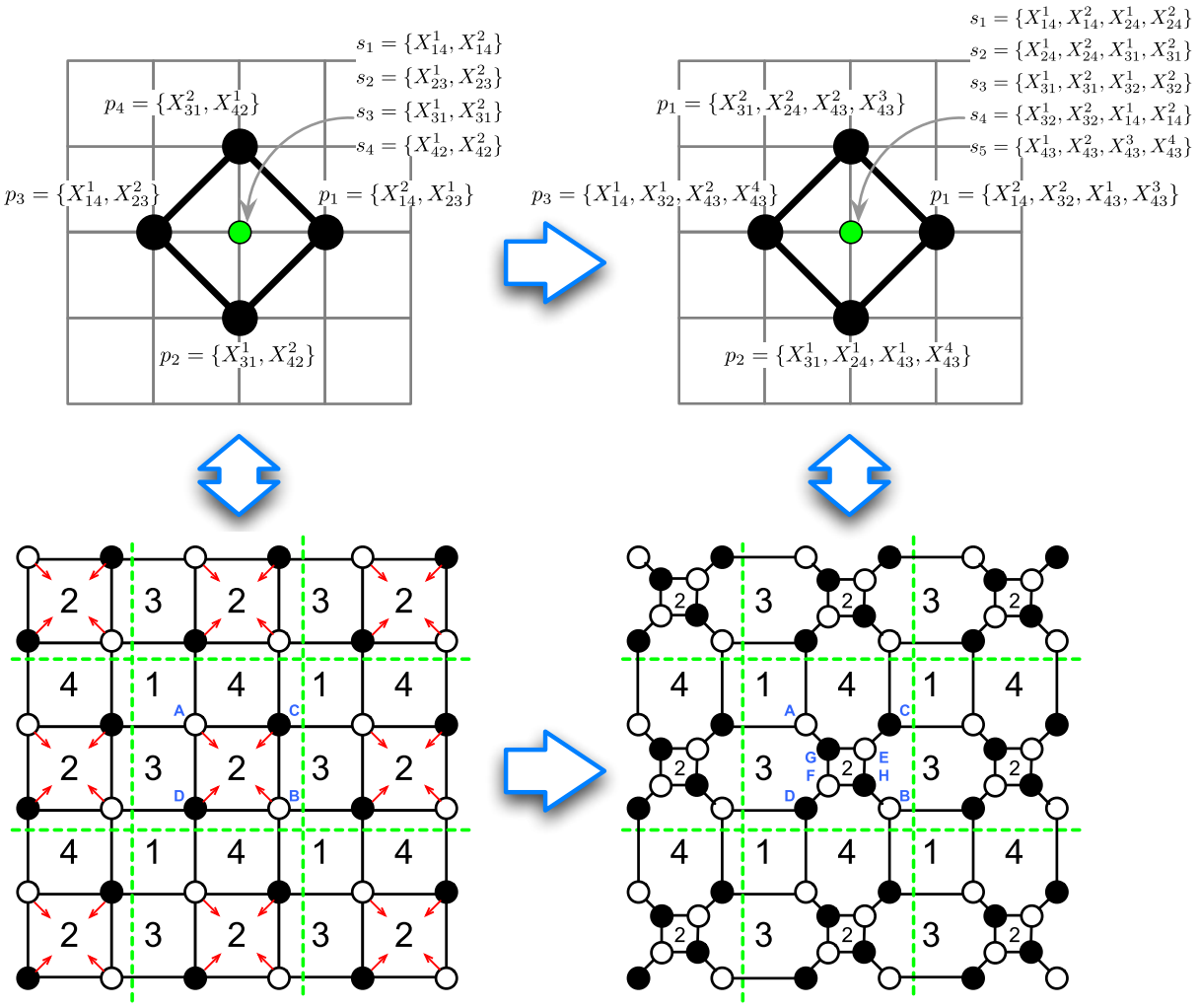


Figure 48. The toric (Seiberg) duality action on the brane tiling of the zeroth Hirzebruch surface F_0 model with corresponding toric diagrams. The points in the toric diagram correspond to GLSM fields which are presented as perfect matchings or sets of bifundamental fields in the brane tiling picture.

whose corresponding brane tiling and toric diagram are shown in the first column of Figure 48. The terms are labelled A to D and the corresponding brane tiling nodes are indicated in Figure 48. By dualizing on the gauge group $U(n_2)$, the superpotential

becomes

$$W_{II} = \underbrace{X^1_{14}X^1_{43}X^1_{31}}_{A} + \underbrace{X^2_{14}X^2_{43}X^2_{31}}_{B} - \underbrace{X^2_{14}X^3_{43}X^1_{31}}_{C} - \underbrace{X^1_{14}X^4_{43}X^2_{31}}_{D} + \underbrace{X^1_{14}X^3_{43}X^2_{31}}_{E} + \underbrace{X^2_{14}X^4_{43}X^1_{31}}_{F} - \underbrace{X^1_{14}X^1_{43}X^1_{31}}_{G} - \underbrace{X^2_{14}X^2_{43}X^2_{31}}_{H} \tag{B.2}$$

and the corresponding new brane tiling and quiver are shown in the second column of Figure 48. One observes that under toric (Seiberg) duality, the number of gauge groups G remains constant, the number of bifundamental fields E and the number of superpotential terms both increase each by 4.

The change in the number of bifundamental fields and superpotential terms corresponds to the change in the number of GLSM fields corresponding to internal points of the corresponding toric diagram. The area of the toric diagram corresponding to the number of gauge groups G remains constant. The two toric diagrams and brane tilings in Figure 48 with the corresponding superpotentials given in (B.1) and (B.2) are called **phases** of the F_0 model.

The duality action often leads to superpotentials with quadratic mass terms. Quadratic mass terms relate to massive fields which become non-dynamical in the IR. The removal of quadratic mass terms and the corresponding deformation of the brane tiling are discussed in the following section.

B.2 Integrating out mass terms

Quadratic terms in the superpotential relate to massive fields which are non-dynamical in the IR [42]. We are interested in the IR regime of the quiver gauge theories above, and therefore need to integrate out the quadratic terms in the superpotential.

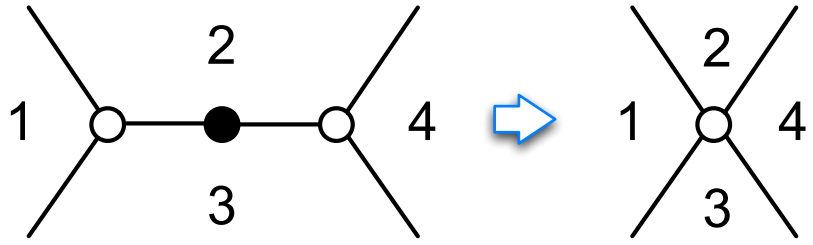


Figure 49. The removal of quadratic mass terms in the superpotential corresponds to the removal of 2-valent vertices in the brane tiling.

The procedure of integrating out quadratic mass terms in the superpotential has a natural interpretation in the brane tiling context as illustrated in Figure 49. Let us consider the superpotential corresponding to the case shown in Figure 49,

$$W_I = \cdots + X_{31}X_{12}\underline{X_{23}} + \underline{X_{32}}X_{24}X_{43} - \underline{X_{23}X_{32}} + \ldots \quad , \tag{B.3}$$

where the quadratic mass term and matter fields involved have been underlined. The removal of the quadratic mass term in (B.3) leads to the new superpotential of the form

$$W_{II} = \cdots + X_{31}X_{12}X_{24}X_{43} + \ldots \quad . \tag{B.4}$$

One observes that the process of integrating out mass terms preserves the toric condition discussed in section §2.2.

B.3 Higgs Mechanism

The Higgs Mechanism has a natural interpretation in the brane tiling picture. By giving a non-zero vacuum expectation value (VEV) to a gauge field in gauge theory I, and integrating out resulting quadratic mass terms in the superpotential as explained above, one obtains a new theory II whose mesonic moduli space is a different toric Calabi-Yau 3-fold to the one of theory I. Giving a VEV to a bifundamental field X_{ij} results in the removal of the corresponding edge in the brane tiling picture. This results in an effective merger between two adjacent faces, analogous of combining two gauge groups $U(n)_i$ and $U(n)_j$ into one.

Let us consider the example of the $\mathbb{C}^3/\mathbb{Z}_2 \times \mathbb{Z}_2$ orbifold theory with orbifold action $(0,1,1)(1,0,1)$. The corresponding brane tiling and toric diagram is shown in Figure 50, and the superpotential is

$$\begin{aligned} W_I = {} & X_{42}X_{23}X_{34} + X_{31}X_{14}X_{43} + X_{24}X_{41}X_{12} + X_{13}X_{32}X_{21} \\ & - X_{42}X_{21}X_{14} - X_{31}X_{12}X_{23} - X_{24}X_{43}X_{32} - X_{13}X_{34}X_{41} \quad . \end{aligned} \tag{B.5}$$

By giving the bifundamental field X_{14} a VEV, such that $\langle X_{14} \rangle = 1$, the superpotential becomes,

$$\begin{aligned} W_{I\prime} = {} & X_{42}X_{23}X_{34} + \underline{X_{31}X_{43}} + X_{24}X_{41}X_{12} + X_{13}X_{32}X_{21} \\ & - \underline{X_{42}X_{21}} - X_{31}X_{12}X_{23} - X_{24}X_{43}X_{32} - X_{13}X_{34}X_{41} \quad , \end{aligned} \tag{B.6}$$

which in turn, by integrating out the above underlined quadratic mass terms, becomes

$$W_{II} = X_{13}X_{32}X_{23}X_{31} + X_{12}X_{21}X_{11} - X_{12}X_{23}X_{32}X_{21} - X_{13}X_{31}X_{11} \quad . \tag{B.7}$$

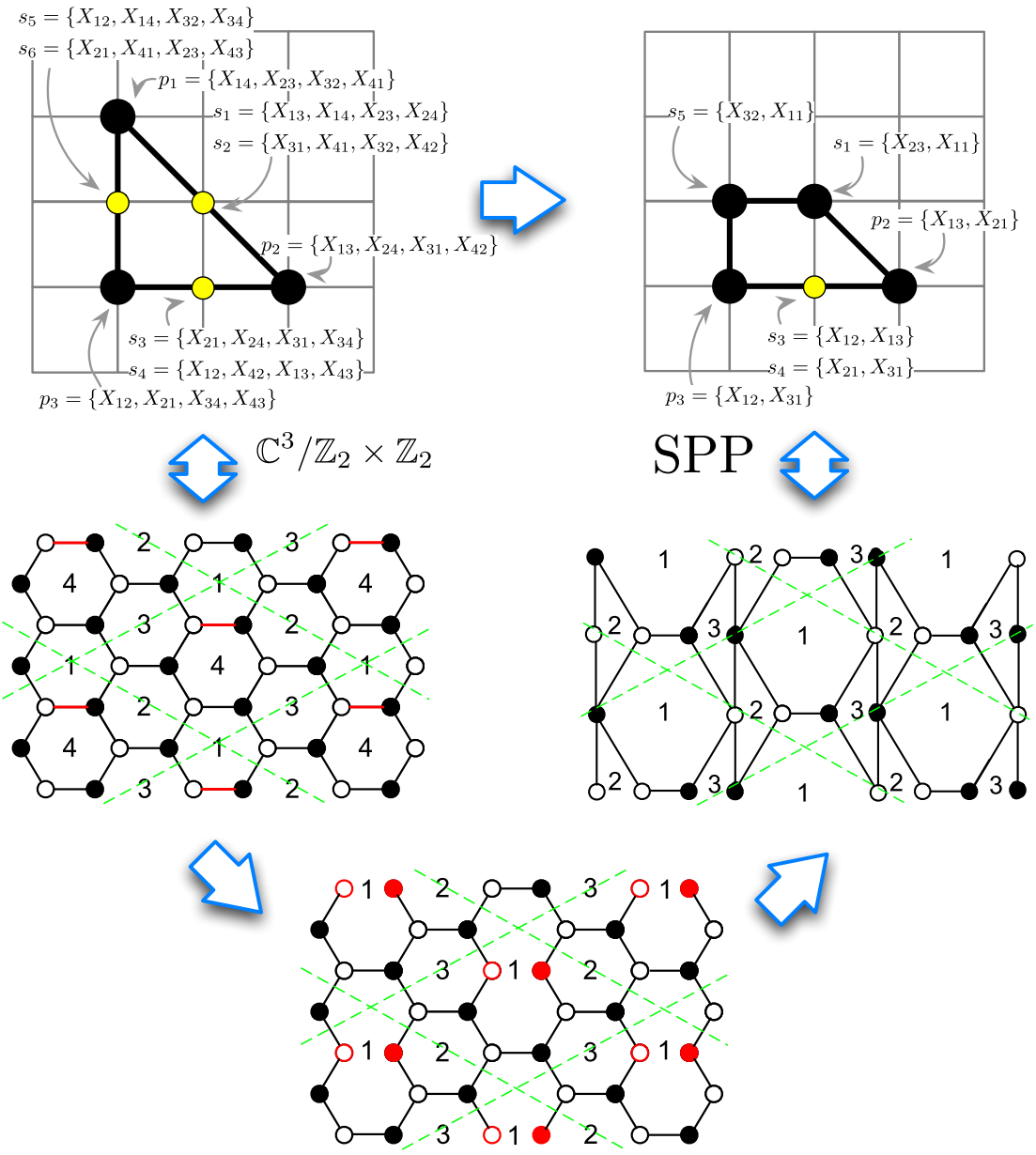


Figure 50. By giving a non-zero vacuum expectation value to the bifundamental field X_{14} of the $\mathbb{C}^3/\mathbb{Z}_2 \times \mathbb{Z}_2$ orbifold theory, one obtains the Suspended Pinch Point theory (SPP). The bifundamental field X_{14} is represented by a red edge in the brane tiling. By setting $\langle X_{14} \rangle = 1$, one obtains quadratic mass terms represented by red nodes in the second brane tiling, which are integrated out to give the third SPP tiling. The nodes of the corresponding toric diagrams are labelled with perfect matching variables and the corresponding sets of bifundamental fields. The Higgsing procedure corresponds to a blow down from $\mathbb{C}^3/\mathbb{Z}_2 \times \mathbb{Z}_2$ to the cone over the Suspended Pinch Point.

Theory II with the above superpotential and brane tiling shown in Figure 50 corresponds to the suspended pinch point (SPP) theory. Thus one has, by giving a VEV to a field in theory I, blown down a toric point in $\mathbb{C}^3/\mathbb{Z}_2 \times \mathbb{Z}_2$ to give the SPP model. Figure 50 shows the perfect matchings and their field content for each toric point of the toric diagrams of $\mathbb{C}^3/\mathbb{Z}_2 \times \mathbb{Z}_2$ and SPP.

The claim is that the combination of toric duality procedures, integrating out mass terms, and higgs mechanisms on the $\mathbb{C}^3/\mathbb{Z}_4 \times \mathbb{Z}_4$ orbifold theory with orbifold action $(1,0,3)(0,1,3)$ results in all possible quiver gauge theories whose mesonic moduli space is toric Calabi-Yau and has a toric diagram which is a reflexive polygon on $\mathbb{Z}^2$.

References

[1] M. R. Douglas and G. W. Moore, *D-branes, Quivers, and ALE Instantons*, hep-th/9603167.

[2] A. Ishii and K. Ueda, *On moduli spaces of quiver representations associated with dimer models*, *ArXiv e-prints* (Oct., 2007) [arXiv:0710.1898].

[3] H. Derksen, J. Weyman, and A. Zelevinsky, *Quivers with potentials and their representations I: Mutations*, *ArXiv e-prints* (Apr., 2007) [arXiv:0704.0649].

[4] N. C. Leung and C. Vafa, *Branes and Toric Geometry*, *ArXiv High Energy Physics - Theory e-prints* (Nov., 1997) [hep-th/9711013].

[5] P. Candelas, M. Lynker, and R. Schimmrigk, *Calabi-Yau Manifolds in Weighted P(4)*, *Nucl. Phys.* **B341** (1990) 383–402.

[6] D. R. Morrison, *Mirror symmetry and rational curves on quintic threefolds: a guide for mathematicians*, *J.AMER.MATH.SOC.* **6** (1993) 223.

[7] V. V. Batyrev, *Dual polyhedra and mirror symmetry for Calabi-Yau hypersurfaces in toric varieties*, *J. Alg. Geom.* **3** (1994) 493–545.

[8] V. Batyrev and D. Dais, *Strong McKay correspondence, string theoretic Hodge numbers and mirror symmetry*, alg-geom/9410001.

[9] V. V. Batyrev and L. A. Borisov, *Dual cones and mirror symmetry for generalized Calabi-Yau manifolds*, . In *Greene, B. (ed.): Yau, S.T. (ed.): Mirror symmetry II* 71-86.

[10] D. Cox and S. Katz, *Mirror symmetry and algebraic geometry.* Mathematical surveys and monographs. American Mathematical Society, 1999.

[11] K. Hori, S. Katz, A. Klemm, R. Pandharipande, R. Thomas, C. Vafa, R. Vakil, and E. Zaslow, *Mirror symmetry*, vol. 1 of *Clay mathematics monographs*. American Mathematical Society, Providence, RI, 2003.

[12] B. Feng, A. Hanany, and Y.-H. He, *D-brane gauge theories from toric singularities and toric duality*, *Nucl. Phys.* **B595** (2001) 165–200, [hep-th/0003085].

[13] B. Feng, A. Hanany, and Y.-H. He, *Phase structure of D-brane gauge theories and toric duality*, *JHEP* **08** (2001) 040, [hep-th/0104259].

[14] B. Feng, S. Franco, A. Hanany, and Y.-H. He, *Unhiggsing the del Pezzo*, *JHEP* **08** (2003) 058, [hep-th/0209228].

[15] B. Feng, S. Franco, A. Hanany, and Y.-H. He, *Symmetries of toric duality*, *JHEP* **12** (2002) 076, [hep-th/0205144].

[16] H. Verlinde and M. Wijnholt, *Building the standard model on a D3-brane*, *JHEP* **0701** (2007) 106, [hep-th/0508089].

[17] V. A. Iskovskih, *Fano 3-folds. i*, *Mathematics of the USSR-Izvestiya* **11** (1977), no. 3 485.

[18] V. A. Iskovskih, *Fano 3-folds. ii*, *Mathematics of the USSR-Izvestiya* **12** (1978), no. 3 469.

[19] G. Ellingsrud, *Complex projective geometry*. London Mathematical Society lecture note series. Cambridge University Press, 1992.

[20] S. Mori and S. Mukai, *Classification of fano 3-folds with b2 $\geq$ 2*, *manuscripta mathematica* **36** (1981) 147–162. 10.1007/BF01170131.

[21] J. Murre, *Classification of fano threefolds according to fano and iskovskih*, . 10.1007/BFb0093585.

[22] S. D. Cutkosky, *On fano 3-folds*, *manuscripta mathematica* **64** (1989) 189–204. 10.1007/BF01160118.

[23] V. V. Batyrev, *Toroidal fano 3-folds*, *Mathematics of the USSR-Izvestiya* **19** (1982), no. 1 13.

[24] V. V. Batyrev, *On the Classification of Toric Fano 4-folds*, *ArXiv Mathematics e-prints* (Jan., 1998) [math/9801107].

[25] M. Kreuzer and B. Nill, *Classification of toric Fano 5-folds*, *ArXiv Mathematics e-prints* (Feb., 2007) [math/0702890].

[26] M. Øbro, *An algorithm for the classification of smooth Fano polytopes*, *ArXiv e-prints* (Apr., 2007) [arXiv:0704.0049].

[27] J. Davey, A. Hanany, N. Mekareeya, and G. Torri, *M2-Branes and Fano 3-folds*, *J.Phys.A* **A44** (2011) 405401, [arXiv:1103.0553].

[28] M. Kreuzer and H. Skarke, *On the Classification of Reflexive Polyhedra*, *Communications in Mathematical Physics* **185** (1997) 495–508, [hep-th/9512204].

[29] M. Kreuzer and H. Skarke, *Classification of Reflexive Polyhedra in Three Dimensions*, *Adv. Theor. Math. Phys.* **2** (1998) 847–864, [hep-th/9805190].

[30] M. Kreuzer and H. Skarke, *Reflexive polyhedra, weights and toric Calabi-Yau fibrations*, *Rev. Math. Phys.* **14** (2002) 343–374, [math/0001106].

[31] M. Kreuzer and H. Skarke, *Complete classification of reflexive polyhedra in four dimensions*, *Adv. Theor. Math. Phys.* **4** (2002) 1209–1230, [hep-th/0002240].

[32] V. Batyrev and M. Kreuzer, *Constructing new Calabi-Yau 3-folds and their mirrors via conifold transitions*, *ArXiv e-prints* (Feb., 2008) [arXiv:0802.3376].

[33] P. Candelas and R. Davies, *New Calabi-Yau Manifolds with Small Hodge Numbers*, *ArXiv e-prints* (Sept., 2008) [arXiv:0809.4681].

[34] P. Candelas and A. Font, *Duality between the webs of heterotic and type II vacua*, *Nuclear Physics B* **511** (Feb., 1998) 295–325, [hep-th/9603170].

[35] Y.-H. He, S.-J. Lee, and A. Lukas, *Heterotic Models from Vector Bundles on Toric Calabi-Yau Manifolds*, *JHEP* **1005** (2010) 071, [arXiv:0911.0865].

[36] Y.-H. He, *An Algorithmic Approach to String Phenomenology*, *Modern Physics Letters A* **25** (2010) 79–90, [arXiv:1001.2419].

[37] P. Candelas, E. Perevalov, and G. Rajesh, *F-theory duals of non-perturbative heterotic $E_8 \times E_8$ vacua in six dimensions*, *Nuclear Physics B* **502** (Feb., 1997) 613–628, [hep-th/9606133].

[38] P. Candelas and H. Skarke, *F-theory, SO(32) and toric geometry*, *Physics Letters B* **413** (Nov., 1997) 63–69, [hep-th/9706226].

[39] H. Skarke, *Reflexive polyhedra and their applications in string and F-theory*, hep-th/0002246.

[40] J. Knapp, M. Kreuzer, C. Mayrhofer, and N.-O. Walliser, *Toric Construction of Global F-Theory GUTs*, *JHEP* **1103** (2011) 138, [arXiv:1101.4908].

[41] A. Hanany and K. D. Kennaway, *Dimer models and toric diagrams*, hep-th/0503149.

[42] S. Franco, A. Hanany, K. D. Kennaway, D. Vegh, and B. Wecht, *Brane Dimers and Quiver Gauge Theories*, *JHEP* **01** (2006) 096, [hep-th/0504110].

[43] S. Franco *et. al.*, *Gauge theories from toric geometry and brane tilings*, *JHEP* **01** (2006) 128, [hep-th/0505211].

[44] A. Hanany and D. Vegh, *Quivers, tilings, branes and rhombi*, *JHEP* **10** (2007) 029, [hep-th/0511063].

[45] A. Hanany, C. P. Herzog, and D. Vegh, *Brane tilings and exceptional collections*, *JHEP* **07** (2006) 001, [hep-th/0602041].

[46] K. D. Kennaway, *Brane Tilings*, *Int. J. Mod. Phys.* **A22** (2007) 2977–3038, [arXiv:0706.1660].

[47] M. Yamazaki, *Brane Tilings and Their Applications*, *Fortsch. Phys.* **56** (2008) 555–686, [arXiv:0803.4474].

[48] A. Hanany, D. Orlando, and S. Reffert, *Sublattice Counting and Orbifolds*, *JHEP* **06** (2010) 051, [arXiv:1002.2981].

[49] J. Davey, A. Hanany, and R.-K. Seong, *Counting Orbifolds*, *JHEP* **06** (2010) 010, [arXiv:1002.3609].

[50] A. Hanany and R.-K. Seong, *Symmetries of Abelian Orbifolds*, *JHEP* **01** (2011) 027, [arXiv:1009.3017].

[51] J. Davey, A. Hanany, and R.-K. Seong, *An Introduction to Counting Orbifolds*, *Fortsch. Phys.* **59** (2011) 677–682, [arXiv:1102.0015].

[52] A. Hanany, V. Jejjala, S. Ramgoolam, and R.-K. Seong, *Calabi-Yau Orbifolds and Torus Coverings*, *JHEP* **09** (2011) 116, [arXiv:1105.3471].

[53] N. Seiberg, *Electric - magnetic duality in supersymmetric nonAbelian gauge theories*, *Nucl.Phys.* **B435** (1995) 129–146, [hep-th/9411149].

[54] B. Feng, A. Hanany, Y.-H. He, and A. M. Uranga, *Toric duality as Seiberg duality and brane diamonds*, *JHEP* **12** (2001) 035, [hep-th/0109063].

[55] C. E. Beasley and M. Ronen Plesser, *Toric duality is Seiberg duality*, *Journal of High Energy Physics* **12** (Dec., 2001) 1–+, [hep-th/0109053].

[56] S. Franco, A. Hanany, and Y.-H. He, *A trio of dualities: Walls, trees and cascades*, *Fortsch. Phys.* **52** (2004) 540–547, [hep-th/0312222].

[57] S. Benvenuti, B. Feng, A. Hanany, and Y.-H. He, *Counting BPS operators in gauge theories: Quivers, syzygies and plethystics*, *JHEP* **11** (2007) 050, [hep-th/0608050].

[58] A. Hanany and C. Romelsberger, *Counting BPS operators in the chiral ring of $N = 2$ supersymmetric gauge theories or $N = 2$ braine surgery*, *Adv. Theor. Math. Phys.* **11** (2007) 1091–1112, [hep-th/0611346].

[59] B. Feng, A. Hanany, and Y.-H. He, *Counting Gauge Invariants: the Plethystic Program*, *JHEP* **03** (2007) 090, [hep-th/0701063].

[60] A. Butti, D. Forcella, A. Hanany, D. Vegh, and A. Zaffaroni, *Counting Chiral Operators in Quiver Gauge Theories*, *JHEP* **11** (2007) 092, [arXiv:0705.2771].

[61] D. Forcella, *Operators and vacua of N=1 field theories*, *Nuovo Cim.* **B125** (2010) 905–914, [arXiv:0912.3444].

[62] A. Hanany, *Counting BPS operators in the chiral ring: The plethystic story*, *AIP Conf.Proc.* **939** (2007) 165–175.

[63] E. Witten, *Phases of N = 2 theories in two dimensions*, *Nucl. Phys.* **B403** (1993) 159–222, [hep-th/9301042].

[64] A. Butti and A. Zaffaroni, *R-charges from toric diagrams and the equivalence of a-maximization and Z-minimization*, *JHEP* **11** (2005) 019, [hep-th/0506232].

[65] D. Forcella, A. Hanany, Y.-H. He, and A. Zaffaroni, *The Master Space of N=1 Gauge Theories*, *JHEP* **0808** (2008) 012, [arXiv:0801.1585].

[66] A. Butti, *Deformations of toric singularities and fractional branes*, *JHEP* **10** (2006) 080, [hep-th/0603253].

[67] B. Feng, Y.-H. He, and F. Lam, *On correspondences between toric singularities and (p,q) webs*, *Nucl.Phys.* **B701** (2004) 334–356, [hep-th/0403133].

[68] D. Forcella, A. Hanany, and A. Zaffaroni, *Master Space, Hilbert Series and Seiberg Duality*, *JHEP* **0907** (2009) 018, [arXiv:0810.4519].

[69] M. Bertolini, F. Bigazzi, and A. Cotrone, *New checks and subtleties for AdS/CFT and a-maximization*, *JHEP* **0412** (2004) 024, [hep-th/0411249].

[70] S. Pinansky, *Quantum deformations from toric geometry*, *JHEP* **03** (2006) 055, [hep-th/0511027].

[71] J. Davey, A. Hanany, and J. Pasukonis, *On the Classification of Brane Tilings*, *JHEP* **01** (2010) 078, [arXiv:0909.2868].

[72] A. Hanany, P. Kazakopoulos, and B. Wecht, *A new infinite class of quiver gauge theories*, *JHEP* **08** (2005) 054, [hep-th/0503177].

[73] S. Benvenuti, A. Hanany, and P. Kazakopoulos, *The toric phases of the Y(p,q) quivers*, *JHEP* **07** (2005) 021, [hep-th/0412279].

[74] S. Benvenuti, S. Franco, A. Hanany, D. Martelli, and J. Sparks, *An infinite family of superconformal quiver gauge theories with Sasaki-Einstein duals*, *JHEP* **06** (2005) 064, [hep-th/0411264].

[75] D. Forcella, *Master Space and Hilbert Series for N=1 Field Theories*, arXiv:0902.2109.

[76] A. Hanany and A. Zaffaroni, *The master space of supersymmetric gauge theories*, *Adv.High Energy Phys.* **2010** (2010) 427891.

[77] D. R. Gulotta, *Properly ordered dimers, R-charges, and an efficient inverse algorithm*, *JHEP* **10** (2008) 014, [arXiv:0807.3012].

[78] B. V. Karpov and D. Y. Nogin, *Three-block exceptional collections over Del Pezzo surfaces*, alg-geom/9703027.

[79] S. Franco, A. Hanany, and P. Kazakopoulos, *Hidden exceptional global symmetries in 4d CFTs*, *JHEP* **07** (2004) 060, [hep-th/0404065].

[80] D. Forcella, A. Hanany, Y.-H. He, and A. Zaffaroni, *Mastering the Master Space*, *Lett.Math.Phys.* **85** (2008) 163–171, [arXiv:0801.3477].

[81] A. Zaffaroni, *The master space of N=1 quiver gauge theories: Counting BPS operators*, . Prepared for 8th Workshop on Continuous Advances in QCD (CAQCD-08), Minneapolis, Minnesota, 15-18 May 2008.

[82] A. Butti and A. Zaffaroni, *From toric geometry to quiver gauge theory: The Equivalence of a-maximization and Z-minimization*, *Fortsch.Phys.* **54** (2006) 309–316, [hep-th/0512240].

[83] A. Hanany, Y.-H. He, V. Jejjala, J. Pasukonis, S. Ramgoolam, *et. al.*, *Invariants of Toric Seiberg Duality*, arXiv:1107.4101.

[84] D. Martelli, J. Sparks, and S.-T. Yau, *The geometric dual of a-maximisation for toric Sasaki- Einstein manifolds*, *Commun. Math. Phys.* **268** (2006) 39–65, [hep-th/0503183].

[85] D. Martelli, J. Sparks, and S.-T. Yau, *Sasaki-Einstein manifolds and volume minimisation*, *Commun. Math. Phys.* **280** (2008) 611–673, [hep-th/0603021].

[86] A. Butti, D. Forcella, and A. Zaffaroni, *Counting BPS baryonic operators in CFTs with Sasaki- Einstein duals*, *JHEP* **06** (2007) 069, [hep-th/0611229].

[87] A. Hanany and R.-K. Seong, *Brane Tilings and Specular Duality*, . work in progress.

[88] B. S. Acharya, J. M. Figueroa-O'Farrill, C. M. Hull, and B. J. Spence, *Branes at conical singularities and holography*, *Adv. Theor. Math. Phys.* **2** (1999) 1249–1286, [hep-th/9808014].

[89] A. Kehagias, *New type IIB vacua and their F-theory interpretation*, *Phys. Lett.* **B435** (1998) 337–342, [hep-th/9805131].